

ENCLOSURE 2 TO SERIAL: HNP-99-032

SHEARON HARRIS NUCLEAR POWER PLANT  
DOCKET NO. 50-400/LICENSE NO. NPF-63  
SPENT FUEL STORAGE  
RE-DESIGNATION OF PROPRIETARY INFORMATION

LICENSING REPORT FOR EXPANDING STORAGE CAPACITY  
IN HARRIS SPENT FUEL POOLS 'C' AND 'D', REVISION 3  
(NON-PROPRIETARY VERSION)

9903220071 990315  
PDR ADDCK 05000400  
P PDR





**HOLTEC**  
INTERNATIONAL

Holtec Center, 555 Lincoln Drive West, Marlton, NJ 08053

Telephone (609) 797-0900

Fax (609) 797-0909

**LICENSING REPORT**  
**for**  
**EXPANDING STORAGE CAPACITY**  
**in**  
**HARRIS SPENT FUEL POOLS C AND D**

**by**

**HOLTEC INTERNATIONAL**  
**555 LINCOLN DRIVE WEST**  
**MARLTON, NJ 08053**

**HOLTEC PROJECT NO. 70324**  
**HOLTEC REPORT HI-971760**  
**REPORT CATEGORY: A**  
**REPORT CLASS: SAFETY RELATED**  
**CLIENT CONTRACT NO. XTA7000024**

**COMPANY PRIVATE**

This document version has all proprietary information removed and has replaced those sections, figures, and tables with highlighting and/or notes to designate the removal of such information. This document is to be used only in connection with the performance of work by Holtec International or its designated subcontractors. Reproduction, publication or presentation, in whole or in part, for any other purpose by any party other than the Client is expressly forbidden.

REVIEW AND CERTIFICATION LOG FOR MULTIPLE AUTHORS

Sheet 1 of 2

REPORT NUMBER: 971760

PROJECT NUMBER: 70324

Document Portion	REVISION 0		REVISION 1		REVISION 2		REVISION 3	
	Author	Reviewer	Author	Reviewer	Author	Reviewer	Author	Reviewer
Chapter 1	S. Pellet SHP 1-22-98	Alvan Siler AS 1/23/98	S. Pellet SHP 4-15-98	Alvan Siler AS 4/15/98	S. Pellet SHP 5-26-98	C. Bullock C.B. 5/26/98	S. Pellet SHP 2-18-99	C. Bullock C.B. 2/18/99
Chapter 2	S. Pellet SHP 1-22-98	Alvan Siler AS 1/23/98	S. Pellet SHP 4-15-98	Alvan Siler AS 4/15/98	S. Pellet SHP 5-26-98	C. Bullock C.B. 5/26/98	S. Pellet SHP 2-18-99	C. Bullock C.B. 2/18/99
Chapter 3	S. Pellet SHP 1-22-98	Alvan Siler AS 1/23/98	S. Pellet SHP 4-15-98	Alvan Siler AS 4/15/98	S. Pellet SHP 5-26-98	C. Bullock C.B. 5/26/98	S. Pellet SHP 2-18-99	C. Bullock C.B. 2/18/99
Chapter 4	Indresh Rantall ER 1-22-98	Alvan Siler AS 1/23/98	Indresh Rantall ER 4/15/98	Alvan Siler AS 4/15/98	S. Pellet SHP 5-26-98	C. Bullock C.B. 5/26/98	S. Pellet SHP 2-18-99	C. Bullock C.B. 2/18/99
Chapter 5	Indresh Rantall ER 1-23/98	Alvan Siler AS 1/23/98	Indresh Rantall ER 4/15/98	Alvan Siler AS 4/15/98	S. Pellet SHP 5-26-98	C. Bullock C.B. 5/26/98	S. Pellet SHP 2-18-99	C. Bullock C.B. 2/18/99
Chapter 6	S. Pellet SHP 1-22-98	Alvan Siler AS 1/23/98	S. Pellet SHP 4-15-98	Alvan Siler AS 4/15/98	S. Pellet SHP 5-26-98	C. Bullock C.B. 5/26/98	S. Pellet SHP 2-18-99	C. Bullock C.B. 2/18/99
Chapter 7	S. Pellet SHP 1-22-98	Alvan Siler AS 1/23/98	S. Pellet SHP 4-15-98	Alvan Siler AS 4/15/98	S. Pellet SHP 5-26-98	C. Bullock C.B. 5/26/98	S. Pellet SHP 2-18-99	C. Bullock C.B. 2/18/99
Chapter 8	S. Pellet SHP 1-22-98	Alvan Siler AS 1/23/98	S. Pellet SHP 4-15-98	Alvan Siler AS 4/15/98	S. Pellet SHP 5-26-98	C. Bullock C.B. 5/26/98	S. Pellet SHP 2-18-99	C. Bullock C.B. 2/18/99
QA APPROVAL	D. Gupta J. Gupta 1-23-98		M. Phipps M. PHIPPS 4/15/98		M. Phipps M. PHIPPS 5/26/98		D. Gupta J. Gupta 2-18-99	
PROJECT MANAGER†	M. J. Phipps 1/23/98		Scott H. Pellet SHP 4-15-98		Scott H. Pellet SHP 5-26-98		Scott H. Pellet SHP 2-18-99	

This document conforms to the requirements of the Design Specification and the applicable sections of the governing codes.

Note: Signatures and printed names are required in the review block.

A revision of this document will be ordered by the Project Manager and carried out if any of its contents is materially affected during evolution of this project. The determination as to the need for revision will be made by the Project Manager with input from others, as deemed necessary by him.

† Must be Project Manager or his designee.

Distribution: C: Client  
M: Designated Manufacturer  
F: Florida Office

THE REVISION CONTROL OF THIS DOCUMENT IS BY A "SUMMARY OF REVISIONS LOG" PLACED BEFORE THE TEXT OF THE REPORT. Form: RCL.02

REVIEW AND CERTIFICATION LOG FOR MULTIPLE AUTHORS

Sheet 2 of 2

REPORT NUMBER: 971760

PROJECT NUMBER: 70324

Document Portion	REVISION 0		REVISION 1		REVISION 2		REVISION 3	
	Author	Reviewer	Author	Reviewer	Author	Reviewer	Author	Reviewer
Chapter 9	S. Pellet SHP 1-22-98	Alan Sola A.S. 1/23/98	S. Pellet SHP 4-5-98	Alan Sola A.S. 4/15/98	S. Pellet SHP 5-26-98	C. Bulatao C.S. 5/26/98	S. Pellet SHP 2-18-99	C. Bulatao C.S. 2/18/99
Chapter 10	S. Pellet SHP 1-22-98	Alan Sola A.S. 1/23/98	S. Pellet SHP 4-5-98	Alan Sola A.S. 4/15/98	N/A	N/A	N/A	N/A
Chapter 100	SHP 5-26-98 S. Pellet SHP 1-22-98	Alan Sola A.S. 1/23/98	S. Pellet SHP 4-5-98	Alan Sola A.S. 4/15/98	S. Pellet SHP 5-26-98	C. Bulatao C.S. 5/26/98	S. Pellet SHP 2-18-99	C. Bulatao C.S. 2/18/99
Chapter 101	S. Pellet SHP 1-22-98	Alan Sola A.S. 1/23/98	S. Pellet SHP 4-15-98	Alan Sola A.S. 4/15/98	S. Pellet SHP 5-26-98	C. Bulatao C.S. 5/26/98	S. Pellet SHP 2-18-99	C. Bulatao C.S. 2/18/99
QA APPROVAL	D. Gupta V. Gupta 1-23-98		M. Phipps M. Phipps 4/15/98		M. Phipps M. Phipps 5/26/98		D. Gupta V. Gupta 2-18-99	
PROJECT MANAGER†	M. Sola M.S. 1/23/98		Scott H. Pellet SHP 4-15-98		Scott H. Pellet SHP 5-26-98		Scott H. Pellet SHP 2-18-99	

This document conforms to the requirements of the Design Specification and the applicable sections of the governing codes.

Note: Signatures and printed names are required in the review block.

\* A revision of this document will be ordered by the Project Manager and carried out if any of its contents is materially affected during evolution of this project. The determination as to the need for revision will be made by the Project Manager with input from others, as deemed necessary by him.

† Must be Project Manager or his designee.

‡ Distribution: C: Client  
M: Designated Manufacturer  
F: Florida Office

THE REVISION CONTROL OF THIS DOCUMENT IS BY A "SUMMARY OF REVISIONS LOG" PLACED BEFORE THE TEXT OF THE REPORT. Form: RCL.02

## SUMMARY OF REVISIONS

Revision 3 contains the following pages:	
COVER PAGE	1 page
REVIEW AND CERTIFICATION LOG	2 pages
QA AND ADMINISTRATIVE INFORMATION LOG	1 page
SUMMARY OF REVISIONS	1 page
TABLE OF CONTENTS	9 pages
1.0 INTRODUCTION	10 pages
2.0 OVERVIEW OF THE PROPOSED CAPACITY EXPANSION	28 pages
3.0 MATERIAL, HEAVY LOAD, AND CONSTRUCTION CONSIDERATIONS	16 pages
4.0 CRITICALITY SAFETY EVALUATION	29 pages
-- APPENDIX 4A	25 pages
5.0 THERMAL-HYDRAULIC CONSIDERATIONS	26 pages
6.0 STRUCTURAL/SEISMIC CONSIDERATIONS	75 pages
7.0 FUEL HANDLING AND CONSTRUCTION ACCIDENTS	25 pages
8.0 FUEL POOL STRUCTURE INTEGRITY CONSIDERATIONS	13 pages
9.0 RADIOLOGICAL EVALUATION	4 pages
10.0 INSTALLATION	9 pages
11.0 ENVIRONMENTAL COST/BENEFIT ASSESSMENT	9 pages
TOTAL	283 pages

Revision 1 contains changes to incorporate comments from CP&L letter 10003481-009 (see Holtec letter 70324SP11).

Revision 2 contains changes to incorporate additional minor CP&L comments. Section 10 "Boral Surveillance Program" has been deleted with following sections renumbered accordingly.

Revision 3 changes the proprietary designation of some information based on discussions with the NRC. This revision does not modify any technical information or textual content.



# TABLE OF CONTENTS

1.0	INTRODUCTION .....	1-1
1.1	References .....	1-6
2.0	OVERVIEW OF THE PROPOSED CAPACITY EXPANSION .....	2-1
2.1	Introduction .....	2-1
2.2	Summary of Principal Design Criteria .....	2-2
2.3	Applicable Codes and Standards .....	2-4
2.4	Quality Assurance Program .....	2-11
2.5	Mechanical Design .....	2-11
2.6	Rack Fabrication .....	2-12
2.6.1	Fabrication Objective .....	2-12
2.6.2	Anatomy of the Harris PWR Rack Module .....	2-13
2.6.3	Anatomy of the Harris BWR Rack Module .....	2-15
3.0	MATERIAL, HEAVY LOAD, AND CONSTRUCTION CONSIDERATIONS .....	3-1
3.1	Introduction .....	3-1
3.2	Structural Materials .....	3-1
3.3	Poison Material (Neutron Absorber) .....	3-1
3.4	Rack Material Compatibility with Coolant .....	3-3
3.5	Heavy Load Considerations for the Proposed Rack Installations .....	3-3
3.6	References .....	3-8
4.0	CRITICALITY SAFETY EVALUATION .....	4-1
4.1	Design Bases .....	4-1
4.2	Summary of Criticality Analyses .....	4-3
4.2.1	Normal Operating Conditions .....	4-3
4.2.1.1	PWR Fuel Results .....	4-3
4.2.1.2	BWR Fuel Results .....	4-4
4.3	Input Parameters .....	4-5
4.3.1	Reference PWR Fuel Assembly and Storage Cell .....	4-5
4.3.2	Reference BWR Fuel Assembly and Storage Cell .....	4-6
4.4	Analytical Methodology .....	4-7
4.4.1	Reference Design Calculations .....	4-7
4.4.2	Burnup Calculations and Uncertainties .....	4-8
4.4.2.1	PWR Fuel Burnup Calculations .....	4-8
4.4.2.2	BWR Fuel Burnup Calculations and Comparison to Vendor Calculations .....	4-8
4.4.3	Effect of Axial Burnup Distribution .....	4-9
4.4.3.1	PWR Fuel Axial Burnup Distribution .....	4-9
4.4.3.2	BWR Fuel Axial Burnup Distribution .....	4-10
4.4.4	Long Term Reactivity Changes .....	4-10
4.5	PWR Storage Rack Criticality Analyses and Tolerance Variations .....	4-11
4.5.1	Nominal Design Case .....	4-11
4.5.2	Uncertainties Due to PWR Rack Manufacturing Tolerances .....	4-11
4.5.2.1	Boron Loading Tolerances .....	4-12

## TABLE OF CONTENTS

4.5.2.2	Boral Width Tolerance .....	4-12
4.5.2.3	Tolerance in Cell Lattice Spacing and Cell Box Inner Dimension .....	4-12
4.5.2.4	Stainless Steel Thickness Tolerance .....	4-12
4.5.2.5	Fuel Enrichment and Density Tolerances .....	4-12
4.6	<u>BWR Storage Rack Criticality Analyses and Tolerance Variations</u> .....	4-13
4.6.1	<u>Nominal Design Case</u> .....	4-13
4.6.2	<u>Uncertainties Due to Manufacturing Tolerances</u> .....	4-14
4.6.2.1	Boron Loading Variation .....	4-14
4.6.2.2	Boral Width Tolerance Variation .....	4-14
4.6.2.3	Tolerance in Cell Lattice Pitch and Inner Box Dimension .....	4-14
4.6.2.4	Stainless Steel Thickness Tolerances .....	4-15
4.6.2.5	Fuel Enrichment and Density Variation .....	4-15
4.6.2.6	Zirconium Flow Channel .....	4-15
4.7	<u>Abnormal and Accident Conditions</u> .....	4-15
4.7.1	<u>Temperature and Water Density Effects</u> .....	4-16
4.7.2	<u>Dropped Fuel Assembly</u> .....	4-16
4.7.3	<u>Lateral Rack Movement</u> .....	4-17
4.7.4	<u>Abnormal Location of a PWR or BWR Fuel Assembly</u> .....	4-17
4.7.5	<u>Eccentric Fuel Positioning</u> .....	4-18
4.8	<u>References</u> .....	4-19
Appendix 4A	“Benchmark Calculations” .....	Total of 25 Pages including 6 figures
4A.1	<u>Introduction and Summary</u> .....	4A-1
4A.2	<u>Effect of Enrichment</u> .....	4A-3
4A.3	<u>Effect of <sup>10</sup>B Loading</u> .....	4A-4
4A.4	<u>Miscellaneous and Minor Parameters</u> .....	4A-5
4A.4.1	<u>Reflector Material and Spacings</u> .....	4A-5
4A.4.2	<u>Fuel Pellet Diameter and Lattice Pitch</u> .....	4A-5
4A.4.3	<u>Soluble Boron Concentration Effects</u> .....	4A-5
4A.5	<u>MOX Fuel</u> .....	4A-6
4A.6	<u>References</u> .....	4A-7
5.0	THERMAL-HYDRAULIC CONSIDERATIONS .....	5-1
5.1	<u>Introduction</u> .....	5-1
5.2	<u>Decay Heat Load Calculations</u> .....	5-2
5.3	<u>Bulk Pool Temperatures</u> .....	5-3
5.4	<u>Local Temperature Analysis</u> .....	5-4
5.4.1	<u>Time-to-Boil</u> .....	5-8
5.5	<u>CFD Analysis of C and D Fuel Pools</u> .....	5-8
5.6	<u>References</u> .....	5-11
6.0	STRUCTURAL/SEISMIC CONSIDERATIONS .....	6-1
6.1	<u>Introduction</u> .....	6-1
6.2	<u>Overview of Rack Structural Analysis Methodology</u> .....	6-1
6.2.1	<u>Background of Analysis Methodology</u> .....	6-2
6.3	<u>Description of Racks</u> .....	6-5

## TABLE OF CONTENTS

6.3.1	<u>Fuel Weights</u> .....	6-5
6.4	<u>Synthetic Time-Histories</u> .....	6-6
6.5	<u>WPMR Methodology</u> .....	6-7
6.5.1	<u>Model Details for Spent Fuel Racks</u> .....	6-7
6.5.1.1	<u>Assumptions</u> .....	6-7
6.5.1.2	<u>Element Details</u> .....	6-9
6.5.2	<u>Fluid Coupling Effect</u> .....	6-10
6.5.2.1	<u>Multi-Body Fluid Coupling Phenomena</u> .....	6-11
6.5.3	<u>Stiffness Element Details</u> .....	6-12
6.5.4	<u>Coefficients of Friction</u> .....	6-13
6.5.5	<u>Governing Equations of Motion</u> .....	6-14
6.6	<u>Structural Evaluation of Spent Fuel Rack Design</u> .....	6-15
6.6.1	<u>Kinematic and Stress Acceptance Criteria</u> .....	6-15
6.6.2	<u>Stress Limit Evaluations</u> .....	6-16
6.6.3	<u>Dimensionless Stress Factors</u> .....	6-18
6.6.4	<u>Loads and Loading Combinations for Spent Fuel Racks</u> .....	6-20
6.7	<u>Parametric Simulations</u> .....	6-21
6.8	<u>Time History Simulation Results</u> .....	6-23
6.8.1	<u>Rack Displacements</u> .....	6-23
6.8.2	<u>Pedestal Vertical Forces</u> .....	6-25
6.8.3	<u>Pedestal Friction Forces</u> .....	6-26
6.8.4	<u>Rack Impact Loads</u> .....	6-27
6.8.4.1	<u>Rack to Rack Impacts</u> .....	6-27
6.8.4.2	<u>Rack to Wall Impacts</u> .....	6-29
6.8.4.3	<u>Fuel to Cell Wall Impact Loads</u> .....	6-29
6.9	<u>Rack Structural Evaluation</u> .....	6-30
6.9.1	<u>Rack Dimensionless Stress Factors for Level B and D Loadings</u> .....	6-30
6.9.1.1	<u>Rack Cell Stress Factors</u> .....	6-31
6.9.2	<u>Pedestal Thread Shear Stress</u> .....	6-32
6.9.3	<u>Local Stresses Due to Impacts</u> .....	6-33
6.9.4	<u>Assessment of Rack Fatigue Margin</u> .....	6-34
6.9.5	<u>Weld Stresses</u> .....	6-37
6.9.6	<u>Bearing Pad Analysis</u> .....	6-39
6.9.7	<u>Level A Evaluation</u> .....	6-40
6.10	<u>Hydrodynamic Loads on Pool Walls</u> .....	6-41
6.11	<u>Conclusions</u> .....	6-42
6.12	<u>References</u> .....	6-43
7.0	<u>FUEL HANDLING AND CONSTRUCTION ACCIDENTS</u> .....	7-1
7.1	<u>Introduction</u> .....	7-1
7.2	<u>Description of Fuel Handling Accidents</u> .....	7-1
7.3	<u>Description of the Rack Drop Accident</u> .....	7-3
7.4	<u>Mathematical Model</u> .....	7-4
7.5	<u>Fuel Drop Results</u> .....	7-5
7.5.1	<u>Shallow Drop Events</u> .....	7-5

## TABLE OF CONTENTS

7.5.2	<u>Deep Drop Events</u> .....	7-5
7.6	<u>Results of Other Drop Scenarios</u> .....	7-6
7.7	<u>Closure</u> .....	7-7
7.8	<u>References</u> .....	7-8
8.0	<b>FUEL POOL STRUCTURE INTEGRITY CONSIDERATIONS</b> .....	8-1
8.1	<u>Introduction</u> .....	8-1
8.2	<u>Description of Pool Structures</u> .....	8-1
8.3	<u>Definition of Loads</u> .....	8-2
8.3.1	<u>Static Loading (Dead Loads and Live Loads)</u> .....	8-2
8.3.2	<u>Seismic Induced Loads</u> .....	8-2
8.3.3	<u>Thermal Loading</u> .....	8-3
8.4	<u>Analysis Procedures</u> .....	8-3
8.4.1	<u>Finite Element Analysis Model</u> .....	8-3
8.4.2	<u>Analysis Methodology</u> .....	8-4
8.4.3	<u>Load Combinations</u> .....	8-6
8.5	<u>Results of Analyses</u> .....	8-7
8.6	<u>Pool Liner</u> .....	8-8
8.7	<u>Conclusions</u> .....	8-9
8.8	<u>References</u> .....	8-10
9.0	<b>RADIOLOGICAL EVALUATION</b> .....	9-1
9.1	<u>Solid Radwaste</u> .....	9-1
9.2	<u>Gaseous Releases</u> .....	9-1
9.3	<u>Personnel Doses</u> .....	9-1
9.4	<u>Anticipated Dose During Re-racking</u> .....	9-2
10.0	<b>INSTALLATION</b> .....	10-1
10.1	<u>Introduction</u> .....	10-1
1.2	<u>Rack Arrangement</u> .....	10-4
10.3	<u>Pool Survey and Inspection</u> .....	10-5
10.4	<u>Pool Cooling and Purification</u> .....	10-6
10.4.1	<u>Pool Cooling</u> .....	10-6
10.4.2	<u>Purification</u> .....	10-6
10.5	<u>Installation of New Racks</u> .....	10-6
10.6	<u>Safety, Environmental &amp; Radiation Control, and ALARA Methods</u> .....	10-8
10.6.1	<u>Safety</u> .....	10-8
10.6.2	<u>Environmental &amp; Radiation Control</u> .....	10-8
10.6.3	<u>ALARA</u> .....	10-8
10.7	<u>Radwaste Material Control</u> .....	10-9
11.0	<b>ENVIRONMENTAL COST/BENEFIT ASSESSMENT</b> .....	11-1
11.1	<u>Introduction</u> .....	11-1
11.2	<u>Imperative for Increased Storage Capacity</u> .....	11-1
11.3	<u>Appraisal of Alternative Options</u> .....	11-1

TABLE OF CONTENTS

---

11.3.1 Alternative Option Summary ..... 11-6  
11.4 Cost Estimate ..... 11-6  
11.5 Resource Commitment ..... 11-7  
11.6 Environmental Considerations ..... 11-8  
11.7 References ..... 11-9

# TABLE OF CONTENTS

## Tables

1.1	Key Haris Plant Information .....	1-7
2.1.1	Geometric and Physical Data for Pool C Rack Modules .....	2-17 and 2-18
2.1.2	Geometric and Physical Data for Pool D Rack Modules .....	2-19
2.5.1	Module Data for Harris Spent Fuel Racks .....	2-20
3.3.1	Boral Experience List - PWRs .....	3-9 and 3-10
3.3.2	Boral Experience List - BWRs .....	3-11 and 3-12
3.3.3	1100 Alloy Aluminum Physical Characteristics .....	3-13
3.3.4	Chemical Composition - Aluminum (1100 Alloy) .....	3-14
3.3.5	Chemical Composition and Physical Properties of Boron Carbide .....	3-15
3.5.1	Heavy Load Handling Compliance Matrix (NUREG-0612) .....	3-16
4.2.1	Summary of Criticality Safety Calculations for PWR Fuel Racks .....	4-20
4.2.2	Summary of Criticality Safety Calculations for BWR Fuel Racks .....	4-21
4.3.1	PWR Fuel Characteristics .....	4-22
4.3.2	BWR Fuel Characteristics .....	4-23
4.4.1	Reactivity Allowance for Uncertainty in Burnup Calculations and the Effect of Axial Burnup Distributions for PWR Fuel .....	4-24
4.5.1	Comparison of MCNP-4A and CASMO-3 Calculations .....	4-25
4.7.1	Reactivity Effects of Temperature and Void .....	4-26
4A.1	Summary of Criticality Benchmark Calculations .....	4A-9 thru 4A-13
4A.2	Comparison of MCNP4a and Keno5a Calculated Reactivities for Various Enrichments .....	4A-14
4A.3	MCNP4a Calculated Reactivities for Critical Experiments with Neutron Absorbers .....	4A-15
4A.4	Comparison of MCNP4a and KENO5a Calculated Reactivities for Various <sup>10</sup> B Loadings .....	4A-16
4A.5	Calculations for Critical Experiments with Thick Lead and Steel Reflectors .....	4A-17
4A.6	Calculations for Critical Experiments with Various Soluble Boron Concentrations .....	4A-18
4A.7	Calculations for Critical Experiments with MOX Fuel .....	4A-19
5.1.1	Partial Listing of Rerack Applications Using Similar Methods of Thermal-Hydraulic Analysis .....	5-12 and 5-13
5.2.1	Decay Periods for a Bounding Pools C and D Storage Configuration .....	5-14
5.2.2	Fuel Assemblies Input Data for Decay Heat Evaluation .....	5-15
5.2.3	Bounding Decay Heat Input from Stored Fuel in Pools C and D .....	5-16
5.4.1	Bounding Fuel Assemblies Hydraulic Flow Resistance Parameters .....	5-17
5.5.1	Pools C and D Dimensional Data .....	5-18

## TABLE OF CONTENTS

---

5.5.2	Bulk and Local Temperature Summary .....	5-19
6.2.1	Partial Listing of Fuel Rack Applications Using DYNARACK .....	6-45 and 6-46
6.3.1	Rack Material Data (200°F) (ASME - Section II, Part D) .....	6-47
6.4.1	Time-History Statistical Correlation Results .....	6-48
6.5.1	Degrees-of-Freedom .....	6-49
6.5.2	(MR216) Numbering System for Gap Elements and Friction Elements in the Pool D Campaign I Model .....	6-50 and 6-51
6.9.1	Comparison of Bounding Calculated Loads/Stresses vs. Code Allowables at Impact and Weld Locations .....	6-52
7.1	Impact Event Data .....	7-9
7.2	Material Definition .....	7-10
8.5.1	Bending and Shear Strength Evaluation .....	8-11
9.4.1	Preliminary Estimate of Person-REM Dose During Reracking .....	9-4

## TABLE OF CONTENTS

### Figures

1.1	Harris Fuel Handling Building Plan Layout .....	1-8
1.2	Storage Configuration for Pool C .....	1-9
1.3	Storage Configuration for Pool D .....	1-10
2.1.1	Pictorial View of Typical Harris Rack Structure .....	2-21
2.6.1	Seam Welded Precision Formed Channels .....	2-22
2.6.2	Three PWR Cells in Elevation View .....	2-23
2.6.3	Three BWR Cells in Elevation View .....	2-24
2.6.4	Composite Box Assembly .....	2-25
2.6.5	Typical Array of Storage Cells .....	2-26
2.6.6	Support Pedestal for Holtec PWR Rack .....	2-27
2.6.7	Support Pedestal for Holtec BWR Rack .....	2-28
4.2.1	Burnup Versus Enrichment for PWR Fuel .....	4-27
4.3.1	a Two Dimensional Representation of the Calculational Model Used for the PWR Storage Rack Analysis .....	4-28
4.3.2	a Two Dimensional Representation of the Calculational Model Used for the BWR Storage Rack Analysis .....	4-29
4A.1	MCNP Calculated k-eff Values for Various Values of the Spectral Index .....	4A-20
4A.2	KENO5a Calculated k-eff Values for Various Values of the Spectral Index .....	4A-21
4A.3	MCNP Calculated k-eff Values at Various U-235 Enrichments .....	4A-22
4A.4	KENO5a Calculated k-eff Values at Various U-235 Enrichments .....	4A-23
4A.5	Comparison of MCNP and KENO5a Calculations for Various Fuel Enrichments .....	4A-24
4A.5	Comparison of MCNP and KENO5a Calculations for Various Boron-10 Areal Densities .....	4A-25
5.3.1	C and D Pools Minimum Total Cooling System Requirements Curve at 137° F Bulk Pool Temperature .....	5-20
5.4.1	Harris C and D Pools Physical Configuration .....	5-21
5.5.1	Plan View of the Harris Pools C and D and CFD Model .....	5-22
5.5.2	Perspective View of the Harris Pools C and D and CFD Model .....	5-23
5.5.3	Peak Local Water Temperature in the Rack Cells .....	5-24
5.5.4	Pools Interconnecting Channel Flow Velocity Vectors Elevation View Plot .....	5-25
5.5.5	Pool Cooling Inlet/Outlet Piping Region Flow Velocity Vectors Plot .....	5-26
6.3.1	Phased Storage Configuration for Pool C .....	6-53
6.3.2	Phased Storage Configuration for Pool D .....	6-54
6.4.1	SFP Time History Accelerogram (X-Direction, OBE) .....	6-55
6.4.2	SFP Time History Accelerogram (Y-Direction, OBE) .....	6-56
6.4.3	SFP Time History Accelerogram (Z-Direction, OBE) .....	6-57

## TABLE OF CONTENTS

---

6.4.4	SFP Time History Accelerogram (X-Direction, SSE) .....	6-58
6.4.5	SFP Time History Accelerogram (Y-Direction, SSE) .....	6-59
6.4.6	SFP Time History Accelerogram (Z-Direction, SSE) .....	6-60
6.5.1	Schematic of the Dynamic Model for DYNARACK .....	6-61
6.5.2	Fuel-to-Rack Impact Springs at Level of Rattling Mass .....	6-62
6.5.3	Two Dimensional View of the Spring-Mass Simulation .....	6-63
6.5.4	Rack Degrees-of-Freedom and Bending Springs .....	6-64
6.5.5	Rack-to-Rack Impact Springs .....	6-65
6.5.6	Bottom Rack Impact Springs - Campaign I - Pool C .....	6-66
6.5.7	Top Rack Impact Springs - Campaign I - Pool C .....	6-67
6.5.8	Bottom Rack Impact Springs - Campaigns II and III - Pool C .....	6-68
6.5.9	Top Rack Impact Springs - Campaigns II and III - Pool C .....	6-69
6.5.10	Bottom Rack Impact Springs - Campaign I - Pool D .....	6-70
6.5.11	Top Rack Impact Springs - Campaign I - Pool D .....	6-71
6.5.12	Bottom Rack Impact Springs - Campaign II - Pool D .....	6-72
6.5.13	Top Rack Impact Springs - Campaign II - Pool D .....	6-73
6.8.1	Vertical Pedestal Time History Loading Plot .....	6-74
6.9.1	Rack Fatigue Finite Element Model .....	6-75
7.2.1	Shallow Drop on a Peripheral Cell .....	7-11
7.2.2	Plan View of Impactor and Impact Zone (Shallow Drop Event) .....	7-12
7.2.3	Deep Drop on a Support Leg Location .....	7-13
7.2.4	Deep Drop on a Center Cell Location .....	7-14
7.3.1	Heaviest Rack Drop .....	7-15
7.5.1	Shallow Drop: Finite Element Model Detail - Impacted Region .....	7-16
7.5.2	Maximum Cell Deformation for Shallow Drop on Exterior Cell .....	7-17
7.5.3	Shallow Drop: Maximum Deformation - Impacted Region Plan .....	7-18
7.5.4	Plan View of Deep Drop Scenarios .....	7-19
7.5.5	Maximum Baseplate Deformation from Deep Drop Scenario .....	7-20
7.6.1	Gate Drop Finite-Element Model .....	7-21
7.6.2	Gate Drop Finite-Element Model, Detail of Impacted Region .....	7-22
7.6.3	Gate Drop Finite-Element Model, Detail of Impacted region (Plan) .....	7-23
7.6.4	Gate Drop Maximum Deformation .....	7-24
7.6.5	Gate Drop Maximum Deformation, Impacted Region Plan .....	7-25
8.2.1	Pool Structure Dimensions .....	8-12
8.4.1	Fuel Handling Building Finite Element Model .....	8-13



The Harris Nuclear Plant (HNP) is a single unit pressurized water reactor installation located in the extreme southwest corner of Wake County, North Carolina, and the southeast corner of Chatham County, North Carolina. The HNP installation is owned by the Carolina Power & Light Company (CP&L) and the North Carolina Eastern Municipal Power Agency (NCEMPA), located in Raleigh, North Carolina. CP&L has the overall responsibility to ensure that plant operations are performed without undue risk to the health and safety of the public. Table 1.1 contains key overview data for HNP's PWR Unit.

HNP was originally named Shearon Harris Nuclear Power Plant (SHNPP) and was initially designed as a four unit nuclear reactor site, of which only Unit 1 was completed. The Fuel Handling Building (FHB), however, was constructed to service all four Units as originally envisioned. During initial licensing, the possibility of transshipment from other Units was recognized and consequently the Spent Fuel Pools were licensed to store both PWR and BWR fuel. Transshipped fuel from the Robinson and Brunswick plants is already in stored in pools A and B.

The FHB is a long narrow structure intended to be sandwiched between the nuclear plants, in order to service all four Units. Each end of the building contains two large pools, with the South end pools (A and B) originally intended to service Units 1 and 4 and the North end pools (C and D) designed to service Units 2 and 3. The layout of the FHB and pools in relationship with Unit 1 is shown in Figure 1.1. The two pools in each end of the building were originally designated as the "New Fuel Pool" for the smaller of the two pools and the "Spent Fuel Pool" for the larger pool. These four pools have since been re-designated as pools A, B, C, and D, where pools A and D represent the smaller pools. All four pools are interconnected through "gated" passages and are capable of storing spent fuel.

Pools A and B, located at the South end of the building, have already been racked and are nearly full. Pool A contains six Region 1 type (6 x 10 cell) PWR racks and three (11 x 11 cell) BWR racks for a total storage capacity of 723 assemblies. Pool A has been, and will continue to be, used to store fresh (unburned) fuel, recently discharged Harris fuel and transshipped fuel. Pool B contains six (7 x 10 cell), five (6 x 10 cell), and one (6 x 8 cell) PWR Region 1 style racks. Pool B also currently contains seventeen (11 x 11 cell) BWR racks, twelve of which have been supplied by Holtec International. Pool B is licensed to store one more (11 x 11 cell) Holtec BWR rack which would increase the total pool storage capacity to 2946 assemblies. The combined pool A and B licensed storage capacity is 3669 assemblies.

Projected operation of the Harris Unit and transshipments from the Robinson and Brunswick Units will continue to demand incremental increases in spent fuel storage capacity. The Carolina Power & Light Company, HNP's principal owner and operator, has entered into a contract with Holtec International of Marlton, N.J. to design maximum density spent fuel storage racks for pools C and D. Under the proposed capacity expansion, fuel storage racks will be installed in campaign phases on an as needed basis. This process is consistent with the incremental capacity expansions already performed in pool B.

Pools C and D are unused and are located in the north end of the Harris Fuel Handling Building. Pool C will provide storage for both PWR and BWR fuel. This pool has nominal dimensions of 27 feet wide by 50 feet long and at maximum storage density can accommodate 927 PWR and 2763 BWR assemblies. Pool D will contain only PWR fuel and with nominal dimensions of 20 feet wide by 32 feet long can accommodate 1025 maximum density storage cells. Proposed storage configurations for pools C and D are provided in Figures 1.2 and 1.3, respectively.

The configuration shown in Figure 1.2 represents the mixture of PWR and BWR storage which will accommodate future storage needs based on the best information currently available. To provide the greatest flexibility in mixture of fuel types, the storage racks were sized to allow

interchangeability. The dimensions of the 9x9 PWR storage rack are nearly identical to those of the 13x13 BWR rack. Therefore, configurations other than those shown in Figure 1.2 are possible by replacing one rack type by the other. The complete geometric fungibility between the 9x9 PWR and 13x13 BWR rack modules affords CP&L the latitude to alter the mix between PWR and BWR storage as the precise need for the two types of spent nuclear fuel storage become known. Interchanging of PWR and BWR modules would be performed after appropriate safety evaluations supported by reanalysis of the criticality, thermal-hydraulic, and structural analyses are successfully conducted to support such a substitution under Subpart 50.59.

The new Holtec racks are free-standing and self-supporting. The principal construction materials for the new racks are SA240-Type 304L stainless steel sheet and plate stock, and SA564-630 (precipitation hardened stainless steel) for the adjustable support spindles. The only non-stainless material utilized in the rack is the neutron absorber material which is a boron carbide and aluminum-composite sandwich available under the patented product name Boral™.

The new Holtec racks are designed to the stress limits of, and analyzed in accordance with, Section III, Division 1, Subsection NF of the ASME Boiler and Pressure Vessel (B&PV) Code. The material procurement, analysis, and fabrication of the rack modules conform to 10CFR50 Appendix B requirements.

The rack design and analysis methodologies employed in the Harris storage capacity expansion are a direct evolution of previous rerack license applications. This Licensing Report documents the design and analyses performed to demonstrate that the new Holtec racks meet all governing requirements of the applicable codes and standards, in particular, "OT Position for Review and Acceptance of Spent Fuel Storage and Handling Applications", USNRC, 1978 and the 1979 Addendum thereto [1.0.1].

Sections 2 and 3 of this report provide an abstract of the design and material information on the new racks.

The criticality safety analysis requires that the neutron multiplication factor for the stored fuel array be bounded by the USNRC  $k_{\text{eff}}$  limit of 0.95 under assumptions of 95% probability and 95% confidence. The criticality safety analysis provided in Section 4 sets the requirements on the Boral panel length and the areal B-10 density for the new high density racks.

Thermal-hydraulic consideration requires that fuel cladding will not fail due to excessive thermal stress, and that the steady state pool bulk temperature will remain within the limits prescribed for the spent fuel pool to satisfy the pool structural strength, operational, and regulatory requirements. The thermal-hydraulic analyses carried out in support of this storage expansion effort are described in Section 5.

Demonstrations of seismic and structural adequacy are presented in Section 6.0. The analysis shows that the primary stresses in the rack module structure will remain below the allowable stresses of the ASME B&PV Code (Subsection NF) [1.0.2]. The structural qualification also includes analytical demonstration that the subcriticality of the stored fuel will be maintained under all postulated accident scenarios in the Harris Final Safety Analysis Report (FSAR). The structural consequences of these postulated accidents are evaluated and presented in Section 7 of this report.

Section 8 contains the structural analysis to demonstrate the adequacy of the spent fuel pool reinforced concrete structure. A synopsis of the geometry of the Harris reinforced concrete structure is also presented in Section 8.

The radiological considerations are documented in Section 9.0. Sections 10, and 11 discuss the salient considerations in the installation of the new racks, and a cost/benefit and



environmental assessment to establish the prudence of CP&L's decision to exercise the wet storage expansion option, respectively.

All computer programs utilized to perform the analyses documented in this licensing report are benchmarked and verified. These programs have been utilized by Holtec International in numerous rerack applications over the past decade.

The analyses presented herein clearly demonstrate that the rack module arrays possess wide margins of safety in respect to all considerations of safety specified in the OT Position Paper, namely, nuclear subcriticality, thermal-hydraulic safety, seismic and structural adequacy, radiological compliance, and mechanical integrity.



## 1.1 References

- [1.0.1] USNRC, "OT Position for Review and Acceptance of Spent Fuel Storage and Handling Applications, April 14, 1978, and Addendum dated January 18, 1979.
- [1.0.2] ASME Boiler & Pressure Vessel Code, Section III, Subsection NF, and Appendices (1995).

Table 1.1	
KEY HARRIS PLANT INFORMATION	
ITEM	DATA
Docket Number	50-400
Capacity, MWe	940
Applied to NRC	9-4-71
Construction Permit	1-27-78
Commercial Operation	1986
Present Capacity	<u>Cells</u>
Pool A	723
Pool B	2946
<b>TOTAL</b>	<b>3669</b>



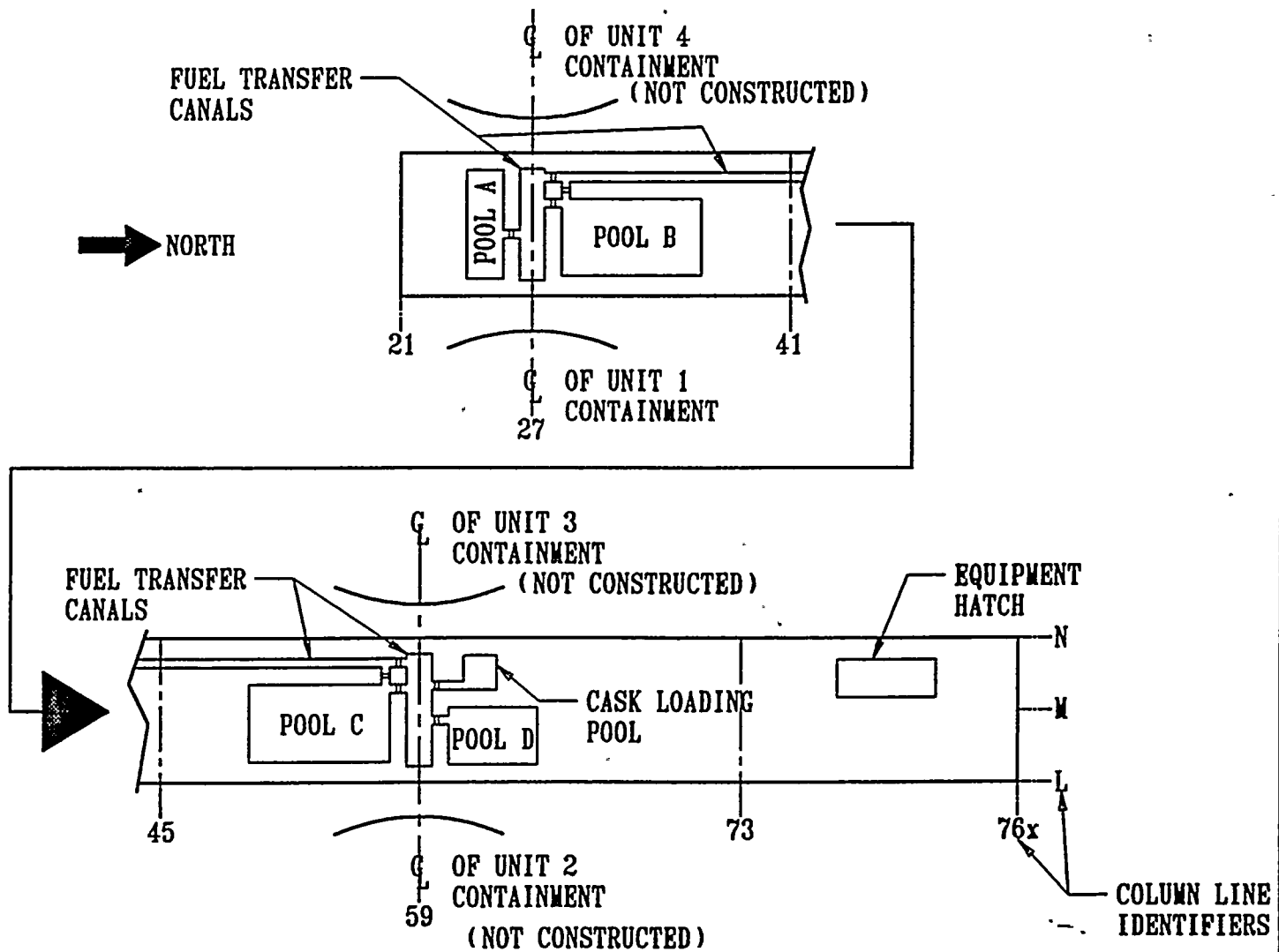


FIGURE 1.1; HARRIS FUEL HANDLING BUILDING PLAN LAYOUT

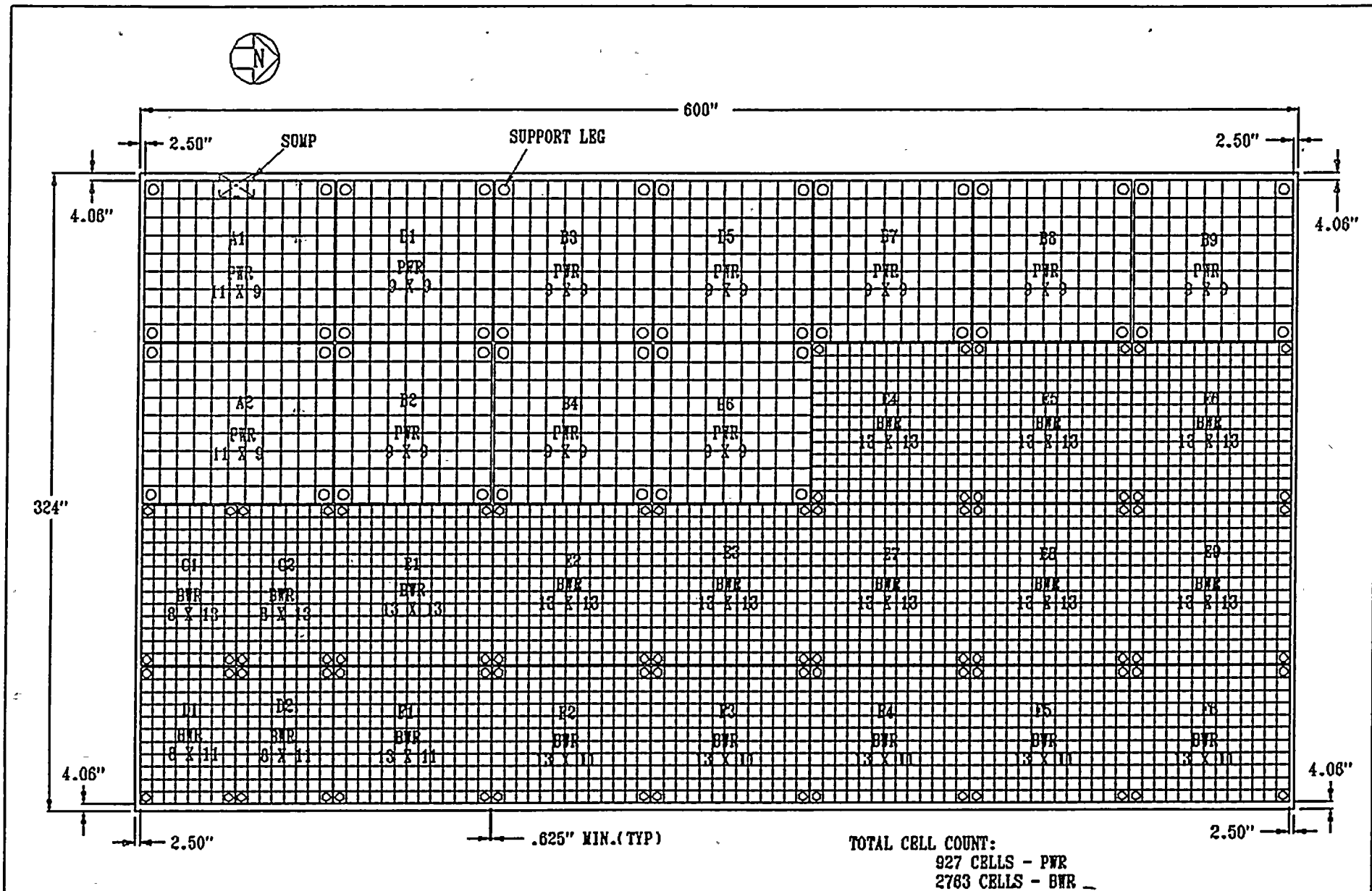


FIGURE 1.2; STORAGE CONFIGURATION FOR POOL C

HI-971760



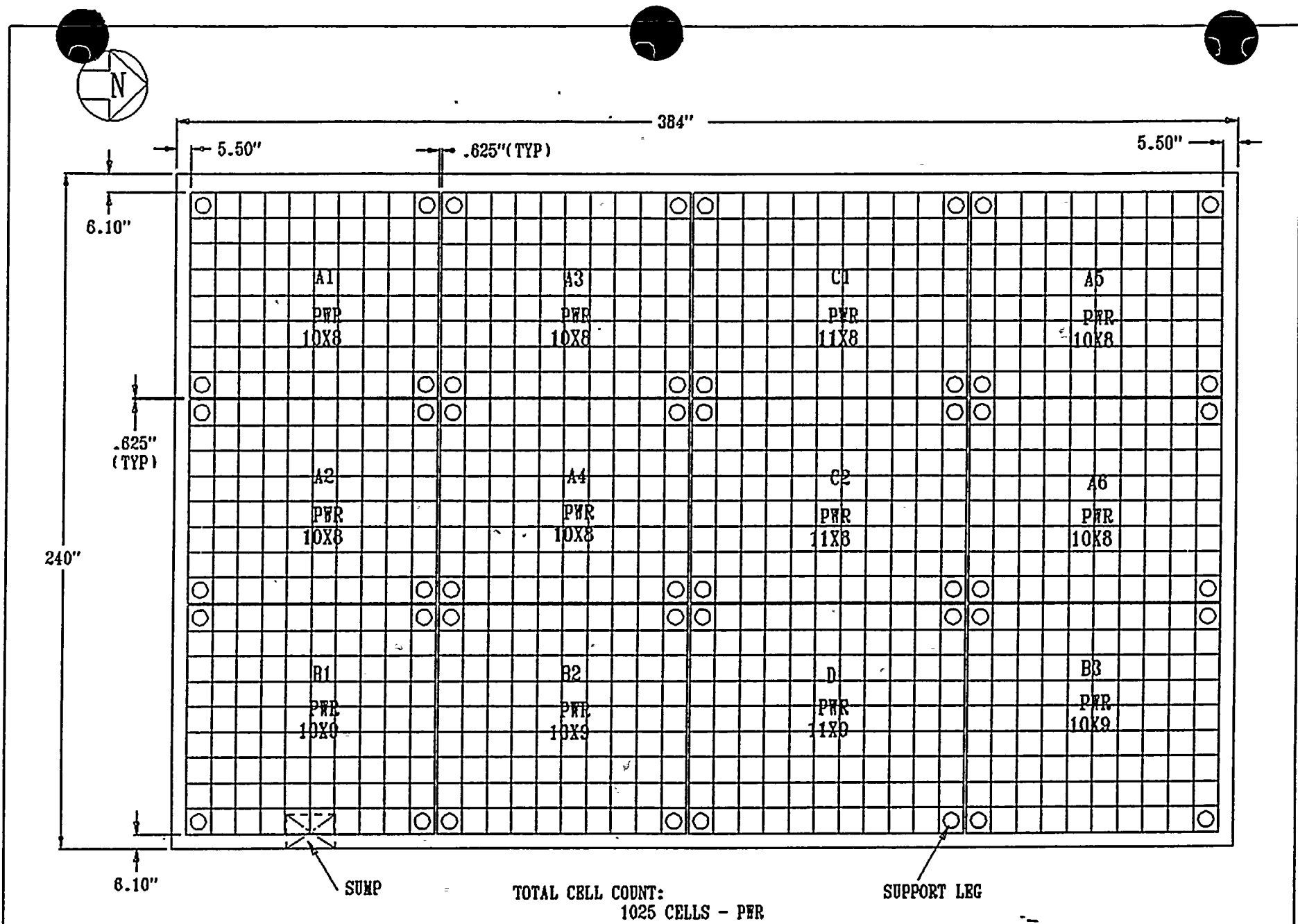


FIGURE 1.3; STORAGE CONFIGURATION FOR POOL D

HI-971760

## 2.0 OVERVIEW OF THE PROPOSED CAPACITY EXPANSION

### 2.1 Introduction

In its currently proposed fully implemented configuration, Pool C will contain eleven PWR racks and nineteen BWR racks. Pool D will contain twelve PWR racks. All storage racks arrays will consist of free-standing modules, made from Type 304L austenitic stainless steel containing prismatic storage cells interconnected through longitudinal welds. A panel of Boral cermet containing a high areal loading of the B-10 isotope provides appropriate neutron attenuation between adjacent storage cells. Figure 2.1.1 provides a schematic of the typical Region 2 storage module proposed for Harris. Data on the cross sectional dimensions, gross weight and cell count for each rack module in pools C and D are presented in Tables 2.1.1 and 2.1.2, respectively.

In the parlance of wet storage technology, the Harris modules are of the so-called non-flux-trap genre and are referred to as Region 2 style racks. Region 2 PWR racks have enrichment/burnup limitations placed on them and storing PWR spent nuclear fuel will be subject to burnup compliance restriction. The BWR storage racks do not require any such limitations since the criticality analyses are performed for the maximum reactivity over burnup.

Each new rack module is supported by four legs which are remotely adjustable. Thus, the racks can be made vertical and the top of the racks can easily be made co-planar with each other. The rack module support legs are engineered to accommodate undulations in the fuel pool and cask pit floor flatness.

A bearing pad interposed between the rack pedestals and the pool liner serves to diffuse the dead load of the loaded racks into the reinforced concrete structure of the pool slab.



The overall design of the Harris racks is similar to those presently in service in the spent fuel pools at many other nuclear plants, among them Zion Nuclear Station of the Commonwealth Edison Company, Donald C. Cook of American Electric Power, and Connecticut Yankee of Northeast Utilities. Altogether, over 50 thousand storage cells of the Harris design have been provided by Holtec International to various nuclear plants around the world.

## 2.2 Summary of Principal Design Criteria

The key design criteria for the new Harris spent fuel racks are set forth in the classical USNRC memorandum entitled "OT Position for Review and Acceptance of Spent Fuel Storage and Handling Applications", April 14, 1978 as modified by amendment dated January 18, 1979. The individual sections of this report expound on the specific design bases derived from the above-mentioned "OT Position Paper". Nevertheless, a brief summary of the design bases for the Harris racks are summarized in the following:

- a. Disposition: All new rack modules are required to be free-standing.
- b. Kinematic Stability: All free-standing modules must be kinematically stable (against tipping or overturning) if a seismic event (which is 150% of the postulated OBE or 110% of the postulated SSE) is imposed on any module.
- c. Structural Compliance: All primary stresses in the rack modules must satisfy the limits postulated in Section III subsection NF of the 1995 ASME Boiler and Pressure Vessel Code.
- d. Thermal-Hydraulic Compliance: The spatial average bulk pool temperature is required to remain under 137°F<sup>†</sup> in the wake of a normal refueling.

In addition to the limitations on the bulk pool temperature, the local water temperature in the Harris pools must remain subcooled (i.e., below the boiling temperature coincident with local hydraulic pressure conditions).

---

<sup>†</sup> The 137°F limit is consistent with that currently in the Harris FSAR and procedures for pools A and B. CP&L is in the process of re-evaluating systems and components to allow for an increase the allowable bulk pool temperature.



- e. Criticality Compliance: Region 2 cells must be able to store the Zircaloy clad fuel of 5 w/o enrichment and 40 MWD/MTU burnup while maintaining the reactivity  $\leq 0.95$ .
- f. Radiological Compliance: The reracking of Harris must not lead to violation of the off-site dose limits, or adversely affect the area dose environment as set forth in the Harris FSAR. The radiological implications of the installation of the new racks also need to be ascertained and deemed to be acceptable.
- g. Pool Structure: The ability of the reinforced concrete structure to satisfy the load combinations set forth in NUREG-0800, SRP 3.8.4 must be demonstrated.
- h. Rack Cyclic Stress Fatigue: In addition to satisfying the primary stress criteria of Subsection NF, the alternating local stresses in the rack structure are evaluated to ensure that the "cumulative damage factor" due to at least ten SSE events does not exceed 1.0.
- i. Liner Integrity: The integrity of the liner under cyclic in-plane loading during a seismic event must be demonstrated. A material fatigue evaluation is performed in accordance with ASME B&PV Code. The alternating local stresses in the liner are evaluated to ensure that the "cumulative damage factor" due to at least ten SSE events does not exceed 1.0.
- j. Bearing Pads: The bearing pads must be sufficiently thick such that the pressure on the liner continues to satisfy the ACI limits during and after a design basis seismic event.
- k. Accident Events: In the event of postulated drop events (uncontrolled lowering of a fuel assembly, for instance), it is necessary to demonstrate that the subcriticality of the rack structure is not compromised.
- l. Construction Events: The field construction services required to be carried out for executing the reracking must be demonstrated to be within the "state of proven art".

The foregoing design bases are further articulated in Sections 4 through 9 of this licensing report.



## 2.3 Applicable Codes and Standards

The following codes, standards and practices are used as applicable for the design, construction, and assembly of the Harris fuel storage racks. Additional specific references related to detailed analyses are given in each section.

### a. Design Codes

- (1) AISC Manual of Steel Construction, 1970 Edition and later.
- (2) ANSI N210-1976, "Design Requirements for Light Water Reactor Spent Fuel Storage Facilities at Nuclear Power Stations" (contains guidelines for fuel rack design).
- (3) American Society of Mechanical Engineers (ASME), Boiler and Pressure Vessel Code Section III, 1986 Edition; ASME Section V, 1986 edition; ASME Section VIII, 1986 Edition; ASME Section IX, 1986 Edition; and ASME Section XI, 1986 Edition.
- (4) ASNT-TC-1A June, 1984 American Society for Nondestructive Testing (Recommended Practice for Personnel Qualifications).
- (5) American Concrete Institute Building Code Requirements for Reinforced Concrete (ACI318-63) and (ACI318-71).
- (6) Code Requirements for Nuclear Safety Related Concrete Structures, ACI349-85/ACI349R-85, and ACI349.1R-80.
- (7) ASME NQA-1, Quality Assurance Program Requirements for Nuclear Facilities
- (8) ASME NQA-2-1989, Quality Assurance Requirements for Nuclear Facility Applications.
- (9) ANSI Y14.5M, Dimensioning and Tolerancing for Engineering Drawings and Related Documentation Practices.
- (10) ACI Detailing Manual - 1980.

b. Material Codes - Standards of ASTM

- (1) E165 - Standard Methods for Liquid Penetrant Inspection.
- (2) A240 - Standard Specification for Heat-Resisting Chromium and Chromium-Nickel Stainless Steel Plate, Sheet and Strip for Fusion-Welded Unfired Pressure Vessels.
- (3) A262 - Detecting Susceptibility to Intergranular Attack in Austenitic Stainless Steel.
- (4) A276 - Standard Specification for Stainless and Heat-Resisting Steel Bars and Shapes.
- (5) A479 - Steel Bars for Boilers & Pressure Vessels.
- (6) ASTM A564, Standard Specification for Hot-Rolled and Cold-Finished Age-Hardening Stainless and Heat-Resisting Steel Bars and Shapes.
- (7) C750 - Standard Specification for Nuclear-Grade Boron Carbide Powder.
- (8) A380 - Recommended Practice for Descaling, Cleaning and Marking Stainless Steel Parts and Equipment.
- (9) C992 - Standard Specification for Boron-Based Neutron Absorbing Material Systems for Use in Nuclear Spent Fuel Storage Racks.
- (10) ASTM E3, Preparation of Metallographic Specimens.
- (11) ASTM E190, Guided Bend Test for Ductility of Welds.
- (12) American Society of Mechanical Engineers (ASME), Boiler and Pressure Vessel Code, Section II-Parts A and C, 1995 Edition.
- (13) NCA3800 - Metallic Material Manufacturer's and Material Supplier's Quality System Program..

c. Welding Codes: ASME Boiler and Pressure Vessel Code, Section IX - Welding and Brazing Qualifications, 1995 Edition.



d. Quality Assurance, Cleanliness, Packaging, Shipping, Receiving, Storage, and Handling Requirements

- (1) ANSI 45.2.1 - Cleaning of Fluid Systems and Associated Components during Construction Phase of Nuclear Power Plants.
- (2) ANSI N45.2.2 - Packaging, Shipping, Receiving, Storage and Handling of Items for Nuclear Power Plants (During the Construction Phase).
- (3) ANSI - N45.2.6 - Qualifications of Inspection, Examination, and Testing Personnel for Nuclear Power Plants (Regulatory Guide 1.58).
- (4) ANSI-N45.2.8, Supplementary Quality Assurance Requirements for Installation, Inspection and Testing of Mechanical Equipment and Systems for the Construction Phase of Nuclear Plants.
- (5) ANSI - N45.2.11, Quality Assurance Requirements for the Design of Nuclear Power Plants.
- (6) ANSI-N45.2.12, Requirements for Auditing of Quality Assurance Programs for Nuclear Power Plants.
- (7) ANSI N45.2.13 - Quality Assurance Requirements for Control of Procurement of Equipment Materials and Services for Nuclear Power Plants (Regulatory Guide 1.123).
- (8) ANSI N45.2.15-18 - Hoisting, Rigging, and Transporting of Items For Nuclear Power Plants.
- (9) ANSI N45.2.23 - Qualification of Quality Assurance Program Audit Personnel for Nuclear Power Plants (Regulatory Guide 1.146).
- (10) ASME Boiler and Pressure Vessel, Section V, Nondestructive Examination, 1995 Edition.
- (11) ANSI - N16.9-75 Validation of Calculation Methods for Nuclear Criticality Safety.

e. Governing NRC Design Documents

- (1) "OT Position for Review and Acceptance of Spent Fuel Storage and Handling Applications," dated April 14, 1978, and the modifications to this document of January 18, 1979.

- (2) NUREG 0612, "Control of Heavy Loads at Nuclear Power Plants", USNRC, Washington, D.C., July, 1980.

f. Other ANSI Standards (not listed in the preceding)

- (1) ANSI/ANS 8.1 (N16.1) - Nuclear Criticality Safety in Operations with Fissionable Materials Outside Reactors.
- (2) ANSI/ANS 8.17, Criticality Safety Criteria for the Handling, Storage, and Transportation of LWR Fuel Outside Reactors.
- (3) N45.2 - Quality Assurance Program Requirements for Nuclear Facilities - 1971.
- (4) N45.2.9 - Requirements for Collection, Storage and Maintenance of Quality Assurance Records for Nuclear Power Plants - 1974.
- (5) N45.2.10 - Quality Assurance Terms and Definitions -1973.
- (6) ANSI/ANS 57.2 (N210) - Design Requirements for Light Water Reactor Spent Fuel Storage Facilities at Nuclear Power Plants.
- (7) N14.6 - American National Standard for Special Lifting Devices for Shipping Containers Weighing 10,000 pounds (4500 kg) or more for Nuclear Materials.
- (8) ANSI/ASME N626-3, Qualification and Duties of Personnel Engaged in ASME Boiler and Pressure Vessel Code Section III, Div. 1, Certifying Activities.
- (9) ANSI Y14.5M, Dimensioning and Tolerancing for Engineering Drawings and Related Documentation Practices.

g. Code-of-Federal Regulations

- (1) 10CFR20 - Standards for Protection Against Radiation.
- (2) 10CFR21 - Reporting of Defects and Non-compliance.
- (3) 10CFR50 Appendix A - General Design Criteria for Nuclear Power Plants.

- (4) 10CFR50 Appendix B - Quality Assurance Criteria for Nuclear Power Plants and Fuel Reprocessing Plants.
- (5) 10CFR61 - Licensing Requirements for Land Disposal of Radioactive Material.
- (6) 10CFR71 - Packaging and Transportation of Radioactive Material.

h. Regulatory Guides

- (1) RG 1.13 - Spent Fuel Storage Facility Design Basis (Revision 2 Proposed).
- (2) RG 1.25 - Assumptions Used for Evaluating the Potential Radiological Consequences of a Fuel Handling Accident in the Fuel Handling and Storage Facility of Boiling and Pressurized Water Reactors.
- (3) RG 1.28 - (ANSI N45.2) - Quality Assurance Program Requirements .
- (4) RG 1.29 - Seismic Design Classification (Rev. 3).
- (5) RG 1.31 - Control of Ferrite Content in Stainless Steel Weld Material.
- (6) RG 1.38 - (ANSI N45.2.2) Quality Assurance Requirements for Packaging, Shipping, Receiving, Storage and Handling of Items for Water-Cooled Nuclear Power Plants.
- (7) RG 1.44 - Control of the Use of Sensitized Stainless Steel.
- (8) RG 1.58 - (ANSI N45.2.6) Qualification of Nuclear Power Plant Inspection, Examination, and Testing Personnel.
- (9) RG 1.60 - Design Response Spectra for Seismic Design of Nuclear Power Plants.
- (10) RG 1.61 - Damping Values for Seismic Design of Nuclear Power Plants, Rev. 0, 1973.
- (11) RG 1.64 - (ANSI N45.2.11) Quality Assurance Requirements for the Design of Nuclear Power Plants.
- (12) RG 1.71 - Welder Qualifications for Areas of Limited Accessibility.

- (13) RG 1.74 - (ANSI N45.2.10) Quality Assurance Terms and Definitions.
- (14) RG 1.85 - Materials Code Case Acceptability - ASME Section 3, Div. 1.
- (15) RG 1.88 - (ANSI N45.2.9) Collection, Storage and Maintenance of Nuclear Power Plant Quality Assurance Records.
- (16) RG 1.92 - Combining Modal Responses and Spatial Components in Seismic Response Analysis.
- (17) RG 1.122 - Development of Floor Design Response Spectra for Seismic Design of Floor-Supported Equipment or Components.
- (18) RG 1.123 - (ANSI N45.2.13) Quality Assurance Requirements for Control of Procurement of Items and Services for Nuclear Power Plants.
- (19) RG 1.124 - Service Limits and Loading Combinations for Class 1 Linear-Type Component Supports, Revision 1, 1978.
- (20) RG 3.4 - Nuclear Criticality Safety in Operations with Fissionable Materials at Fuels and Materials Facilities.
- (21) RG 3.41 - Validation of Computational Methods for Nuclear Criticality Safety, Revision 1, 1977.
- (22) RG 8.8 - Information Relative to Ensuring that Occupational Radiation Exposure at Nuclear Power Plants will be as Low as Reasonably Achievable (ALARA).
- (23) DG-8006, "Control of Access to High and Very High Radiation Areas in Nuclear Power Plants".
- (24) IE Information Notice 83-29 - Fuel Binding Caused by Fuel Rack Deformation.
- (25) RG 8.38 - Control of Access to High and Very High Radiation Areas in Nuclear Power Plants, June, 1993.

i. Branch Technical Position

- (1) CPB 9.1-1 - Criticality in Fuel Storage Facilities.

- (2) ASB 9-2 - Residual Decay Energy for Light-Water Reactors for Long-Term Cooling.

j. Standard Review Plan

- (1) SRP 3.2.1 - Seismic Classification.
- (2) SRP 3.2.2 - System Quality Group Classification.
- (3) SRP 3.7.1 - Seismic Design Parameters.
- (4) SRP 3.7.2 - Seismic System Analysis.
- (5) SRP 3.7.3 - Seismic Subsystem Analysis.
- (6) SRP 3.8.4 - Other Seismic Category I Structures (including Appendix D), Technical Position on Spent Fuel Rack.
- (7) SRP 3.8.5 - Foundations for Seismic Category I Structures, Revision 1, 1981.
- (8) SRP 9.1.2 - Spent Fuel Storage, Revision 3, 1981.
- (9) SRP 9.1.3 - Spent Fuel Pool Cooling and Cleanup System.
- (10) SRP 9.1.4 - Light Load Handling System.
- (11) SRP 9.1.5 - Heavy Load Handling System.
- (12) SRP 15.7.4 - Radiological Consequences of Fuel Handling Accidents.

k. AWS Standards

- (1) AWS D1.1 - Structural Welding Code, Steel.
- (2) AWS D1.3 - Structure Welding Code - Sheet Steel.
- (3) AWS D9.1 - Welding of Sheet Metal.
- (4) AWS A2.4 - Standard Symbols for Welding, Brazing and Nondestructive Examination.
- (5) AWS A3.0 - Standard Welding Terms and Definitions.

- (6) AWS A5.12 - Tungsten Arc-welding Electrodes.
- (7) AWS QC1 - Standards and Guide for Qualification and Certification of Welding Inspectors.

#### 2.4 Quality Assurance Program

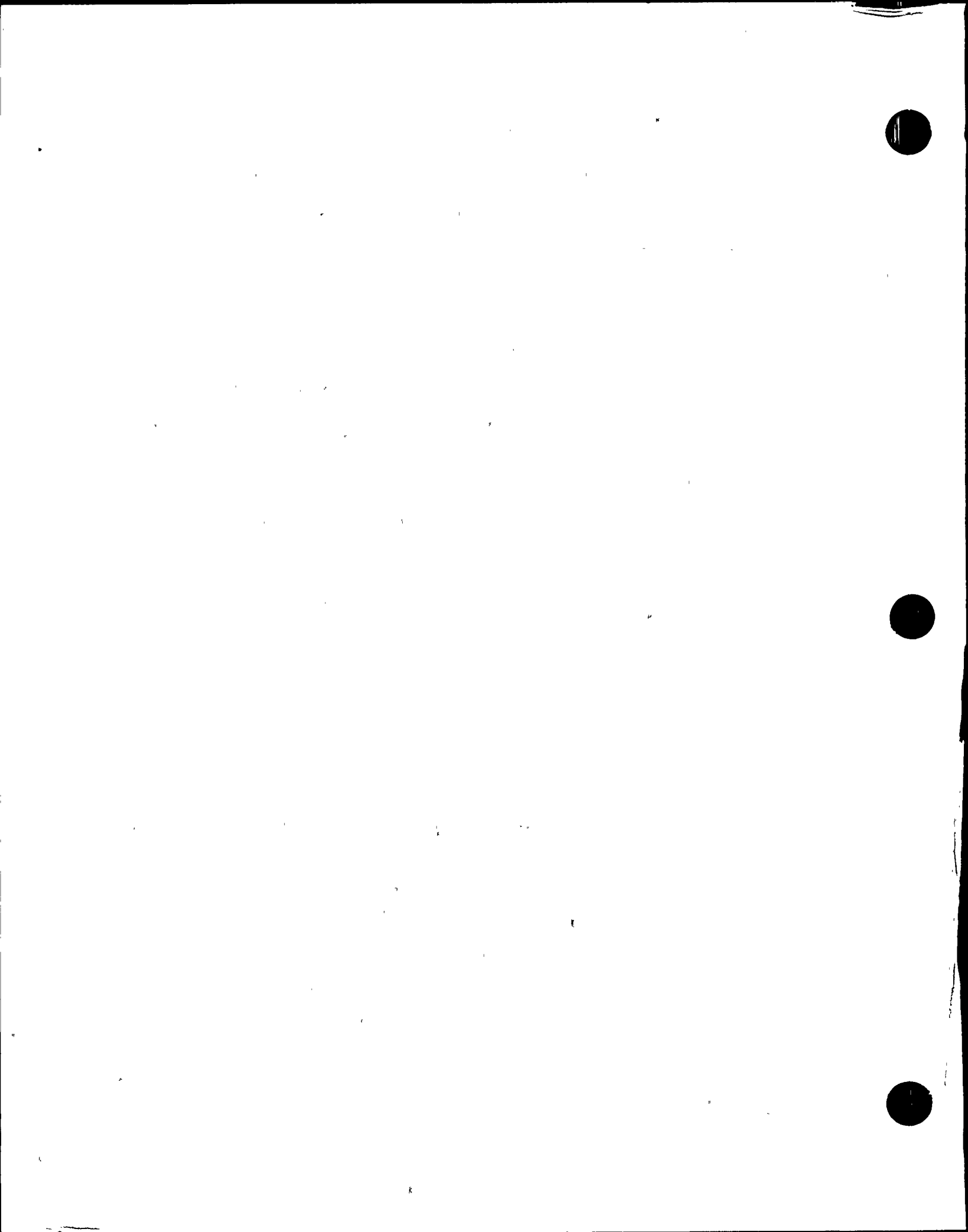
The governing quality assurance requirements for design of the Harris spent fuel racks are enunciated in 10CFR50 Appendix B. The quality assurance program for design of the Harris racks is described in Holtec's Nuclear Quality Assurance Manual, which has been reviewed and approved by the Carolina Power & Light Company. This program is designed to provide a flexible but highly controlled system for the design, analysis and licensing of customized components in accordance with various codes, specifications, and regulatory requirements.

The manufacturing of the racks will be performed in accordance with the requirements set forth in 10CFR50 Appendix B.

#### 2.5 Mechanical Design

The Harris rack modules are designed as cellular structures such that each fuel assembly has a prismatic square opening with conformal lateral support and a flat horizontal bearing surface. The basic characteristics of the Harris spent fuel racks are summarized in Table 2.5.1. The design of the PWR and BWR storage racks are very similar. The major differences are in the cell inside dimension and pitch, the baseplate flow holes, the support legs, and the poison width and length.

A central objective in the design of the new rack modules is to maximize their structural rigidity while minimizing their inertial mass. Accordingly, the Harris modules have been designed to simulate multi-flange beam structures. The multiple flanges are formed from the numerous cell walls in the rack cross-sectional array. These cells are connected through intermittent welds. The weld lengths, location, and size were chosen during the original



design of this rack style/series to ensure adequate strength and to adjust the natural frequency of the rack modules to avoid resonance. In general, this effort has resulted in excellent detuning characteristics with respect to the applicable seismic events.

## 2.6 Rack Fabrication

This subsection presents an item-by-item description of the anatomy of the Harris rack modules in the context of the fabrication methodology. The object of this section is to provide a self-contained description of rack module construction for the Harris fuel pool to enable an independent appraisal of the adequacy of design.

### 2.6.1 Fabrication Objective

The requirements in manufacturing the high density storage racks for Harris may be stated in four interrelated points:

1. The rack modules are fabricated in such a manner that there is no weld splatter on the storage cell surfaces which would come in contact with the fuel assembly.
2. The storage locations are constructed so that redundant flow paths for the coolant are available.
3. The fabrication process involves operational sequences which permit immediate verification by the inspection staff.
4. The storage cells are connected to each other by austenitic stainless steel corner welds which leads to a honeycomb lattice construction. The extent of welding is selected to "detune" the racks from the stipulated seismic input motion.



## 2.6.2 Anatomy of the Harris PWR Rack Module

In addition to the composite box assembly, the baseplate and the support legs constitute the principal components of the Harris fuel rack modules. The following description provides details of all of the major rack components.

- i. Composite box subassembly: The rack module manufacturing begins with fabrication of the "box". The boxes are fabricated from two precision formed channels by seam welding in a machine equipped with copper chill bars and pneumatic clamps to minimize distortion due to welding heat input. The minimum weld penetration is 80% of the box metal gage. This process results in a square cross section box, as shown in Figure 2.6.1. The clear inside dimension of the PWR box cell is 8.80".

A sheathing is attached to each side of the box with the poison material installed in the sheathing cavity. The design objective calls for attaching Boral tightly on the box surface. This is accomplished by die forming the internal and external boral sheathings to provide end flares with smooth edges, as shown in Figure 2.6.4. The flanges of the sheathing are welded to the box using skip welds and spot welds. The sheathings serve to locate and position the poison sheet accurately, and to preclude its movement under seismic conditions. The PWR Boral dimensions are 145" long and 7.5" wide.

The square cross section box with Boral panels affixed to its external surfaces is referred to as the "composite box assembly". Each composite box has at least two one inch diameter lateral holes punched near its bottom edge to provide auxiliary flow holes. For those cells located over support legs, four flow holes are required to compensate for the loss of the baseplate flow holes described below.

The composite boxes are arranged in a checkerboard array and welded edge-to-edge to form an assemblage of storage cell locations, as shown in Figure 2.6.5. Filler panels and corner angles are welded to the edges of boxes at the outside boundary of the rack to complete the formation of the peripheral cells. The inter-box welding and pitch adjustment are accomplished by small longitudinal connectors. The connectors are sized and placed to ensure that the 8.8" inside cell clear dimension on developed boxes is maintained after inclusion of any reductions from the sheathing. This assemblage of box assemblies results in a honeycomb structure with axial, flexural and torsional rigidity depending on the extent of intercell welding provided. It can be seen from Figure 2.6.5 that all



four corners of each interior box are connected to the contiguous boxes resulting in a well-defined path for "shear flow".

- ii. **Baseplate:** A 3/4 inch thick baseplate provides a continuous horizontal surface for supporting the fuel assemblies. The baseplate has a 5 inch diameter hole in each cell location, except at lift locations. For the lift locations the flow holes are modified to provide a smaller hole to match the dimensions of the BWR rack flow holes (3.8125" diameter) and slotted ears to allow insertion and engagement of the lifting rig. Matching the BWR flow hole dimensions allows for a single tool to be used to lift both rack styles. The cross sectional area of the modified lift location flow holes is only slightly smaller than the 5" diameter holes, because of the added area provided by the slotted ears. The location of all baseplate holes coincide with the cell centerlines. The baseplate is attached to the base of the cell assemblage by fillet welds and extends horizontally approximately 1/4" beyond the periphery of the rack.
- iii. **The neutron absorber material:** As mentioned in the preceding section, Boral is used as the neutron absorber material. Each storage cell side is equipped with one integral Boral sheet (poison material), except for the outer walls of some of the peripheral rack cells. Only one Boral sheet is required between adjacent cells containing fuel. Therefore, outer rack walls which face each other do not both require Boral, consequently one of the two racks may be fabricated without poison along one outer wall.
- iv. **Sheathing:** As described earlier, the sheathing serves as the locator and retainer of the poison material.
- v. **Support legs:** All support legs are the adjustable type as shown in Figure 2.6.6. The 1/2 inch diameter top (female threaded) portion is made of austenitic steel material. The 1/2 inch diameter bottom (male threaded) part is made of 17:4 Ph series stainless steel to avoid galling problems. Each support leg is equipped with a readily accessible socket to enable remote leveling of the rack after its placement in the pool. The support legs are located at the centerlines of cells to ensure accessibility of the levelling tool through the 5 inch diameter flow hole in the baseplate.

The assembly of the rack modules is carried out by welding the composite boxes in a vertical fixture with the precision fabricated baseplate serving as the bottom positioner.

### 2.6.3 Anatomy of the Harris BWR Rack Module

- i. Composite box subassembly: The fabrication of the boxes for the BWR racks is similar to that of the PWR racks. The inside cell clear dimension is reduced to 6.06" to properly support the smaller BWR assembly. Each box has two inch diameter lateral holes punched near its bottom edge to provide auxiliary flow holes.

The smaller BWR assembly dimensions require the Boral and sheathing to be smaller than the PWR version. The BWR Boral dimensions are 150" long and 5" wide for inside cell walls and 3.5" wide for rack periphery walls, if available, otherwise 5" wide will also be used at these locations. Sheathing is similar to the PWR version, except smaller to accommodate the smaller Boral dimensions.

The composite box assemblage is prepared in identical fashion to the PWR racks and will also appear much the same as the typical array shown in Figure 2.6.5.

- ii. Baseplate: The 3/4" baseplate is fabricated to run continuously beneath the entire array of cell assemblage. Similar to the PWR racks, flow holes are placed on the centerlines of each rack cell. The flow holes in the BWR racks are prepared to accommodate and support the bottom BWR assembly nozzle by providing a 3.8125 inch opening which is tapered larger at the top to conform to the configuration of the BWR lower fitting. At lift locations ears are included to allow for insertion and engagement of the lift rig. The baseplate is attached to the base of the cell assemblage by fillet welds and extends horizontally approximately 1/4" beyond the periphery of the rack cells.
- iii. The neutron absorber material: As mentioned in the preceding section, Boral is used as the neutron absorber material. Each storage cell side is equipped with one integral Boral sheet (poison material), except for the outer walls of some of the peripheral rack cells. Only one Boral sheet is required between adjacent cells containing fuel. Therefore, outer rack walls which face each other do not both require Boral and consequently one of the two racks may be fabricated without poison along one outer wall. Similarly, for cells facing the pool walls, Boral shielding is not required.
- iv. Sheathing: As described earlier, the sheathing serves as the locator and retainer of the poison material.
- v. Support legs: All support legs are the adjustable type as shown in Figure 2.6.7. The inch diameter top (female threaded) portion is made of austenitic steel

material. The bottom (male threaded) part is made of 17:4 Ph series stainless steel to avoid galling problems. Gusset plates are welded to each of the support legs. Each support leg is equipped with a readily accessible socket to enable remote leveling of the rack after its placement in the pool. The support legs are located at the centerlines of cells to ensure accessibility of the levelling tool through the 3.8125 inch diameter flow hole.

One advantage of the BWR assembly configuration is that it provides open areas at its base to allow coolant flow directly up and through the assembly. The rack design exploits this advantage by allowing flow through the baseplate holes, even at locations where support legs would normally interfere. This flow is accomplished by providing 3.8125 inch diameter flow holes in the support legs.

The assembly of the rack modules is carried out by welding the composite boxes in a vertical fixture with the precision fabricated baseplate serving as the bottom positioner.

An elevation view of three PWR and BWR storage cells is shown in Figures 2.6.2 and 2.6.3, respectively.

Table 2.1.1

GEOMETRIC AND PHYSICAL DATA FOR POOL C RACK MODULES<sup>†</sup>

Rack I.D. ††	Type	Number of Cells		Number of Cells Per Module	Dimension (inches)		Shipping Weight (lbs)	Submerged Weight (lbs)
		N-S	E-W		N-S Direction	E-W Direction		
A1	PWR	11	9	99	99.5	81.5	14,770	12,850
A2	PWR	11	9	99	99.5	81.5	15,620	13,590
B1	PWR	9	9	81	81.5	81.5	12,250	10,660
B2	PWR	9	9	81	81.5	81.5	12,940	11,260
B3	PWR	9	9	81	81.5	81.5	12,250	10,660
B4	PWR	9	9	81	81.5	81.5	12,600	10,960
B5	PWR	9	9	81	81.5	81.5	12,250	10,660
B6	PWR	9	9	81	81.5	81.5	12,600	10,960
B7	PWR	9	9	81	81.5	81.5	12,250	10,660
B8	PWR	9	9	81	81.5	81.5	12,250	10,660
B9	PWR	9	9	81	81.5	81.5	11,910	10,360
C1	BWR	8	13	104	50.5	81.5	9,710	8,450
C2	BWR	8	13	104	50.5	81.5	9,710	8,450
D1	BWR	8	11	88	50.5	69.0	8,460	7,360
D2	BWR	8	11	88	50.5	69.0	8,460	7,360

† All dimensions are rounded off to the nearest 0.5 inch, and all weights are rounded off to the nearest 10 lbs.

†† See Figure 1.2 for pool configuration.

Table 2.1.1 (Cont'd.)

## GEOMETRIC AND PHYSICAL DATA FOR POOL C RACK MODULES†

Rack I.D. ††	Type	Number of Cells		Number of Cells Per Module	Dimension (inches)		Shipping Weight (lbs)	Submerged Weight (lbs)
		N-S	E-W		N-S Direction	E-W Direction		
E1	BWR	13	13	169	81.5	81.5	15,370	13,370
E2	BWR	13	13	169	81.5	81.5	15,700	13,660
E3	BWR	13	13	169	81.5	81.5	15,700	13,660
E4	BWR	13	13	169	81.5	81.5	15,700	13,660
E5	BWR	13	13	169	81.5	81.5	15,700	13,660
E6	BWR	13	13	169	81.5	81.5	15,370	13,370
E7	BWR	13	13	169	81.5	81.5	15,700	13,660
E8	BWR	13	13	169	81.5	81.5	15,700	13,660
E9	BWR	13	13	169	81.5	81.5	15,370	13,370
F1	BWR	13	11	143	81.5	69.0	13,380	11,640
F2	BWR	13	11	143	81.5	69.0	13,380	11,640
F3	BWR	13	11	143	81.5	69.0	13,380	11,640
F4	BWR	13	11	143	81.5	69.0	13,380	11,640
F5	BWR	13	11	143	81.5	69.0	13,380	11,640
F6	BWR	13	11	143	81.5	69.0	13,100	11,400

† All dimensions are rounded off to the nearest 0.5 inch, and all weights are rounded off to the nearest 10 lbs.

†† See Figure 1.2 for pool configuration.

Table 2.1.2

GEOMETRIC AND PHYSICAL DATA FOR POOL D RACK MODULES<sup>†</sup>

Rack I.D. <sup>††</sup>	Type	Number of Cells		Number of Cells Per Module	Dimension (inches)		Shipping Weight (lbs)	Submerged Weight (lbs)
		N-S	E-W		N-S Direction	E-W Direction		
A1	PWR	10	8	80	90.5	72.5	12,080	10,510
A2	PWR	10	8	80	90.5	72.5	12,460	10,840
A3	PWR	10	8	80	90.5	72.5	12,080	10,510
A4	PWR	10	8	80	90.5	72.5	12,460	10,840
A5	PWR	10	8	80	90.5	72.5	11,770	10,240
A6	PWR	10	8	80	90.5	72.5	12,150	10,570
B1	PWR	10	9	90	90.5	81.5	13,900	12,090
B2	PWR	10	9	90	90.5	81.5	13,900	12,090
B3	PWR	10	9	90	90.5	81.5	13,550	11,790
C1	PWR	11	8	88	99.5	72.5	13,200	11,480
C2	PWR	11	8	88	99.5	72.5	13,620	11,850
D	PWR	11	9	99	99.5	81.5	15,190	13,220

<sup>†</sup> All dimensions are rounded off to the nearest 0.5 inch, and all weights are rounded off to the nearest 10 lbs.

<sup>††</sup> See Figure 1.3 for pool configuration.

Table 2.5.1

MODULE DATA FOR HARRIS SPENT FUEL RACKS

Parameter	PWR	BWR
Storage cell inside dimension (nominal)	8.80 in.	6.06 in.
Cell pitch (nominal)	9.00 in.	6.25 in.
Storage cell height (above the baseplate)	169 in.	169 in.
Baseplate hole size (away from pedestal)	5.0 in.	3.8125 in.
Baseplate thickness	0.75 in.	0.75 in.
Support leg height (nominal)	5.5 in.	5.5 in.
Support leg type	Remotely adjustable legs	Remotely adjustable legs
Number of support pedestals	4	4
Remote lifting and handling provisions	Yes	Yes
Poison material	Boral	Boral
Poison length	145 in	150 in.
Poison width	7.5 in	5.0 in. (interior) / 3.5 in. (exterior) †

† Narrower 3.5" exterior Boral will be used subject to availability, otherwise the 5.0" width will be used.

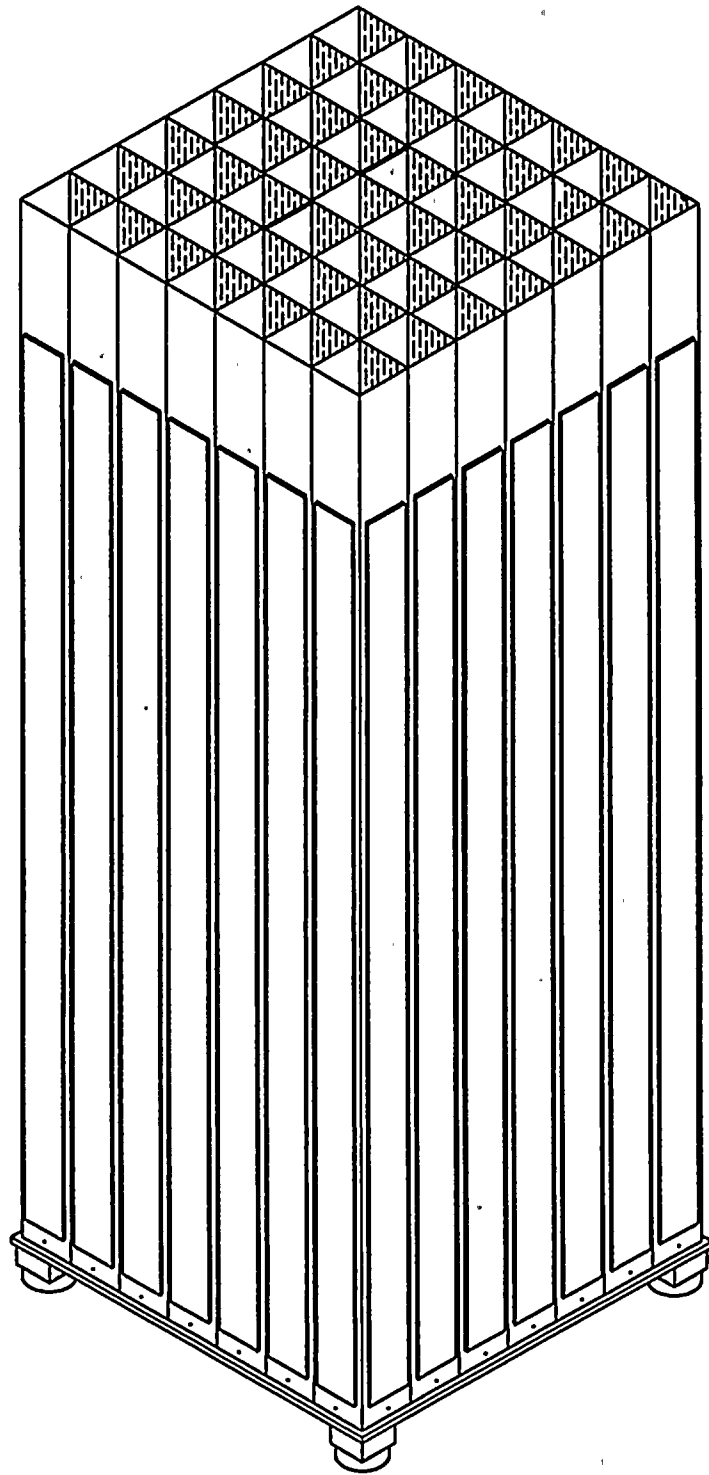


FIGURE 2.1.1; PICTORIAL VIEW OF TYPICAL HARRIS RACK STRUCTURE

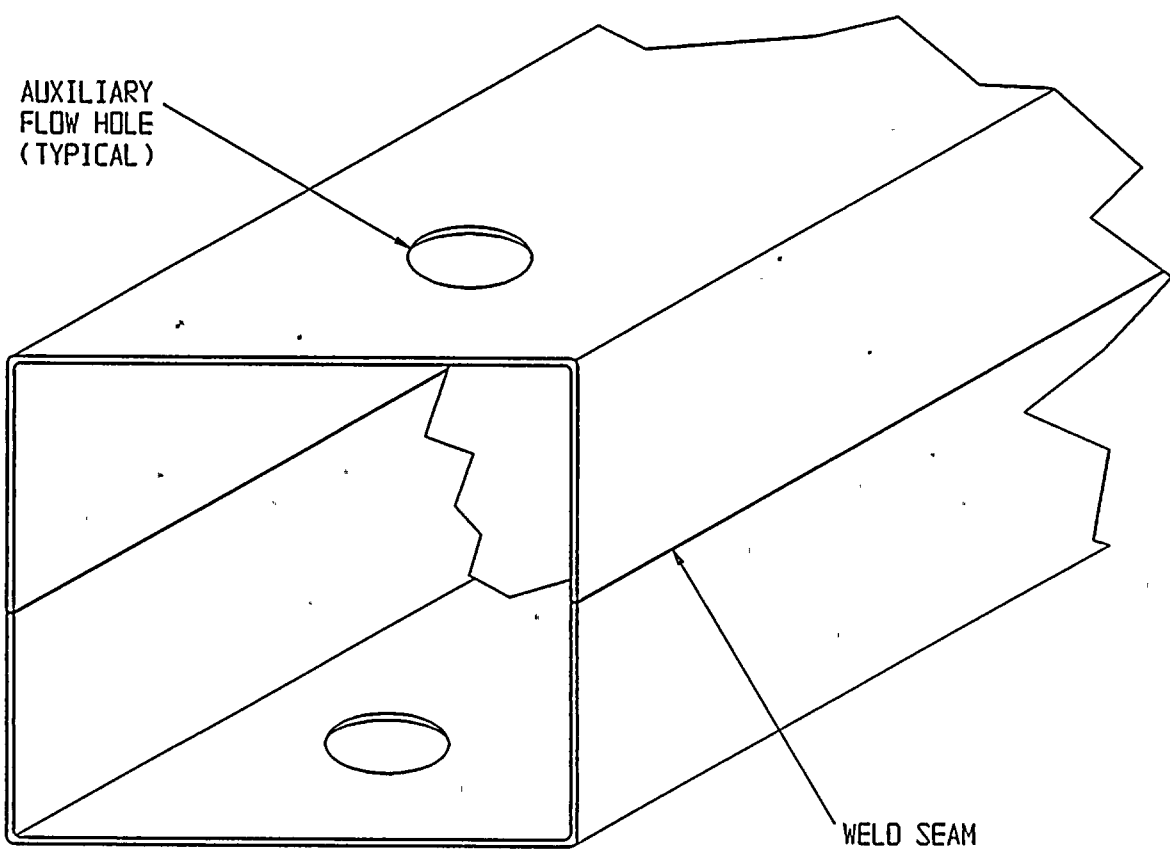


FIGURE 2.6.1; SEAM WELDED PRECISION FORMED CHANNELS

HI-971760

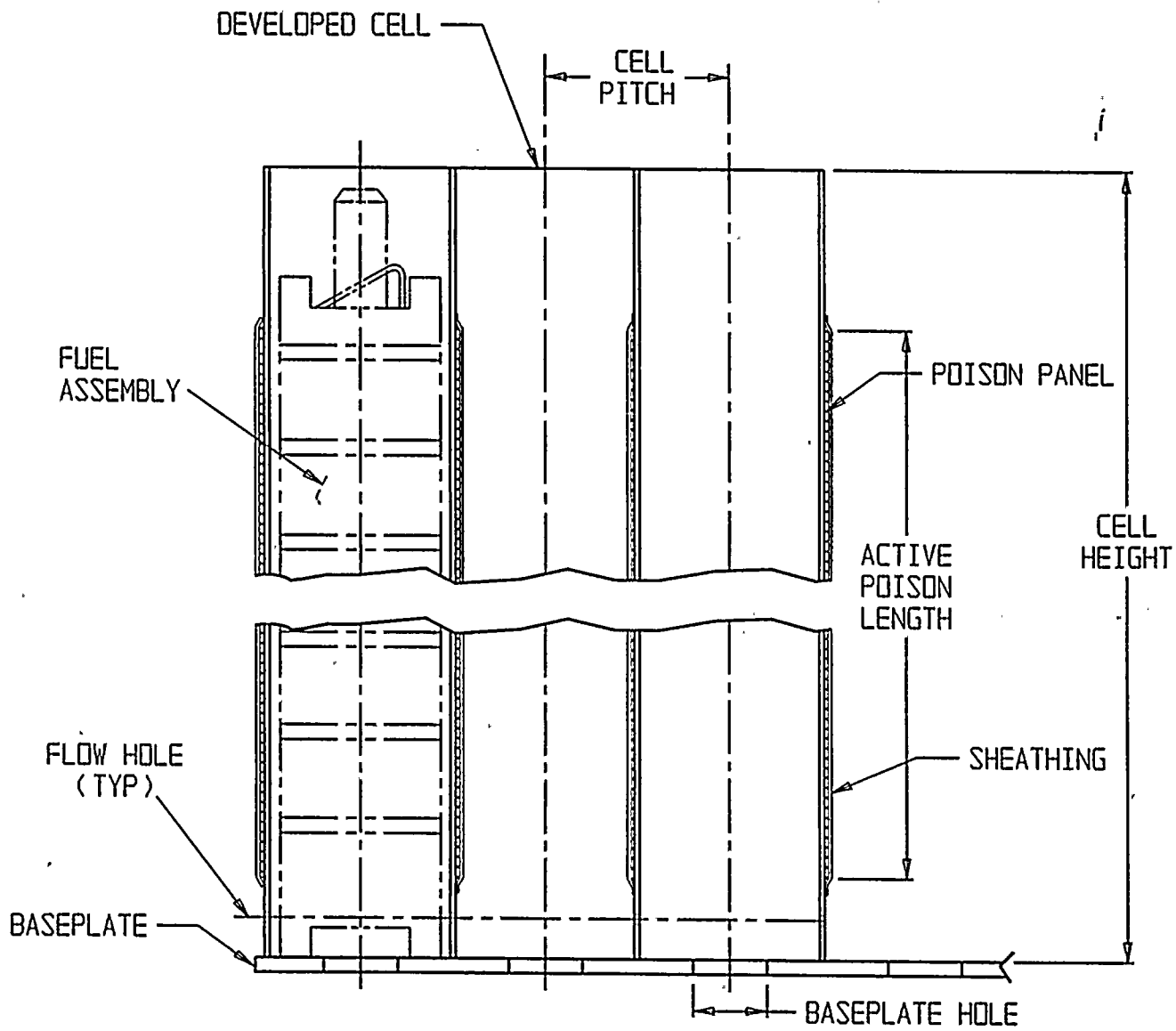


FIGURE 2.6.2; THREE PWR CELLS IN ELEVATION VIEW

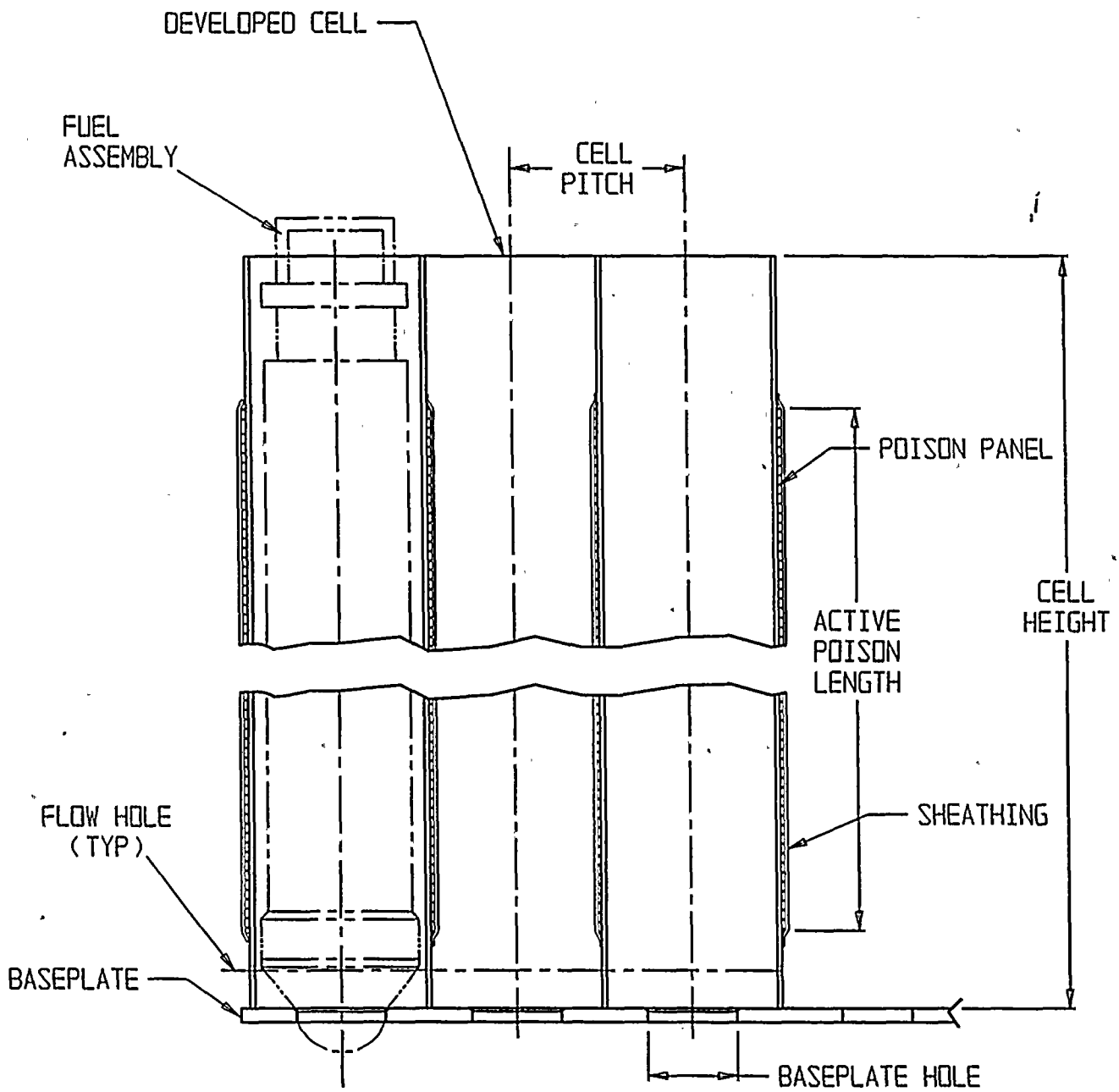


FIGURE 2.6.3; THREE BWR CELLS IN ELEVATION VIEW

HI-971760

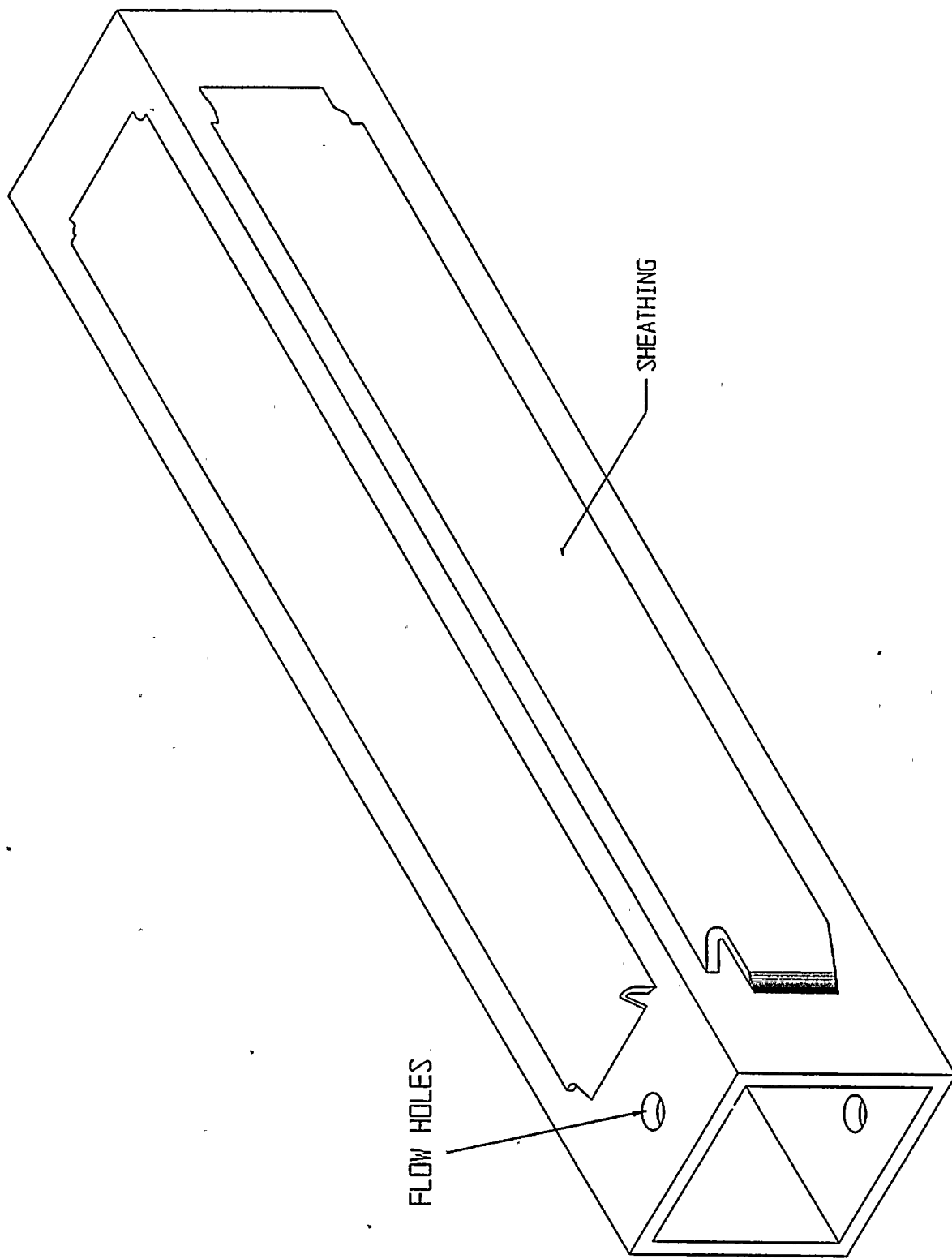


FIGURE 2-6-4: COMPOSITE BOX ASSEMBLY

HI-971760

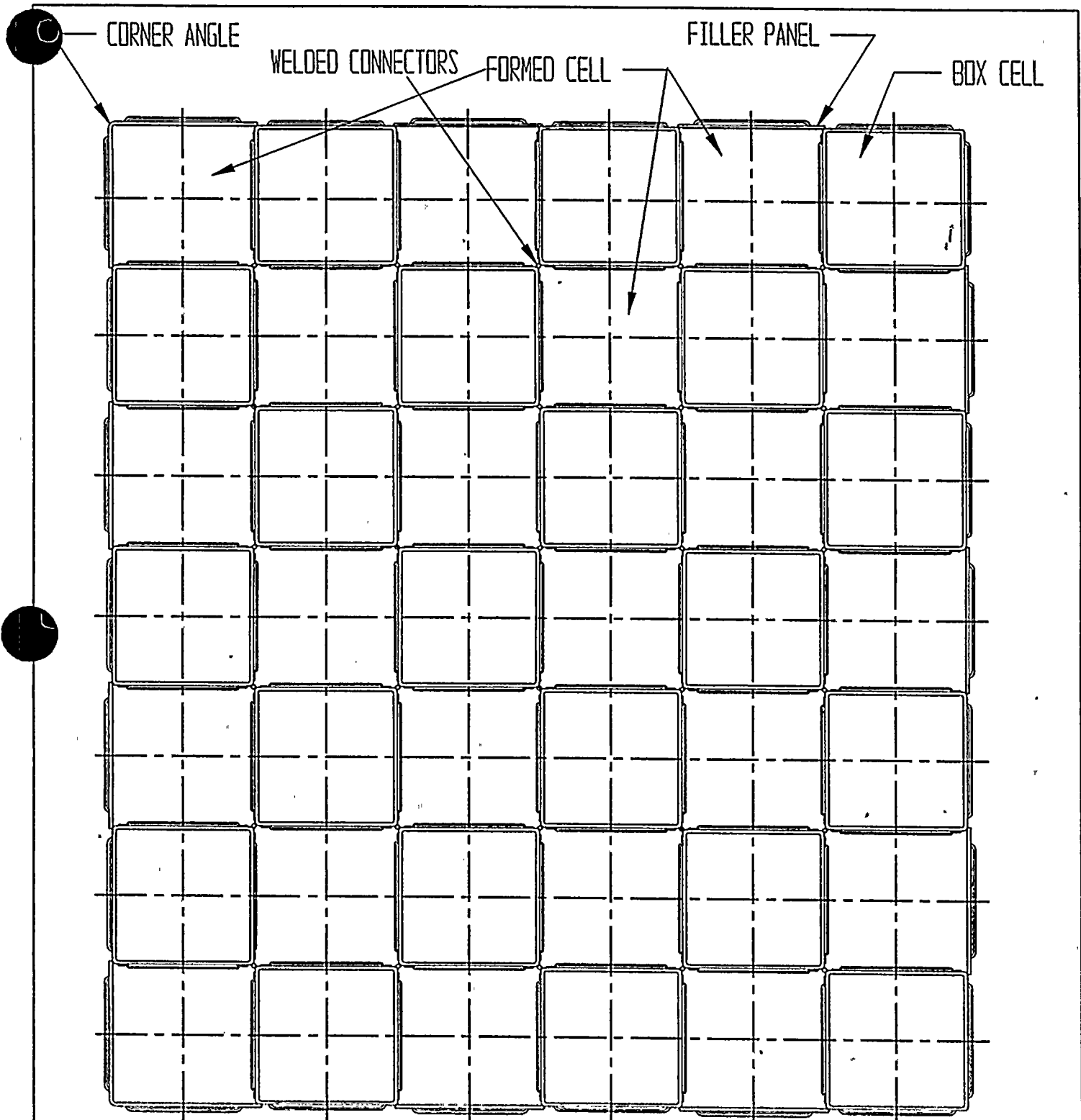


FIGURE 2.6.5; TYPICAL ARRAY OF STORAGE CELLS  
(NON-FLUX TRAP CONSTRUCTION)

HI- 971760

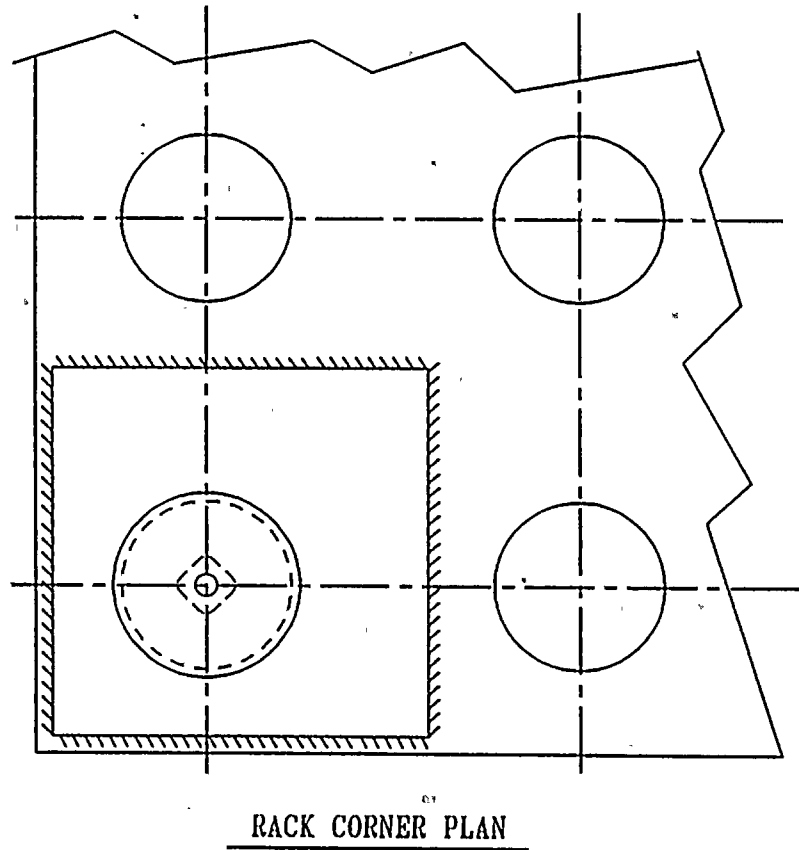
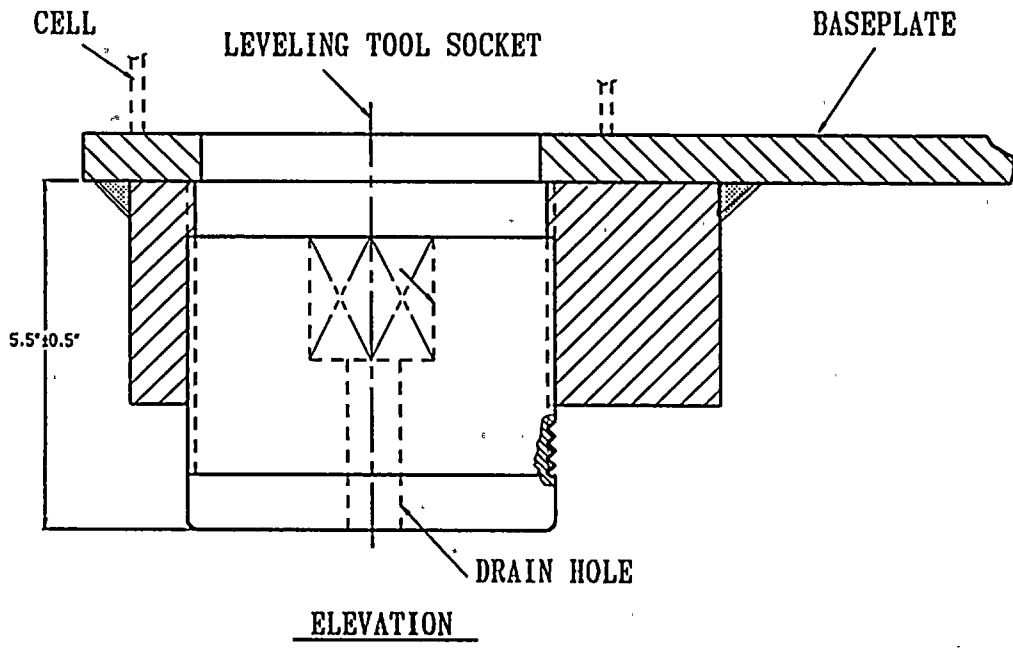


FIGURE 2.6.6; SUPPORT PEDESTAL FOR PWR RACK

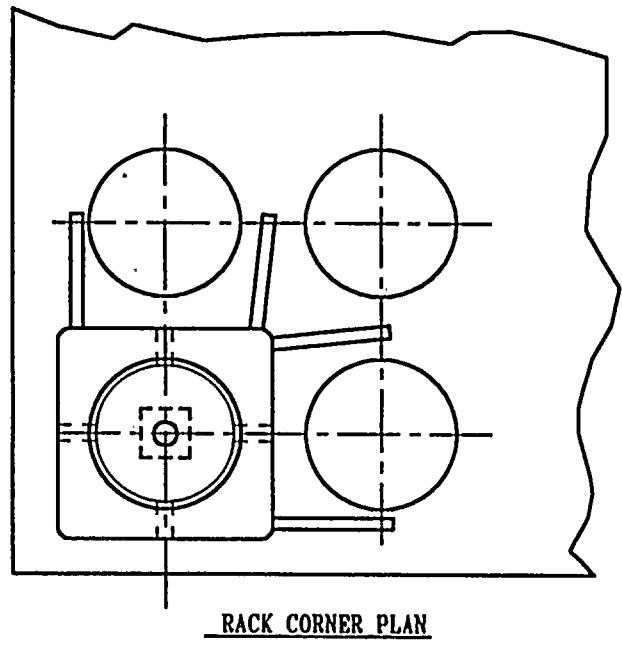
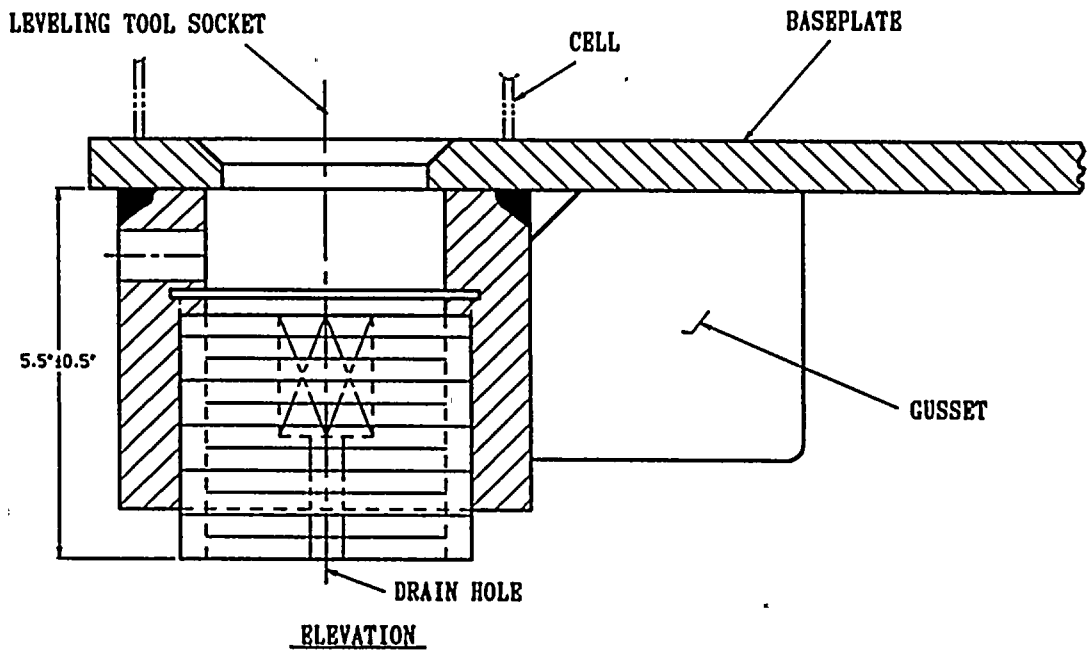


FIGURE 2.6.7; SUPPORT PEDESTAL FOR HOLTEC BWR RACKS

HI-971760



## 3.0 MATERIAL, HEAVY LOAD, AND CONSTRUCTION CONSIDERATIONS

### 3.1 Introduction

Safe storage of nuclear fuel in the Harris pools requires that the materials utilized in the rack fabrication be of proven durability and be compatible with the pool water environment. Likewise, all activities during the rack installations must comply with the provisions of NUREG-0612 to eliminate the potential of construction accidents. This section provides a synopsis of the considerations with regard to long-term service life and short-term construction safety.

### 3.2 Structural Materials

The following structural materials are utilized in the fabrication of the new spent fuel racks:

- a. ASME SA240-304L for all sheet metal stock
- b. Internally threaded support legs: ASME SA240-304L
- c. Externally threaded support spindle: ASME SA564-630 precipitation hardened, stainless steel (heat treated to 1100°F)
- d. Weld material - per the following ASME specification: SFA 5.9 ER308L

### 3.3 Poison Material (Neutron Absorber)

The racks employ Boral™, a patented product of AAR Manufacturing, as the neutron absorber material. Boral is a thermal neutron poison material composed of boron carbide and 1100 alloy aluminum. Boron carbide is a compound having a high boron content in a physically stable and chemically inert form. The 1100 alloy aluminum is a lightweight metal with high tensile strength which is protected from corrosion by a highly resistant oxide film. The two materials, boron carbide and aluminum, are chemically compatible and ideally suited for long-term use in the radiation, thermal and chemical environment of a nuclear reactor or a spent fuel pool. Boral has been shown [3.3.1] to be superior to alternative materials previously used as neutron absorbers in storage racks.

Boral has been the most widely used neutron absorbing material in fuel rack applications over the past 20 years. Its use in the spent fuel pools as the neutron absorbing material can be attributed to its proven performance (over 150 pool years of experience) and the following unique characteristics:

- i. The content and placement of boron carbide provides a very high removal cross-section for thermal neutrons.
- ii. Boron carbide, in the form of fine particles, is homogeneously dispersed throughout the central layer of the Boral panels.
- iii. The boron carbide and aluminum materials in Boral do not degrade as a result of long-term exposure to radiation.
- iv. The neutron absorbing central layer of Boral is clad with permanently bonded surfaces of aluminum.
- v. Boral is stable, strong, durable, and corrosion resistant.

Boral will be manufactured by AAR Manufacturing under the control and surveillance of a Quality Assurance/Quality Control Program that conforms to the requirements of 10CFR50 Appendix B, "Quality Assurance Criteria for Nuclear Power Plants". As indicated in Tables 3.3.1 and 3.3.2, Boral has been licensed by the USNRC for use in numerous PWR and BWR spent fuel storage racks and has been extensively used in international nuclear installations.

#### Boral Material Characteristics

**Aluminum:** Aluminum is a silvery-white, ductile metallic element that is the most abundant in the earth's crust. The 1100 alloy aluminum is used extensively in heat exchangers, pressure vessels and storage tanks, chemical equipment, reflectors, and sheet metal work.

It has high resistance to corrosion in industrial and marine atmospheres. Aluminum has atomic number of 13, atomic weight of 26.98, specific gravity of 2.69 and valence of 3. The physical, mechanical and chemical properties of the 1100 alloy aluminum are listed in Tables 3.3.3 and 3.3.4.

The excellent corrosion resistance of the 1100 alloy aluminum is provided by the protective oxide film that develops on its surface from exposure to the atmosphere or water. This film prevents the loss of metal from general corrosion or pitting corrosion.

**Boron Carbide:** The boron carbide contained in Boral is a fine granulated powder that conforms to ASTM C-750-80 nuclear grade Type III. The material conforms to the chemical composition and properties listed in Table 3.3.5.

References [3.3.2], [3.3.3], and [3.3.4] provide further discussion as to the suitability of these materials for use in spent fuel storage module applications.

#### 3.4 Rack Material Compatibility with Coolant

All materials used in the construction of the Holtec racks have an established history of in-pool usage. Their physical, chemical and radiological compatibility with the pool environment is an established fact.

Austenitic stainless steel (304L) is perhaps the most widely used stainless alloy in nuclear power plants, since it provides both high strength and non-corrosive properties.

#### 3.5 Heavy Load Considerations for the Proposed Rack Installations

The Fuel Handling Building auxiliary crane will be used for installation of the new storage racks in pools C and D. The Spent Fuel Cask Handling Crane (CHC) cannot be used for rack installation, since travel limitations prohibit its movement over the spent fuel pools. Storage capacity will be increased starting in the south end of pool C and proceeding north. This installation pattern will enable the storage racks to be manipulated without lifts over spent fuel.

The auxiliary crane is a single failure proof crane and is currently rated for 10 tons. A 20 ton hoist will be attached to the auxiliary crane hook to prevent submergence of the auxiliary crane hook. The auxiliary crane was used for installation of storage racks in pool B. Rigging and procedures for pools C and D rack installation will be similar to those used previously.

The maximum lift weight during rack installation is determined by the following table.

Item	Weight (lbs)
Rack	15,700 (maximum)
Lift Rig	1,200
Rigging	500
20 ton hoist	1,420
Total Lift	18,820

The rack sizes were limited to ensure that the crane and lifting components remain single failure proof and it may be seen that the maximum lift of 18,820 lbs is below the auxiliary crane rating of 20,000 lbs. As a result, the auxiliary crane, which can travel over both pools C and D, is qualified to accept the anticipated load during the rack installation project.

A remotely engagable lift rig, meeting NUREG-0612 [3.5.1] stress criteria, will be used to lift the new modules. The rig is designed for handling both PWR and BWR racks. The new rack lift rig consists of independently loaded lift rods in a lift configuration which ensures that failure of one traction rod will not result in uncontrolled lowering of the load being carried by the rig (which complies with the duality feature called for in Section 5.1.6(3a) of NUREG 0612).

The rigs have the following attributes:

- a. The traction rod is designed to prevent loss of its engagement with the rig in the locked position. Moreover, the locked configuration can be directly verified from above the pool water without the aid of an underwater camera.
- b. The stress analysis of the rigs will be carried out using a finite element code, and the primary stress limits in ANSI 14.6-1978 [3.5.2] will be shown to be met by detailed analysis.
- c. The rigs will be load tested with 300% of the maximum weight to be lifted. The test weight will be maintained in the air for 10 minutes. All critical weld joints will be liquid penetrant examined to establish the soundness of all critical joints.

Pursuant to the defense-in-depth approach of NUREG-0612, the following additional measures of safety will be undertaken for the racking operation.

- i. The crane used in the project will be given a preventive maintenance checkup and inspection per the Harris maintenance procedures before the beginning of the racking operation.
- ii. Safe load paths will be developed for moving the new racks in the Fuel Handling Building. The racks will not be carried directly over any fuel located in the pool.
- iii. The rack upending and laying down will be carried out in an area which precludes any adverse interaction with safety related equipment.
- iv. All crew members involved in the use of the lifting and upending equipment will be given training similar to that utilized in previous rack installation operations.

The rack installation activities will require Harris PNSC approval and will be conducted in accordance with written procedures which will be reviewed and approved by Carolina Power & Light.

The proposed heavy loads compliance will be in accordance with the objectives of the CP&L, NRC-approved submittal to NUREG-0612. The guidelines of NUREG-0612 call for measures to "provide an adequate defense-in-depth for handling of heavy loads near spent fuel...". The NUREG-0612 guidelines cite four major causes of load handling accidents, namely

- i. operator errors
- ii. rigging failure
- iii. lack of adequate inspection
- iv. inadequate procedures

The Harris racking program ensures maximum emphasis on mitigating the potential load drop accidents by implementing measures to eliminate shortcomings in all aspects of the operation including the four aforementioned areas. A summary of the measures specifically planned to deal with the major causes is provided below.

**Operator errors:** As mentioned above, CP&L plans to provide comprehensive training to the installation crew. All training shall be in compliance with ANSI B30.2 [3.5.3].

**Rigging failure:** The lifting device designed for handling and installation of the new racks at Harris has redundancies in the lift legs and lift eyes such that there are four independent load members. Failure of any one load bearing member would not lead to uncontrolled lowering of the load. The rig complies with all provisions of ANSI 14.6 [3.5.2], including compliance with the primary stress criteria, load testing at 300% of maximum lift load, and dye examination of critical welds.

The Harris rig design is similar to the rigs used in the initial racking or the rerack of numerous other plants, such as Hope Creek, Millstone Unit 1, Indian Point Unit Two, Ulchin II, Laguna Verde, J.A. FitzPatrick and Three Mile Island Unit 1.

**Lack of adequate inspection:** The designer of the racks will develop a set of QC hold points which will require inspections and approvals prior to proceeding. Additional hold points will be established for activities during the installatin process. These inspection points have been proven to significantly reduce any requirement for rework or instances of erroneous installation in numerous prior rerack projects.

**Inadequate procedures:** CP&L is developing various operating procedures to address operations pertaining to the rack installation effort, including, but not limited to, mobilization, rack handling, upending, lifting, installation, verticality, alignment, dummy gage testing, site safety, and ALARA compliance. Many of the procedures will be the same or revisions to those developed and currently in use for rack installations in pool B.

The series of operating procedures planned for Harris rack installations are the successors of the procedures successfully implemented in previous projects.



Table 3.5.1 provides a synopsis of the requirements delineated in NUREG-0612, and their intended compliance.

- [3.3.1] "Nuclear Engineering International," July 1997 issue, pp 20-23.
- [3.3.2] "Spent Fuel Storage Module Corrosion Report," Brooks & Perkins Report 554, June 1, 1977.
- [3.3.3] "Suitability of Brooks & Perkins Spent Fuel Storage Module for Use in PWR Storage Pools," Brooks & Perkins Report 578, July 7, 1978.
- [3.3.4] "Boral Neutron Absorbing/Shielding Material - Product Performance Report," Brooks & Perkins Report 624, July 20, 1982.
- [3.5.1] NUREG-0612, "Control of Heavy Loads at Nuclear Power Plants," July 1980.
- [3.5.2] ANSI N14.6-1978, Standard for Special Lifting Devices for Shipping Containers Weighing 10000 Pounds or more for Nuclear Materials," American National Standard Institute, Inc., 1978.
- [3.5.3] ANSI/ASME B30.2, "Overhead and Gantry Cranes, (Top Running Bridge, Single or Multiple Girder, Top Running Trolley Hoist)," American Society of Mechanical Engineers, 1983.
- [3.5.4] ANSI/ASME B30.20, "Below-the-Hook Lifting Devices," American Society of Mechanical Engineers, 1993.
- [3.5.5] CMMA Specification 70, "Electrical Overhead Travelling Cranes," Crane Manufacturers Association of America, Inc., 1983.
- [3.5.6] ANSI/ASME B30.20, "Below-the-Hook Lifting Devices," American Society of Mechanical Engineers, 1993.

Table 3.3.1

## BORAL EXPERIENCE LIST - PWRs

Plant	Utility	Docket No.	Mfg. Year
Maine Yankee	Maine Yankee Atomic Power	50-309	1977
Donald C. Cook	Indiana & Michigan Electric	50-315/316	1979
Sequoyah 1,2	Tennessee Valley Authority	50-327/328	1979
Salem 1,2	Public Service Electric & Gas	50-272/311	1980
Zion 1,2	Commonwealth Edison Co.	50-295/304	1980
Bellefonte 1, 2	Tennessee Valley Authority	50-438/439	1981
Yankee Rowe	Yankee Atomic Power	50-29	1964/1983
Indian Point 3	NY Power Authority	50-286	1987
Byron 1,2	Commonwealth Edison Co.	50-454/455	1988
Braidwood 1,2	Commonwealth Edison Co.	50-456/457	1988
Yankee Rowe	Yankee Atomic Power	50-29	1988
Three Mile Island I	GPU Nuclear	50-289	1990
Sequoyah (rerack)	Tennessee Valley Authority	50-327	1992
Donald C. Cook (rerack)	American Electric Power	50-315/316	1992
Beaver Valley Unit 1	Duquesne Light Company	50-334	1993
Fort Calhoun	Omaha Public Power District	50-285	1993
Zion 1 & 2 (rerack)	Commonwealth Edison Co.	50-295/304	1993
Salem Units 1 & 2 (rerack)	Public Gas and Electric Company	50-272/311	1995
Haddam Neck	Connecticut Yankee Atomic Power Company	50-213	1996
Gosgen	Kernkraftwerk Gosgen-Daniken AG (Switzerland)	--	1984
Koeberg 1,2	ESCOM (South Africa)	--	1985
Beznau 1,2	Nordostschweizerische Kraftwerke AG (Switzerland)	--	1985

Table 3.3.1 (Cont'd.)

BORAL EXPERIENCE LIST - PWRs

Plant	Utility	Docket No.	Mfg. Year
12 various Plants	Electricite de France (France)	--	1986
Ulchin Unit 1	Korea Electric Power Company (Korea)	--	1995
Ulchin Unit 2	Korea Electric Power Company (Korea)	--	1996
Kori-4	Korea Electric Power Company (Korea)	--	1996
Yonggwang 1,2	Korea Electric Power Company (Korea)	--	1996
Sizewell B	Nuclear Electric, plc (United Kingdom)	--	1997
Angra 1	Furnas Centrais-Elétricas SA (Brazil)	--	1997

Table 3.3.2

## BORAL EXPERIENCE LIST - BWRs

Plant	Utility	Docket No.	Mfg. Year
Cooper	Nebraska Public Power	50-298	1979
J.A. FitzPatrick	NY Power Authority	50-333	1978
Duane Arnold	Iowa Electric Light & Power	50-331	1979
Browns Ferry 1,2,3	Tennessee Valley Authority	50-259/260/296	1980
Brunswick 1,2	Carolina Power & Light	50-324/325	1981
Clinton	Illinois Power	50-461/462	1981
Dresden 2,3	Commonwealth Edison Company	50-237/249	1981
E.I. Hatch 1,2	Georgia Power	50-321/366	1981
Hope Creek	Public Service Electric & Gas	50-354/355	1985
Humboldt Bay	Pacific Gas & Electric Company	50-133	1985
LaCrosse	Dairyland Power	50-409	1976
Limerick 1,2	Philadelphia Electric Company	50-352/353	1980
Monticello	Northern States Power	50-263	1978
Peachbottom 2,3	Philadelphia Electric	50-277/278	1980
Perry 1,2	Cleveland Electric Illuminating	50-440/441	1979
Pilgrim	Boston Edison Company	50-293	1978
Susquehanna 1,2	Pennsylvania Power & Light	50-387,388	1979
Vermont Yankee	Vermont Yankee Atomic Power	50-271	1978/1986
Hope Creek	Public Service Electric & Gas	50-354/355	1989
Shearon Harris Pool B	Carolina Power & Light	50-401	1991
Duane Arnold	Iowa Electric Light & Power	50-331	1993
Pilgrim	Boston Edison Company	50-293	1993
LaSalle 1	Commonwealth Edison Company	50-373	1992
Millstone Unit 1	Northeast Utilities	50-245	1989
James A. FitzPatrick	NY Power Authority	50-333	1990
Hope Creek	Public Service Electric & Gas Company	50-354	1991



Table 3.3.2 (Cont'd.)

BORAL EXPERIENCE LIST - BWRs

Plant	Utility	Docket No.	Mfg. Year
Duane Arnold Energy Center	Iowa Electric Power Company	50-331	1994
Limerick Units 1,2	PECO Energy	50-352/50-353	1994
Shearon Harris Pool 'B'	Carolina Power & Light Company	50-400	1996
Nine Mile Point Unit 1	Niagara Mohawk Power Corporation	50-220	1997
Chinshan 1,2	Taiwan Power Company (Taiwan)	--	1986
Kuosheng 1,2	Taiwan Power Company (Taiwan)	--	1991
Laguna Verde 1,2	Comision Federal de Electricidad (Mexico)	--	1991



1  
2  
3  
4  
5  
6  
7  
8  
9  
10  
11  
12  
13  
14  
15  
16  
17  
18  
19  
20  
21  
22  
23  
24  
25  
26  
27  
28  
29  
30  
31  
32  
33  
34  
35  
36  
37  
38  
39  
40  
41  
42  
43  
44  
45  
46  
47  
48  
49  
50  
51  
52  
53  
54  
55  
56  
57  
58  
59  
60  
61  
62  
63  
64  
65  
66  
67  
68  
69  
70  
71  
72  
73  
74  
75  
76  
77  
78  
79  
80  
81  
82  
83  
84  
85  
86  
87  
88  
89  
90  
91  
92  
93  
94  
95  
96  
97  
98  
99  
100



Table 3.3.3

1100 ALLOY ALUMINUM PHYSICAL CHARACTERISTICS

Density	0.098 lb/in <sup>3</sup>
Melting Range	1190°F - 1215°F
Thermal Conductivity (77°F)	128 BTU/hr/ft <sup>2</sup> /F/ft
Coefficient of Thermal Expansion (68°F - 212°F)	13.1 x 10 <sup>-6</sup> in/in-°F
Specific Heat (221°F)	0.22 BTU/lb/°F
Modulus of Elasticity	10 x 10 <sup>6</sup> psi
Tensile Strength (75°F)	13,000 psi (annealed) 18,000 psi (as rolled)
Yield Strength (75°F)	5,000 psi (annealed) 17,000 psi (as rolled)
Elongation (75°F)	35-45% (annealed) 9-20% (as rolled)
Hardness (Brinell)	23 (annealed) 32 (as rolled)
Annealing Temperature	650°F

Table 3.3.4 CHEMICAL COMPOSITION - ALUMINUM (1100 ALLOY)	
99.00% min.	Aluminum
1.00% max.	Silicone and Iron
0.05-0.20% max.	Copper
0.05% max.	Manganese
0.10% max.	Zinc
0.15% max.	Other

Table 3.3.5

**CHEMICAL COMPOSITION AND PHYSICAL PROPERTIES  
OF BORON CARBIDE**

CHEMICAL COMPOSITION (WEIGHT PERCENT)	
Total boron	70.0 min.
B <sup>10</sup> isotopic content in natural boron	18.0
Boric oxide	3.0 max.
Iron	2.0 max.
Total boron plus total carbon	94.0 min.
PHYSICAL PROPERTIES	
Chemical formula	B <sub>4</sub> C
Boron content (weight percent)	78.28%
Carbon content (weight percent)	21.72%
Crystal structure	rhombohedral
Density	0.0907 lb/in <sup>3</sup>
Melting Point	4442°F
Boiling Point	6332°F

Table 3.5.1

HEAVY LOAD HANDLING COMPLIANCE MATRIX (NUREG-0612)

Criterion	Compliance
1. Are safe load paths defined for the movement of heavy loads to minimize the potential of impact, if dropped, on irradiated fuel?	Yes
2. Will procedures be developed to cover: identification of required equipment, inspection and acceptance criteria required before movement of load, steps and proper sequence for handling the load, defining the safe load paths, and special precautions?	Yes
3. Will crane operators be trained and qualified?	Yes
4. Will special lifting devices meet the guidelines of ANSI 14.6-1978?	Yes
5. Will non-custom lifting devices be installed and used in accordance with ANSI B30.20, latest edition?	Yes
6. Will the cranes be inspected and tested prior to use in rack installation?	Yes
7. Does the crane meet the intent of ANSI B30.2-1976 and CMMA-70?	Yes

## 4.0 CRITICALITY SAFETY EVALUATION

### 4.1 Design Bases

The high density spent fuel PWR and BWR storage racks for Harris Pools C and D are designed in accordance with the applicable codes listed below. The rack design and fuel storage configuration acceptance criteria is to show that the effective neutron multiplication factor,  $k_{eff}$ , is equal to or less than 0.95 with the racks fully loaded with fuel of the highest anticipated reactivity, and flooded with un-borated water at a temperature corresponding to the highest reactivity. The maximum calculated reactivity includes a margin for uncertainty in reactivity calculations including mechanical tolerances. All uncertainties are statistically combined, with uncertainties applied conservatively to calculate the final  $k_{eff}$  which must be shown to be less than 0.95 with a 95% probability at a 95% confidence level [4.1.1]. Reactivity effects of abnormal and accident conditions have also been evaluated to assure that under credible abnormal and accident conditions, the reactivity will not exceed the limiting design basis value.

Applicable codes, standards, and regulations or pertinent sections thereof, include the following:

- General Design Criteria 62, Prevention of Criticality in Fuel Storage and Handling.
- USNRC Standard Review Plan, NUREG-0800, Section 9.1.2, Spent Fuel Storage, Rev. 3 - July 1981.
- USNRC letter of April 14, 1978, to all Power Reactor Licensees - OT Position for Review and Acceptance of Spent Fuel Storage and Handling Applications, including modification letter dated January 18, 1979.
- USNRC Regulatory Guide 1.13, Spent Fuel Storage Facility Design Basis, Rev. 2 (proposed), December 1981.
- ANSI ANS-8.17-1984, Criticality Safety Criteria for the Handling, Storage and Transportation of LWR Fuel Outside Reactors.
- ANSI/ANS-57.2-1983, Design Requirements for Light Water Reactor Spent Fuel Storage Facilities at Nuclear Power Plants.

- ANSI N210-1976, Design Objectives for Light Water Reactor Spent Fuel Storage Facilities at Nuclear Power Plants.

USNRC guidelines and the applicable ANSI standards specify that the maximum effective multiplication factor,  $k_{eff}$ , including uncertainties, shall be less than or equal to 0.95. The infinite multiplication factor,  $k_{inf}$ , is calculated for an infinite array, neglecting neutron losses due to leakage from the actual storage rack, and therefore is a higher and more conservative value. In the present criticality safety evaluation of the Harris storage racks, the design basis criterion was assumed to be a  $k_{inf}$  of less than 0.95, which is more conservative than the limit specified in the regulatory guidelines.

To ensure that the true reactivity will always be less than the calculated reactivity, the following conservative assumptions were made:

- Moderator is un-borated water at a temperature (4°C) that results in the highest reactivity.
- In all cases (except for the assessment of peripheral effects and certain abnormal/accident conditions where neutron leakage is inherent), the infinite multiplication factor,  $k_{inf}$ , was used rather than the effective multiplication factor,  $k_{eff}$  (i.e., neutron loss from radial and axial leakage neglected).
- Neutron absorption in minor structural members is neglected, i.e., spacer grids are analytically replaced by water.
- The racks were assumed to be fully loaded with the most reactive fuel authorized to be stored in the facility. In the analysis, no credit was taken for any control rods or burnable poison (IFBA rods for the PWR fuel or gadolinia for BWR fuel), or soluble boron in the pool water which may be present.
- In-core depletion calculations assume conservative operating conditions, highest fuel and moderator temperature, an allowance for the soluble boron concentrations during in-core PWR operations and an allowance for voids during in-core BWR operations.

The PWR spent fuel storage racks are designed to accommodate any and all of the fuel assemblies listed in Table 4.3.1 with a maximum enrichment of 5 wt%  $^{235}\text{U}$ . To assure the acceptability of the racks for storage of any and all of the above assembly types, the most



reactive fuel assembly type was identified and used as the design basis fuel assembly. The Westinghouse 15x15 assembly was determined to have the highest reactivity at zero burnup and as a function of burnup for an initial 5 wt%  $^{235}\text{U}$  enrichment and therefore was used as the design basis PWR fuel assembly.

The BWR spent fuel storage racks are designed to accommodate any and all of the fuel assemblies listed in Table 4.3.2 with a maximum planar average enrichments of 4.6 wt.%  $^{235}\text{U}$ . Each fuel assembly type was analyzed independently to determine its acceptability in the rack. It is noted that individual fuel rods can have enrichments that are less than or greater than the maximum planar average enrichment.

## 4.2 Summary of Criticality Analyses

### 4.2.1 Normal Operating Conditions

#### 4.2.1.1 PWR Fuel Results

The design basis PWR fuel assembly is a 15 x 15 Westinghouse fuel assembly containing  $\text{UO}_2$  at a maximum initial enrichment of 5.0 wt%  $^{235}\text{U}$ . All fuel assembly types listed in Table 4.3.1 were also evaluated and the Westinghouse 15x15 assembly was shown to exhibit the highest reactivity for the high density PWR storage racks at Harris.

The NRC guidelines specify that the limiting  $k_{\text{eff}}$  of 0.95 under normal storage conditions should be evaluated in the absence of soluble boron. Consequences of abnormal and accident conditions have also been evaluated assuming no soluble boron, where "abnormal" refers to conditions (such as higher water temperatures) which may reasonably be expected to occur during the lifetime of the plant and "accident" refers to conditions which are not expected to occur but nevertheless must be protected against.

The criticality analyses of the spent fuel storage pool are summarized in Table 4.2.1 for the design basis storage conditions. The maximum  $k_{\text{inf}}$  is 0.9450 (95% probability at the 95% con-

fidence level) for the enrichment-burnup combinations shown in Figure 4.2.1. The calculated maximum reactivity includes burnup-dependent allowances for uncertainty in depletion calculations and for the axial distribution in burnup. Reactivity allowances for manufacturing tolerances and calculational uncertainties are also included. As cooling time increases in long-term storage, decay of Pu-241 and growth of Am-241 results in a significant decrease in reactivity, which will provide a continuously increasing subcriticality margin for the next 100 years.

The racks can safely accommodate fuel of various initial enrichments and discharge fuel burnups, provided the combination falls within the acceptable domain above the curve in Figure 4.2.1. For convenience, the minimum (limiting) burnup data for unrestricted storage can be described as a linear function of the initial enrichment (E, in weight percent  $^{235}\text{U}$ ) which conservatively encompasses the limiting burnup data. The equation for this curve is shown in Figure 4.2.1 and provided below.

For Unrestricted Storage of  
the following PWR fuel assemblies

Westinghouse 17x17 Std

Westinghouse 17x17 V5

Westinghouse 15x15

Siemens 17x17

Siemens 15x15

the enrichment must be less than or equal to 5 wt%  $^{235}\text{U}$  and the burnup must  
satisfy the minimum burnup requirements

$$\text{Minimum Burnup in MWD/MTU} = 12114 * E - 19123$$

The burnup criteria will be implemented by appropriate administrative procedures to ensure verified burnup as specified in the proposed Regulatory Guide 1.13, Revision 2, prior to fuel transfer into Spent Fuel Pools C or D.

#### 4.2.1.2 BWR Fuel Results

All BWR fuel assembly types being considered were explicitly analyzed to determine the acceptability for storage in Spent Fuel Pool C. The maximum planar average enrichment was

assumed for all rods in the assembly and no credit was taken for gadolinia which might be present.

The criticality safety was evaluated at the burnup corresponding to a  $k_{inf}$  of 1.32 in the Standard Cold Core Geometry (SCCG). SCCG is defined as an infinite array of fuel assemblies on a 6-inch lattice spacing at 20°C, without any control absorber or voids.

The maximum  $k_{inf}$  in the BWR storage rack was determined to be 0.9443 (95% probability at the 95% confidence level) including all known calculational and manufacturing uncertainties. In addition, a conservative allowance of 0.01  $\Delta k$  for possible differences between fuel vendor calculations and those reported here was included. This allowance also encompasses any uncertainty in the burnup calculations.

The basic calculations supporting the criticality safety of the Harris fuel storage racks for the design basis fuel are summarized in Table 4.2.2. For the design basis fuel, the fuel storage rack satisfies the USNRC criterion of a maximum  $k_{eff}$  less than or equal to 0.95.

The acceptance criteria for storage of spent BWR fuel in Harris Pool C can be summarized in the following manner.

<p>For Unrestricted Storage of the following BWR fuel assemblies</p> <p>GE 3, GE 4, GE 5, GE 6, GE 7, GE 8, GE 9, GE 10, GE 13</p> <p>the maximum planar average enrichment must be less than or equal to 4.6 wt.% <sup>235</sup>U and the <math>k_{inf}</math> in standard cold core geometry must be less than or equal to 1.32</p>
---

### 4.3 Input Parameters

#### 4.3.1 Reference PWR Fuel Assembly and Storage Cell

The design basis PWR fuel assembly is a 15x15 array of fuel rods with 21 rods replaced by 21 control rod guide tubes. Table 4.3.1 summarizes the PWR fuel assembly design specifications

for all fuel assemblies analyzed. Figure 4.3.1 shows the calculational model of the PWR spent fuel storage cell containing a 15x15 assembly.

The design basis for the Region 2 type storage cells is fuel of 5.0 wt.%  $^{235}\text{U}$  maximum initial enrichment burned to 41,447 MWD/MTU. The storage cells, consisting of an egg-crate structure, are composed of stainless steel walls with a single fixed neutron absorber panel, Boral, in a 0.107 inch channel. These cells are located on a lattice spacing of  $9.017 \pm$  [redacted] inch. The  $0.075 \pm$  [redacted] thick steel walls define a storage cell which has a  $8.8 \pm$  [redacted] inch nominal inside dimension. The Boral absorber has a thickness of  $0.098 \pm$  [redacted] inch and a nominal B-10 areal density of  $0.0302 \text{ g/cm}^2$  (minimum of [redacted]  $\text{g/cm}^2$ ). The width of the Boral absorber panel is  $7.5 \pm$  [redacted] inches. Boral panels are not needed or used on the exterior walls of modules facing non-fueled regions, i.e., the pool walls. However, at least one boral panel is used between storage racks.

#### 4.3.2 Reference BWR Fuel Assembly and Storage Cell

The design basis BWR fuel assembly, used for uncertainty calculations, is a standard 8x8 array of BWR fuel rods containing  $\text{UO}_2$  clad in Zircaloy (60 fuel rods with 4 water rods). Design parameters for all BWR fuel assemblies analyzed are summarized in Table 4.3.2. Figure 4.3.2 shows the calculational model of a BWR storage rack cell containing an 8x8 assembly.

The BWR storage cells, consisting of an egg-crate structure, are composed of stainless steel walls with a single fixed neutron absorber panel, Boral, in a 0.08 inch channel. These cells are located on a lattice spacing of  $6.25 \pm$  [redacted] inch. The  $0.075 \pm$  [redacted] thick steel walls define a storage cell which has a  $6.06 \pm$  [redacted] inch nominal inside dimension. The Boral absorber has a thickness of  $0.075 \pm$  [redacted] inch and a nominal B-10 areal density of  $0.0162 \text{ g/cm}^2$  (minimum of [redacted]  $\text{g/cm}^2$ ). The width of the Boral absorber panel is  $5.0 \pm$  [redacted] inches. Boral panels are not needed or used on the exterior walls of modules facing non-fueled regions, i.e., the pool walls. However, at least one boral panel is used between storage racks. The boral panel used on the outside of the

BWR racks is 3.5 inch in width. The minimum B-10 loading on these panels is identical to the loading on the internal panels.

#### 4.4 Analytical Methodology

##### 4.4.1 Reference Design Calculations

In the fuel rack analyses, the primary criticality analyses of the high density spent fuel storage racks were performed with a two-dimensional multigroup transport theory technique, using the CASMO-3 computer code [4.4.1 - 4.4.4]. Since CASMO-3 can not be directly compared to critical experiments, a calculational bias is not available for CASMO-3. Therefore, independent verification calculations were made with a Monte Carlo technique utilizing the MCNP-4A computer code [4.4.5]. Benchmark calculations, presented in Appendix A, indicate a bias of  $0.0009 \pm 0.0011$  for MCNP-4A, evaluated at the 95% probability, 95% confidence level. The MCNP-4A bias and uncertainty were included in the MCNP-4A to CASMO-3 comparison as discussed in Section 4.5.

CASMO-3 was also used for burnup calculations and for evaluating small reactivity increments associated with manufacturing tolerances. In the geometric model used in the calculations, each fuel rod and its cladding were described explicitly and reflecting boundary conditions (zero neutron current) were used in the axial direction and at the Boral and steel plates between storage cells. These boundary conditions have the effect of creating an infinite array of storage cells in all directions.

MCNP-4A was used to determine reactivity effects, to calculate the reactivity for fuel misloading outside the racks and to determine the effect of having PWR and BWR racks adjacent to each other. MCNP-4A Monte Carlo calculations inherently include a statistical uncertainty due to the random nature of neutron tracking. To minimize the statistical uncertainty of the MCNP-4A calculated reactivity, a minimum of 600,000 neutron histories in 200 generations of 3000 neutrons each, are accumulated in each calculation.

#### 4.4.2 Burnup Calculations and Uncertainties

CASMO-3 was used for burnup calculations during core operations. CASMO-3 has been extensively verified [4.4.4, 4.4.6] against Monte Carlo calculations, reactor operations, and heavy-element concentrations in irradiated fuel. In addition, Johansson [4.4.7] has obtained very good agreement in calculations of close-packed, high-plutonium-content, experimental configurations.

##### 4.4.2.1 PWR Fuel Burnup Calculations

Since critical experiment data with spent fuel is not available for determining the uncertainty in burnup-dependent reactivity calculations, an allowance for uncertainty in reactivity was assigned based upon other considerations. Assuming the uncertainty in depletion calculations is less than 5% of the total reactivity decrement, a burnup dependent uncertainty in reactivity for burnup calculations may be assigned. Table 4.4.1 summarizes results of the burnup analyses to determine the allowances for uncertainties in burnup calculations. The reactivity allowances for uncertainties in burnup are listed for three different burnup ranges: less than 30,000 MWD/MTU, between 30,000 and 40,000 MWD/MTU, and between 40,000 and 45,000 MWD/MTU. The appropriate uncertainty was used for each burnup range in determining the acceptable burnup versus enrichment combinations depicted in Figure 4.2.1. The allowance for uncertainty in burnup calculations is believed to be a conservative estimate, particularly in view of the substantial reactivity decrease with aged fuel as discussed in Section 4.4.4.

##### 4.4.2.2 BWR Fuel Burnup Calculations and Comparison to Vendor Calculations

CASMO-3 was used to perform depletion calculations and to calculate the  $k_{inf}$  in the SCCG. As discussed, there are no depleted fuel critical experiments with which to benchmark CASMO-3's depletion calculations. Therefore a reactivity allowance for uncertainty in depletion is needed. Instead of using 5% of the reactivity decrement, as in the case of the PWR assemblies, a flat

reactivity allowance of  $0.01 \Delta k$  is used. This value is not statistically combined with the other uncertainties but rather added directly to the calculated  $k_{inf}$ . The allowance is used to also encompass any potential differences between the SCCG calculations performed here and the vendor calculations.

#### 4.4.3 Effect of Axial Burnup Distribution

Initially, fuel loaded into the reactor will burn with a slightly skewed cosine power distribution. As burnup progresses, the burnup distribution will tend to flatten, becoming more highly burned in the central regions than in the upper and lower ends. At high burnup, the more reactive fuel near the ends of the fuel assembly (less than average burnup) occurs in regions of lower reactivity worth due to neutron leakage. Consequently, it would be expected that over most of the burnup history, distributed burnup fuel assemblies would exhibit a slightly lower reactivity than that calculated for the average burnup. As burnup progresses, the distribution, to some extent, tends to be self-regulating as controlled by the axial power distribution, precluding the existence of large regions of significantly reduced burnup.

Generic analytic results of the axial burnup effect have been provided by Turner [4.4.8] based upon calculated and measured axial burnup distributions. These analyses confirm the minor and generally negative reactivity effect of the axially distributed burnup, becoming positive at burnups greater than about 30,000 MWD/MTU. The trends observed [4.4.8] suggest the possibility of a small positive reactivity effect above 30,000 MWD/MTU increasing to slightly over  $1\% \Delta k$  at 40,000 MWD/MTU.

##### 4.4.3.1 PWR Fuel Axial Burnup Distribution

Calculations for the Harris storage racks with PWR fuel of three different average burnups were made using an axial burnup distribution representative of spent PWR fuel<sup>1</sup>. At lower burnups, the

---

<sup>1</sup> The axial burnup distribution measured on spent fuel from the Surry plant was used as representative of PWR fuel.

reactivity increment is smaller as indicated in Table 4.4.1, being negative at 30,000 MWD/MTU and at lower burnups. No credit is taken for this negative reactivity effect at the lower burnups other than the suggestion of additional conservatism. Furthermore, the reactivity significantly decreases with time in storage (Section 4.4.4 below) providing a continuously increasing margin below the 0.95 limit.

The appropriate reactivity allowance for the effect of axial burnup distribution was used for each burnup range in determining the acceptable burnup versus enrichment values in Figure 4.2.1.

#### 4.4.3.2 BWR Fuel Axial Burnup Distribution

The burnup at which  $k_{inf}$  in the SCCG reaches 1.32 is approximately 12,000 MWD/MTU. As discussed above and in [4.4.8] the effect of using the explicit axial burnup distribution as opposed to an average burnup distribution results in a negative effect on reactivity. Therefore, no reactivity allowance for axial burnup distribution is applied to the BWR fuel analysis.

#### 4.4.4 Long Term Reactivity Changes

At reactor shutdown, the reactivity of the fuel initially decreases due to the growth of Xe-135. Subsequently, the Xenon decays and the reactivity increases to a maximum at several hundred hours when the Xenon is gone. Over the next 30 years, the reactivity continuously decreases due primarily to Pu-241 decay and Americium growth. At lower burnup, the reactivity decrease will be less pronounced since less Pu-241 would have been produced. No credit is taken for this long-term decrease in reactivity other than to indicate additional and increasing conservatism in the design criticality analysis.



## 4.5 PWR Storage Rack Criticality Analyses and Tolerance Variations

### 4.5.1 Nominal Design Case

The principal method of analysis for the racks was the CASMO-3 code, using the restart option in CASMO-3 to analytically transfer fuel of a specified burnup into the storage rack configuration at a reference temperature of 4°C (39°F). Calculations were made for fuel of several different initial enrichments and, at each enrichment, a limiting  $k_{inf}$  value was established which includes reactivity allowances for manufacturing tolerances, the uncertainty in the burnup analyses and for the effect of the axial burnup distribution on reactivity. The restart CASMO-3 calculations (cold, no-Xenon, rack geometry) were then interpolated to define the burnup value yielding the limiting  $k_{inf}$  value for each enrichment. A line was fitted to these converged burnup values and this line defines the boundary of the acceptable domain shown in Figure 4.2.1.

An independent MCNP-4A calculation was performed to verify the acceptability of the reference criticality analyses. Fuel of 5.0 wt% initial enrichment was analyzed by MCNP-4A and by CASMO-3. The results of this comparison are presented in Table 4.5.1. In comparing the MCNP values to the CASMO-3 values, the MCNP-4A calculational bias and calculational statistics were included. In addition, the MCNP-4A model correctly included the effect of axial neutron leakage which the CASMO-3 calculations conservatively neglect. Since the MCNP-4A model is at 20 °C and the CASMO-3 model is at 4 °C, a temperature correction had to be applied to the MCNP-4A result. The MCNP-4A result confirms that the reference CASMO-3 calculations are conservative.

### 4.5.2 Uncertainties Due to PWR Rack Manufacturing Tolerances

All reactivity allowances for manufacturing tolerances are summarized below and listed in Table 4.2.1. Since the tolerances are statistically independent, the allowances are statistically combined into a single reactivity allowance which was used in the final calculations (see Table 4.2.1).

#### 4.5.2.1 Boron Loading Tolerances

The Boral absorber panels used in the storage cells are 0.098 inch thick with a nominal B-10 areal density of 0.0302 g/cm<sup>2</sup>. The manufacturing limit of B-10 loading assures that at any point the minimum B-10 areal density will not be less than [REDACTED] g/cm<sup>2</sup>. Differential CASMO-3 calculations indicate that this tolerance limit results in an incremental reactivity uncertainty of  $\pm 0.0041 \Delta k$ .

#### 4.5.2.2 Boral Width Tolerance

The reference storage cell design uses a Boral absorber width of  $7.50 \pm$  [REDACTED] inch. CASMO-3 differential calculations show that this tolerance results in a reactivity uncertainty of  $\pm 0.0009 \Delta k$ .

#### 4.5.2.3 Tolerance in Cell Lattice Spacing and Cell Box Inner Dimension

Since the Region 2 style racks do not utilize a water gap between storage cells, the manufacturing tolerance on inner box dimension is identical to the tolerance on the storage cell lattice spacing. The inner box dimension is  $8.8 \pm$  [REDACTED] inches. This corresponds to an uncertainty in reactivity of  $\pm 0.0017 \Delta k$  as determined with CASMO-3.

#### 4.5.2.4 Stainless Steel Thickness Tolerance

The nominal thickness of the stainless steel box wall is 0.075 inch with a tolerance of  $\pm$  [REDACTED] inch, resulting in an uncertainty in reactivity of  $\pm 0.0005 \Delta k$  as calculated with CASMO-3.

#### 4.5.2.5 Fuel Enrichment and Density Tolerances

The maximum fuel enrichment was specified as 5.0 wt.% <sup>235</sup>U + 0.0/- 0.05. This uncertainty results in a negative reactivity effect which is not credited in this analysis. The UO<sub>2</sub> density was [REDACTED]. CASMO-3 calculations show that the reactivity allowance for this tolerance is  $\pm 0.0014 \Delta k$ .

## 4.6 BWR Storage Rack Criticality Analyses and Tolerance Variations

### 4.6.1 Nominal Design Case

The two-dimensional CASMO-3 code was used as the principal method of analysis for the Harris spent fuel pool BWR racks. CASMO-3 was used to perform depletion calculations on the fuel assembly and using the restart option in CASMO-3 the fuel of a specified burnup was analytically transferred into the storage rack at a reference temperature of 4°C (39°F). The same fuel of a specified burnup was also analytically transferred into the standard cold core geometry (SCCG) configuration which is an infinite lattice with 6 inch spacing at a temperature of 20°C without any burnable absorber or control blades and no voids. All Xenon which was present during the depletion calculations was removed during the restarts in the rack and SCCG. The reactivity effects of the natural uranium blanket normally located at the ends of the assemblies were conservatively neglected since an infinite fuel length was used.

All fuel assemblies specified were analyzed at the maximum enrichment specified. The maximum  $k_{inf}$  in the SCCG was specified as 1.32. Using the CASMO-3 results, the burnup corresponding to a  $k_{inf}$  in the SCCG of 1.32 was determined and the corresponding  $k_{inf}$  in the rack was determined. The reactivity adjustments were added to the rack  $k_{inf}$  to determine the maximum value and this was compared against the 0.95  $k_{eff}$  limit. Based on this analysis, all specified fuel assemblies are acceptable for storage as stated in Section 4.2.1.2. Table 4.2.2 provides the final results of the BWR fuel assembly calculations.

An independent MCNP-4A calculation was used to verify the acceptability of the reference criticality analyses. Fuel of 4.6 wt% initial enrichment was analyzed by MCNP-4A and by CASMO-3. The results of this comparison are presented in Table 4.5.1. In comparing the MCNP values to the CASMO values, the MCNP-4A calculational bias and calculational statistics were included. In addition, the MCNP-4A model correctly included the effect of axial neutron leakage which the CASMO-3 calculations conservatively neglect. Since the MCNP-4A model is at 20 °C



and the CASMO-3 model is at 4 °C, a temperature correction had to be applied to the MCNP-4A result. The MCNP-4A result confirm that the reference CASMO-3 calculations are conservative.

#### 4.6.2 Uncertainties Due to Manufacturing Tolerances

The reactivity effects associated with manufacturing tolerances are discussed below and shown in Table 4.2.2. Since the tolerances are statistically independent, the allowances are statistically combined into a single reactivity allowance which was used in the final calculations (see Table 4.2.2).

##### 4.6.2.1 Boron Loading Variation

The Boral absorber panels used in the storage cells are nominally 0.075 inch thick, with a B-10 areal density of 0.0162 g/cm<sup>2</sup>. The manufacturing tolerance limit in B-10 content, including both thickness and composition tolerances assures that the minimum boron-10 areal density will not be less than [REDACTED] g/cm<sup>2</sup>. Differential CASMO-3 calculations indicate that this tolerance limit results in an incremental reactivity uncertainty of  $\pm 0.0053 \Delta k$ .

##### 4.6.2.2 Boral Width Tolerance Variation

The reference storage cell design uses a Boral panel width of 5.00 inches. The tolerance on the Boral width is  $\pm$  [REDACTED] inch. Calculations using CASMO-3 showed that this tolerance corresponds to a  $\pm 0.0018 \Delta k$  uncertainty.

##### 4.6.2.3 Tolerance in Cell Lattice Pitch and Inner Box Dimension

Since the Region 2 style racks do not utilize a water gap between storage cells, the manufacturing tolerance on inner box dimension is identical to the tolerance on the storage cell lattice spacing. The inner box dimension is 6.06  $\pm$  [REDACTED] inches. This corresponds to an uncertainty in reactivity of  $\pm 0.0037 \Delta k$  as determined with CASMO-3.



#### 4.6.2.4 Stainless Steel Thickness Tolerances

The nominal thickness of the stainless steel box is  $0.075 \pm$  [redacted] inches. The maximum positive reactivity effect of the expected stainless steel thickness tolerances was calculated to be  $\pm 0.0005 \Delta k$  using CASMO-3.

#### 4.6.2.5 Fuel Enrichment and Density Variation

The maximum planar average fuel enrichment was specified for each fuel assembly analyzed. Therefore, there is no reactivity allowance for variations in enrichment since the absolute maximum was used for all calculations.

The  $UO_2$  density was specified for each fuel assembly analyzed. The maximum tolerance on the density is  $\pm$  [redacted] g/cc. CASMO-3 calculations show that the reactivity allowance for this tolerance is  $\pm 0.0023 \Delta k$ .

#### 4.6.2.6 Zirconium Flow Channel

Elimination of the zirconium flow channel results in a small (approximately  $0.0024 \Delta k$ ) decrease in reactivity. More significant is a positive reactivity effect resulting from potential bulging of the zirconium channel, which moves the channel wall outward toward the Boral absorber. It is conservatively assumed that the maximum bulging that could occur would result in the channel touching the cell walls. Since this would not occur over the entire length of the channel, the model assumed that the entire channel was enlarged so that the mid-point of the channel wall was placed equidistant between the nominal channel outer dimension and the cell wall. This results in an incremental reactivity of  $+ 0.0045 \Delta k$  as determined with MCNP-4A.

### 4.7 Abnormal and Accident Conditions

Strict administrative controls on the fuel transfer to Pools C and D will preclude fuel which is outside the range of the previously stated acceptance criteria from being brought into the spent

fuel pool. Therefore, the only potential abnormal and accident conditions that exist are the misplacement of a fuel assembly outside the rack or the dropping of a fuel assembly on top of the rack. It is also possible to inadvertently place a BWR spent fuel assembly in the PWR rack.

#### 4.7.1 Temperature and Water Density Effects

The spent fuel pool temperature coefficient of reactivity is negative. Using the minimum temperature of 4°C, therefore, assures that the true reactivity will always be lower than the calculated value regardless of the temperature. Temperature effects on reactivity have been calculated and the results are shown in Table 4.7.1. Introducing voids in the water internal to the storage cell (to simulate boiling) decreased reactivity, as shown in the table. Boiling at the submerged depth of the racks would occur at approximately 122°C.

#### 4.7.2 Dropped Fuel Assembly

For a drop on top of the rack, the fuel assembly will come to rest horizontally on top of the rack with a minimum separation distance from the fuel in the rack of more than 12 inches (which is considered infinite), including an estimated allowance for deformation under seismic or accident conditions. At this separation distance, the effect on reactivity is insignificant.

It is also possible to vertically drop an assembly into a location occupied by another assembly. Such a vertical impact would at most cause a small compression of the stored assembly, reducing the water-to-fuel ratio and thereby reducing reactivity. In addition the distance between the active fuel regions of both assemblies will be more than sufficient to ensure no neutron interaction between the two assemblies.

Dropping an assembly into an unoccupied cell could result in a localized deformation of the baseplate of the rack. The resultant effect would be the lowering of a single fuel assembly by the amount of the deformation. This could potentially result in the active fuel height no longer being covered by the boral. The immediate eight surrounding fuel cells could also be affected.

However, the amount of deformation for these cells would be considerably less. The amount of localized deformation would not exceed three inches for a PWR assembly and would therefore be considerably less for the lighter BWR assembly. The criticality effect of this drop accident has been conservatively analyzed and it has been shown that this localized event (nine storage cells at most) has a negligible impact on reactivity.

#### 4.7.3 Lateral Rack Movement

Lateral motion of the rack modules under seismic conditions could potentially alter the spacing between rack modules. Region 2 storage cells do not use a flux-trap and the reactivity is therefore insensitive to the spacing between modules. The spacing between modules is sufficiently large to preclude adverse interaction even with the maximum seismically-induced reduction in spacing.

#### 4.7.4 Abnormal Location of a PWR or BWR Fuel Assembly

Strict administrative controls will prevent an unacceptable assembly, as determined by the acceptance criteria stated in Section 4.2, from being transferred to Harris Pools C and D. Therefore, the only potential mislocation of a fuel assembly is the mislocation of a fuel assembly of equal or lower reactivity to the design basis outside a PWR or BWR rack. Since the racks will have a Boron panel on the outside face (when the outside face is not against a wall) the reactivity effect of a misloaded fuel assembly outside the rack is negligible because of the neutron leakage that occurs from the rack itself. Therefore, the conservative infinite lattice calculations that were performed have  $k_{inf}$  values that are higher than any potential mislocation accidents.

Another mislocation event could occur with a BWR assembly. This would be the inadvertent placement of a BWR assembly in the PWR racks. Since, the BWR assembly is significantly smaller than a PWR assembly, the reactivity effect of placing a BWR assembly in the PWR rack is negligible. The reverse scenario of misplacing a PWR



assembly in the BWR rack is impossible because of the size of the PWR assembly.

#### 4.7.5 Eccentric Fuel Positioning

The fuel assembly is assumed to be normally located in the center of the storage rack cell and in the case of the BWR rack there are bottom fittings and spacers that mechanically restrict lateral movement of the fuel assemblies. Nevertheless, MCNP-4A calculations were made with the fuel assemblies assumed to be in the corner of the storage rack cell (four-assembly cluster at closest approach). These calculations indicated that eccentric fuel positioning results in a decrease in reactivity (by about 0.0051 for the PWR assemblies and 0.0091 for the BWR assemblies). The highest reactivity, therefore, corresponds to the reference design with the fuel assemblies positioned in the center of the storage cells.

## 4.8 References

- [4.1.1] M. G. Natrella, Experimental Statistics, National Bureau of Standards Handbook 91, August 1963.
- [4.4.1] A. Ahlin, M. Edenius, H. Haggblom, "CASMO - A Fuel Assembly Burnup Program," AE-RF-76-4158, Studsvik report (proprietary).
- [4.4.2] A. Ahlin and M. Edenius, "CASMO - A Fast Transport Theory Depletion Code for LWR Analysis," *ANS Transactions*, Vol. 26, p. 604, 1977.
- [4.4.3] M. Edenius, A. Ahlin, and B. H. Forssen, "CASMO-3 A Fuel Assembly Burnup Program, Users Manual", Studsvik/NFA-87/7, Studsvik Energitechnik AB, November 1986.
- [4.4.4] M. Edenius and A. Ahlin, "CASMO-3: New Features, Benchmarking, and Advanced Applications," *Nuclear Science and Engineering*, 100, 342-351, (1988).
- [4.4.5] J.F. Briesmeister, Editor, "MCNP - A General Monte Carlo N-Particle Transport Code, Version 4A," LA-12625, Los Alamos National Laboratory (1993).
- [4.4.6] E. E. Pilat, "Methods for the Analysis of Boiling Water Reactors (Lattice Physics)," YAEC-1232, Yankee Atomic Electric Co., December 1980.
- [4.4.7] E. Johansson, "Reactor Physics Calculations on Close-Packed Pressurized Water Reactor Lattices," *Nuclear Technology*, Vol. 68, pp. 263-268, February 1985.
- [4.4.8] S. E. Turner, "Uncertainty Analysis - Burnup Distributions", presented at the DOE/SANDIA Technical Meeting on Fuel Burnup Credit, Special Session, ANS/ENS Conference, Washington, D.C., November 2, 1988.

Table 4.2.1

## Summary of Criticality Safety Calculations for the PWR Fuel Racks

Fuel Assembly		Westinghouse 15x15
Enrichment		5%
Temperature		4°C
Burnup from Calculation (MWD/MTU)		41,352
Burnup from Curve (MWD/MTU)		41,447
CASMO-3 $k_{inf}$		0.9126
Uncertainties		
UO <sub>2</sub> density	0.0014	
Inner box dimension	0.0017	
Box wall thickness	0.0005	
Boral width	0.0009	
B-10 loading	0.0041	
Burnup	0.0160	
Total Uncertainty at 95%/95%		0.0167
Effect of Axial Burnup Distribution		0.0157
Maximum $k_{inf}$		<hr/> 0.9450
Regulatory Limit		0.9500

## Notes:

1. Only the most reactive assembly is shown.
2. The total uncertainty is a statistical combination of the manufacturing uncertainties.

Table 4.2.2

## Summary of Criticality Safety Calculations for the BWR Fuel Racks

Fuel Assembly	GE 3	GE 4	GE 7	GE 8	GE 9	GE 10	GE 13
Temperature	4°C						
SCCG $k_{inf}$	1.32	1.32	1.32	1.32	1.32	1.32	1.32
Enrichment	4.6	4.6	4.6	4.6	4.6	4.6	4.6
CASMO-3 $k_{inf}$	0.9163	0.9140	0.9192	0.9214	0.9207	0.9201	0.9227
Uncertainties							
UO <sub>2</sub> density	0.0023						
Inner box dimension	0.0037						
Box wall thickness	0.0005						
Boral width	0.0018						
B-10 loading	0.0053						
Total uncertainty at 95%/95%	0.0071	0.0071	0.0071	0.0071	0.0071	0.0071	0.0071
Channel bulging	0.0045	0.0045	0.0045	0.0045	0.0045	0.0045	0.0045
Uncertainty for burnup and vendor comparison	0.0100	0.0100	0.0100	0.0100	0.0100	0.0100	0.0100
Maximum $k_{inf}$	0.9379	0.9356	0.9408	0.9430	0.9423	0.9417	0.9443
Regulatory Limit	0.9500	0.9500	0.9500	0.9500	0.9500	0.9500	0.9500

## Notes:

1. The total uncertainty is a statistical combination of the manufacturing uncertainties.
2. The GE 13 assembly has part length rods. Two CASMO-3 calculations were performed: one with all rods present and the other with only the full length rods present. The most reactive configuration was the second and the  $k_{inf}$  from this configuration is presented.
3. The GE 5 and GE 6 are identical to the GE 7 for the fuel parameters analyzed and therefore the GE 5 and GE 6 have a maximum  $k_{inf}$  equivalent to the GE 7.
4. The enrichment is the planar average enrichment.

Table 4.3.1  
PWR Fuel Characteristics

Fuel Assembly	Westinghouse 17x17 Std	Westinghouse 17x17 V5	Westinghouse 15x15	Siemens 17x17	Siemens 15x15
NOTE: All Dimensions in inches					
Clad O.D.	0.374	0.360	0.422	0.376	0.424
Clad I.D.	0.329	0.315	0.373	0.328	0.364
Clad Material	Zr-4	Zr-4	Zr-4	Zr-4	Zr-4
Pellet Diameter	0.3225	0.3088	0.3659	0.3215	0.357
Stack Density	10.41	10.41	10.41		
Maximum Enrichment	5.0	5.0	5.0	5.0	5.0
Active Fuel Length	144	144	144	144	144
Number Fuel Rods	264	264	204	264	204
Fuel Rod Pitch	0.496	0.496	0.563	0.496	0.563
Number of Thimbles	24/1	24/1	21	25	21
Thimble O.D.	0.482/0.484	0.474/0.476	0.546	0.480	0.544
Thimble I.D.	0.450/0.448	0.442/0.440	0.512	0.448	0.511

The highlighted data in the table above is the property of Westinghouse or Siemens and is proprietary information provided in confidence. Access to this information shall be limited to those individuals having a need for such access and shall not be disclosed or transmitted to any organization without the written permission of Westinghouse or Siemens, respectively.

Table 4.3.2  
BWR Fuel Characteristics

Fuel Assembly	GE 3	GE 4	GE 7	GE 8	GE 9	GE 10	GE 13
NOTE: All dimensions in inches							
Clad O.D.	0.563	0.493	0.483	0.483	0.483	0.483	0.440
Clad I.D.	0.489	0.425	0.419	0.419	0.419	0.419	0.419
Clad Material	Zr-2	Zr-2	Zr-2	Zr-2	Zr-2	Zr-2	Zr-2
Pellet Diameter	0.477	0.416	0.410	0.411	0.411	0.411	0.411
Stack Density	10.31	10.40	10.54	10.58	10.54	10.54	10.54
Maximum Enrichment	4.6	4.6	4.6	4.6	4.6	4.6	4.6
SCCG $k_{inf}$	$\leq 1.32$	$\leq 1.32$	$\leq 1.32$	$\leq 1.32$	$\leq 1.32$	$\leq 1.32$	$\leq 1.32$
Active Fuel Length	144	146	150	150	150	150	150
Fuel Rod Array	7x7	8x8	8x8	8x8	8x8	8x8	9x9
Number Fuel Rods	49	63	62	60	60	60	74
Fuel Rod Pitch	0.738	0.640	0.640	0.640	0.640	0.640	0.566
Number of Water Rods	0	1	2	4	1	1	2
Water Rod O.D.		0.493	0.591	0.591/ 0.483	1.34	1.34	0.980
Water Rod I.D.		0.425	0.531	0.531/ 0.431	1.26	1.26	1.26
Channel I.D.	5.278	5.278	5.278	5.278	5.278	5.278	5.278
Channel Thickness	0.080	0.080	0.080	0.080	0.080	0.070	0.070

Notes:

1. The GE 13 assembly has 8 part length rods.
2. The GE 5 and GE 6 are identical to the GE 7 for the fuel parameters listed.
3. The enrichment is the maximum planar average enrichment.

The highlighted data in the table above is the property of GE and is proprietary information provided in confidence. Access to this information shall be limited to those individuals having a need for such access and shall not be disclosed or transmitted to any organization without the written permission of GE.

Table 4.4.1

Reactivity Allowance for Uncertainty in Burnup Calculations  
and the Effect of Axial Burnup Distributions for PWR Fuel

Calculated Burnup (MWD/MTU)	Applicable Burnup Range (MWD/MTU)	$\Delta k$	
		Uncertainty in Burnup	Effect of Axial Burnup Distribution
45,000	40,000-45,000	0.0160	0.0157
40,000	30,000-40,000	0.0143	0.0090
30,000	< 30,000	0.0110	Negative

Notes:

1. The uncertainty in burnup was calculated by taking 5% of the reactivity decrement from zero burnup to the calculated burnup using CASMO-3.
2. The effect of the axial burnup distribution was calculated using MCNP-4A by comparing results from two cases: the first had a uniform axial burnup and the second had a distributed axial burnup distribution represented by 10 axial zones.
3. The effect of the axial burnup distribution is negative at and below 30,000 MWD/MTU, therefore, conservatively no reactivity adjustment was made.

Table 4.5.1  
Comparison of MCNP-4A and CASMO-3 Calculations

	PWR Rack	BWR Rack
Fuel Assembly	W 15x15	GE 8
Enrichment	5.0	4.6
Temperature	4°C	4°C
MCNP-4A $k_{eff}$	1.2004	0.9993
Uncertainties		
Calculational Statistics	0.0020	
Bias Uncertainty	0.0011	
Total Uncertainty at 95%/95%	0.0023	0.0023
Temperature correction from 20°C to 4°C	0.0020	0.0020
Bias	0.0009	0.0009
MCNP-4A Maximum $k_{eff}$	1.2056	1.0045
CASMO-3 $k_{inf}$	1.2076	1.0126

Notes:

1. The MCNP-4A calculation correctly includes the effect of axial neutron leakage.



Table 4.7.1  
Reactivity Effects of Temperature and Void

Temperature	Incremental Reactivity Effect - $\Delta k$ (relative to reference)	
	PWR Rack	BWR Rack
4°C (39°F)	reference	reference
20°C (68°F)	-0.0020	-0.0020
60°C (140°F)	-0.0093	-0.0093
120°C (248°F)	-0.0247	-0.0240
120°C with 10% void	-0.0492	-0.0446



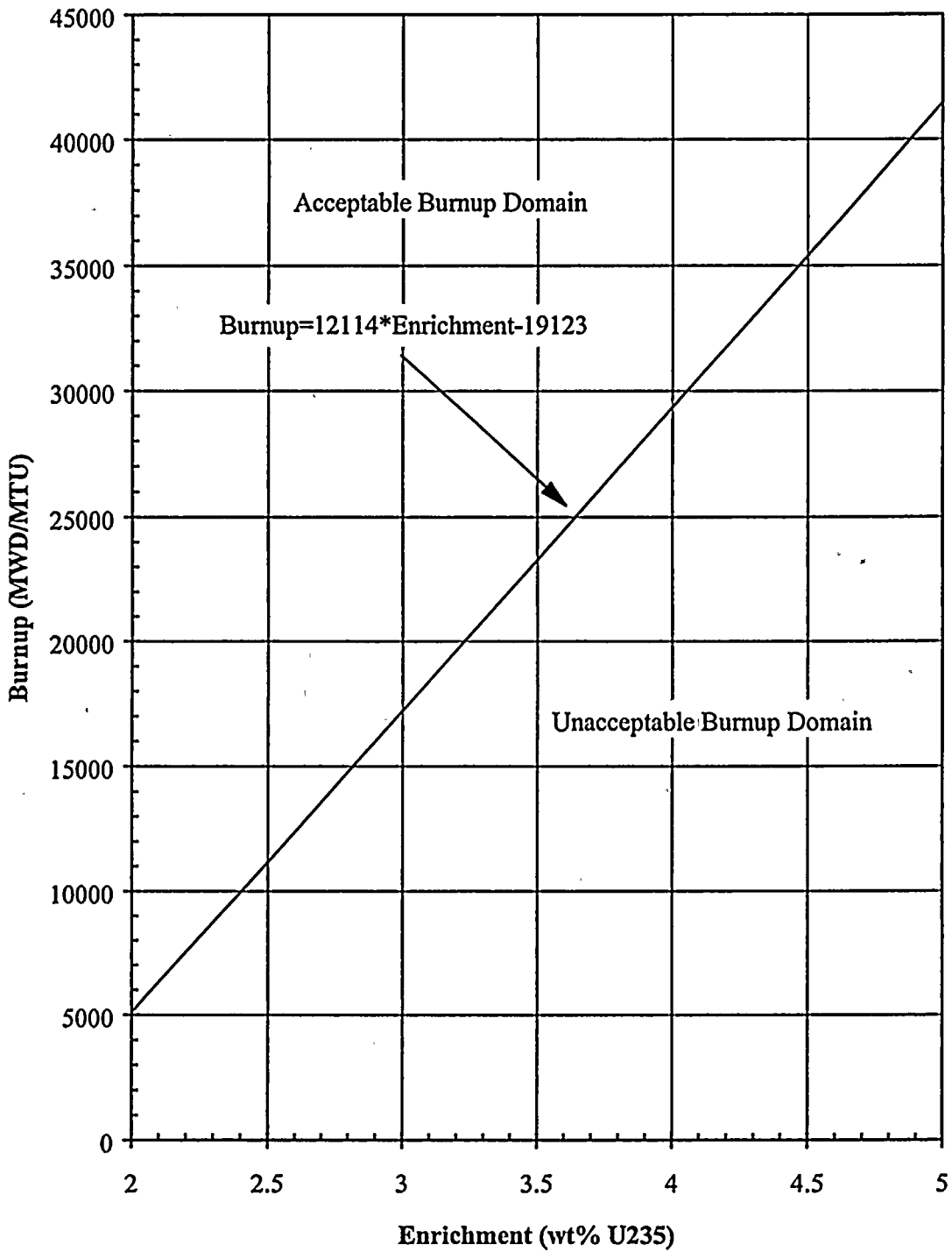
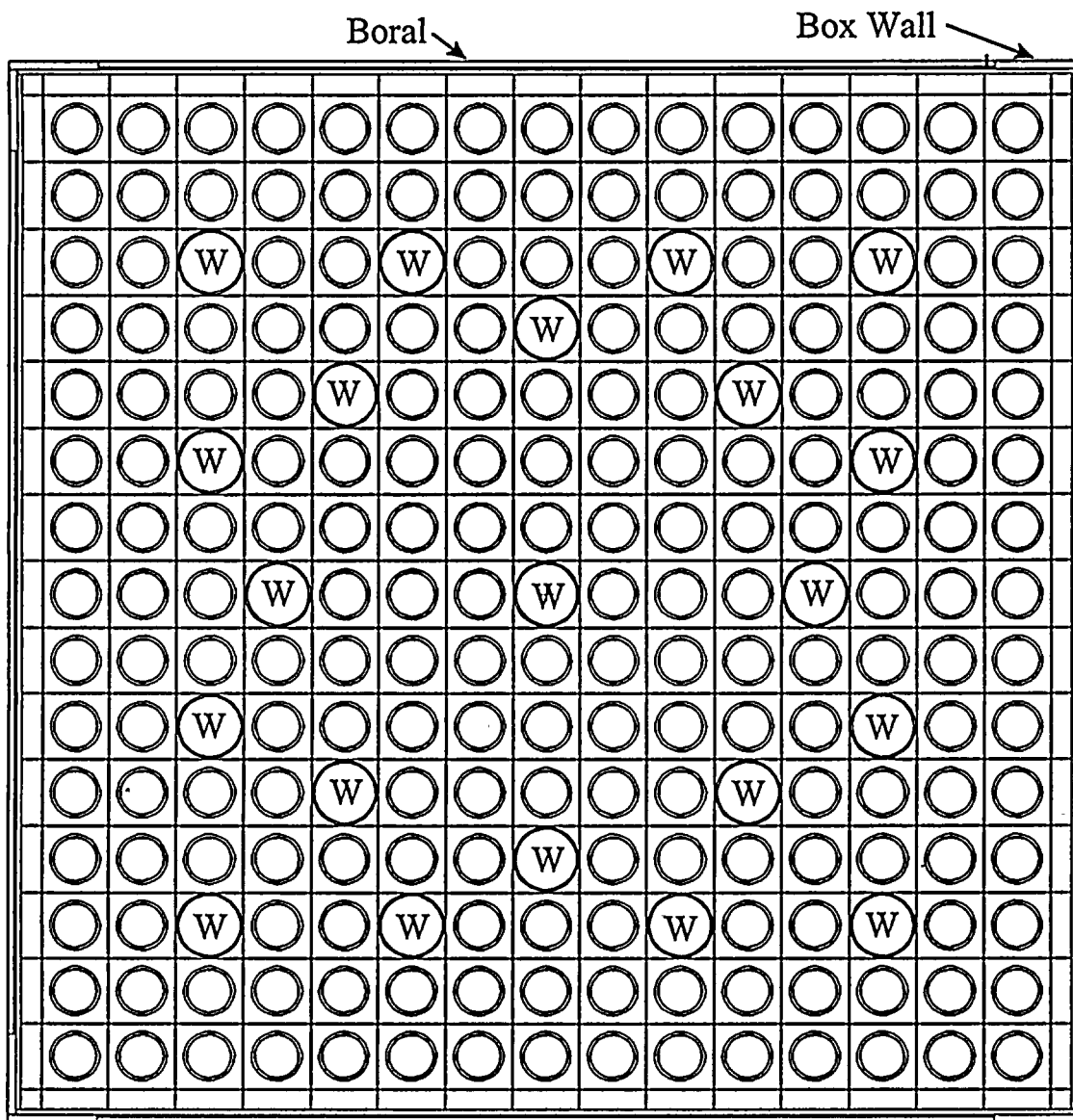


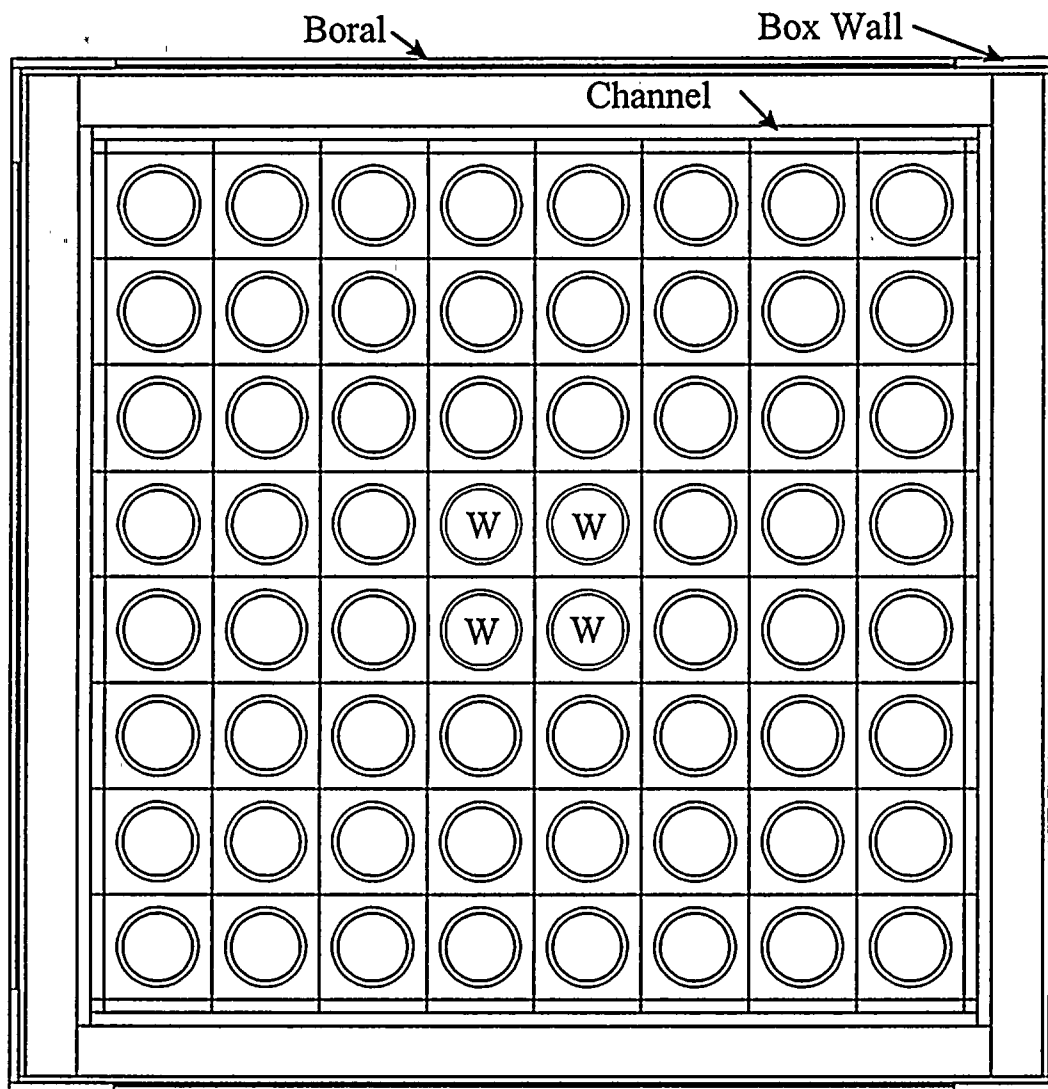
Figure 4.2.1: Burnup Versus Enrichment for PWR Fuel





W = guide tubes

Figure 4.3.1: This is a two dimensional representation of the calculational model used for the PWR storage rack analysis showing a Westinghouse 15x15 fuel design. This figure was drawn with the two dimensional plotter in MCNP-4A.



W = water rod

Figure 4.3.2: This is a two dimensional representation of the calculational model used for the BWR storage rack analysis showing a GE 8 fuel design. This figure was drawn with the two dimensional plotter in MCNP-4A.

## APPENDIX 4A: BENCHMARK CALCULATIONS

### 4A.1 INTRODUCTION AND SUMMARY

Benchmark calculations have been made on selected critical experiments, chosen, in so far as possible, to bound the range of variables in the rack designs. Two independent methods of analysis were used, differing in cross section libraries and in the treatment of the cross sections. MCNP4a [4A.1] is a continuous energy Monte Carlo code and KENO5a [4A.2] uses group-dependent cross sections. For the KENO5a analyses reported here, the 238-group library was chosen, processed through the NITAWL-II [4A.2] program to create a working library and to account for resonance self-shielding in uranium-238 (Nordheim integral treatment). The 238 group library was chosen to avoid or minimize the errors<sup>†</sup> (trends) that have been reported (e.g., [4A.3 through 4A.5]) for calculations with collapsed cross section sets.

In rack designs, the three most significant parameters affecting criticality are (1) the fuel enrichment, (2) the <sup>10</sup>B loading in the neutron absorber, and (3) the lattice spacing (or water-gap thickness if a flux-trap design is used). Other parameters, within the normal range of rack and fuel designs, have a smaller effect, but are also included in the analyses.

Table 4A.1 summarizes results of the benchmark calculations for all cases selected and analyzed, as referenced in the table. The effect of the major variables are discussed in subsequent sections below. It is important to note that there is obviously considerable overlap in parameters since it is not possible to vary a single parameter and maintain criticality; some other parameter or parameters must be concurrently varied to maintain criticality.

One possible way of representing the data is through a spectrum index that incorporates all of the variations in parameters. KENO5a computes and prints the "energy of the average lethargy causing fission" (EALF). In MCNP4a, by utilizing the tally option with the identical 238-group energy structure as in KENO5a, the number of fissions in each group may be collected and the EALF determined (post-processing).

---

<sup>†</sup> Small but observable trends (errors) have been reported for calculations with the 27-group and 44-group collapsed libraries. These errors are probably due to the use of a single collapsing spectrum when the spectrum should be different for the various cases analyzed, as evidenced by the spectrum indices.

Figures 4A.1 and 4A.2 show the calculated  $k_{eff}$  for the benchmark critical experiments as a function of the EALF for MCNP4a and KENO5a, respectively (UO<sub>2</sub> fuel only). The scatter in the data (even for comparatively minor variation in critical parameters) represents experimental error<sup>†</sup> in performing the critical experiments within each laboratory, as well as between the various testing laboratories. The B&W critical experiments show a larger experimental error than the PNL criticals. This would be expected since the B&W criticals encompass a greater range of critical parameters than the PNL criticals.

Linear regression analysis of the data in Figures 4A.1 and 4A.2 show that there are no trends, as evidenced by very low values of the correlation coefficient (0.13 for MCNP4a and 0.21 for KENO5a). The total bias (systematic error, or mean of the deviation from a  $k_{eff}$  of exactly 1.000) for the two methods of analysis are shown in the table below.

Calculational Bias of MCNP4a and KENO5a	
MCNP4a	0.0009 ± 0.0011
KENO5a	0.0030 ± 0.0012

The bias and standard error of the bias were derived directly from the calculated  $k_{eff}$  values in Table 4A.1 using the following equations<sup>††</sup>, with the standard error multiplied by the one-sided K-factor for 95% probability at the 95% confidence level from NBS Handbook 91 [4A.18] (for the number of cases analyzed, the K-factor is ~2.05 or slightly more than 2).

$$\bar{k} = \frac{1}{n} \sum_1^n k_i \quad (4A.1)$$

† A classical example of experimental error is the corrected enrichment in the PNL experiments, first as an addendum to the initial report and, secondly, by revised values in subsequent reports for the same fuel rods.

†† These equations may be found in any standard text on statistics, for example, reference [4A.6] (or the MCNP4a manual) and is the same methodology used in MCNP4a and in KENO5a.

$$\sigma_{\bar{k}}^2 = \frac{\sum_{i=1}^n k_i^2 - (\sum_{i=1}^n k_i)^2 / n}{n(n-1)} \quad (4A.2)$$

$$Bias = (1 - \bar{k}) \pm K \sigma_{\bar{k}} \quad (4A.3)$$

where  $k_i$  are the calculated reactivities of  $n$  critical experiments;  $\sigma_{\bar{k}}$  is the unbiased estimator of the standard deviation of the mean (also called the standard error of the bias (mean));  $K$  is the one-sided multiplier for 95% probability at the 95% confidence level (NBS Handbook 91 [4A.18]).

Formula 4.A.3 is based on the methodology of the National Bureau of Standards (now NIST) and is used to calculate the values presented on page 4.A-2. The first portion of the equation,  $(1 - \bar{k})$ , is the actual bias which is added to the MCNP4a and KENO5a results. The second term,  $K\sigma_{\bar{k}}$ , is the uncertainty or standard error associated with the bias. The  $K$  values used were obtained from the National Bureau of Standards Handbook 91 and are for one-sided statistical tolerance limits for 95% probability at the 95% confidence level. The actual  $K$  values for the 56 critical experiments evaluated with MCNP4a and the 53 critical experiments evaluated with KENO5a are 2.04 and 2.05, respectively.

The bias values are used to evaluate the maximum  $k_{eff}$  values for the rack designs. KENO5a has a slightly larger systematic error than MCNP4a, but both result in greater precision than published data [4A.3 through 4A.5] would indicate for collapsed cross section sets in KENO5a (SCALE) calculations.

#### 4A.2 Effect of Enrichment

The benchmark critical experiments include those with enrichments ranging from 2.46 w/o to 5.74 w/o and therefore span the enrichment range for rack designs. Figures 4A.3 and 4A.4 show the calculated  $k_{eff}$  values (Table 4A.1) as a function of the fuel enrichment reported for the critical experiments. Linear regression analyses for these data confirms that there are no trends, as indicated by low values of the correlation coefficients (0.03 for MCNP4a and 0.38 for KENO5a). Thus, there are no corrections to the bias for the various enrichments.

As further confirmation of the absence of any trends with enrichment, a typical configuration was calculated with both MCNP4a and KENO5a for various enrichments. The cross-comparison of calculations with codes of comparable sophistication is suggested in Reg. Guide 3.41. Results of this comparison, shown in Table 4A.2 and Figure 4A.5, confirm no significant difference in the calculated values of  $k_{eff}$  for the two independent codes as evidenced by the 45° slope of the curve. Since it is very unlikely that two independent methods of analysis would be subject to the same error, this comparison is considered confirmation of the absence of an enrichment effect (trend) in the bias.

#### 4A.3 Effect of $^{10}\text{B}$ Loading

Several laboratories have performed critical experiments with a variety of thin absorber panels similar to the Boral panels in the rack designs. Of these critical experiments, those performed by B&W are the most representative of the rack designs. PNL has also made some measurements with absorber plates, but, with one exception (a flux-trap experiment), the reactivity worth of the absorbers in the PNL tests is very low and any significant errors that might exist in the treatment of strong thin absorbers could not be revealed.

Table 4A.3 lists the subset of experiments using thin neutron absorbers (from Table 4A.1) and shows the reactivity worth ( $\Delta k$ ) of the absorber.<sup>†</sup>

No trends with reactivity worth of the absorber are evident, although based on the calculations shown in Table 4A.3, some of the B&W critical experiments seem to have unusually large experimental errors. B&W made an effort to report some of their experimental errors. Other laboratories did not evaluate their experimental errors.

To further confirm the absence of a significant trend with  $^{10}\text{B}$  concentration in the absorber, a cross-comparison was made with MCNP4a and KENO5a (as suggested in Reg. Guide 3.41). Results are shown in Figure 4A.6 and Table 4A.4 for a typical geometry. These data substantiate the absence of any error (trend) in either of the two codes for the conditions analyzed (data points fall on a 45° line, within an expected 95% probability limit).

---

<sup>†</sup> The reactivity worth of the absorber panels was determined by repeating the calculation with the absorber analytically removed and calculating the incremental ( $\Delta k$ ) change in reactivity due to the absorber.



#### 4A.4 Miscellaneous and Minor Parameters

##### 4A.4.1 Reflector Material and Spacings

PNL has performed a number of critical experiments with thick steel and lead reflectors.<sup>†</sup> Analysis of these critical experiments are listed in Table 4A.5 (subset of data in Table 4A.1). There appears to be a small tendency toward overprediction of  $k_{\text{eff}}$  at the lower spacing, although there are an insufficient number of data points in each series to allow a quantitative determination of any trends. The tendency toward overprediction at close spacing means that the rack calculations may be slightly more conservative than otherwise.

##### 4A.4.2 Fuel Pellet Diameter and Lattice Pitch

The critical experiments selected for analysis cover a range of fuel pellet diameters from 0.311 to 0.444 inches, and lattice spacings from 0.476 to 1.00 inches. In the rack designs, the fuel pellet diameters range from 0.303 to 0.3805 inches O.D. (0.496 to 0.580 inch lattice spacing) for PWR fuel and from 0.3224 to 0.494 inches O.D. (0.488 to 0.740 inch lattice spacing) for BWR fuel. Thus, the critical experiments analyzed provide a reasonable representation of power reactor fuel. Based on the data in Table 4A.1, there does not appear to be any observable trend with either fuel pellet diameter or lattice pitch, at least over the range of the critical experiments applicable to rack designs.

##### 4A.4.3 Soluble Boron Concentration Effects

Various soluble boron concentrations were used in the B&W series of critical experiments and in one PNL experiment, with boron concentrations ranging up to 2550 ppm. Results of MCNP4a (and one KENO5a) calculations are shown in Table 4A.6. Analyses of the very high boron concentration experiments (> 1300 ppm) show a tendency to slightly overpredict reactivity for the three experiments exceeding 1300 ppm. In turn, this would suggest that the evaluation of the racks with higher soluble boron concentrations could be slightly conservative.

---

<sup>†</sup> Parallel experiments with a depleted uranium reflector were also performed but not included in the present analysis since they are not pertinent to the Holtec rack design.

The number of critical experiments with  $\text{PuO}_2$  bearing fuel (MOX) is more limited than for  $\text{UO}_2$  fuel. However, a number of MOX critical experiments have been analyzed and the results are shown in Table 4A.7. Results of these analyses are generally above a  $k_{\text{eff}}$  of 1.00, indicating that when Pu is present, both MCNP4a and KENO5a overpredict the reactivity. This may indicate that calculation for MOX fuel will be expected to be conservative, especially with MCNP4a. It may be noted that for the larger lattice spacings, the KENO5a calculated reactivities are below 1.00, suggesting that a small trend may exist with KENO5a. It is also possible that the overprediction in  $k_{\text{eff}}$  for both codes may be due to a small inadequacy in the determination of the Pu-241 decay and Am-241 growth. This possibility is supported by the consistency in calculated  $k_{\text{eff}}$  over a wide range of the spectral index (energy of the average lethargy causing fission).

References

- [4A.1] J.F. Briesmeister, Ed., "MCNP4a - A General Monte Carlo N-Particle Transport Code, Version 4A; Los Alamos National Laboratory, LA-12625-M (1993).
- [4A.2] SCALE 4.3, "A Modular Code System for Performing Standardized Computer Analyses for Licensing Evaluation", NUREG-0200 (ORNL-NUREG-CSD-2/U2/R5, Revision 5, Oak Ridge National Laboratory, September 1995.
- [4A.3] M.D. DeHart and S.M. Bowman, "Validation of the SCALE Broad Structure 44-G Group ENDF/B-Y Cross-Section Library for Use in Criticality Safety Analyses", NUREG/CR-6102 (ORNL/TM-12460) Oak Ridge National Laboratory, September 1994.
- [4A.4] W.C. Jordan et al., "Validation of KENO.V.a", CSD/TM-238, Martin Marietta Energy Systems, Inc., Oak Ridge National Laboratory, December 1986.
- [4A.5] O.W. Hermann et al., "Validation of the Scale System for PWR Spent Fuel Isotopic Composition Analysis", ORNL-TM-12667, Oak Ridge National Laboratory, undated.
- [4A.6] R.J. Larsen and M.L. Marx, An Introduction to Mathematical Statistics and its Applications, Prentice-Hall, 1986.
- [4A.7] M.N. Baldwin et al., Critical Experiments Supporting Close Proximity Water Storage of Power Reactor Fuel, BAW-1484-7, Babcock and Wilcox Company, July 1979.
- [4A.8] G.S. Hoovier et al., Critical Experiments Supporting Underwater Storage of Tightly Packed Configurations of Spent Fuel Pins, BAW-1645-4, Babcock & Wilcox Company, November 1991.
- [4A.9] L.W. Newman et al., Urania Gadolinia: Nuclear Model Development and Critical Experiment Benchmark, BAW-1810, Babcock and Wilcox Company, April 1984.

- [4A.10] J.C. Manaranche et al., "Dissolution and Storage Experimental Program with 4.75 w/o Enriched Uranium-Oxide Rods," Trans. Am. Nucl. Soc. 33: 362-364 (1979).
- [4A.11] S.R. Bierman and E.D. Clayton, Criticality Experiments with Subcritical Clusters of 2.35 w/o and 4.31 w/o  $^{235}\text{U}$  Enriched  $\text{UO}_2$  Rods in Water with Steel Reflecting Walls, PNL-3602, Battelle Pacific Northwest Laboratory, April 1981.
- [4A.12] S.R. Bierman et al., Criticality Experiments with Subcritical Clusters of 2.35 w/o and 4.31 w/o  $^{235}\text{U}$  Enriched  $\text{UO}_2$  Rods in Water with Uranium or Lead Reflecting Walls, PNL-3926, Battelle Pacific Northwest Laboratory, December, 1981.
- [4A.13] S.R. Bierman et al., Critical Separation Between Subcritical Clusters of 4.31 w/o  $^{235}\text{U}$  Enriched  $\text{UO}_2$  Rods in Water with Fixed Neutron Poisons, PNL-2615, Battelle Pacific Northwest Laboratory, October 1977.
- [4A.14] S.R. Bierman, Criticality Experiments with Neutron Flux Traps Containing Voids, PNL-7167, Battelle Pacific Northwest Laboratory, April 1990.
- [4A.15] B.M. Durst et al., Critical Experiments with 4.31 wt %  $^{235}\text{U}$  Enriched  $\text{UO}_2$  Rods in Highly Borated Water Lattices, PNL-4267, Battelle Pacific Northwest Laboratory, August 1982.
- [4A.16] S.R. Bierman, Criticality Experiments with Fast Test Reactor Fuel Pins in Organic Moderator, PNL-5803, Battelle Pacific Northwest Laboratory, December 1981.
- [4A.17] E.G. Taylor et al., Saxton Plutonium Program Critical Experiments for the Saxton Partial Plutonium Core, WCAP-3385-54, Westinghouse Electric Corp., Atomic Power Division, December 1965.
- [4A.18] M.G. Natrella, Experimental Statistics, National Bureau of Standards, Handbook 91, August 1963.

Table 4A.1

Summary of Criticality Benchmark Calculations

Reference	Identification	Enrich.	Calculated $k_{eff}$		EALF <sup>†</sup> (eV)		
			MCNP4a	KENO5a	MCNP4a	KENO5a	
1	B&W-1484 (4A.7)	Core I	2.46	0.9964 ± 0.0010	0.9898 ± 0.0006	0.1759	0.1753
2	B&W-1484 (4A.7)	Core II	2.46	1.0008 ± 0.0011	1.0015 ± 0.0005	0.2553	0.2446
3	B&W-1484 (4A.7)	Core III	2.46	1.0010 ± 0.0012	1.0005 ± 0.0005	0.1999	0.1939
4	B&W-1484 (4A.7)	Core IX	2.46	0.9956 ± 0.0012	0.9901 ± 0.0006	0.1422	0.1426
5	B&W-1484 (4A.7)	Core X	2.46	0.9980 ± 0.0014	0.9922 ± 0.0006	0.1513	0.1499
6	B&W-1484 (4A.7)	Core XI	2.46	0.9978 ± 0.0012	1.0005 ± 0.0005	0.2031	0.1947
7	B&W-1484 (4A.7)	Core XII	2.46	0.9988 ± 0.0011	0.9978 ± 0.0006	0.1718	0.1662
8	B&W-1484 (4A.7)	Core XIII	2.46	1.0020 ± 0.0010	0.9952 ± 0.0006	0.1988	0.1965
9	B&W-1484 (4A.7)	Core XIV	2.46	0.9953 ± 0.0011	0.9928 ± 0.0006	0.2022	0.1986
10	B&W-1484 (4A.7)	Core XV <sup>††</sup>	2.46	0.9910 ± 0.0011	0.9909 ± 0.0006	0.2092	0.2014
11	B&W-1484 (4A.7)	Core XVI <sup>††</sup>	2.46	0.9935 ± 0.0010	0.9889 ± 0.0006	0.1757	0.1713
12	B&W-1484 (4A.7)	Core XVII	2.46	0.9962 ± 0.0012	0.9942 ± 0.0005	0.2083	0.2021
13	B&W-1484 (4A.7)	Core XVIII	2.46	1.0036 ± 0.0012	0.9931 ± 0.0006	0.1705	0.1708



Table 4A.1

Summary of Criticality Benchmark Calculations

	Reference	Identification	Enrich.	Calculated $k_{eff}$		EALF <sup>†</sup> (eV)	
				MCNP4a	KENO5a	MCNP4a	KENO5a
14	B&W-1484 (4A.7)	Core XIX	2.46	0.9961 ± 0.0012	0.9971 ± 0.0005	0.2103	0.2011
15	B&W-1484 (4A.7)	Core XX	2.46	1.0008 ± 0.0011	0.9932 ± 0.0006	0.1724	0.1701
16	B&W-1484 (4A.7)	Core XXI	2.46	0.9994 ± 0.0010	0.9918 ± 0.0006	0.1544	0.1536
17	B&W-1645 (4A.8)	S-type Fuel, w/886 ppm B	2.46	0.9970 ± 0.0010	0.9924 ± 0.0006	1.4475	1.4680
18	B&W-1645 (4A.8)	S-type Fuel, w/746 ppm B	2.46	0.9990 ± 0.0010	0.9913 ± 0.0006	1.5463	1.5660
19	B&W-1645 (4A.8)	SO-type Fuel, w/1156 ppm B	2.46	0.9972 ± 0.0009	0.9949 ± 0.0005	0.4241	0.4331
20	B&W-1810 (4A.9)	Case 1 1337 ppm B	2.46	1.0023 ± 0.0010	NC	0.1531	NC
21	B&W-1810 (4A.9)	Case 12 1899 ppm B	2.46/4.02	1.0060 ± 0.0009	NC	0.4493	NC
22	French (4A.10)	Water Moderator 0 gap	4.75	0.9966 ± 0.0013	NC	0.2172	NC
23	French (4A.10)	Water Moderator 2.5 cm gap	4.75	0.9952 ± 0.0012	NC	0.1778	NC
24	French (4A.10)	Water Moderator 5 cm gap	4.75	0.9943 ± 0.0010	NC	0.1677	NC
25	French (4A.10)	Water Moderator 10 cm gap	4.75	0.9979 ± 0.0010	NC	0.1736	NC
26	PNL-3602 (4A.11)	Steel Reflector, 0 separation	2.35	NC	1.0004 ± 0.0006	NC	0.1018

Table 4A.1

Summary of Criticality Benchmark Calculations

Reference	Identification	Enrich.	Calculated $k_{eff}$		EALF <sup>†</sup> (eV)		
			MCNP4a	KENO5a	MCNP4a	KENO5a	
27	PNL-3602 (4A.11)	Steel Reflector, 1.321 cm sepn.	2.35	0.9980 ± 0.0009	0.9992 ± 0.0006	0.1000	0.0909
28	PNL-3602 (4A.11)	Steel Reflector, 2.616 cm sepn	2.35	0.9968 ± 0.0009	0.9964 ± 0.0006	0.0981	0.0975
29	PNL-3602 (4A.11)	Steel Reflector, 3.912 cm sepn.	2.35	0.9974 ± 0.0010	0.9980 ± 0.0006	0.0976	0.0970
30	PNL-3602 (4A.11)	Steel Reflector, infinite sepn.	2.35	0.9962 ± 0.0008	0.9939 ± 0.0006	0.0973	0.0968
31	PNL-3602 (4A.11)	Steel Reflector, 0 cm sepn.	4.306	NC	1.0003 ± 0.0007	NC	0.3282
32	PNL-3602 (4A.11)	Steel Reflector, 1.321 cm sepn.	4.306	0.9997 ± 0.0010	1.0012 ± 0.0007	0.3016	0.3039
33	PNL-3602 (4A.11)	Steel Reflector, 2.616 cm sepn.	4.306	0.9994 ± 0.0012	0.9974 ± 0.0007	0.2911	0.2927
34	PNL-3602 (4A.11)	Steel Reflector, 5.405 cm sepn.	4.306	0.9969 ± 0.0011	0.9951 ± 0.0007	0.2828	0.2860
35	PNL-3602 (4A.11)	Steel Reflector, Infinite sepn. <sup>††</sup>	4.306	0.9910 ± 0.0020	0.9947 ± 0.0007	0.2851	0.2864
36	PNL-3602 (4A.11)	Steel Reflector, with Boral Sheets	4.306	0.9941 ± 0.0011	0.9970 ± 0.0007	0.3135	0.3150
37	PNL-3926 (4A.12)	Lead Reflector, 0 cm sepn.	4.306	NC	1.0003 ± 0.0007	NC	0.3159
38	PNL-3926 (4A.12)	Lead Reflector, 0.55 cm sepn.	4.306	1.0025 ± 0.0011	0.9997 ± 0.0007	0.3030	0.3044
39	PNL-3926 (4A.12)	Lead Reflector, 1.956 cm sepn.	4.306	1.0000 ± 0.0012	0.9985 ± 0.0007	0.2883	0.2930

Table 4A.1

## Summary of Criticality Benchmark Calculations

Reference	Identification	Enrich.	Calculated $k_{eff}$		EALF <sup>†</sup> (eV)		
			MCNP4a	KENO5a	MCNP4a	KENO5a	
40	PNL-3926 (4A.12)	Lead Reflector, 5.405 cm sepn.	4.306	0.9971 ± 0.0012	0.9946 ± 0.0007	0.2831	0.2854
41	PNL-2615 (4A.13)	Experiment 004/032 - no absorber	4.306	0.9925 ± 0.0012	0.9950 ± 0.0007	0.1155	0.1159
42	PNL-2615 (4A.13)	Experiment 030 - Zr plates	4.306	NC	0.9971 ± 0.0007	NC	0.1154
43	PNL-2615 (4A.13)	Experiment 013 - Steel plates	4.306	NC	0.9965 ± 0.0007	NC	0.1164
44	PNL-2615 (4A.13)	Experiment 014 - Steel plates	4.306	NC	0.9972 ± 0.0007	NC	0.1164
45	PNL-2615 (4A.13)	Exp. 009 1.05% Boron-Steel plates	4.306	0.9982 ± 0.0010	0.9981 ± 0.0007	0.1172	0.1162
46	PNL-2615 (4A.13)	Exp. 012 1.62% Boron-Steel plates	4.306	0.9996 ± 0.0012	0.9982 ± 0.0007	0.1161	0.1173
47	PNL-2615 (4A.13)	Exp. 031 - Boral plates	4.306	0.9994 ± 0.0012	0.9969 ± 0.0007	0.1165	0.1171
48	PNL-7167 (4A.14)	Experiment 214R - with flux trap	4.306	0.9991 ± 0.0011	0.9956 ± 0.0007	0.3722	0.3812
49	PNL-7167 (4A.14)	Experiment 214V3 - with flux trap	4.306	0.9969 ± 0.0011	0.9963 ± 0.0007	0.3742	0.3826
50	PNL-4267 (4A.15)	Case 173 - 0 ppm B	4.306	0.9974 ± 0.0012	NC	0.2893	NC
51	PNL-4267 (4A.15)	Case 177 - 2550 ppm B	4.306	1.0057 ± 0.0010	NC	0.5509	NC
52	PNL-5803 (4A.16)	MOX Fuel - Type 3.2 Exp. 21	20% Pu	1.0041 ± 0.0011	1.0046 ± 0.0006	0.9171	0.8868

Table 4A.1

## Summary of Criticality Benchmark Calculations

Reference	Identification	Enrich.	Calculated $k_{eff}$		EALF <sup>†</sup> (eV)		
			MCNP4a	KENO5a	MCNP4a	KENO5a	
53	PNL-5803 (4A.16)	MOX Fuel - Type 3.2 Exp. 43	20% Pu	1.0058 ± 0.0012	1.0036 ± 0.0006	0.2968	0.2944
54	PNL-5803 (4A.16)	MOX Fuel - Type 3.2 Exp. 13	20% Pu	1.0083 ± 0.0011	0.9989 ± 0.0006	0.1665	0.1706
55	PNL-5803 (4A.16)	MOX Fuel - Type 3.2 Exp. 32	20% Pu	1.0079 ± 0.0011	0.9966 ± 0.0006	0.1139	0.1165
56	WCAP-3385 (4A.17)	Saxton Case 52 PuO <sub>2</sub> 0.52" pitch	6.6% Pu	0.9996 ± 0.0011	1.0005 ± 0.0006	0.8665	0.8417
57	WCAP-3385 (4A.17)	Saxton Case 52 U 0.52" pitch	5.74	1.0000 ± 0.0010	0.9956 ± 0.0007	0.4476	0.4580
58	WCAP-3385 (4A.17)	Saxton Case 56 PuO <sub>2</sub> 0.56" pitch	6.6% Pu	1.0036 ± 0.0011	1.0047 ± 0.0006	0.5289	0.5197
59	WCAP-3385 (4A.17)	Saxton Case 56 borated PuO <sub>2</sub>	6.6% Pu	1.0008 ± 0.0010	NC	0.6389	NC
60	WCAP-3385 (4A.17)	Saxton Case 56 U 0.56" pitch	5.74	0.9994 ± 0.0011	0.9967 ± 0.0007	0.2923	0.2954
61	WCAP-3385 (4A.17)	Saxton Case 79 PuO <sub>2</sub> 0.79" pitch	6.6% Pu	1.0063 ± 0.0011	1.0133 ± 0.0006	0.1520	0.1555
62	WCAP-3385 (4A.17)	Saxton Case 79 U 0.79" pitch	5.74	1.0039 ± 0.0011	1.0008 ± 0.0006	0.1036	0.1047

Notes: NC stands for not calculated.

<sup>†</sup> EALF is the energy of the average lethargy causing fission.

<sup>††</sup> These experimental results appear to be statistical outliers ( $> 3\sigma$ ) suggesting the possibility of unusually large experimental error. Although they could justifiably be excluded, for conservatism, they were retained in determining the calculational basis.

Table 4A.2

COMPARISON OF MCNP4a AND KENO5a CALCULATED REACTIVITIES<sup>†</sup>  
FOR VARIOUS ENRICHMENTS

Enrichment	Calculated $k_{eff} \pm 1\sigma$	
	MCNP4a	KENO5a
3.0	0.8465 $\pm$ 0.0011	0.8478 $\pm$ 0.0004
3.5	0.8820 $\pm$ 0.0011	0.8841 $\pm$ 0.0004
3.75	0.9019 $\pm$ 0.0011	0.8987 $\pm$ 0.0004
4.0	0.9132 $\pm$ 0.0010	0.9140 $\pm$ 0.0004
4.2	0.9276 $\pm$ 0.0011	0.9237 $\pm$ 0.0004
4.5	0.9400 $\pm$ 0.0011	0.9388 $\pm$ 0.0004

<sup>†</sup> Based on the GE 8x8R fuel assembly.



Table 4A.3

MCNP4a CALCULATED REACTIVITIES FOR  
CRITICAL EXPERIMENTS WITH NEUTRON ABSORBERS

Ref.	Experiment		$\Delta k$ Worth of Absorber	MCNP4a Calculated $k_{eff}$	EALF <sup>†</sup> (eV)
4A.13	PNL-2615	Boral Sheet	0.0139	0.9994±0.0012	0.1165
4A.7	B&W-1484	Core XX	0.0165	1.0008±0.0011	0.1724
4A.13	PNL-2615	1.62% Boron-steel	0.0165	0.9996±0.0012	0.1161
4A.7	B&W-1484	Core XIX	0.0202	0.9961±0.0012	0.2103
4A.7	B&W-1484	Core XXI	0.0243	0.9994±0.0010	0.1544
4A.7	B&W-1484	Core XVII	0.0519	0.9962±0.0012	0.2083
4A.11	PNL-3602	Boral Sheet	0.0708	0.9941±0.0011	0.3135
4A.7	B&W-1484	Core XV	0.0786	0.9910±0.0011	0.2092
4A.7	B&W-1484	Core XVI	0.0845	0.9935±0.0010	0.1757
4A.7	B&W-1484	Core XIV	0.1575	0.9953±0.0011	0.2022
4A.7	B&W-1484	Core XIII	0.1738	1.0020±0.0011	0.1988
4A.14	PNL-7167	Expt 214R flux trap	0.1931	0.9991±0.0011	0.3722

<sup>†</sup>EALF is the energy of the average lethargy causing fission.

Table 4A.4

COMPARISON OF MCNP4a AND KENO5a  
CALCULATED REACTIVITIES<sup>†</sup> FOR VARIOUS <sup>10</sup>B LOADINGS

<sup>10</sup> B, g/cm <sup>2</sup>	Calculated $k_{eff} \pm 1\sigma$	
	MCNP4a	KENO5a
0.005	1.0381 ± 0.0012	1.0340 ± 0.0004
0.010	0.9960 ± 0.0010	0.9941 ± 0.0004
0.015	0.9727 ± 0.0009	0.9713 ± 0.0004
0.020	0.9541 ± 0.0012	0.9560 ± 0.0004
0.025	0.9433 ± 0.0011	0.9428 ± 0.0004
0.03	0.9325 ± 0.0011	0.9338 ± 0.0004
0.035	0.9234 ± 0.0011	0.9251 ± 0.0004
0.04	0.9173 ± 0.0011	0.9179 ± 0.0004

<sup>†</sup> Based on a 4.5% enriched GE 8x8R fuel assembly.



Table 4A.5

CALCULATIONS FOR CRITICAL EXPERIMENTS WITH  
THICK LEAD AND STEEL REFLECTORS<sup>†</sup>

Ref.	Case	E, wt%	Separation, cm	MCNP4a $k_{eff}$	KENO5a $k_{eff}$
4A.11	Steel Reflector	2.35	1.321	0.9980±0.0009	0.9992±0.0006
		2.35	2.616	0.9968±0.0009	0.9964±0.0006
		2.35	3.912	0.9974±0.0010	0.9980±0.0006
		2.35	∞	0.9962±0.0008	0.9939±0.0006
4A.11	Steel Reflector	4.306	1.321	0.9997±0.0010	1.0012±0.0007
		4.306	2.616	0.9994±0.0012	0.9974±0.0007
		4.306	3.405	0.9969±0.0011	0.9951±0.0007
		4.306	∞	0.9910±0.0020	0.9947±0.0007
4A.12	Lead Reflector	4.306	0.55	1.0025±0.0011	0.9997±0.0007
		4.306	1.956	1.0000±0.0012	0.9985±0.0007
		4.306	5.405	0.9971±0.0012	0.9946±0.0007

<sup>†</sup> Arranged in order of increasing reflector-fuel spacing.

Table 4A.6

CALCULATIONS FOR CRITICAL EXPERIMENTS WITH VARIOUS SOLUBLE BORON CONCENTRATIONS

Reference	Experiment	Boron Concentration, ppm	Calculated $k_{eff}$	
			MCNP4a	KENO5a
4A.15	PNL-4267	0	$0.9974 \pm 0.0012$	-
4A.8	B&W-1645	886	$0.9970 \pm 0.0010$	$0.9924 \pm 0.0006$
4A.9	B&W-1810	1337	$1.0023 \pm 0.0010$	-
4A.9	B&W-1810	1899	$1.0060 \pm 0.0009$	-
4A.15	PNL-4267	2550	$1.0057 \pm 0.0010$	-

Table 4A.7

## CALCULATIONS FOR CRITICAL EXPERIMENTS WITH MOX FUEL

Reference	Case <sup>†</sup>	MCNP4a		KENO5a	
		$k_{\text{eff}}$	EALF <sup>††</sup>	$k_{\text{eff}}$	EALF <sup>††</sup>
PNL-5803 [4A.16]	MOX Fuel - Exp. No. 21	1.0041±0.0011	0.9171	1.0046±0.0006	0.8868
	MOX Fuel - Exp. No. 43	1.0058±0.0012	0.2968	1.0036±0.0006	0.2944
	MOX Fuel - Exp. No. 13	1.0083±0.0011	0.1665	0.9989±0.0006	0.1706
	MOX Fuel - Exp. No. 32	1.0079±0.0011	0.1139	0.9966±0.0006	0.1165
WCAP-3385-54 [4A.17]	Saxton @ 0.52" pitch	0.9996±0.0011	0.8665	1.0005±0.0006	0.8417
	Saxton @ 0.56" pitch	1.0036±0.0011	0.5289	1.0047±0.0006	0.5197
	Saxton @ 0.56" pitch borated	1.0008±0.0010	0.6389	NC	NC
	Saxton @ 0.79" pitch	1.0063±0.0011	0.1520	1.0133±0.0006	0.1555

Note: NC stands for not calculated

† Arranged in order of increasing lattice spacing.

†† EALF is the energy of the average lethargy causing fission.

## 5.0 THERMAL-HYDRAULIC CONSIDERATIONS

### 5.1 Introduction

This section provides a summary of the methods, models, analyses and numerical results to demonstrate the compliance of Harris Spent Fuel Pools C and D with the provisions of Section III of the USNRC "OT Position Paper for Review and Acceptance of Spent Fuel Storage and Handling Applications", (April 14, 1978) for a bounding configuration. Similar methods of thermal-hydraulic analysis have been used in other rerack licensing projects (see Table 5.1.1).

The thermal-hydraulic qualification analyses for the rack array may be broken down into the following categories:

- (i) Evaluation of the long-term decay heat load, which is the cumulative spent fuel decay heat generation from all fuel assemblies stored in the C and D pools.
- (ii) Evaluation of the steady-state bulk pool temperatures when forced cooling is available. The bulk pool temperatures are required to be maintained  $\leq 137^{\circ}\text{F}$ <sup>†</sup> under normal conditions with fuel pool cooling in operation.
- (iii) Determination of the maximum pool local temperature at steady bulk pool temperatures.
- (iv) Evaluation of the potential for flow bypass from pool inlet to outlet in the absence of a sparger line to the spent fuel pools racks.
- (v) Evaluation of the "time-to-boil" if all forced heat rejection paths from the pool are lost.

---

<sup>†</sup> The 137°F limit is consistent with that currently in the Harris FSAR and procedures for pools A and B. CP&L is in the process of re-evaluating systems and components to allow for an increase in the allowable bulk pool temperature.

This section presents a synopsis of the analysis methods employed, and final results. The decay heat load calculation is conservatively performed in accordance with the provisions of USNRC Branch Technical Position ASB9-2, "Residual Decay Energy for Light Water Reactors for Long Term Cooling", Rev. 2, July, 1981.

The Pool C and D fuel rack configurations for proposed expansion are depicted in Figures 1.2 and 1.3. A total of 1,952 PWR cells and 2,763 BWR cells will be available in a bounding configuration to maximize fuel storage capacity.

To determine the limiting decay heat in the Harris spent fuel pools, a projected bounding decay period for fuel scenario is considered as shown in Table 5.2.1. The in-core irradiation time and limiting assembly specific power inputs are provided in Table 5.2.2. The C and D spent fuel pools (SFPs) are designated to store old fuel which has been cooled for at least 5 years. The fuel is envisaged to be transhipped from Brunswick and Robinson plants or shuffled from Harris' Pools A and/or B.

Since the decay heat load from the old assemblies varies very slowly as a function of time, the long-term decay heat in the bounding configuration is assumed to be constant. Based on the discharge scenario and fuel assemblies characteristics listed in Tables 5.2.1 and 5.2.2, the combined Pools C and D decay heat rates are determined and summarized in Table 5.2.3.

The decay heat load to the two pools (C and D) will be removed by several passive and active heat rejection mechanisms, as listed below:

- (a) Heat loss by pool surface evaporation
- (b) Radiation heat loss from pool surface to fuel handling building extremities
- (c) Natural convection heat transfer to fuel building air
- (d) Heat loss through pool concrete walls
- (e) Forced convection cooling of SFP surface by HVAC system forced air ventilation
- (f) Forced cooling by SFP water circulation through a heat exchanger

In the interest of conservatism, no credit is applied to removing heat by any of the mechanisms listed above from (a) to (e). Consequently, all of the decay heat generated in the C and D pools is considered to be removed by the forced flow of SFP cooling water circulating through a heat exchanger, which transfers heat to the CCW system. In a forced SFP cooling scenario, hot water from the pool is circulated by a pump through an exchanger cooled by the CCW system. The cooled SFP water is then directed back to the C and D pools. The decay heat load in the C and D pools is from old fuel discharges, which is relatively constant (i.e., steady heat load). Therefore, at equilibrium conditions, the total decay heat load to the pool is equal to the heat removed by the cooling system and a constant bulk temperature is maintained in the C and D pools.

The heat removal capacity of the SFP cooling system is principally characterized by two parameters, namely the water circulation flow rate and the fuel pool inlet water temperature. The bulk pool temperature of pools C and D is required to be maintained at or below 137°F<sup>†</sup>. The minimum SFP water flow rate required to comply with this bulk pool temperature criterion is thus a function of the fuel pool inlet water temperature. This requirement is graphically illustrated in Figure 5.3.1. A SFP cooling system design point, which is on the curve, satisfies the minimum cooling requirements. A design point above this curve exceeds the SFP cooling

---

<sup>†</sup> The 137°F limit is consistent with that currently in the Harris FSAR and procedures for pools A and B. CP&L is in the process of re-evaluating systems and components to allow for an increase in the allowable bulk pool temperature.



requirements. Therefore, Figure 5.3.1 establishes the thermal-hydraulic design basis for SFP cooling system capacity and the final cooling system design shall comply with these flow vs. inlet temperature parameters.

#### 5.4 Local Temperature Analysis

In this section, we present the methodology for calculating the local temperatures when forced cooling is available to the Pool C only. The results from evaluations performed with forced cooling in pool C only are conservative, since the pool cooling system will be connected to both pools and cooling water will be discharged to both pools. Therefore, these evaluations predict conservative local temperatures, especially in pool D.

Truncation of sparger lines has become a standard pool modification procedure in rerack campaigns in recent years. Over a dozen SFPs reracked in the past several years have removed sparger lines to enable a high density storage layout and thus maximize pool capacity. Absence of a sparger in the Harris C and D pools removes the mechanistic feed of cold water into the bottom plenum of the fuel racks. It is not apparent from heuristic reasoning alone that the cooled water delivered to the pool would not bypass the hot fuel racks and the stored spent fuel in the two pools and exit through the outlet piping. To demonstrate adequate cooling of fuel in the two areas, it is therefore necessary to rigorously quantify the velocity field in the pool created by the interaction of buoyancy driven flows and water ingress/egress. A CFD analysis for this demonstration is required. The objective of this study is to demonstrate that the principal thermal-hydraulic criteria of ensuring local subcooled conditions in the pool is met for the bounding fuel storage configuration. An outline of the CFD approach is described in the following.

Figure 5.4.1 depicts the fuel Pools C and D physical configuration in plan view. The two pools are connected by a transfer canal. Pool piping connections for introducing cooling water and discharge of heated water are shown for both pools. Currently, SFP cooling system design work

is in progress to provide a forced cooling system which will provide suction and discharge to both pools. Thermal-hydraulic adequacy of the two pools shall be conservatively demonstrated by assuming that forced cooling is available to only Pool C. Adequate cooling of Pool D is enabled by a buoyancy-driven flow of relatively cooler bulk Pool C water to Pool D through the interconnecting transfer canal. Decay heat inputs to both pools are based on a bounding fuel storage configuration and spent fuel cooling times. The buoyancy-induced cooling of Pool D is demonstrated by performing a rigorous Computational Fluid Dynamics (CFD) analysis of the temperature and flow fields in the two pools. The CFD methodology is discussed in the next subsection. An additional assumption about the location of cooling inlet and outlet piping is included in the analysis to result in an extremely conservative thermal-hydraulic portrayal of the two interconnected pools. The pool cooling inlet and outlet piping connections are assumed to be located on the southeast end of the pool. Thus, forced cooling of the pool is in a diagonally opposite (i.e., farthest) corner from the northwest location of the connection from Pool C to the transfer canal. The forced cooling ingress and egress locations are in close proximity to each other and at the same elevation. The potential for flow bypass from inlet to outlet is conservative, since the modeled locations are closer than the actual relative positions.

There are several significant geometric and thermal-hydraulic features of the Harris SFPs which need to be considered for a rigorous CFD analysis. From a fluid flow modeling standpoint, there are two regions to be considered. One region is the bulk pool region where the classical Navier-Stokes equations are solved with turbulence effects included. The other region is the heat generating fuel assemblies located in the spent fuel racks located near the bottom of the SFP. In this region, water flow is directed vertically upwards due to buoyancy forces through relatively small flow channels formed by stored fuel assembly rod arrays in each rack cell. This situation shall be modeled as a porous solid region in which fluid flow is governed by the classical Darcy's Law:

$$\frac{\partial P}{\partial x_i} = - \frac{\mu}{K(i)} v_i - C\rho|v|v_i / 2$$



where  $\delta p / \delta X_i$  is the pressure gradient,  $K(i)$ ,  $V_i$  and  $C$  are the corresponding permeability, velocity and inertial resistance parameters and  $\mu$  is the fluid viscosity. Bounding permeability and inertial resistance parameters for the rack cells loaded with PWR or BWR fuel is determined based on friction factor correlations for laminar flow conditions typically encountered due to low buoyancy induced velocities and small size of the flow channels. A large number of fuel assembly types have been analyzed for hydraulic flow resistance [5.4.1] determination. Table 5.4.1 provides flow resistance parameters which bound all PWR and BWR fuel assembly types which were analyzed in this study.

The pool geometry requires an adequate portrayal of large scale and small scale features, spatially distributed heat sources in the spent fuel racks and water inlet/outlet configuration. Relatively cooler bulk pool water normally flows down through the narrow fuel rack outline to pool wall liner clearance known as the downcomer. Near the bottom of the racks, the flow turns from a vertical to horizontal direction into the bottom plenum supplying cooling water to the rack cells. Heated water issuing out of the top of the racks mixes with the bulk pool water. An adequate modeling of these features on the CFD program involves meshing the large scale bulk pool region and small scale downcomer and bottom plenum regions with sufficient number of computational cells to capture the bulk and local features of the flow field.

The CFD analysis is performed on the industry standard FLUENT [5.4.2] fluid flow and heat transfer modeling program. The FLUENT code enables buoyancy flow and turbulence effects to be included in the CFD analysis. Turbulence effects are modeled by relating time-varying "Reynolds's Stresses" to the mean bulk flow quantities with the following turbulence modeling options:

- (i)  $\kappa$ - $\epsilon$  Model
- (ii) RNG  $\kappa$ - $\epsilon$  Model
- (iii) Reynolds Stress Model

The  $\kappa$ - $\epsilon$  model is considered appropriate for the fuel pool CFD analysis. Rigorous modeling of fluid flow problems requires a numerical solution to the classical Navier-Stokes equations of fluid motion [5.4.3].

The governing equations (in modified form for turbulent flows with buoyancy effects included) can be written as:

$$\frac{\partial \rho_o u_i}{\partial t} + \frac{\partial \rho_o u_i u_j}{\partial x_j} = \frac{\partial}{\partial x_j} \left[ \mu \left( \frac{\partial u_i}{\partial x_j} + \frac{\partial u_j}{\partial x_i} \right) \right] - \frac{\partial p}{\partial x_i} - \rho_o \beta (T - T_o) g_i + \frac{\partial \rho_o \langle u'_i u'_j \rangle}{\partial x_j}$$

where  $u_i$  are the three time-averaged velocity components.  $\rho \langle u'_i u'_j \rangle$  are time-averaged Reynolds stresses derived from the turbulence induced fluctuating velocity components  $u'_i$ ,  $\rho_o$  is the fluid density at temperature  $T_o$ ,  $\beta$  is the coefficient of thermal expansion,  $\mu$  is the fluid viscosity,  $g_i$  are the components of gravitational acceleration and  $x_j$  are the Cartesian coordinate directions. The Reynolds stress tensor is expressed in terms of the mean flow quantities by defining a turbulent viscosity  $\mu_t$  and a turbulent velocity scale  $\kappa^{1/2}$  as shown below [5.4.4]:

$$\rho \langle u'_i u'_j \rangle = 2/3 \rho \kappa \delta_{ij} - \mu_t \left[ \frac{\partial u_i}{\partial x_j} + \frac{\partial u_j}{\partial x_i} \right]$$

The procedure to obtain the turbulent viscosity and velocity length scales involves a solution of two additional transport equations for kinetic energy ( $\kappa$ ) and rate of energy dissipation ( $\epsilon$ ). This methodology is known as the  $\kappa$ - $\epsilon$  model for turbulent flows as described by Launder and Spalding [5.4.5].

#### 5.4.1 Time-to-Boil

If all heat exchanger assisted forced pool cooling becomes unavailable, then the pool water will begin to rise in temperature and eventually will reach the normal bulk boiling temperature at 212°F. The time to reach the boiling point will be the shortest when the loss of forced cooling occurs at the point in time when the bulk pool temperature is at its maximum calculated value for a bounding fuel storage configuration. The calculation is conservatively performed for a bounding decay heat load to the pool, no credit for evaporation cooling and no credit for thermal inertia of racks. The amount of water holdup above the racks in the two pools is in excess of 48,000 ft<sup>3</sup> (2.9 x 10<sup>6</sup> lbs) of water. The maximum rate of temperature rise of bulk pools water at a bounding 15.63 million Btu/hr decay heat input (Table 5.2.3) is therefore less than 5.4°F/hr with no water makeup. If the initial temperature is conservatively assumed to be at a uniform maximum bulk average limit of 140°F<sup>†</sup>, then the time to reach normal boiling point of the bulk pool is in excess of 13 hours. This is a relatively long time period for operator action to start makeup water and re-initiate forced cooling to the pool.

#### 5.5 CFD Analysis of C and D Fuel Pools

A summary of pools dimensional data used to generate a Computational Fluid Dynamics (CFD) model of the two interconnected C and D pools is provided in Table 5.5.1. The CFD model provides a determination of the difference between the peak local and bulk pool temperatures. The local temperature corresponding to the maximum bulk pool temperature can then be determined by adding this local temperature rise to the bulk temperature limit. In the CFD model, a *minimum* bounding downcomer gap between racks outline to pool liner is applied as noted in Table 5.5.1. In this manner, the downcomer water flow path hydraulic resistance is *maximized*. Consequently, the local rack cell temperature predictions shall be conservatively maximized. The background constant decay heat input to the pool is modeled as a uniform volumetric heat source term in the active fuel region of the Pools C and D racks. The total heat

---

<sup>†</sup> The assumption of an initial temperature of 140°F is conservative, since the bulk pool temperature is currently limited to 137°F.



generating volume is calculated to be  $657 \text{ m}^3$ . Thus, from the total decay heat input (Table 5.2.3), the volumetric heat source term is determined to be  $6,956 \text{ W/m}^3$ .

A plan view of the three-dimensional CFD model is presented in Figure 5.5.1. In this view, the two pools with an interconnected transfer canal is depicted. The water inlet/outlet connections are shown modeled in the top left end corner of the Pool C. The racks outline, modeled as a porous media, is depicted in blue color. A perspective view of the CFD model is presented in Figure 5.5.2. The bottom of the transfer canal, as shown in this figure, is at the same elevation as the top of the racks. The average background decay heat is applied to the model as a volumetric heat source term in the active fuel region of the fuel racks. The CFD model of the C and D pools is solved to obtain converged temperature and velocity profiles. The results obtained from the analysis are discussed next.

Peak local water temperature in the rack cells is shown as a contour plot in cross sectional plan view as shown in Figure 5.5.3. The plan view elevation is within the region of the racks above the active fuel region, but below the top of the racks.

An exchange of cold and hot water streams from the Pool D to Pool C is determined by the CFD solution with only pool C cooled by a forced cooling system. This exchange of cold and hot water between the two bulk pools is illustrated as a flow velocity vectors plot (Figure 5.5.4) in the pools' interconnecting channel. The peak local temperature is  $6.8^\circ\text{F}$  above the water temperature at the cooling system discharge from pool. Consequently, the peak local temperature corresponding to the maximum bulk pool temperature limit is obtained by adding this local temperature rise. Table 5.5.2 provides the bulk and local temperature summaries. The peak  $143.8^\circ\text{F}$  local temperature is below the local water boiling temperature by a large margin.

Figure 5.5.5 provides a flow velocity vectors plot in the pool cooling inlet/outlet piping region. The pool inlet piping is modeled to be 12 inches below the pool water level and the pool outlet piping suction is adjacent to the inlet piping discharge at the same elevation. From the velocity vectors plot, it is apparent that no bypass of incoming water to outlet is indicated for an



extremely conservative configuration. In the actual pool piping arrangement for Pool C, the water inlet and outlet connections are widely separated. Consequently, it is concluded that any water bypass from inlet to outlet is *not* possible.

References

- [5.4.1] Holtec Report HI-951325, "HI-STAR 100 System Thermal Design Package".
- [5.4.2] "QA Documentation and Validation of the FLUENT Version 4.3 CFD Analysis Program", Holtec Report HI-961444.
- [5.4.3] Batchelor, G.K., "An Introduction to Fluid Dynamics", Cambridge University Press, 1967.
- [5.4.4] Hinze, J.O., "Turbulence", McGraw Hill Publishing Co., New York, NY, 1975.
- [5.4.5] Launder, B.E., and Spalding, D.B., "Lectures in Mathematical Models of Turbulence", Academic Press, London, 1972.

Table 5.1.1

PARTIAL LISTING OF RERACK APPLICATIONS USING  
SIMILAR METHODS OF THERMAL-HYDRAULIC ANALYSIS

PLANT	DOCKET NO.
Enrico Fermi Unit 2	USNRC 50-341
Quad Cities 1 and 2	USNRC 50-254, 50-265
Rancho Seco	USNRC 50-312
Grand Gulf Unit 1	USNRC 50-416
Oyster Creek	USNRC 50-219
Pilgrim	USNRC 50-293
V.C. Summer	USNRC 50-395
Diablo Canyon Units 1 and 2	USNRC 50-275, 50-455
Byron Units 1 and 2	USNRC 50-454, 50-455
Braidwood Units 1 and 2	USNRC 50-456, 50-457
Vogtle Unit 2	USNRC 50-425
St. Lucie Unit 1	USNRC 50-425
Millstone Point Unit 1	USNRC 50-245
D.C. Cook Units 1 and 2	USNRC 50-315, 50-316
Indian Point Unit 2	USNRC 50-247
Three Mile Island Unit 1	USNRC 50-289
J.A. FitzPatrick	USNRC 50-333
Shearon Harris	USNRC 50-400
Hope Creek	USNRC 50-354
Kuosheng Units 1 and 2	Taiwan Power Company
Chin Shan Units 1 and 2	Taiwan Power Company



1  
 2  
 3  
 4  
 5  
 6  
 7  
 8  
 9  
 10  
 11  
 12  
 13  
 14  
 15  
 16  
 17  
 18  
 19  
 20  
 21  
 22  
 23  
 24  
 25  
 26  
 27  
 28  
 29  
 30  
 31  
 32  
 33  
 34  
 35  
 36  
 37  
 38  
 39  
 40  
 41  
 42  
 43  
 44  
 45  
 46  
 47  
 48  
 49  
 50  
 51  
 52  
 53  
 54  
 55  
 56  
 57  
 58  
 59  
 60  
 61  
 62  
 63  
 64  
 65  
 66  
 67  
 68  
 69  
 70  
 71  
 72  
 73  
 74  
 75  
 76  
 77  
 78  
 79  
 80  
 81  
 82  
 83  
 84  
 85  
 86  
 87  
 88  
 89  
 90  
 91  
 92  
 93  
 94  
 95  
 96  
 97  
 98  
 99  
 100

Table 5.1.1 (continued)

PARTIAL LISTING OF RERACK APPLICATIONS USING  
SIMILAR METHODS OF THERMAL-HYDRAULIC ANALYSIS

PLANT	DOCKET NO.
Ulchin Unit 2	Korea Electric Power Corporation
Laguna Verde Units 1 and 2	Comision Federal de Electricidad
Zion Station Units 1 and 2	USNRC 50-295, 50-304
Sequoyah	USNRC 50-327, 50-328
La Salle Unit One	USNRC 50-373
Duane Arnold	USNRC 50-331
Fort Calhoun	USNRC 50-285
Nine Mile Point Unit One	USNRC 50-220
Beaver Valley Unit One	USNRC 50-334
Limerick Unit 2	USNRC 50-353
Ulchin Unit 1	Korea Electric Power Corporation

Table 5.2.1

DECAY PERIODS FOR A BOUNDING POOLS C AND D  
STORAGE CONFIGURATION

PWR Fuel Assemblies		BWR Fuel Assemblies	
Number of Assys	Decay Period	Number of Assys	Decay Period
172	5 years	456	5 years
172	7 years	456	7 years
172	9 years	456	9 years
172	11 years	456	11 years
172	13 years	456	13 years
172	15 years	483	15 years
172	17 years		
172	19 years		
172	21 years		
172	23 years		
232	25 years		



Table 5.2.2	
FUEL ASSEMBLIES INPUT DATA FOR DECAY HEAT EVALUATION	
Item	Value
PWR Assembly Irradiation Time	1,915 EFPD <sup>†</sup>
PWR Assembly Specific Power	19.11 MWt
BWR Assembly Irradiation Time	2,028 EFPD
BWR Assembly Specific Power	4.66 MWt

---

<sup>†</sup> Effective Full Power Days



Table 5.2.3 BOUNDING DECAY HEAT INPUT FROM STORED FUEL IN POOLS C AND D	
Fuel Assemblies	Decay Heat Load (Million Btu/hr)
BWR Fuel Assemblies	4.47
PWR Fuel Assemblies	11.16
Total	15.63 (4.57 MW)

Table 5.4.1

BOUNDING FUEL ASSEMBLIES HYDRAULIC FLOW RESISTANCE PARAMETERS

Parameter	Value
Permeability	$10^{-6} \text{ m}^2$
Inertial Resistance Factor	$95 \text{ m}^{-1}$

Table 5.5.1

POOLS C AND D DIMENSIONAL DATA

Parameter	Value
Pool C: Length Width	597.88" 320.60"
Pool D: Length Width	383.36" 237.79"
Water Depth	38.5 ft
Pools-to-Transfer Canal Channel Width	24"
Bottom Plenum	6"
Pool C Downcomers North Wall South Wall East Wall West Wall	1.44" <sup>†</sup> 1.44" 2.36" 2.36"
Pool D Downcomers North Wall South Wall East Wall West Wall	5.15" 5.0" 5.0" 5.0"

<sup>†</sup> A minimum uniform downcomer gap equal to 1.44" applied to both pools for CFD analysis.

Table 5.5.2

BULK AND LOCAL TEMPERATURES SUMMARY

Item	Temperature (°F) †
Local temperature rise above bulk	6.8
Bulk pool maximum temperature limit	137.0
Peak Local Temperature	143.8

---

† Local temperature values are conservatively computed based on neglecting forced cooling to pool D, as discussed at the beginning of Section 5.4

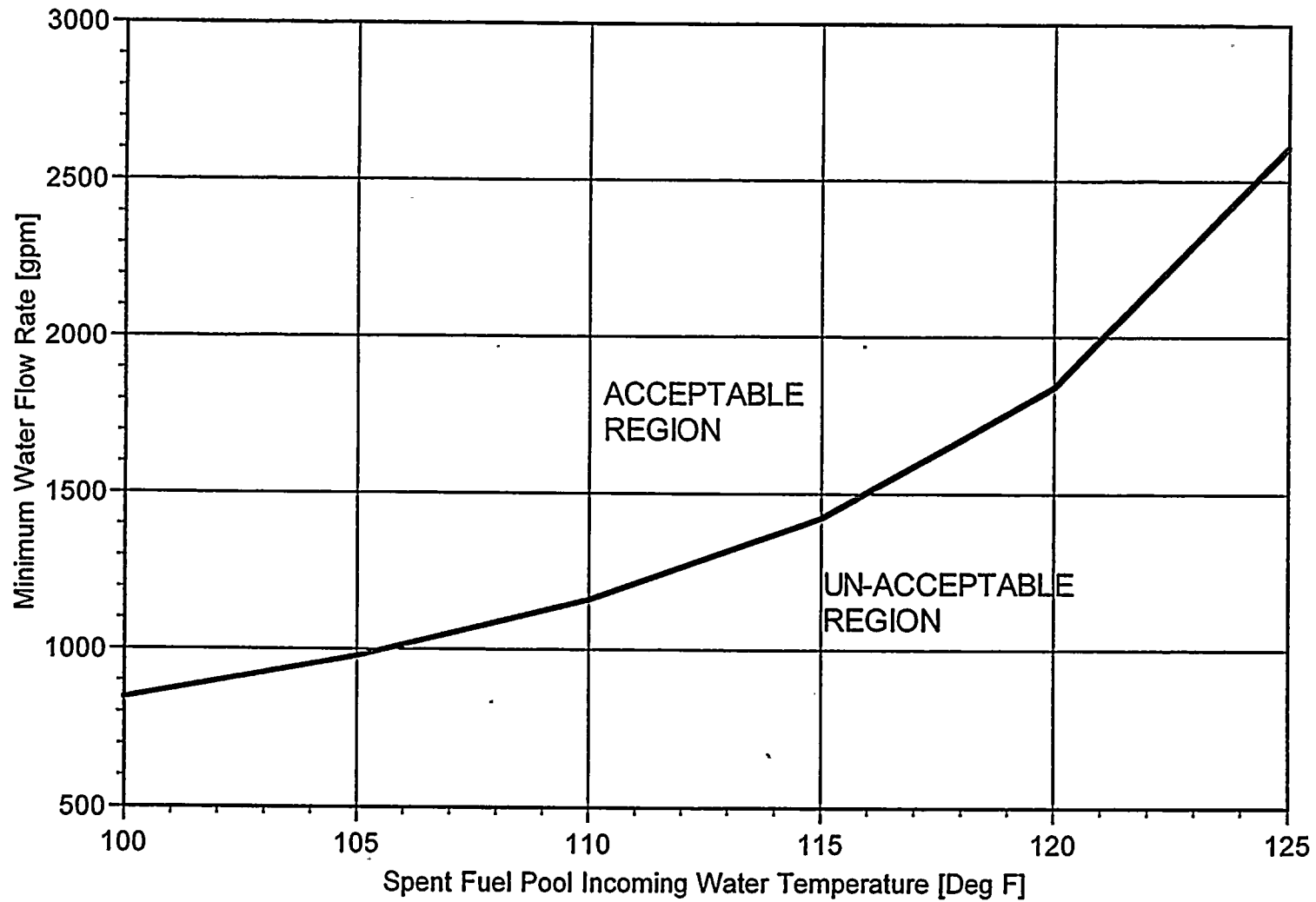


FIGURE 5.3.1: C AND D POOLS MINIMUM TOTAL COOLING SYSTEM REQUIREMENTS CURVE AT 137 Deg. F BULK POOL TEMPERATURE

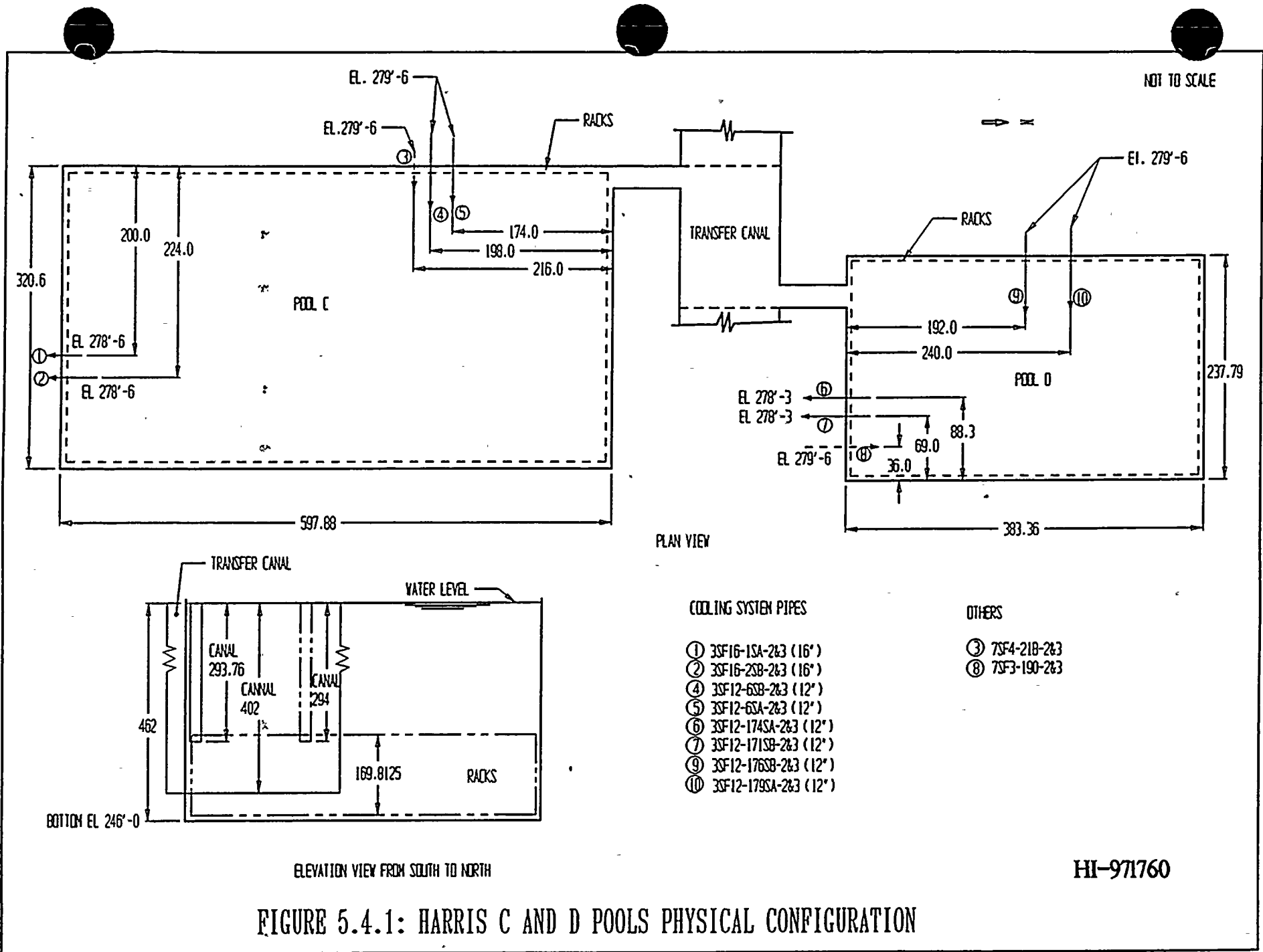


FIGURE 5.4.1: HARRIS C AND D POOLS PHYSICAL CONFIGURATION

HI-971760

70324\HI971760\5\_4\_1

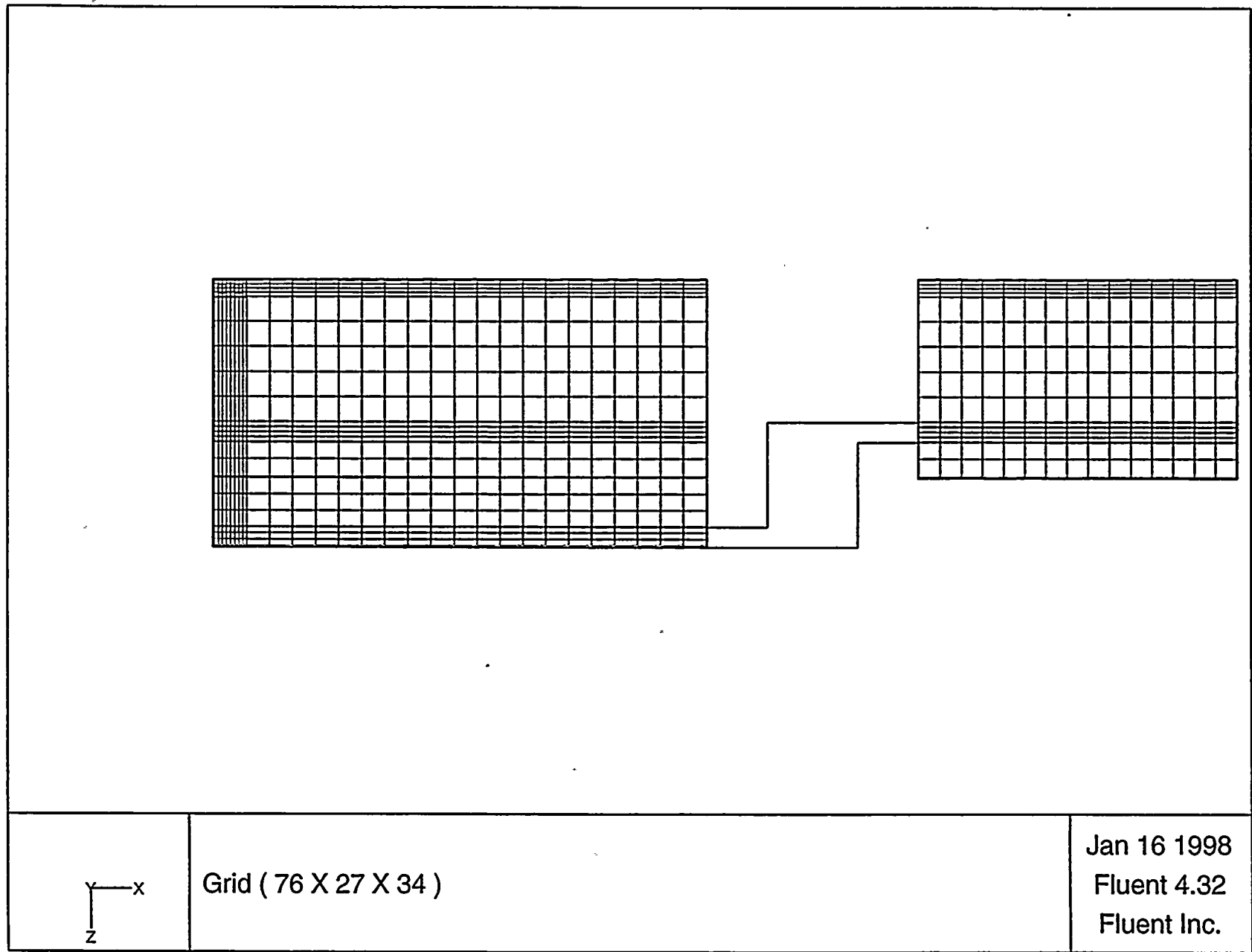
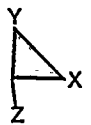
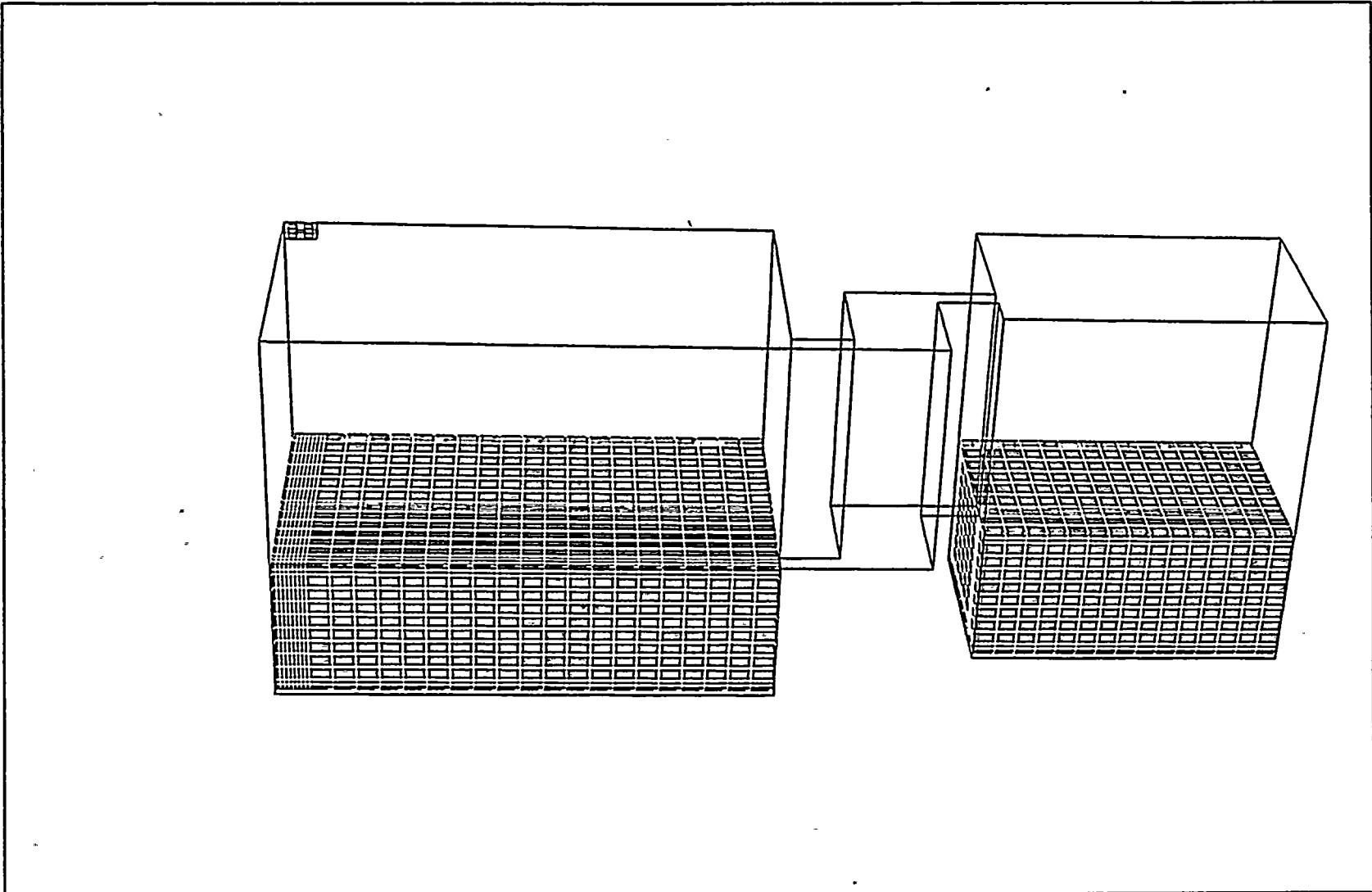


FIGURE 5.5.1: PLAN VIEW OF THE HARRIS POOLS C AND D CFD MODEL

HI-971760



Grid ( 76 X 27 X 34 )

Jan 15 1998  
Fluent 4.32  
Fluent Inc.

FIGURE 5.5.2: PERSPECTIVE VIEW OF THE HARRIS POOLS C AND D CFD MODEL

HI-971760

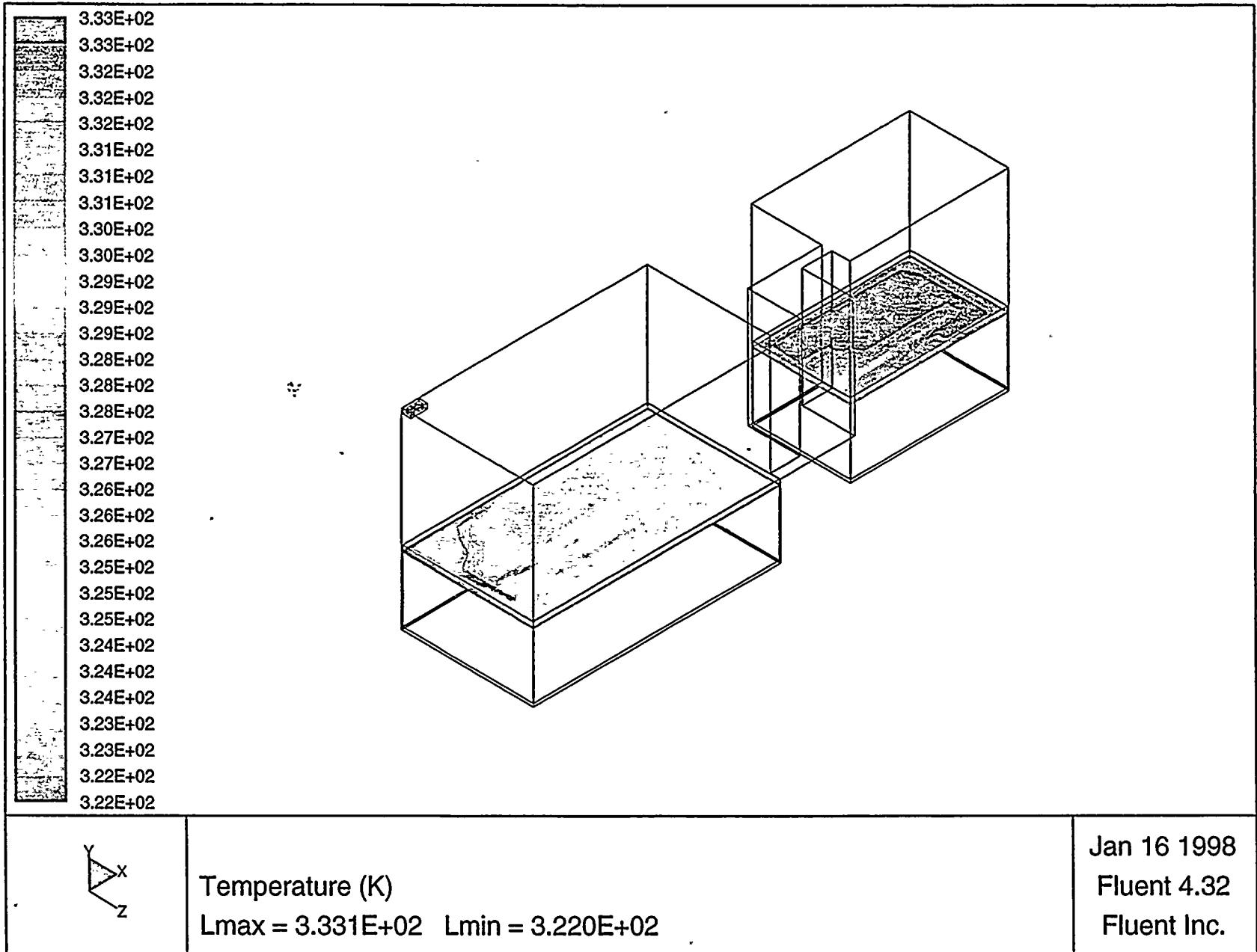


FIGURE 5.5.3: PEAK LOCAL WATER TEMPERATURE IN THE RACK CELLS

HI-971760

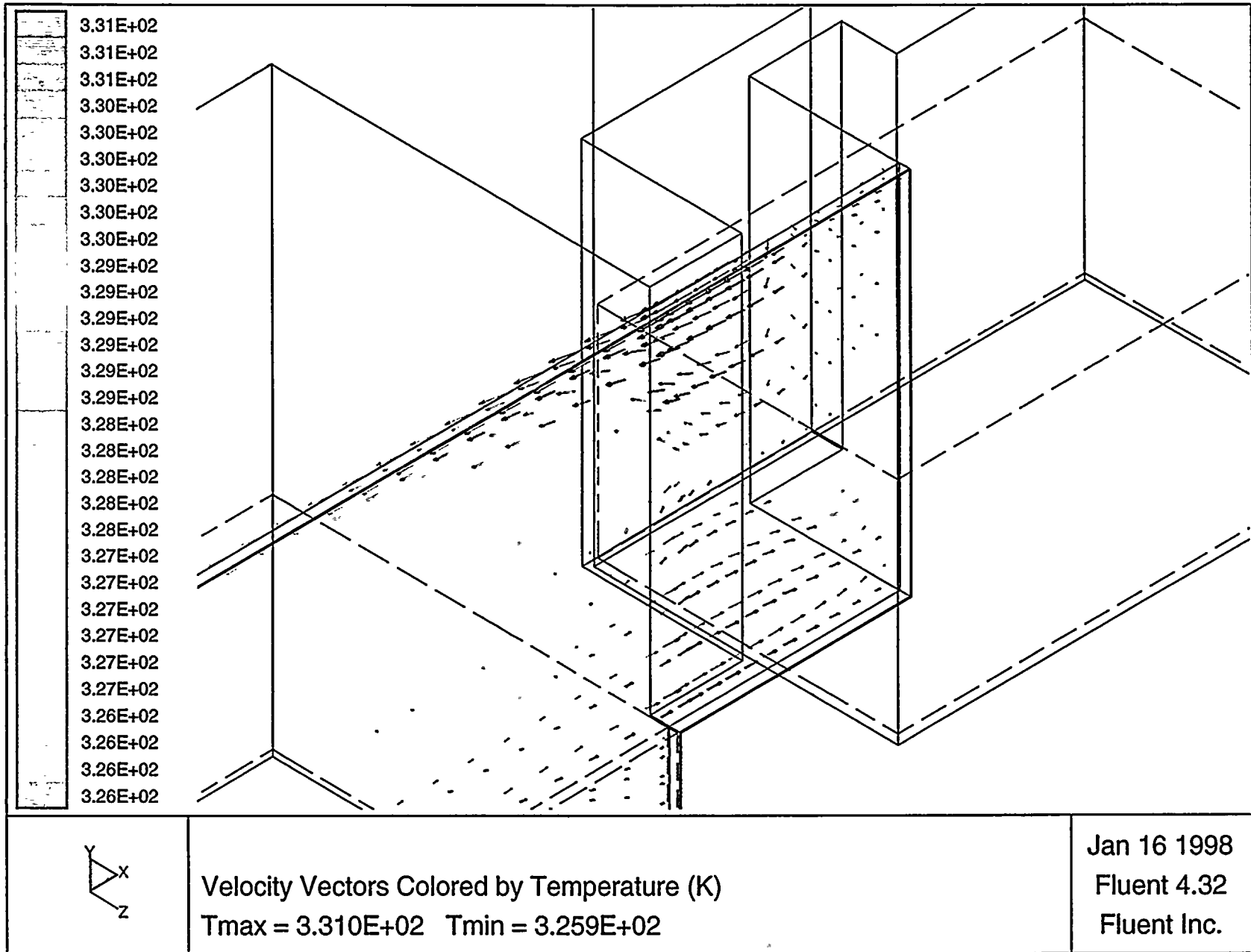


FIGURE 5.5.4: POOLS INTERCONNECTING CHANNEL FLOW VELOCITY VECTORS ELEVATION VIEW PLOT



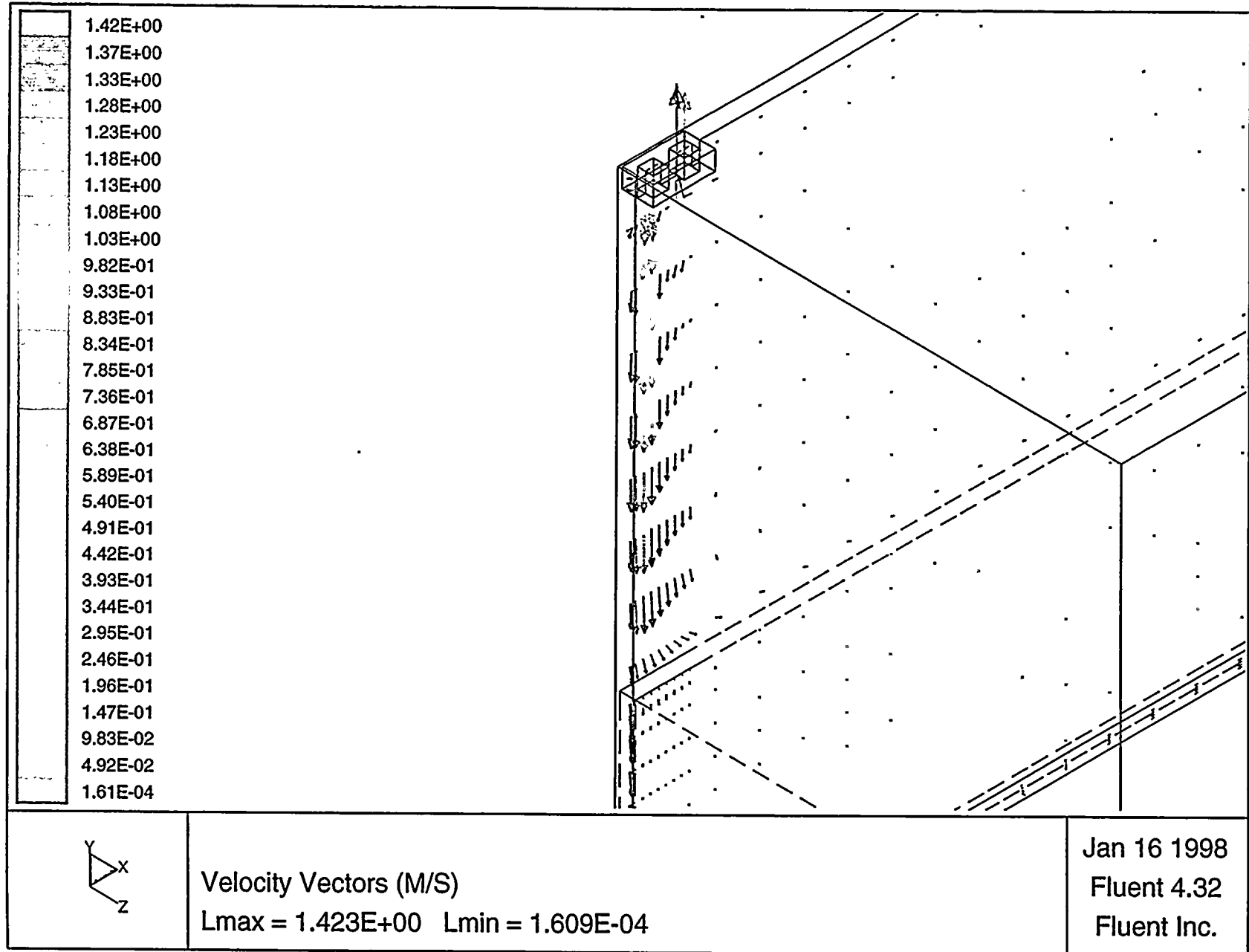


FIGURE 5.5.5: POOL COOLING INLET/OUTLET PIPING REGION FLOW VELOCITY VECTORS PLOT

## 6.0 STRUCTURAL/SEISMIC CONSIDERATIONS

### 6.1 Introduction

This section considers the structural adequacy of the new maximum density spent fuel racks under all loadings postulated for normal, seismic, and accident conditions at Harris. The existing spent fuel storage racks are also examined for stability during the installation process. The analyzed storage rack configurations with the new racks in place are shown in Figures 1.2 and 1.3.

The analyses undertaken to confirm the structural integrity of the racks are performed in compliance with the USNRC Standard Review Plan [6.1.1] and the OT Position Paper [6.1.2]. For each of the analyses, an abstract of the methodology, modeling assumptions, key results, and summary of parametric evaluations are presented. Delineation of the relevant criteria are discussed in the text associated with each analysis.

### 6.2 Overview of Rack Structural Analysis Methodology

The response of a free-standing rack module to seismic inputs is highly nonlinear and involves a complex combination of motions (sliding, rocking, twisting, and turning), resulting in impacts and friction effects. Some of the unique attributes of the rack dynamic behavior include a large fraction of the total structural mass in a confined rattling motion, friction support of rack pedestals against lateral motion, and large fluid coupling effects due to deep submergence and independent motion of closely spaced adjacent structures.

Linear methods, such as modal analysis and response spectrum techniques, cannot accurately simulate the structural response of such a highly nonlinear structure to seismic excitation. An accurate simulation is obtained only by direct integration of the nonlinear equations of motion with the three pool slab acceleration time-histories applied as the forcing functions acting simultaneously.

Whole Pool Multi-Rack (WPMR) analysis is the vehicle utilized in this project to simulate the dynamic behavior of the complex storage rack structures. The following sections provide the basis for this selection and discussion on the development of the methodology.

#### 6.2.1 Background of Analysis Methodology

Reliable assessment of the stress field and kinematic behavior of the rack modules calls for a conservative dynamic model incorporating all *key attributes* of the actual structure. This means that the model must feature the ability to execute the concurrent motion forms compatible with the free-standing installation of the modules.

The model must possess the capability to effect momentum transfers which occur due to rattling of fuel assemblies inside storage cells and the capability to simulate lift-off and subsequent impact of support pedestals with the pool liner (or bearing pad). The contribution of the water mass in the interstitial spaces around the rack modules and within the storage cells must be modeled in an accurate manner since erring in quantification of fluid coupling on either side of the actual value is no guarantee of conservatism.

The Coulomb friction coefficient at the pedestal-to-pool liner (or bearing pad) interface may lie in a rather wide range and a conservative value of friction cannot be prescribed *a priori*. In fact, a perusal of results of rack dynamic analyses in numerous docket (Table 6.2.1) indicates that an upper bound value of the coefficient of friction often maximizes the computed rack displacements as well as the equivalent elastostatic stresses.

In short, there are a large number of parameters with potential influence on the rack kinematics. The comprehensive structural evaluation must deal with all of these without sacrificing conservatism.

The three-dimensional single rack dynamic model introduced by Holtec International in the Enrico Fermi Unit 2 rack project (ca. 1980) and used in some 50 rerack projects since that time (Table 6.2.1) addresses most of the above mentioned array of parameters. The details of this methodology are also published in the permanent literature [6.2.1]. Despite the versatility of the 3-D seismic model, the accuracy of the single rack simulations has been suspect due to one key element; namely, hydrodynamic participation of water around the racks. During dynamic rack motion, hydraulic energy is either drawn from or added to the moving rack, modifying its submerged motion in a significant manner. Therefore, the dynamics of one rack affects the motion of all others in the pool.

A dynamic simulation which treats only one rack, or a small grouping of racks, is intrinsically inadequate to predict the motion of rack modules with any quantifiable level of accuracy. Three-dimensional Whole Pool Multi-Rack analyses carried out on several previous plants demonstrate that single rack simulations under predict rack displacement during seismic responses [6.2.2].

Briefly, the 3-D rack model dynamic simulation, involving one or more spent fuel racks, handles the array of variables as follows:

Interface Coefficient of Friction: Parametric runs are made with upper bound and lower bound values of the coefficient of friction. The limiting values are based on experimental data which have been found to be bounded by the values 0.2 and 0.8. Simulations are also performed with the array of pedestals having randomly chosen coefficients of friction in a Gaussian distribution with a mean of 0.5 and lower and upper limits of 0.2 and 0.8, respectively. In the fuel rack simulations, the Coulomb friction interface between rack support pedestal and liner is simulated by piecewise linear (friction) elements. These elements function only when the pedestal is physically in contact with the pool liner.



Rack Beam Behavior: Rack elasticity, relative to the rack base, is included in the model by introducing linear springs to represent the elastic bending action, twisting, and extensions.

Impact Phenomena: Compression-only gap elements are used to provide for opening and closing of interfaces such as the pedestal-to-bearing pad interface, and the fuel assembly-to-cell wall interface. These interface gaps are modeled using nonlinear spring elements. The term "nonlinear spring" is a generic term used to denote the mathematical representation of the condition where a restoring force is not linearly proportional to displacement.

Fuel Loading Scenario: The fuel assemblies are conservatively assumed to rattle in unison which obviously exaggerates the contribution of impact against the cell wall.

Fluid Coupling: Holtec International extended Fritz's classical two-body fluid coupling model to multiple bodies and utilized it to perform the first two-dimensional multi-rack analysis (Diablo Canyon, ca. 1987). Subsequently, laboratory experiments were conducted to validate the multi-rack fluid coupling theory. This technology was incorporated in the computer code DYNARACK (a.k.a. MR216) [6.2.4] which handles simultaneous simulation of all racks in the pool as a Whole Pool Multi-Rack 3-D analysis. This development was first utilized in Chinshan, Oyster Creek, in earlier projects at the Harris plant [6.2.1, 6.2.3] and, subsequently, in numerous other rerack projects. The WPMR analyses have corroborated the accuracy of the single rack 3-D solutions in predicting the maximum structural stresses, and also serve to improve predictions of rack kinematics.

For closely spaced racks, demonstration of kinematic compliance is verified by including all modules in one comprehensive simulation using a WPMR model. In WPMR analysis, all rack modules are modeled simultaneously and the coupling effect due to this multi-body motion is included in the analysis. Due to the superiority of this technique in predicting the dynamic behavior of closely spaced submerged storage racks, the Whole Pool Multi-Rack analysis methodology is used for this project.

## 6.3

Description of Racks

The implementation of the storage capacity increase in pools C and D will be performed on an as needed basis through incremental phases (campaigns). Figures 6.3.1 and 6.3.2 identify the fully implemented configuration and also designates which racks will be included in each of the campaigns. The new high density storage racks are analyzed for the anticipated configurations at the completion of each of the installation campaigns. Evaluated configurations of the two pools are also handled separately, since the pools are physically separated by the surrounding concrete walls. The analyzed configurations considered are described as follows:

<u>Pool</u>	<u>Campaign</u>	<u>Incremental Number of Racks</u>	<u>Incremental Number of Storage Locations</u>
C	I	14	1680
	II	10	1260
	III	6	750
D	I	6	500
	II	6	525

The materials utilized in fabrication of the rack components are identified in Table 6.3.1.

The cartesian coordinate system utilized within the rack dynamic model has the following nomenclature:

- x = Horizontal axis along plant North
- y = Horizontal axis along plant West
- z = Vertical axis upward from the rack base

6.3.1 Fuel Weights

For the dynamic rack simulations, the dry PWR fuel weight is taken to be 1600 lbs and the dry BWR fuel weight is taken to be 680 lbs.



The synthetic time-histories in three orthogonal directions (N-S, E-W, and vertical) are generated in accordance with the provisions of SRP 3.7.1 [6.4.1]. In order to prepare an acceptable set of acceleration time-histories, Holtec International's proprietary code GENEQ [6.4.2] is utilized.

A preferred criterion for the synthetic time-histories in SRP 3.7.1 calls for both the response spectrum and the power spectral density corresponding to the generated acceleration time-history to envelope their target (design basis) counterparts with only finite enveloping inflections. The time-histories for the pools have been generated to satisfy this preferred (and more rigorous) criterion. The seismic files also satisfy the requirements of statistical independence mandated by SRP 3.7.1.

Figures 6.4.1 through 6.4.3 and 6.4.4 through 6.4.6 provide plots of the time-history accelerograms which were generated over a 20 second duration for OBE and SSE events, respectively.

Results of the correlation function of the three time-histories are given in Table 6.4.1. Absolute values of the correlation coefficients are shown to be less than 0.15, indicating that the desired statistical independence of the three data sets has been met.

Recognizing that the analysis work effort must deal with both stress and displacement criteria, the sequence of model development and analysis steps that are undertaken are summarized in the following:

- a. Prepare 3-D dynamic models suitable for a time-history analysis of the new maximum density racks. These models include the assemblage of all rack modules in each pool. Include all fluid coupling interactions and mechanical coupling appropriate to performing an accurate non-linear simulation. This 3-D simulation is referred to as a Whole Pool Multi-Rack model.
- b. Perform 3-D dynamic analyses on various physical conditions (such as coefficient of friction and extent of cells containing fuel assemblies). Archive appropriate displacement and load outputs from the dynamic model for post-processing.
- c. Perform stress analysis of high stress areas for the limiting case of all the rack dynamic analyses. Demonstrate compliance with ASME Code Section III, Subsection NF limits on stress and displacement.

#### 6.5.1 Model Details for Spent Fuel Racks

The dynamic modeling of the rack structure is prepared with special consideration of all nonlinearities and parametric variations. Particulars of modeling details and assumptions for the Whole Pool Multi-Rack analysis of racks are given in the following:

##### 6.5.1.1 Assumptions

- a. The fuel rack structure motion is captured by modeling the rack as a 12 degree-of-freedom structure. Movement of the rack cross-section at any height is described by six degrees-of-freedom of the rack base and six degrees-of-freedom at the rack top. In this manner, the response of the module, relative to the baseplate, is captured in the dynamic analyses once suitable springs are introduced to couple the rack degrees-of-freedom and simulate rack stiffness.

- b. Rattling fuel assemblies within the rack are modeled by five lumped masses located at  $H$ ,  $.75H$ ,  $.5H$ ,  $.25H$ , and at the rack base ( $H$  is the rack height measured above the baseplate). Each lumped fuel mass has two horizontal displacement degrees-of-freedom. Vertical motion of the fuel assembly mass is assumed equal to rack vertical motion at the baseplate level. The centroid of each fuel assembly mass can be located off-center, relative to the rack structure centroid at that level, to simulate a partially loaded rack.
- c. Seismic motion of a fuel rack is characterized by random rattling of fuel assemblies in their individual storage locations. All fuel assemblies are assumed to move in-phase within a rack. This exaggerates computed dynamic loading on the rack structure and, therefore, yields conservative results.
- d. Fluid coupling between rack and fuel assemblies, and between rack and wall, is simulated by appropriate inertial coupling in the system kinetic energy. Inclusion of these effects uses the methods of [6.5.2, 6.5.3] for rack/assembly coupling and for rack-to-rack coupling.
- e. Fluid damping and form drag are conservatively neglected.
- f. Sloshing is found to be negligible at the top of the rack and is, therefore, neglected in the analysis of the rack.
- g. Potential impacts between the cell walls of the new racks and the contained fuel assemblies are accounted for by appropriate compression-only gap elements between masses involved. The possible incidence of rack-to-wall or rack-to-rack impact is simulated by gap elements at the top and bottom of the rack in two horizontal directions. Bottom gap elements are located at the baseplate elevation. The initial gaps reflect the presence of baseplate extensions, and the rack stiffnesses are chosen to simulate local structural detail.
- h. Pedestals are modeled by gap elements in the vertical direction and as "rigid links" for transferring horizontal stress. Each pedestal support is linked to the pool liner (or bearing pad) by two friction springs. The spring rate for the friction springs includes any lateral elasticity of the stub pedestals. Local pedestal vertical spring stiffness accounts for floor elasticity and for local rack elasticity just above the pedestal.
- i. Rattling of fuel assemblies inside the storage locations causes the gap between fuel assemblies and cell wall to change from a maximum of twice the nominal gap to a theoretical zero gap. Fluid coupling coefficients are based on the nominal gap in order to provide a conservative measure of fluid resistance to gap closure.

- j. The model for the rack is considered supported, at the base level, on four pedestals modeled as non-linear compression only gap spring elements and eight piecewise linear friction spring elements; these elements are properly located with respect to the centerline of the rack beam, and allow for arbitrary rocking and sliding motions.

#### 6.5.1.2 Element Details

Figure 6.5.1 shows a schematic of the dynamic model of a single rack. The schematic depicts many of the characteristics of the model including all of the degrees-of-freedom and some of the spring restraint elements.

Table 6.5.1 provides a complete listing of each of the 22 degrees-of-freedom for a rack model. Six translational and six rotational degrees-of-freedom (three of each type on each end) describe the motion of the rack structure. Rattling fuel mass motions (shown at nodes 1\*, 2\*, 3\*, 4\*, and 5\* in Figure 6.5.1) are described by ten horizontal translational degrees-of-freedom (two at each of the five fuel masses). The vertical fuel mass motion is assumed (and modeled) to be the same as that of the rack baseplate.

Figure 6.5.2 depicts the fuel to rack impact springs (used to develop potential impact loads between the fuel assembly mass and rack cell inner walls) in a schematic isometric. Only one of the five fuel masses is shown in this figure. Four compression only springs, acting in the horizontal direction, are provided at each fuel mass.

Figure 6.5.3 provides a 2-D schematic elevation of the storage rack model, discussed in more detail in Section 6.5.3. This view shows the vertical location of the five storage masses and some of the support pedestal spring members.

Figure 6.5.4 shows the modeling technique and degrees-of-freedom associated with rack elasticity. In each bending plane a shear and bending spring simulate elastic effects [6.5.4].



Linear elastic springs coupling rack vertical and torsional degrees-of-freedom are also included in the model.

Figure 6.5.5 depicts a single rack module with its surrounding impact springs (used to develop potential impact loads between racks or between rack and wall). Figures 6.5.6 through 6.5.13 show the rack numbering schemes used for the WPMR analyses of both pools. These figures also provide the numbering scheme for all of the rack periphery compression only gap elements.

### 6.5.2 Fluid Coupling Effect

In its simplest form, the so-called "fluid coupling effect" [6.5.2, 6.5.3] can be explained by considering the proximate motion of two bodies under water. If one body (mass  $m_1$ ) vibrates adjacent to a second body (mass  $m_2$ ), and both bodies are submerged in frictionless fluid, then Newton's equations of motion for the two bodies are:

$$(m_1 + M_{11}) \ddot{X}_1 + M_{12} \ddot{X}_2 = \text{applied forces on mass } m_1 + O(X_1^2)$$

$$M_{21} \ddot{X}_1 + (m_2 + M_{22}) \ddot{X}_2 = \text{applied forces on mass } m_2 + O(X_2^2)$$

$\ddot{X}_1$ , and  $\ddot{X}_2$  denote absolute accelerations of masses  $m_1$  and  $m_2$ , respectively, and the notation  $O(X^2)$  denotes nonlinear terms.

$M_{11}$ ,  $M_{12}$ ,  $M_{21}$ , and  $M_{22}$  are fluid coupling coefficients which depend on body shape, relative disposition, etc. Fritz [6.5.3] gives data for  $M_{ij}$  for various body shapes and arrangements. The fluid adds mass to the body ( $M_{11}$  to mass  $m_1$ ), and an inertial force proportional to acceleration of the adjacent body (mass  $m_2$ ). Thus, acceleration of one body affects the force field on another. This force field is a function of inter-body gap, reaching large values for small gaps. Lateral motion of a fuel assembly inside a storage location encounters this effect.

For example, fluid coupling behavior will be experienced between nodes 2 and 2\* in Figure 6.5.1. The rack analysis also contains inertial fluid coupling terms which model the effect of fluid in the gaps between adjacent racks.

Terms modeling the effects of fluid flowing between adjacent racks in a single rack analysis suffer from the inaccuracies described earlier. These terms are usually computed assuming that all racks adjacent to the rack being analyzed are vibrating in-phase or 180° out of phase. The WPMR analyses do not require any assumptions with regard to phase.

Rack-to-rack gap elements have initial gaps set to 100% of the physical gap between the racks or between outermost racks and the adjacent pool walls.

#### 6.5.2.1 Multi-Body Fluid Coupling Phenomena

During the seismic event, all racks in the pool are subject to the input excitation simultaneously. The motion of each free-standing module would be autonomous and independent of others as long as they did not impact each other and no water were present in the pool. While the scenario of inter-rack impact is not a common occurrence and depends on rack spacing, the effect of water – the so-called fluid coupling effect – is a universal factor. As noted in Ref. [6.5.2, 6.5.4], the fluid forces can reach rather large values in closely spaced rack geometries. It is, therefore, essential that the contribution of the fluid forces be included in a comprehensive manner. This is possible only if all racks in the pool are *allowed* to execute 3-D motion in the mathematical model. For this reason, single rack or even multi-rack models involving only a portion of the racks in the pool, are inherently inaccurate. The Whole Pool Multi-Rack model removes this intrinsic limitation of the rack dynamic models by simulating the 3-D motion of all modules simultaneously. The fluid coupling effect, therefore, encompasses interaction between *every* set of racks in the pool, i.e., the motion of one rack produces fluid forces on all other racks and on the pool walls. Stated more formally, both near-field and far-field fluid coupling effects are included in the analysis.

The derivation of the fluid coupling matrix [6.5.5] relies on the classical inviscid fluid mechanics principles, namely the principle of continuity and Kelvin's recirculation theorem. While the derivation of the fluid coupling matrix is based on no artificial construct, it has been nevertheless verified by an extensive set of shake table experiments [6.5.5].

### 6.5.3 Stiffness Element Details

Table 6.5.2 lists all spring elements used in the 3-D, 22-DOF, rack model for Campaign I of pool D. This set of elements is chosen since it represents the smallest of the models and provides a sufficient example to describe spring element numbering of Campaign II of pool D and the larger pool C models, which are similar. Three element types are used in the rack models. Type 1 are linear elastic elements used to represent the beam-like behavior of the integrated rack cell matrix. Type 2 elements are the piece-wise linear friction springs used to develop the appropriate forces between the rack pedestals and the supporting bearing pads. Type 3 elements are non-linear gap elements which model gap closures and subsequent impact loadings (i.e., between fuel assemblies and the storage cell inner walls, and rack outer periphery spaces).

A detailed numbering scheme for the rack-to-rack and rack-to-wall gap elements for each of the pool models is provided in Figures 6.5.6 through 6.5.13.

If the simulation model is restricted to two dimensions (one horizontal motion plus one vertical motion, for example), for the purposes of model clarification only, then Figure 6.5.3 describes the configuration. This simpler model is used to elaborate on the various stiffness modeling elements.

Type 3 gap elements modeling impacts between fuel assemblies and racks have local stiffness  $K_i$  in Figure 6.5.3. In Table 6.5.2, for example, type 3 gap elements 5 through 8 act on the rattling fuel mass at the rack top. Support pedestal spring rates  $K_s$  are modeled by type 3 gap

elements 1 through 4, as listed in Table 6.5.2. Local compliance of the concrete floor is included in  $K_s$ . The type 2 friction elements listed in Table 6.5.2 are shown in Figure 6.5.3 as  $K_f$ . The spring elements depicted in Figure 6.5.4 represent type 1 elements.

Friction at support/liner interface is modeled by the piecewise linear friction springs with suitably large stiffness  $K_f$  up to the limiting lateral load  $\mu N$ , where  $N$  is the current compression load at the interface between support and liner. At every time-step during transient analysis, the current value of  $N$  (either zero if the pedestal has lifted off the liner, or a compressive finite value) is computed.

The gap element  $K_s$ , modeling the effective compression stiffness of the structure in the vicinity of the support, includes stiffness of the pedestal, local stiffness of the underlying pool slab, and local stiffness of the rack cellular structure above the pedestal.

The previous discussion is limited to a 2-D model solely for simplicity. Actual analyses incorporate 3-D motions and include all stiffness elements listed in Table 6.5.2.

#### 6.5.4 Coefficients of Friction

To eliminate the last significant element of uncertainty in rack dynamic analyses, multiple simulations are performed to adjust the friction coefficient ascribed to the support pedestal/pool bearing pad interface. These friction coefficients are chosen consistent with the two bounding extremes from Rabinowicz's data [6.5.1]. Simulations are also performed by imposing intermediate value friction coefficients developed by a random number generator with Gaussian normal distribution characteristics. The assigned values are then held constant during the

entire simulation in order to obtain reproducible results.<sup>†</sup> Thus, in this manner, the WPMR analysis results are brought closer to the realistic structural conditions.

The coefficient of friction ( $\mu$ ) between the pedestal supports and the pool floor is indeterminate. According to Rabinowicz [6.5.1], results of 199 tests performed on austenitic stainless steel plates submerged in water show a mean value of  $\mu$  to be 0.503 with standard deviation of 0.125. Upper and lower bounds (based on twice standard deviation) are 0.753 and 0.253, respectively. Analyses are therefore performed for coefficient of friction values of 0.2 (lower limit) and for 0.8 (upper limit), and for random friction values clustered about a mean of 0.5. The bounding values of  $\mu = 0.2$  and 0.8 have been found to envelope the upper limit of module response in previous rereck projects.

#### 6.5.5 Governing Equations of Motion

Using the structural model discussed in the foregoing, equations of motion corresponding to each degree-of-freedom are obtained using Lagrange's Formulation [6.5.4]. The system kinetic energy includes contributions from solid structures and from trapped and surrounding fluid. The final system of equations obtained have the matrix form:

$$[M] \left[ \frac{d^2 q}{dt^2} \right] = [Q] + [G]$$

where:

[M] - total mass matrix (including structural and fluid mass contributions). The size of this matrix will be  $22n \times 22n$  for a WPMR analysis ( $n$  = number of racks in the model).

---

<sup>†</sup> It is noted that MR216 has the capability to change the coefficient of friction at any pedestal at each instant of contact based on a random reading of the computer clock cycle. However, exercising this option would yield results that could not be reproduced. Therefore, the random choice of coefficients is made only once per run.



- q - the nodal displacement vector relative to the pool slab displacement (the term with q indicates the second derivative with respect to time, i.e., acceleration)
- [G] - a vector dependent on the given ground acceleration
- [Q] - a vector dependent on the spring forces (linear and nonlinear) and the coupling between degrees-of-freedom

The above column vectors have length 22n. The equations can be rewritten as follows:

$$\left[ \frac{d^2q}{dt^2} \right] = [M]^{-1} [Q] + [M]^{-1} [G]$$

This equation set is mass uncoupled, displacement coupled at each instant in time. The numerical solution uses a central difference scheme built into the proprietary computer program MR216 [6.2.4].

## 6.6 Structural Evaluation of Spent Fuel Rack Design

### 6.6.1 Kinematic and Stress Acceptance Criteria

There are two sets of criteria to be satisfied by the rack modules:

#### a. Kinematic Criteria

Per Reference [6.1.1], in order to be qualified as a physically stable structure it is necessary to demonstrate that an isolated rack in water would not overturn when an event of magnitude:

- 1.5 times the upset seismic loading condition is applied.
- 1.1 times the faulted seismic loading condition is applied.

#### b. Stress Limit Criteria

Stress limits must not be exceeded under the postulated load combinations provided herein.

## 6.6.2 Stress Limit Evaluations

The stress limits presented below apply to the rack structure and are derived from the ASME Code, Section III, Subsection NF [6.6.1]. Parameters and terminology are in accordance with the ASME Code. Material properties are obtained from the ASME Code, Section II, Part D [6.6.2], and are listed in Table 6.3.1.

### (i) Normal and Upset Conditions (Level A or Level B)

- a. Allowable stress in tension on a net section is:

$$F_t = 0.6 S_y$$

Where,  $S_y$  = yield stress at temperature, and  $F_t$  is equivalent to primary membrane stress.

- b. Allowable stress in shear on a net section is:

$$F_v = .4 S_y$$

- c. Allowable stress in compression on a net section

$$F_a = S_y \left( .47 - \frac{k \ell}{444 r} \right)$$

$kl/r$  for the main rack body is based on the full height and cross section of the honeycomb region and does not exceed 120 for all sections.

$\ell$  = unsupported length of component

$k$  = length coefficient which gives influence of boundary conditions. The following values are appropriate for the described end conditions:

= 1 (simple support both ends)

= 2 (cantilever beam)

= 1/2 (clamped at both ends)

$r$  = radius of gyration of component

- d. Maximum allowable bending stress at the outermost fiber of a net section, due to flexure about one plane of symmetry is:

$$F_b = 0.60 S_y \quad (\text{equivalent to primary bending})$$

- e. Combined bending and compression on a net section satisfies:

$$\frac{f_a}{F_a} + \frac{C_{mx} f_{bx}}{D_x F_{bx}} + \frac{C_{my} f_{by}}{D_y F_{by}} < 1$$

where:

$f_a$  = Direct compressive stress in the section

$f_{bx}$  = Maximum bending stress along x-axis

$f_{by}$  = Maximum bending stress along y-axis

$C_{mx}$  = 0.85

$C_{my}$  = 0.85

$D_x$  =  $1 - (f_a/F'_{cx})$

$D_y$  =  $1 - (f_a/F'_{cy})$

$F'_{cx,cy}$  =  $(\pi^2 E)/(2.15 (kl/r)_{x,y}^2)$

$E$  = Young's Modulus

and subscripts x,y reflect the particular bending plane.

- f. Combined flexure and compression (or tension) on a net section:

$$\frac{f_a}{0.6S_y} + \frac{f_{bx}}{F_{bx}} + \frac{f_{by}}{F_{by}} < 1.0$$

The above requirements are to be met for both direct tension or compression.

- g. Welds

Allowable maximum shear stress on the net section of a weld is given by:

$$F_w = 0.3 S_u$$

where  $S_u$  is the weld material ultimate strength at temperature. For fillet weld legs in contact with base metal, the shear stress on the gross section is limited to  $0.4S_y$ , where  $S_y$  is the base material yield strength at temperature.

(ii) Level D Service Limits

Section F-1334 (ASME Section III, Appendix F) [6.6.2], states that the limits for the Level D condition are the minimum of  $1.2 (S_y/F_y)$  or  $(0.7S_u/F_y)$  times the corresponding limits for the Level A condition.  $S_u$  is ultimate tensile stress at the specified rack design temperature. Examination of material properties for 304L stainless demonstrates that 1.2 times the yield strength is less than the 0.7 times the ultimate strength.

Exceptions to the above general multiplier are the following:

- a) Stresses in shear shall not exceed the lesser of  $0.72S_y$  or  $0.42S_u$ . In the case of the Austenitic Stainless material used here,  $0.72S_y$  governs.
- b) Axial Compression Loads shall be limited to 2/3 of the calculated buckling load.
- c) Combined Axial Compression and Bending - The equations for Level A conditions shall apply except that:

$$F_a = 0.667 \times \text{Buckling Load} / \text{Gross Section Area},$$

and the terms  $F'_{ex}$  and  $F'_{ey}$  may be increased by the factor 1.65.

- d) For welds, the Level D allowable maximum weld stress is not specified in Appendix F of the ASME Code. An appropriate limit for weld throat stress is conservatively set here as:

$$F_w = (0.3 S_u) \times \text{factor}$$

where:

$$\text{factor} = (\text{Level D shear stress limit}) / (\text{Level A shear stress limit})$$

### 6.6.3 Dimensionless Stress Factors

For convenience, the stress results are presented in dimensionless form. Dimensionless stress factors are defined as the ratio of the actual developed stress to the specified limiting value. The limiting value of each stress factor is 1.0, based on the allowable strengths for each level, for Levels A, B, and D (where  $1.2S_y < .7S_u$ ).

The stress factors reported are:

$R_1$  = Ratio of direct tensile or compressive stress on a net section to its allowable value (note pedestals only resist compression)

$R_2$  = Ratio of gross shear on a net section in the x-direction to its allowable value

$R_3$  = Ratio of maximum x-axis bending stress to its allowable value for the section

$R_4$  = Ratio of maximum y-axis bending stress to its allowable value for the section

$R_5$  = Combined flexure and compressive factor (as defined in the foregoing)

$R_6$  = Combined flexure and tension (or compression) factor (as defined in the foregoing)

$R_7$  = Ratio of gross shear on a net section in the y-direction to its allowable value

The applicable loads and their combinations which must be considered in the seismic analysis of rack modules are excerpted from Refs. [6.1.2] and [6.6.3].

The load combinations considered are identified below:

Loading Combination	Service Level
D + L D + L + T <sub>o</sub> D + L + T <sub>o</sub> + E	Level A
D + L + T <sub>a</sub> + E D + L + T <sub>o</sub> + P <sub>f</sub>	Level B
D + L + T <sub>a</sub> + E' D + L + T <sub>o</sub> + F <sub>d</sub>	Level D  The functional capability of the fuel racks must be demonstrated.

- D = Dead weight-induced loads (including fuel assembly weight)  
 L = Live Load (not applicable for the fuel rack, since there are no moving objects in the rack load path)  
 P<sub>f</sub> = Upward force on the racks caused by postulated stuck fuel assembly  
 F<sub>d</sub> = Impact force from accidental drop of the heaviest load from the maximum possible height.  
 E = Operating Basis Earthquake (OBE)  
 E' = Safe Shutdown Earthquake (SSE)  
 T<sub>o</sub> = Differential temperature induced loads (normal operating or shutdown condition based on the most critical transient or steady state condition)  
 T<sub>a</sub> = Differential temperature induced loads (the highest temperature associated with the postulated abnormal design conditions)

T<sub>a</sub> and T<sub>o</sub> produce local thermal stresses. The worst thermal stress field in a fuel rack is obtained when an isolated storage location has a fuel assembly generating heat at maximum postulated rate and surrounding storage locations contain no fuel. Heated water makes unobstructed contact with the inside of the storage walls, thereby producing maximum possible

temperature difference between adjacent cells. Secondary stresses produced are limited to the body of the rack; that is, support pedestals do not experience secondary (thermal) stresses.

## 6.7 Parametric Simulations

Whole Pool Multi-Rack (WPMR) simulations have been performed to investigate the structural integrity of each rack array. Pools C and D had separate runs performed for the SSE seismic event considering pools filled and partially filled with racks. The partially filled pools represent interim configurations subsequent to the installation campaigns identified for each pool in Figures 6.3.1 and 6.3.2. The configurations were considered with friction coefficients of 0.8, 0.2, and a gaussian distribution with a mean of 0.5 (i.e., random coefficient of friction (COF) with upper and lower limits of 0.8 and 0.2). The SSE simulations were performed and conservatively compared against the allowables for OBE events. This process eliminated the need for performing OBE simulations to significantly reduce the number of runs needed. Due to the mild SSE earthquake postulated for Harris, this conservative evaluation technique yielded satisfactory design margins.

The overturning check simulations were performed to determine the behavior of the highest aspect (width/length) ratio racks under both the OBE and SSE events. The overturning check simulations considered a single rack (i.e., no dynamic fluid coupling to walls or other racks) half full with fuel all loaded along the long side of the rack.

The rack numbering schemes used to identify the racks in each simulation model are introduced in Figures 6.5.6 through 6.5.13. The circled rack numbers in the figures correspond to the rack numbers shown in the following tables.

The following table presents a complete listing of the simulations discussed herein. Consideration of the parameters described above resulted in the following runs:

<b>Run</b>	<b>Simulation Description</b>	<b>COF</b>	<b>Event</b>
1	Pool C (Campaign I)	0.8	SSE
2	Pool C (Campaign I)	0.2	SSE
3	Pool C (Campaign I)	Random	SSE
4	Pool C (Campaign II)	0.8	SSE
5	Pool C (Campaign II)	0.2	SSE
6	Pool C (Campaign II)	Random	SSE
7	Pool C (Campaign III - Full)	0.8	SSE
8	Pool C (Campaign III - Full)	0.2	SSE
9	Pool C (Campaign III - Full)	Random	SSE
10	Pool D (Campaign I)	0.8	SSE
11	Pool D (Campaign I)	0.2	SSE
12	Pool D (Campaign I)	Random	SSE
13	Pool D (Campaign II - Full)	0.8	SSE
14	Pool D (Campaign II - Full)	0.2	SSE
15	Pool D (Campaign II - Full)	Random	SSE
16	Single Holtec Rack Overturning Check	0.8	OBE x 1.5
17	Single HoltecRack Overturning Check	0.8	SSE x 1.1

The results from the MR216 runs may be seen in the raw data output files. The MR216 output files archive all of the loads and displacements at key locations within each of the rack modules at every time step throughout the entire time history duration. However, due to the huge quantity of output data, a post-processor is used to scan for worst case conditions and develop the stress factors discussed in subsection 6.6.3.

Further reduction in this bulk of information is provided in this section by extracting the worst case values from the parameters of interest; namely displacements, support pedestal forces, impact loads, and stress factors. This section also summarizes other analyses performed to develop and evaluate structural member stresses which are not determined by the post processor.

#### 6.8.1 Rack Displacements

A tabulated summary of the maximum displacement for each simulation is provided below with the location/direction terms defined as follows:

uxt = displacement of top corner of rack, relative to the slab, in the East-West direction for pool C racks and in the North-South direction for pool D rack modules.

uyt = displacement of top corner of rack, relative to the slab, in the North-South direction for pool C racks and in the East-West direction for pool D rack modules.

Simulations 16 and 17 were performed to evaluate the potential for overturning of a single Holtec rack isolated in the pool without any fluid coupling to adjacent racks or walls. This simulation was performed to account for the unlikely possibility of a seismic event occurring during the installation process.

The following maximum rack displacements (in inches) are obtained for each of the runs:

Pool	Event	Run	COF	Maximum Displacement (inches)	Location/ Direction	Rack
Pool C Campaign I	SSE	1	0.8	1.132	uxt	16
	SSE	2	0.2	0.631	uyt	5
	SSE	3	Random	0.878	uxt	16
Pool C Campaign II	SSE	4	0.8	1.494	uxt	28
	SSE	5	0.2	0.917	uxt	1
	SSE	6	Random	0.878	uxt	16
Pool C Campaign III	SSE	7	0.8	0.617	uyt	29
	SSE	8	0.2	0.740	uyt	1
	SSE	9	Random	0.684	uyt	3
Pool D Campaign I	SSE	10	0.8	0.520	uxt	2
	SSE	11	0.2	0.390	uyt	3
	SSE	12	Random	0.521	uxt	2
Pool D Campaign II	SSE	13	0.8	0.575	uyt	1
	SSE	14	0.2	0.595	uyt	1
	SSE	15	Random	0.576	uyt	1
Tipover: Single Holtec Rack	OBE	16	0.8	0.347	uyt	PWR
Tipover: Single Holtec Rack	SSE	17	0.8	1.054	uyt	PWR

The largest displacement of 1.494 occurs in run 4 for rack 28 in the X direction. Since this displacement maintains the centroid of the rack well within the boundaries represented by the support pedestals, there is no possibility of rack overturning (tipover).

## 6.8.2 Pedestal Vertical Forces

Pedestal number 1 for each rack is located in the +X, -Y corner of each rack. Numbering increases counterclockwise around the periphery of the rack. The following bounding vertical pedestal forces (in kips) are obtained for each run:

Pool	Event	Run	COF	Maximum Pedestal Load (kips)	Rack	Ped.
Pool C Campaign I	SSE	1	0.8	122	5	4
	SSE	2	0.2	115	5	4
	SSE	3	Random	123	5	1
Pool C Campaign II	SSE	4	0.8	153	5	2
	SSE	5	0.2	121	9	2
	SSE	6	Random	134	9	1
Pool C Campaign III	SSE	7	0.8	113	7	4
	SSE	8	0.2	110	9	1
	SSE	9	Random	122	26	1
Pool D Campaign I	SSE	10	0.8	118	5	4
	SSE	11	0.2	112	5	1
	SSE	12	Random	114	5	4
Pool D Campaign II	SSE	13	0.8	135	11	2
	SSE	14	0.2	116	11	4
	SSE	15	Random	130	11	4

As may be seen, the highest pedestal load is 153,000 lbs and occurs in run 4 for pedestal 2 of rack 5. Figure 6.8.1 provides a plot of the vertical force of this pedestal transmitted to the bearing pad over the entire duration of the SFP, 0.8 COF, SSE, campaign II simulation.

### 6.8.3 Pedestal Friction Forces

The maximum (x or y direction) shear load (in kips) bounding all pedestals for each simulation are reported below and are obtained by inspection of the complete tabular data.

Pool	Event	Run	COF	Maximum Friction Load (kips)	Rack
Pool C Campaign I	SSE	1	0.8	46	11
	SSE	2	0.2	22.3	8
	SSE	3	Random	41.7	13
Pool C Campaign II	SSE	4	0.8	44.2	13
	SSE	5	0.2	22.2	9
	SSE	6	Random	40.9	11
Pool C Campaign III	SSE	7	0.8	43.4	3
	SSE	8	0.2	19.7	7
	SSE	9	Random	45.8	26
Pool D Campaign I	SSE	10	0.8	45.6	1
	SSE	11	0.2	19.7	2
	SSE	12	Random	34.4	1
Pool D Campaign II	SSE	13	0.8	42.3	11
	SSE	14	0.2	22.3	1
	SSE	15	Random	42.4	11

## 6.8.4 Rack Impact Loads

A freestanding rack, by definition, is a structure subject to potential impacts during a seismic event. Impacts arise from rattling of the fuel assemblies in the storage rack locations and, in some instances, from localized impacts between the racks, or between a peripheral rack and the pool wall. The following sections discuss the bounding values of these impact loads.

### 6.8.4.1 Rack to Rack Impacts

As is often the case with close rack spacing, some rack to rack impacts occur. The following instantaneous maximum impact forces and locations are identified for each of the simulations performed. Listings are only given for those simulations within which an impact occurred. The element numbering is identified in Figures 6.5.6 through 6.5.13.

Run	Impact Load (kips)	Element	Location	Run	Impact Load (kips)	Element	Location
1	3.0	494	Top	5	11.3	814	Bottom
1	8.1	503	Top	5	8.1	817	Top
1	8.1	504	Top	5	8.1	818	Top
1	8.1	583	Top	5	4.9	831	Bottom
1	8.1	584	Top	5	8.4	937	Bottom
2	8.1	493	Top	5	5.6	945	Bottom
2	8.1	494	Top	5	6.4	991	Bottom
3	6.7	493	Top	5	6.5	992	Bottom
3	8.1	494	Top	6	8.1	736	Top
3	8.1	503	Top	6	1.9	746	Top
3	8.1	504	Top	6	8.1	759	Top
3	3.0	539	Top	6	7.9	760	Top
3	2.1	540	Top	6	8.1	781	Top
3	8.1	583	Top	6	8.1	782	Top
3	8.1	584	Top	6	8.1	789	Top
3	8.1	599	Top	6	8.1	790	Top

Run	Impact Load (kips)	Element	Location	Run	Impact Load (kips)	Element	Location
3	8.1	600	Top	6	4.9	799	Top
4	5.3	736	Top	6	8.1	817	Top
4	8.1	759	Top	6	8.1	818	Top
4	8.1	760	Top	6	1.2	827	Top
4	8.1	781	Top	6	8.1	828	Top
4	8.1	782	Top	6	8.1	835	Top
4	8.1	799	Top	6	8.1	836	Top
4	8.1	800	Top	6	1.9	914	Top
4	8.1	817	Top	6	1.8	946	Bottom
4	8.1	818	Top	6	8.1	949	Top
4	8.1	827	Top	6	8.1	950	Top
4	8.1	828	Top	6	8.1	979	Top
4	8.1	835	Top	6	8.1	980	Top
4	8.1	836	Top	6	2.6	982	Bottom
4	8.1	907	Top	6	8.1	986	Top
4	8.1	908	Top	6	12.9	992	Bottom
4	8.1	913	Top	7	8.1	913	Top
4	8.1	914	Top	7	8.1	914	Top
4	8.1	979	Top	7	5.3	949	Top
4	8.1	980	Top	7	0.8	950	Top
5	6.7	736	Top	8	8.0	991	Bottom
5	16.7	743	Bottom	8	11.3	992	Bottom
5	7.7	744	Bottom	9	8.1	913	Top
5	10.7	756	Bottom	9	8.1	914	Top
5	4.5	777	Bottom	9	8.1	949	Top
5	22.1	778	Bottom	9	7.8	950	Top
5	16.1	813	Bottom				

#### 6.8.4.2 Rack to Wall Impacts

Storage racks do not impact the pool walls under any simulation.

#### 6.8.4.3 Fuel to Cell Wall Impact Loads

A review of the results from each simulation allows determination of the maximum instantaneous impact load between fuel assembly and fuel cell wall at any modeled impact site. The maximum values obtained are reported in the following table.

Pool	Event	Run	COF	Maximum Fuel Impact Load (lbs)	Rack
Pool C Campaign I	SSE	1	0.8	532	2
	SSE	2	0.2	562	5
	SSE	3	Random	605	2
Pool C Campaign II	SSE	4	0.8	531	25
	SSE	5	0.2	548	9
	SSE	6	Random	535	22
Pool C Campaign III	SSE	7	0.8	525	17
	SSE	8	0.2	527	17
	SSE	9	Random	515	17
Pool D Campaign I	SSE	10	0.8	473	1
	SSE	11	0.2	591	4
	SSE	12	Random	473	1
Pool D Campaign II	SSE	13	0.8	472	12
	SSE	14	0.2	462	12
	SSE	15	Random	472	12

The maximum fuel to cell wall impact load is 605 pounds. Based on fuel manufacturer's data, loads of this magnitude will not damage the fuel assembly.

## 6.9 Rack Structural Evaluation

### 6.9.1 Rack Dimensionless Stress Factors for Level B and D Loadings

The vertical and shear forces at the bottom casting-pedestal interface are available as a function of time. The maximum values for the stress factors defined in Section 6.6.3 can be determined for every pedestal in the array of racks by scanning this data to select the limiting loads and performing calculations to determine member stresses. These two tasks are performed by a post-processor. With this information available, the structural integrity of the pedestal can be assessed and reported. The net section maximum (in time) bending moments and shear forces can also be determined at the bottom casting-rack cellular structure interface for each spent fuel rack in the pool. This allows the evaluation of the maximum stress in the limiting rack cell (box).

The tables presented in this section provide limiting stress factor results for male and female pedestals, and for the entire spent fuel rack cellular cross section just above the bottom casting. These locations are the most heavily loaded net sections in the structure so that satisfaction of the stress factor criteria at these locations ensures that the overall structural criteria set forth in Section 6.6.1 are met.

The tables below develop stress factors for all of the SSE (Level D) simulations based on the associated SSE allowables. However, as stated above the intent is to evaluate the stresses developed from the SSE loadings with the allowables associated with OBE (Level B). Since the OBE allowables are  $\frac{1}{2}$  of the SSE allowables, this comparison may be conservatively performed by reducing the acceptable stress ratio to 0.5. This is very conservative, since the actual OBE loads which should be compared against the OBE allowable would be much lower than the SSE loads herein.

### 6.9.1.1 Rack Cell Stress Factors

The rack cell dimensionless stress factors for each of the simulations are as follows:

Pool	Event	Run	COF	Maximum R6 Stress Factor	Rack
Pool C Campaign I	SSE	1	0.8	0.494	11
	SSE	2	0.2	0.289	9
	SSE	3	Random	0.384	9
Pool C Campaign II	SSE	4	0.8	0.454	6
	SSE	5	0.2	0.221	13
	SSE	6	Random	0.452	6
Pool C Campaign III	SSE	7	0.8	0.409	3
	SSE	8	0.2	0.266	3
	SSE	9	Random	0.432	24
Pool D Campaign I	SSE	10	0.8	0.230	1
	SSE	11	0.2	0.224	3
	SSE	12	Random	0.230	1
Pool D Campaign II	SSE	13	0.8	0.224	11
	SSE	14	0.2	0.227	3
	SSE	15	Random	0.232	2

The values for all other defined stress factors are also archived. As may be seen, all of the stress factors are well below 1.0. Therefore, the stresses developed during SSE conditions remain below the allowable SSE range and the rack modules are satisfactory to withstand the loadings. Note that stress factors for these SSE simulations are calculated based on SSE allowable strengths. However, since none of the stress factors exceed 0.5, the rack structures also adequately withstand the OBE conditions.

## 6.9.2 Pedestal Thread Shear Stress

The average shear stress in the thread engagement region is given below for the limiting pedestal in each simulation.

Pool	Event	Run	COF	Maximum Thread Shear Stress (psi)	Rack
Pool C Campaign I	SSE	1	0.8	4,682	11
	SSE	2	0.2	4,382	9
	SSE	3	Random	4,607	5
Pool C Campaign II	SSE	4	0.8	5,731	5
	SSE	5	0.2	4,532	9
	SSE	6	Random	5,019	9
Pool C Campaign III	SSE	7	0.8	4,232	7
	SSE	8	0.2	4,120	9
	SSE	9	Random	4,570	26
Pool D Campaign I	SSE	10	0.8	3,003	5
	SSE	11	0.2	2,850	5
	SSE	12	Random	2,901	5
Pool D Campaign II	SSE	13	0.8	3,435	11
	SSE	14	0.2	2,952	11
	SSE	15	Random	3,307	11

The ultimate strength of the female part of the pedestal is 66,200 psi. The yield stress for the female pedestal material is 21,300 psi, as shown in Table 6.3.1. The male pedestal material has much greater strength and is therefore not a controlling factor in the design. The allowable shear stress for Level B conditions is 0.4 times the yield stress which gives 8,520 psi. The allowable shear stress for Level D conditions is the lesser of:  $0.72 S_y = 15,336$  psi or  $0.42 S_u = 27,804$  psi. Therefore, the former criteria controls.



The largest thread shear stress computed by the post-processor is 5,731 psi. Since this value is below the allowable stresses for both OBE and DBE conditions, the thread shear stresses are within the acceptable range.

### 6.9.3 Local Stresses Due to Impacts

Impact loads at the pedestal base (discussed in subsection 6.8.2) produce stresses in the pedestal for which explicit stress limits are prescribed in the Code. The post-processor reports the stress factors in the pedestals which are developed, in part, from these impact stresses. The reported pedestal stress factors are included in the discussion above in Section 6.9.1.1 along with the rack cell stress factors. However, the post-processor does not develop stress factors for the localized areas of the cellular and baseplate regions of the racks which experience fuel to cell wall, rack to rack, and rack to wall impact loads. These impact loads produce stresses which attenuate rapidly away from the loaded region. This behavior is characteristic of secondary stresses.

Even though limits on secondary stresses are not prescribed in the Code for Class 3 NF structures, evaluations were made to ensure that the localized impacts do not lead to plastic deformations in the storage cells which affect the subcriticality of the stored fuel array.

#### a. Impact Loading Between Fuel Assembly and Cell Wall

Local cell wall integrity is conservatively estimated from peak impact loads. Plastic analysis is used to obtain the limiting impact load which would lead to gross permanent deformation. Table 6.9.1 indicates that the limiting impact load (of 3,238 lbf, including a safety factor of 2.0) is much greater than the highest calculated impact load value (of 605 lbf, see subsection 6.8.4.3) obtained from any of the rack analyses. Therefore, fuel impacts do not represent a significant concern with respect to fuel rack cell deformation.

b. Impacts Between Adjacent Racks

As may be seen from subsection 6.8.4.1, the bottom (baseplate) of the storage racks will impact each other at a few locations during seismic events. Since the loading is presented edge-on to the 3/4" baseplate membrane, the distributed stresses after local deformation will be negligible. The impact loading will be distributed over a large area (a significant portion of the entire baseplate length of about 50.4 (minimum) inches by its 3/4 inch thickness). The resulting compressive stress from the highest impact load of 26,200 lbs distributed over 37 sq. inches is only 708 psi, which is negligible. Therefore, any deformation will not effect the configuration of the stored fuel.

Additional impacts will be experienced at the tops of some storage racks. These impacts will result in local yielding of the rack cell walls whenever the load exceeds 8,100 lbs. However, localized damage from all of these impacts occurs above the fuel active region. The fuel configuration and poison areas remain unaffected. Therefore, these impacts are acceptable.

6.9.4 Assessment of Rack Fatigue Margin

Deeply submerged high density spent fuel storage racks arrayed in close proximity to each other in a free-standing configuration behave primarily as a nonlinear cantilevered structure when subjected to 3-D seismic excitations. In addition to the pulsations in the vertical load at each pedestal, lateral friction forces at the pedestal/bearing pad-liner interface, which help prevent or mitigate lateral sliding of the rack, also exert a time-varying moment in the baseplate region of the rack. The friction-induced lateral forces act simultaneously in x and y directions with the requirement that their vectorial sum does not exceed  $\mu V$ , where  $\mu$  is the limiting interface coefficient of friction and V is the concomitant vertical thrust on the liner (at the *given* time instant). As the vertical thrust at a pedestal location changes, so does the



maximum friction force,  $F$ , that the interface can exert. In other words, the lateral force at the pedestal/liner interface,  $F$ , is given by

$$F \leq \mu N (\tau)$$

where  $N$  (vertical thrust) is the time-varying function of  $\tau$ .  $F$  does not always equal  $\mu N$ ; rather,  $\mu N$  is the maximum value it can attain at any time; the actual value, of course, is determined by the dynamic equilibrium of the rack structure.

In summary, the horizontal friction force at the pedestal/liner interface is a function of time; its magnitude and direction of action varies during the earthquake event.

The time-varying lateral (horizontal) and vertical forces on the extremities of the support pedestals produce stresses at the root of the pedestals in the manner of an end-loaded cantilever. The stress field in the cellular region of the rack is quite complex, with its maximum values located in the region closest to the pedestal. The maximum magnitude of the stresses depends on the severity of the pedestal end loads and on the geometry of the pedestal/rack baseplate region.

Alternating stresses in metals produce metal fatigue if the amplitude of the stress cycles is sufficiently large. In high density racks designed for sites with moderate to high postulated seismic action, the stress intensity amplitudes frequently reach values above the material endurance limit, leading to expenditure of the fatigue "usage" reserve in the material.

Because the locations of maximum stress (viz., the pedestal/rack baseplate junction) and the close placement of racks, a post-earthquake inspection of the high stressed regions in the racks is not feasible. Therefore, the racks must be engineered to withstand multiple earthquakes without reliance of nondestructive inspections for post-earthquake integrity assessment. The fatigue life evaluation of racks is an integral aspect of a sound design.

The time-history method of analysis, deployed in this report, provides the means to obtain a complete cycle history of the stress intensities in the highly stressed regions of the rack. Having determined the amplitude of the stress intensity cycles and their number, the cumulative damage factor,  $U$ , can be determined using the classical Miner's rule

$$U = \sum \frac{n_i}{N_i}$$

where  $n_i$  is the number of stress intensity cycles of amplitude  $\sigma_i$ , and  $N_i$  is the permissible number of cycles corresponding to  $\sigma_i$  from the ASME fatigue curve for the material of construction.  $U$  must be less than or equal to 1.0.

To evaluate the cumulative damage factor, a finite element model of a portion of the spent fuel rack in the vicinity of a support pedestal is constructed in sufficient detail to provide an accurate assessment of stress intensities. Figure 6.9.1 shows the essentials of the finite element model. The finite element solutions for unit pedestal loads in three orthogonal directions are combined to establish the maximum value of stress intensity as a function of the three unit pedestal loads. Using the archived results of the spent fuel rack dynamic analyses (pedestal load histories versus time), enables a time-history of stress intensity to be established at the most limiting location. This permits establishing a set of alternating stress intensity ranges versus cycles for several seismic events. Following ASME Code guidelines for computing  $U$ , it is found that  $U = 0.464$  due to the combined effect of 21 SSE events. This cumulative damage factor is below the ASME Code limit of 1.0 and therefore, fatigue failure is not expected. Selection of 21 SSE events represents a conservative evaluation compared to other previous fatigue assessments which were based on the damage resulting from 10 SSE events, as discussed in the Harris FSAR.

### 6.9.5 Weld Stresses

Weld locations subjected to significant seismic loading are at the bottom of the rack at the baseplate-to-cell connection, at the top of the pedestal support at the baseplate connection, and at cell-to-cell connections. Bounding values of resultant loads are used to qualify the connections.

#### a. Baseplate-to-Rack Cell Welds

Reference [6.6.1] (ASME Code Section III, Subsection NF) permits, for Level A or B conditions, an allowable weld stress  $\tau = .3 S_u = 19860$  psi. As stated in subsection 3.4.2 the allowable may be increased for Level D by the ratio  $(15336/8520) = 1.8$ , giving an allowable of 35,748 psi.

Weld dimensionless stress factors are produced through the use of a simple conversion (ratio) factor applied to the corresponding stress factor in the adjacent rack material. A 2.15 factor for PWR racks is based on the differences in material thickness and length versus weld throat dimension and length:

$$Ratio = \frac{0.075 * 8.875}{0.0625 * 0.7071 * 7} = 2.15165$$

Similarly, a 1.49 factor for BWR racks is developed as follows:

$$Ratio = \frac{0.075 * 6.135}{0.0625 * 0.7071 * 7} = 1.48736$$

The highest predicted weld stress for DBE is calculated from the highest R6 value (see subsection 6.9.1.1) as follows:

$$R6 * [(0.6) F_y] * Ratio = \\ 0.494 [(0.6) 21,300] * 2.144 = 13,574 \text{ psi}$$

this value is less than the OBE allowable weld stress value, which is 19,860. Therefore, all weld stresses between the baseplate and cell wall base are acceptable.

b. Baseplate-to-Pedestal Welds

The weld between the baseplate and support pedestal are evaluated by development of a finite element model of the bearing pad/base plate interface and appropriate application of the maximum pedestal loads. The maximum weld stress was determined to be 10,194 psi, which is much less than the OBE allowable weld stress value of 19,860 psi. The results are also shown in Table 6.9.1.

c. Cell-to-Cell Welds

Cell-to-cell connections are made using a series of connecting welds along the cell height. Stresses in storage cell to cell welds develop due to fuel assembly impacts with the cell wall. These weld stresses are conservatively calculated by assuming that fuel assemblies in adjacent cells are moving out of phase with one another so that impact loads in two adjacent cells are in opposite directions; this tends to separate the two cells from each other at the weld.

Table 6.9.1 gives results for the maximum allowable load that can be transferred by these welds based on the available weld area. An upper bound on the load required to be transferred is also given in Table 6.9.1 and is much lower than the allowable load. This upper bound value is very conservatively obtained by applying the bounding rack-to-fuel impact load from any simulation in two orthogonal directions simultaneously,



and multiplying the result by 2 to account for the simultaneous impact of two assemblies. An equilibrium analysis at the connection then yields the upper bound load to be transferred. It is seen from the results in Table 6.9.1 that the calculated load is well below the allowable.

#### 6.9.6 Bearing Pad Analysis

To protect the pool slab from high localized dynamic loadings, bearing pads are placed between the pedestal base and the slab. Fuel rack pedestals impact on these bearing pads during a seismic event and pedestal loading is transferred to the liner. Bearing pad dimensions are set to ensure that the average pressure on the slab surface due to a static load plus a dynamic impact load does not exceed the American Concrete Institute, ACI-349 [6.9.1] limit on bearing pressures. Section 10.17 of [6.9.2] gives the design bearing strength as

$$f_b = \phi (.85 f_c') \epsilon$$

where  $\phi = .7$  and  $f_c'$  is the specified concrete strength for the spent fuel pool.  $\epsilon = 1$ , except when the supporting surface is wider on all sides than the loaded area. In that case,  $\epsilon = (A_2/A_1)^{.5}$ , but not more than 2.  $A_1$  is the actual loaded area, and  $A_2$  is an area greater than  $A_1$  and is defined in [6.9.2]. Using a value of  $\epsilon > 1$  includes credit for the confining effect of the surrounding concrete. It is noted that this criteria is in conformance with the ultimate strength primary design methodology of the American Concrete Institute in use since 1971. For Harris, the concrete compressive strength is  $f_c' = 4,000$  psi. The allowable bearing pressure is conservatively computed by taking  $\epsilon=1$  to account for lack of total concrete confinement in the leak chase region and a stress reduction factor of  $\phi=0.7$ . Thus, the maximum allowable concrete bearing pressure is 2,380 psi.

The maximum vertical pedestal load is 153,000 lbs (SSE event). The bearing pad selected is 1.5" thick, austenitic stainless steel plate stock. The average pressure at the pad to liner



interface is computed and compared against the above-mentioned limit. Calculations show that the average pressure at the slab/liner interface is 2,168 psi which is below the allowable value of 2,380 psi, providing a factor of safety of 1.1.

Therefore, the bearing pad design devised for the Harris pools C and D is deemed appropriate for the prescribed loadings.

#### 6.9.7 Level A Evaluation

The Level A condition is not a governing condition for spent fuel racks since the general level of loading is far less than Level B loading. To illustrate this, the heaviest (fully loaded) spent fuel rack (which is an 11X9 PWR rack) is considered under the dead weight load. It is shown below that the maximum pedestal load is low and that further stress evaluations are unnecessary.

#### LEVEL A MAXIMUM PEDESTAL LOAD

Dry Weight of Largest PWR Holtec Rack	=	15,700 lbf <sup>†</sup>
Dry Weight of 99 PWR Fuel Assemblies	=	158,400 lbf
Total Dry Weight	=	174,100 lbf <sup>††</sup>
Total Buoyant Weight (0.87 × Total Dry Weight)	=	151,467 lbf
Load per Pedestal	=	37,867 lbf

The stress allowables for the normal condition is the same as for the upset condition. An upset condition pedestal load may be conservatively (bounded on the low side) determined for the

---

<sup>†</sup> Conservative weight corresponding to the heaviest rack, which is a BWR storage rack. The heaviest PWR rack nominal weight is 15,620 lb.

<sup>††</sup> This weight exceeds the weight of the heaviest fully loaded BWR rack, which is [15,700 lb + (13x13) x 680 lb] = 130,620 lb.



purpose of comparing with the load above by dividing the DBE pedestal load by a factor of 2.0. This would result in an OBE pedestal load of  $153,000 \div 2 = 76,500$ , which is still much greater than the calculated Level A load. Since this load (and the corresponding stress throughout the rack members) is much greater than the 37,867 lb load calculated above, the Upset (OBE) condition controls over normal (Gravity) condition. Therefore, no further evaluation is necessary for Level A.

#### 6.10 Hydrodynamic Loads on Pool Walls

The maximum hydrodynamic pressures (in psi) that develop between the fuel racks and the spent fuel pool walls will occur at those conditions and locations of greatest relative displacements. The greatest displacement was shown in Section 6.8.1 to be 1.494 inches, which occurs in rack 28 under simulation number 4. The maximum hydrodynamic pressure during this simulation was determined to be 19 psi. This hydrodynamic pressure was considered in the evaluation of the Fuel Handling Building and Pool structure.

## 6.11 Conclusions

- Time history simulations, including all non-linear impact and interface friction effects, have been applied to evaluate the structural margins in the Holtec spent fuel racks.
- The totality of simulations provide an extensive set of results for loads, stresses, and displacements, which taken together, demonstrate that the spent fuel racks meet the input specification and the governing Code requirements.
- Evaluation of structural margins have been performed for the array of racks in each pool with all racks loaded with fuel. The requirements of the specification and the governing Code documents are met for Level A, Level B, and Level D conditions.
- Based on all results presented in tabular form above the spent fuel racks are demonstrated to be acceptable for the service intended.



- [6.1.1] USNRC NUREG-0800, Standard Review Plan, June 1987.
- [6.1.2] (USNRC Office of Technology) "OT Position for Review and Acceptance of Spent Fuel Storage and Handling Applications", dated April 14, 1978, and January 18, 1979 amendment thereto.
- [6.2.1] Soler, A.I. and Singh, K.P., "Seismic Responses of Free Standing Fuel Rack Constructions to 3-D Motions", Nuclear Engineering and Design, Vol. 80, pp. 315-329 (1984).
- [6.2.2] Soler, A.I. and Singh, K.P., "Some Results from Simultaneous Seismic Simulations of All Racks in a Fuel Pool", INNM Spent Fuel Management Seminar X, January, 1993.
- [6.2.3] Singh, K.P. and Soler, A.I., "Seismic Qualification of Free Standing Nuclear Fuel Storage Racks - the Chin Shan Experience, Nuclear Engineering International, UK (March 1991).
- [6.2.4] Holtec Proprietary Report HI-961465 - WPMR Analysis User Manual for Pre&Post Processors & Solver, August, 1997.
- [6.4.1] USNRC Standard Review Plan, NUREG-0800 (Section 3.7.1, Rev. 2, 1989).
- [6.4.2] Holtec Proprietary Report HI-89364 - Verification and User's Manual for Computer Code GENEQ, January, 1990.
- [6.5.1] Rabinowicz, E., "Friction Coefficients of Water Lubricated Stainless Steels for a Spent Fuel Rack Facility," MIT, a report for Boston Edison Company, 1976.
- [6.5.2] Singh, K.P. and Soler, A.I., "Dynamic Coupling in a Closely Spaced Two-Body System Vibrating in Liquid Medium: The Case of Fuel Racks," 3rd International Conference on Nuclear Power Safety, Keswick, England, May 1982.
- [6.5.3] Fritz, R.J., "The Effects of Liquids on the Dynamic Motions of Immersed Solids," Journal of Engineering for Industry, Trans. of the ASME, February 1972, pp 167-172.

- [6.5.4] Levy, S. and Wilkinson, J.P.D., "The Component Element Method in Dynamics with Application to Earthquake and Vehicle Engineering," McGraw Hill, 1976.
- [6.5.5] Paul, B., "Fluid Coupling in Fuel Racks: Correlation of Theory and Experiment", (Proprietary), NUSCO/Holtec Report HI-88243.
- [6.6.1] ASME Boiler & Pressure Vessel Code, Section III, Subsection NF, 1995 Edition.
- [6.6.2] ASME Boiler & Pressure Vessel Code, Section II, Part D, 1995 Edition.
- [6.6.3] USNRC Standard Review Plan, NUREG-0800 (Section 3.8.4, Rev. 2, 1989).
- [6.9.1] ACI 349-85, Code Requirements for Nuclear Safety Related Concrete Structures, American Concrete Institute, Detroit, Michigan, 1985.
- [6.9.2] ACI 318-95, Building Code requirements for Structural Concrete," American Concrete Institute, Detroit, Michigan, 1995.

Table 6.2.1

## PARTIAL LISTING OF FUEL RACK APPLICATIONS USING DYNARACK

PLANT	DOCKET NUMBER(s)	YEAR
Enrico Fermi Unit 2	USNRC 50-341	1980
Quad Cities 1 & 2	USNRC 50-254, 50-265	1981
Rancho Seco	USNRC 50-312	1982
Grand Gulf Unit 1	USNRC 50-416	1984
Oyster Creek	USNRC 50-219	1984
Pilgrim	USNRC 50-293	1985
V.C. Summer	USNRC 50-395	1984
Diablo Canyon Units 1 & 2	USNRC 50-275, 50-323	1986
Byron Units 1 & 2	USNRC 50-454, 50-455	1987
Braidwood Units 1 & 2	USNRC 50-456, 50-457	1987
Vogtle Unit 2	USNRC 50-425	1988
St. Lucie Unit 1	USNRC 50-335	1987
Millstone Point Unit 1	USNRC 50-245	1989
Chinshan	Taiwan Power	1988
D.C. Cook Units 1 & 2	USNRC 50-315, 50-316	1992
Indian Point Unit 2	USNRC 50-247	1990
Three Mile Island Unit 1	USNRC 50-289	1991
James A. FitzPatrick	USNRC 50-333	1990
Shearon Harris	USNRC 50-400	1991
Hope Creek	USNRC 50-354	1990

Table 6.2.1

PARTIAL LISTING OF FUEL RACK APPLICATIONS USING DYNARACK

PLANT	DOCKET NUMBER(s)	YEAR
Kuosheng Units 1 & 2	Taiwan Power Company	1990
Ulchin Unit 2	Korea Electric Power Co.	1990
Laguna Verde Units 1 & 2	Comision Federal de Electricidad	1991
Zion Station Units 1 & 2	USNRC 50-295, 50-304	1992
Sequoyah	USNRC 50-327, 50-328	1992
LaSalle Unit 1	USNRC 50-373	1992
Duane Arnold Energy Center	USNRC 50-331	1992
Fort Calhoun	USNRC 50-285	1992
Nine Mile Point Unit 1	USNRC 50-220	1993
Beaver Valley Unit 1	USNRC 50-334	1992
Salem Units 1 & 2	USNRC 50-272, 50-311	1993
Limerick	USNRC 50-352, 50-353	1994
Ulchin Unit 1	KINS	1995
Yonggwang Units 1 & 2	KINS	1996
Kori-4	KINS	1996
Connecticut Yankee	USNRC 50-213	1996
Angra Unit 1	Brazil	1996
Sizewell B	United Kingdom	1996

**Table 6.3.1**  
**RACK MATERIAL DATA (200°F)**  
**(ASME - Section II, Part D)**

Material	Young's Modulus E (psi)	Yield Strength S <sub>y</sub> (psi)	Ultimate Strength S <sub>u</sub> (psi)
SA240; 304L S.S.	27.6 x 10 <sup>6</sup>	21,300	66,200
<b>SUPPORT MATERIAL DATA (200°F)</b>			
SA240, Type 304L (upper part of support feet)	27.6 x 10 <sup>6</sup>	21,300	66,200
SA-564-630 (lower part of support feet; age hardened at 1100°F)	28.5 x 10 <sup>6</sup>	106,300	140,000

**Table 6.4.1**  
**TIME-HISTORY STATISTICAL CORRELATION RESULTS**

OBE	
Data1 to Data2	0.0295
Data1 to Data3	0.0392
Data2 to Data3	0.0169
DBE	
Data1 to Data2	0.0183
Data1 to Data3	0.0588
Data2 to Data3	0.0299



**Table 6.5.1**  
**Degrees-of-freedom**

LOCATION (Node)	DISPLACEMENT			ROTATION		
	$U_x$	$U_y$	$U_z$	$\theta_x$	$\theta_y$	$\theta_z$
1	$p_1$	$p_2$	$p_3$	$q_4$	$q_5$	$q_6$
2	$p_7$	$p_8$	$p_9$	$q_{10}$	$q_{11}$	$q_{12}$
Node 1 is assumed to be attached to the rack at the bottom most point. Node 2 is assumed to be attached to the rack at the top most point. Refer to Figure 6.5.1 for node identification.						
2*	$p_{13}$	$p_{14}$				
3*	$p_{15}$	$p_{16}$				
4*	$p_{17}$	$p_{18}$				
5*	$p_{19}$	$p_{20}$				
1*	$p_{21}$	$p_{22}$				
where the relative displacement variables $q_i$ are defined as: $p_i = q_i(t) + U_x(t) \quad i = 1,7,13,15,17,19,21$ $\quad = q_i(t) + U_y(t) \quad i = 2,8,14,16,18,20,22$ $\quad = q_i(t) + U_z(t) \quad i = 3,9$ $\quad = q_i(t) \quad i = 4,5,6,10,11,12$ $p_i$ denotes absolute displacement (or rotation) with respect to inertial space $q_i$ denotes relative displacement (or rotation) with respect to the floor slab * denotes fuel mass nodes $U(t)$ are the three known earthquake displacements						

**Table 6.5.2  
(MR216) NUMBERING SYSTEM  
FOR GAP ELEMENTS AND FRICTION ELEMENTS  
IN THE POOL D, CAMPAIGN I, MODEL**

**I. Nonlinear Springs (Type 3 Gap Elements - 212 Total)**

Number	Rack No.	Description
1	1	Support S1, Z compression-only element
2	1	Support S2, Z compression-only element
3	1	Support S3, Z compression-only element
4	1	Support S4, Z compression-only element
5	1	X rack/fuel assembly impact element between nodes 2 and 2*
6	1	X rack/fuel assembly impact element between nodes 2 and 2*
7	1	Y rack/fuel assembly impact element between nodes 2 and 2*
8	1	Y rack/fuel assembly impact element between nodes 2 and 2*
9-24	1	Impact elements corresponding to the remaining rattling fuel masses at nodes 1*, 3*, 4* and 5* (similar to elements 5 thru 8)
25-28	2	Z compression-only elements for Supports S1, S2, S3, and S4
29-48	2	Impact elements corresponding to the rattling masses at nodes 1*, 2*, 3*, 4* and 5*
49-144	3-6	Impact elements similar to those above
145-212	varies	rack/rack and rack/wall elements at top and bottom of racks (see Figures 6.5.6 and 6.5.7)

**Table 6.5.2  
(MR216) NUMBERING SYSTEM  
FOR GAP ELEMENTS AND FRICTION ELEMENTS  
IN THE POOL D, CAMPAIGN I MODEL**

**II. Linear Springs (Type 1 Elements - 36 Total)**

Number	Rack No.	Description
1	1	Rack beam bending element (x-z plane)
2	1	Rack shear deformation element (x-z plane)
3	1	Rack beam bending element (y-z plane)
4	1	Rack shear deformation element (y-z plane)
5	1	Rack beam axial deformation element
6	1	Rack beam torsional deformation element
7-12	2	Similar to elements 1 thru 6
13-36	3-6	Similar to elements 1 thru 6

**III. Piece-wise Linear Friction Springs (Type 2 Elements - 48 Total)**

Number	Rack No.	Description
1	1	Pedestal 1, X direction
2	1	Pedestal 1, Y direction
3	1	Pedestal 2, X direction
4	1	Pedestal 2, Y direction
5	1	Pedestal 3, X direction
6	1	Pedestal 3, Y direction
7	1	Pedestal 4, X direction
8	1	Pedestal 4, Y direction
9-16	2	Similar to elements 1 thru 8
17-48	3-6	Similar to elements 1 thru 8

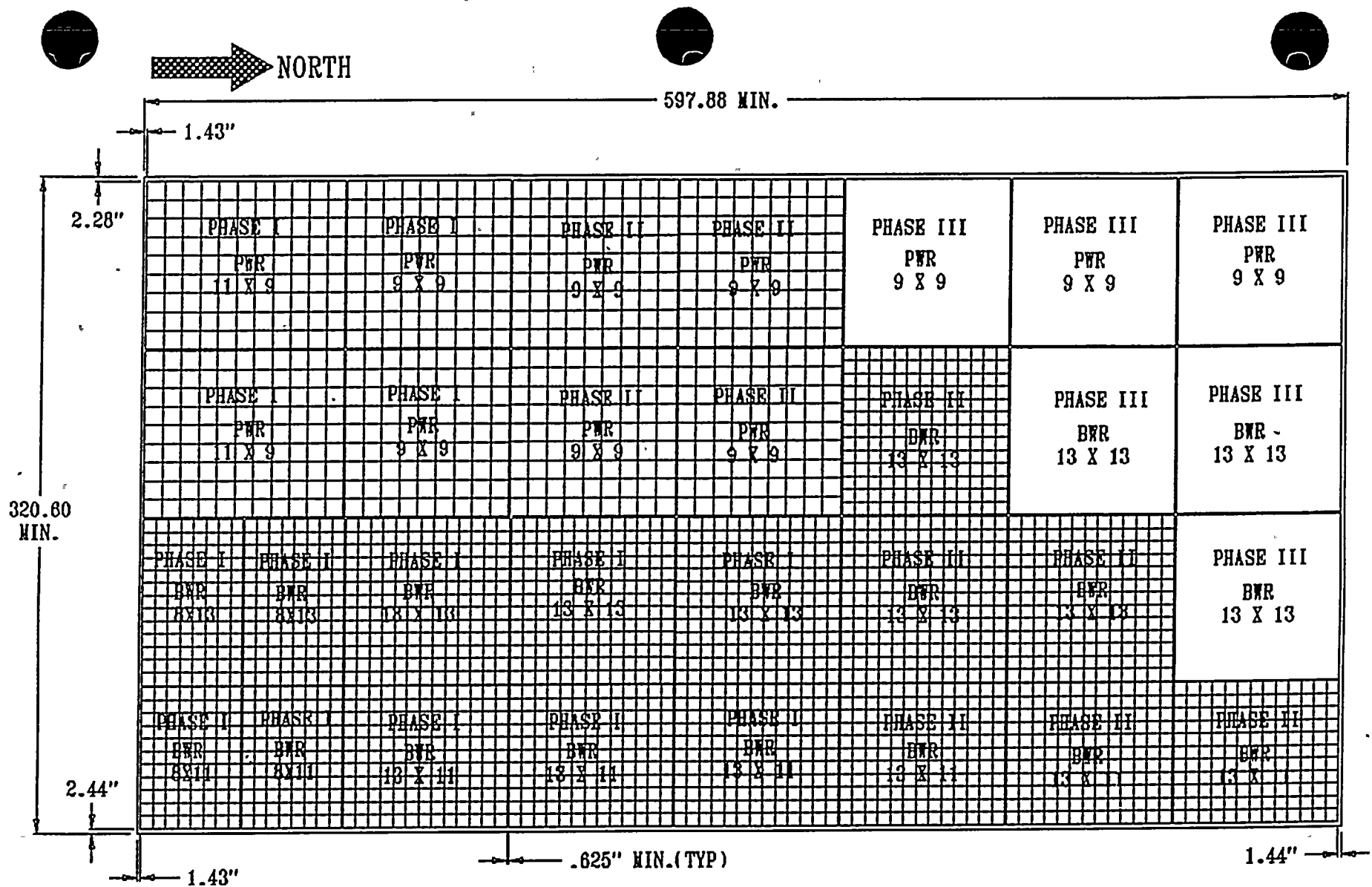
**Table 6.9.1**  
**COMPARISON OF BOUNDING CALCULATED LOADS/STRESSES**  
**VS.**  
**CODE ALLOWABLES**  
**AT IMPACT AND WELD LOCATIONS**

Item/Location	DBE Calculated	OBE Allowable
Fuel assembly/cell wall impact, lbf.	605 *	3,238 **
Rack/baseplate weld, psi	13,574	19,860
Female pedestal/baseplate weld, psi	10,194	19,860
Cell/cell welds, lbf.	1,711 ***	3,195

\* See Section 6.8.4.3.

\*\* Based on the limit load for a cell wall. The allowable load on the fuel assembly itself may be less than this value but is greater than 605 lbs.

\*\*\* Based on the fuel assembly to cell wall impact load simultaneously applied in two orthogonal directions.



PHASE I CELL COUNT :  
 360 CELLS - PWR  
 1320 CELLS - BWR

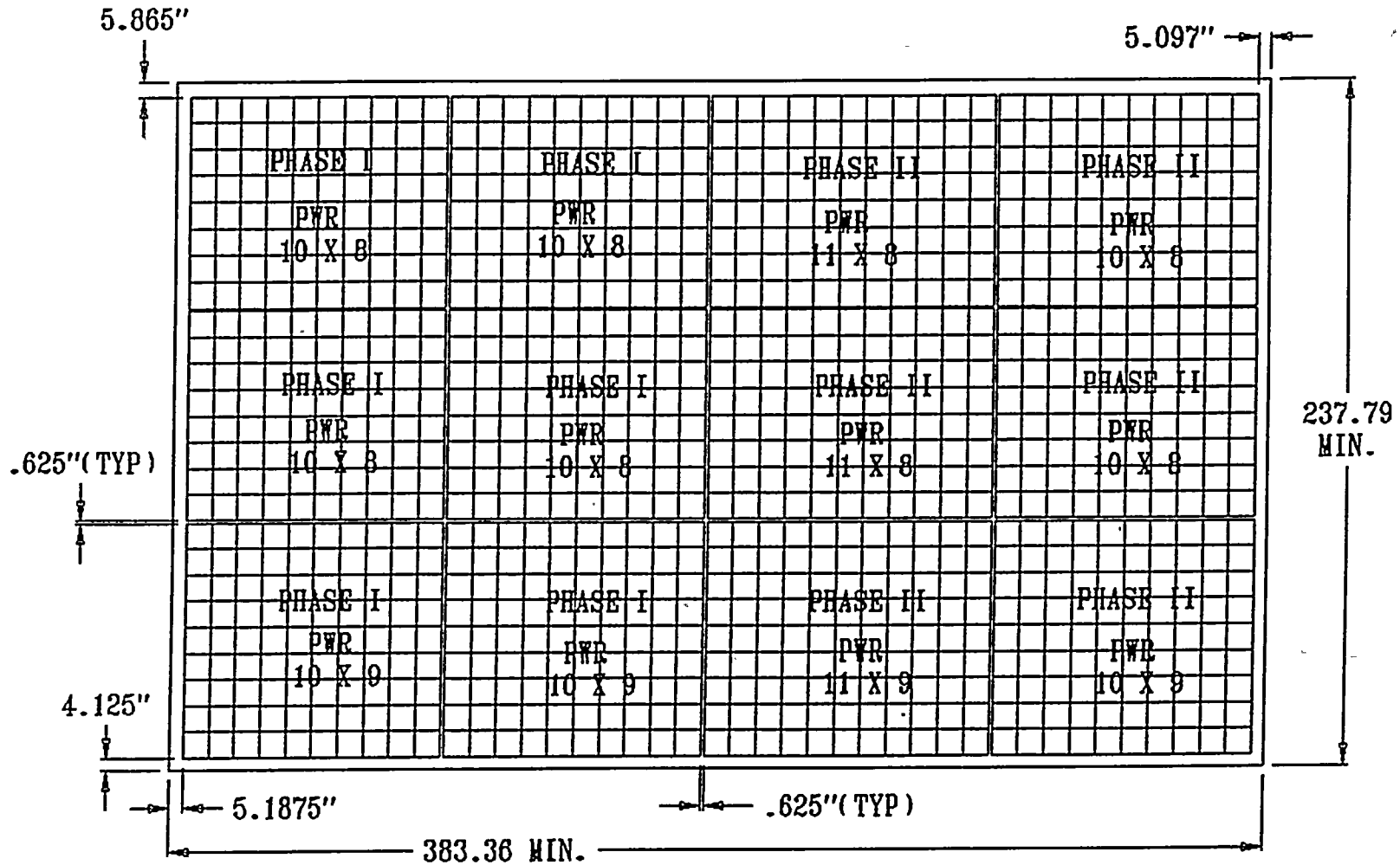
PHASE II CELL COUNT :  
 324 CELLS - PWR  
 936 CELLS - BWR

PHASE III CELL COUNT :  
 243 CELLS - PWR  
 507 CELLS - BWR

TOTAL CELL COUNT :  
 927 CELLS - PWR  
 2763 CELLS - BWR

FIGURE 6.3.1; PHASED STORAGE CONFIGURATION FOR POOL C





PHASE I CELL COUNT:  
500 CELLS - PWR

PHASE II CELL COUNT:  
525 CELLS - PWR

TOTAL CELL COUNT:  
1025 CELLS - PWR

FIGURE 6.3.2; PHASED STORAGE CONFIGURATION FOR POOL D



Harris Plant  
Spent Fuel Pool Time History Accelerogram  
X direction Bounding Spectra (2% Damping)

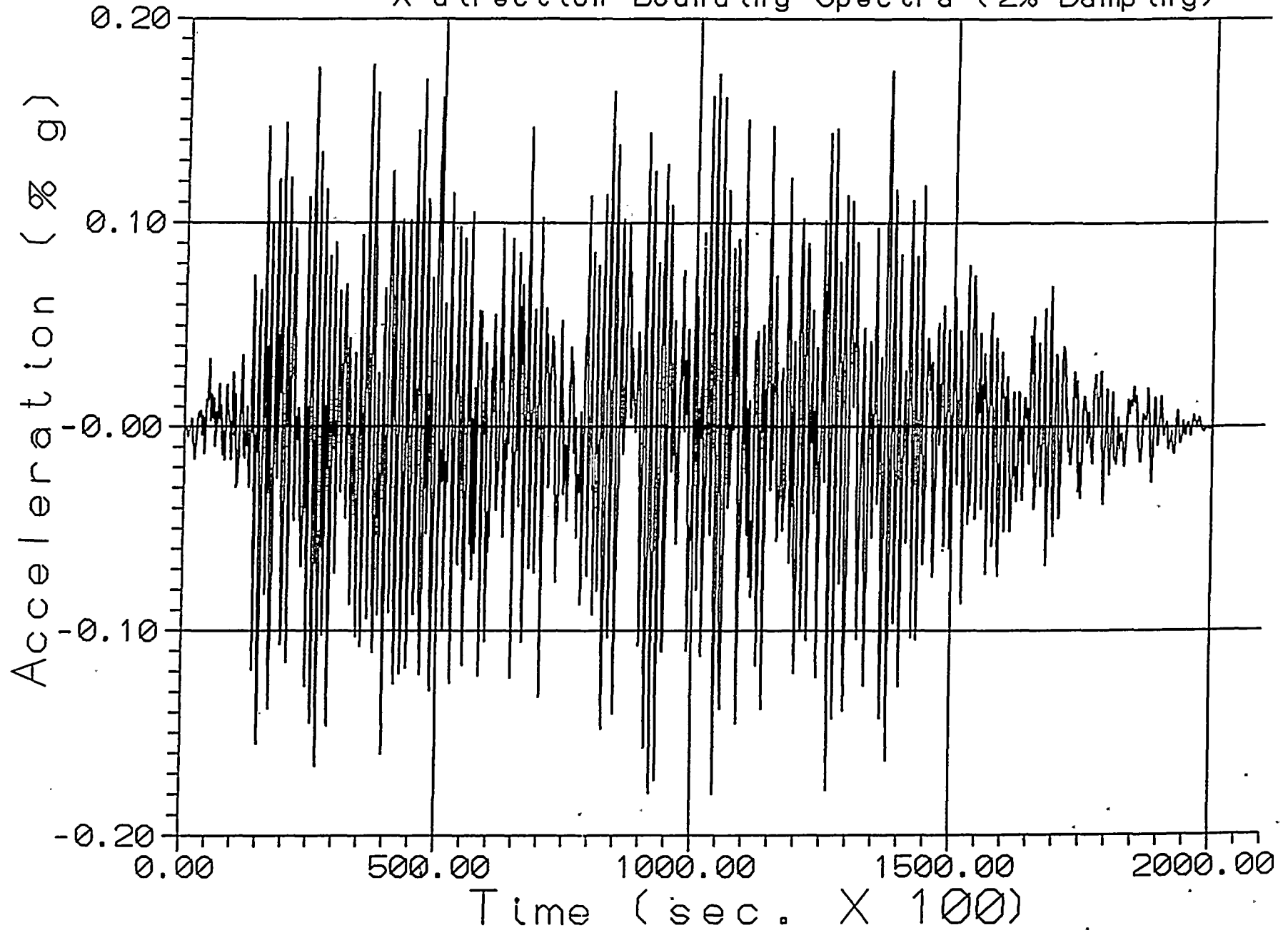


Figure 6.41

Harris Plant  
Spent Fuel Pool Time History Accelerogram  
Y direction Bounding Spectra (2% Damping)

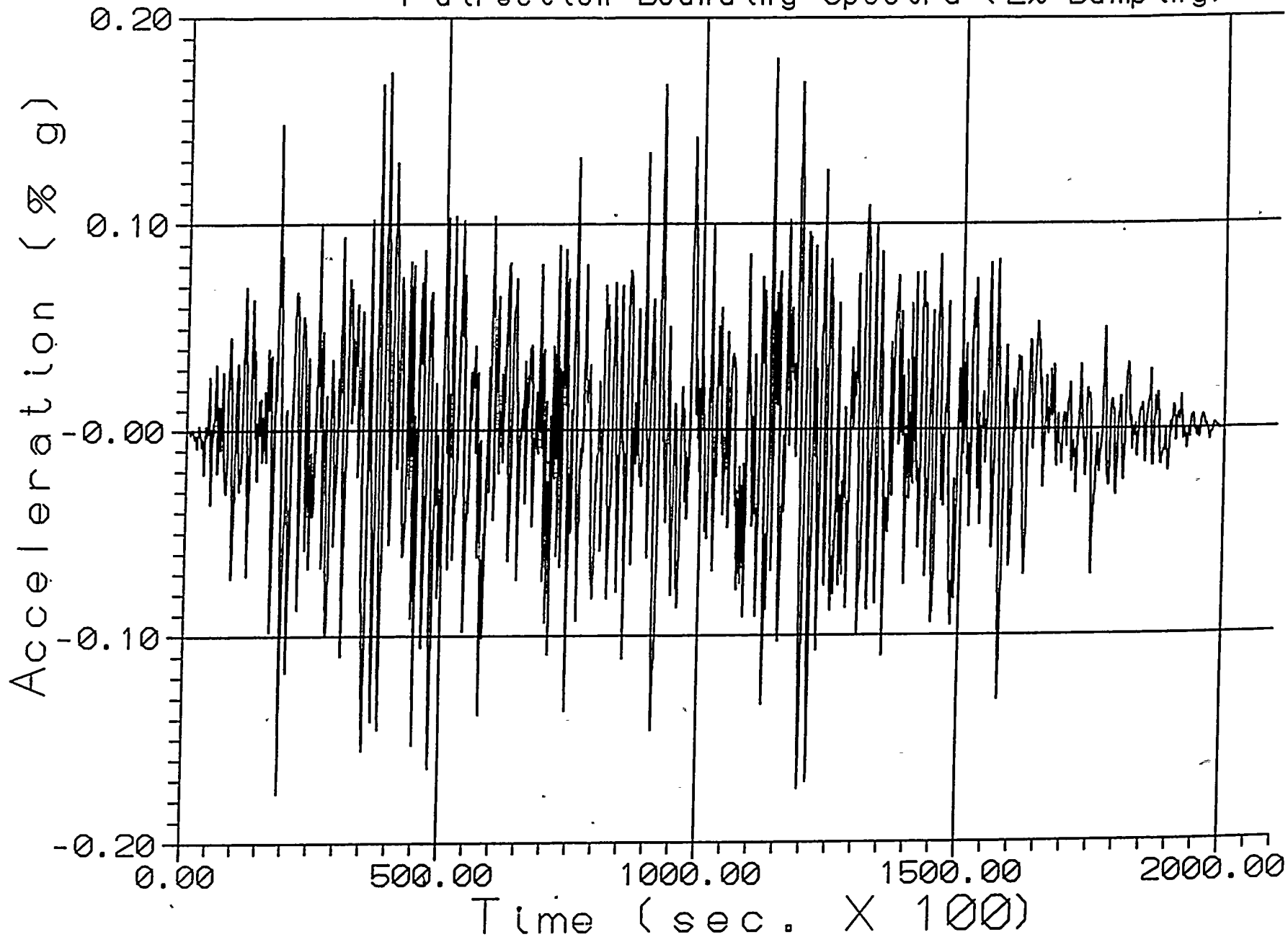


Figure 6.42



Harris Plant  
Spent Fuel Pool Time History Accelerogram  
Z direction Bounding Spectra (2% Damping)

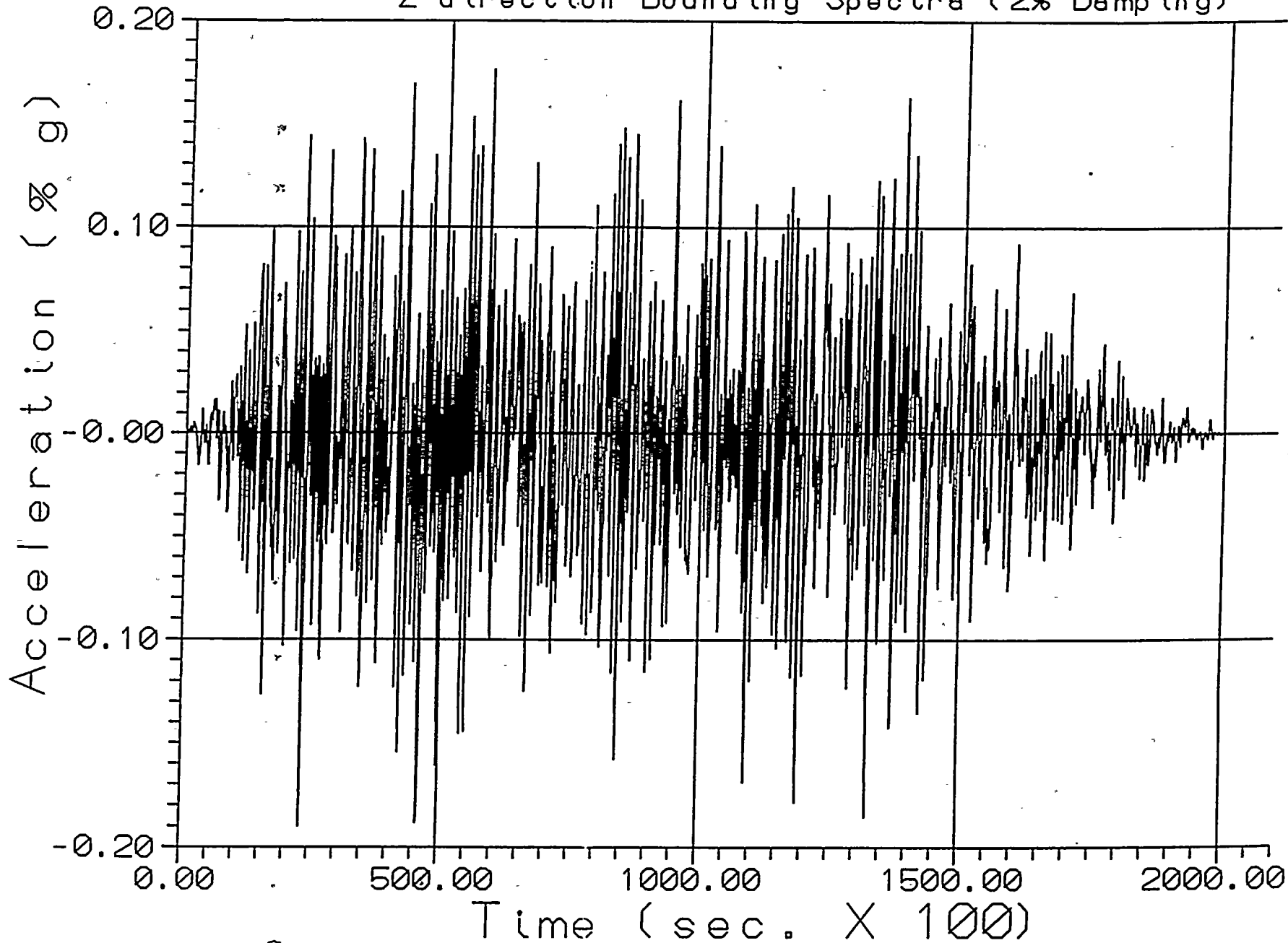


Figure 6.43<sup>a</sup>



Harris Plant  
Spent Fuel Pool Time History Accelerogram  
X direction Bounding Spectra (4% Damping)

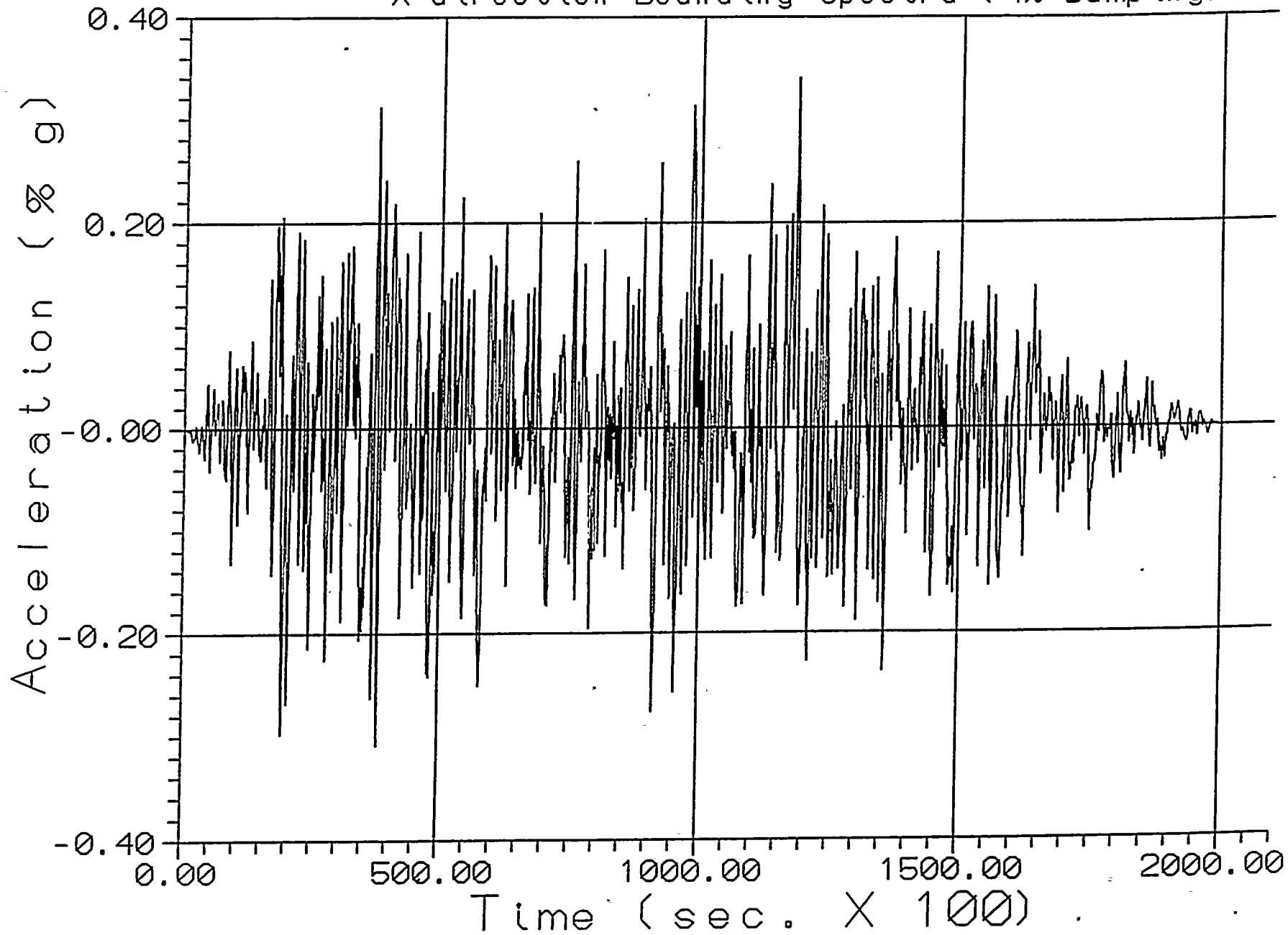


Figure 6.4.4



Harris Plant  
Spent Fuel Pool Time History Accelerogram  
Y direction Bounding Spectra (4% Damping)

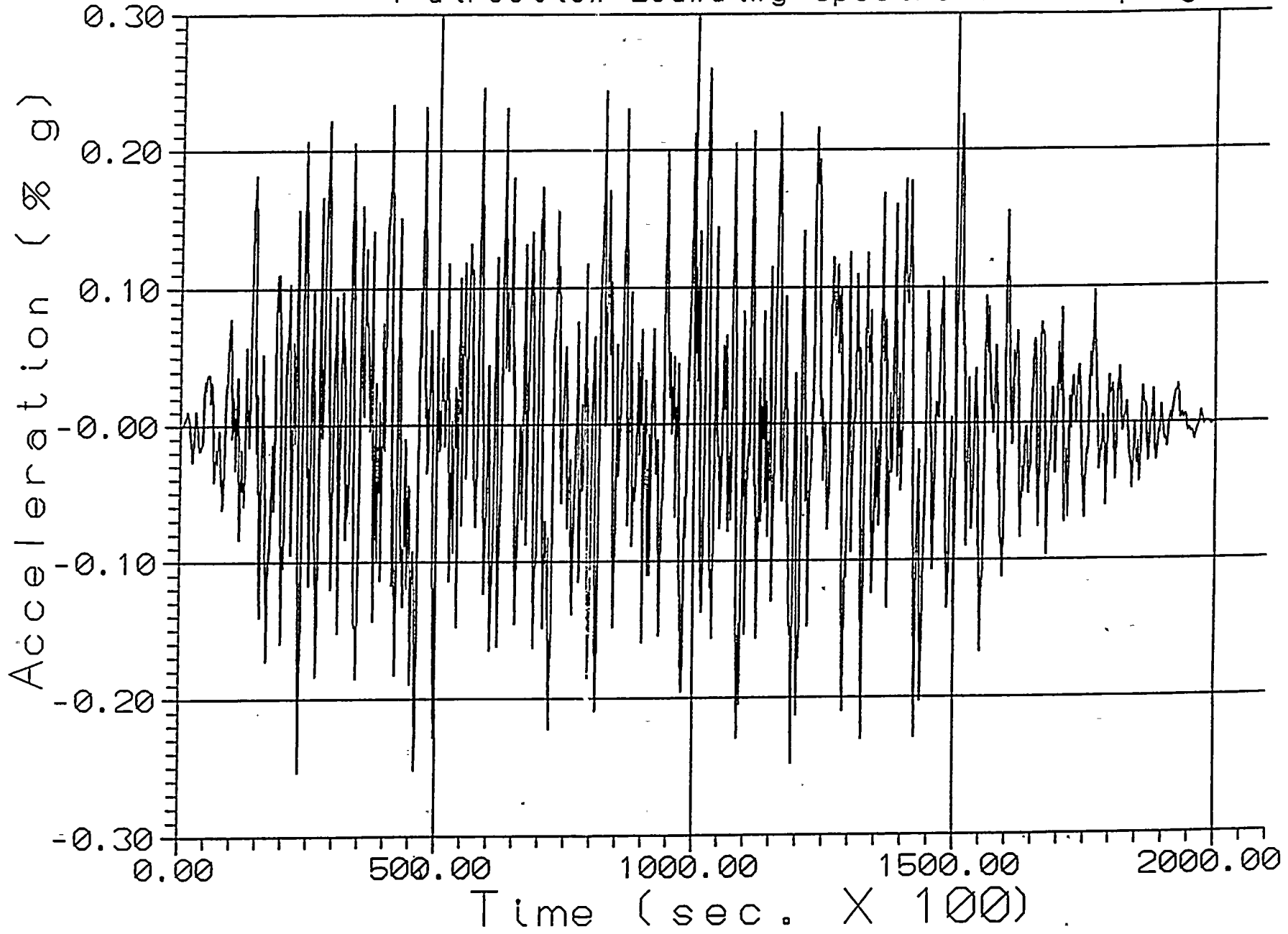


Figure 6.4.5

Harris Plant  
Spent Fuel Pool Time History Accelerogram  
Z direction Bounding Spectra (4% Damping)

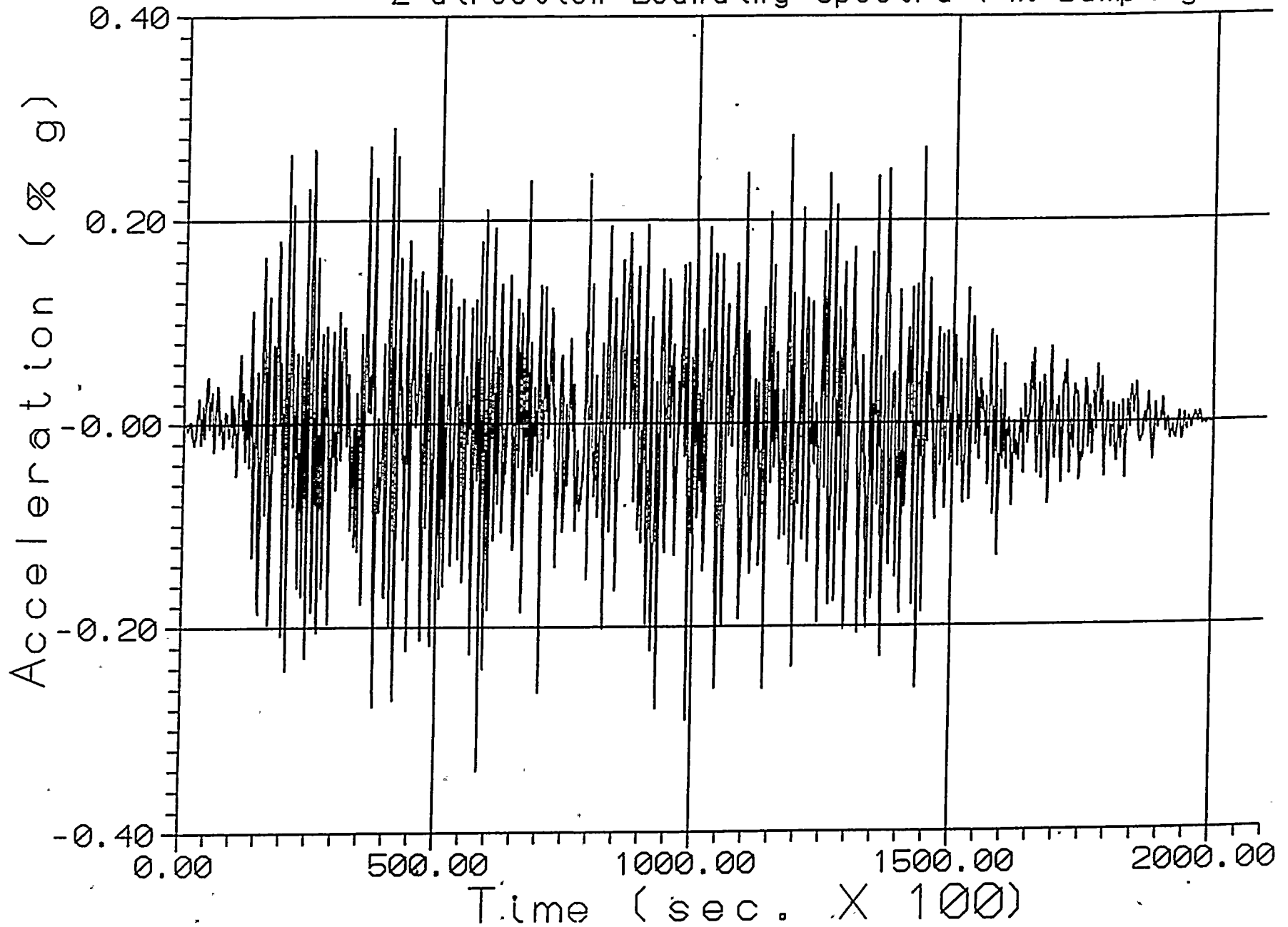


Figure 6.4.6

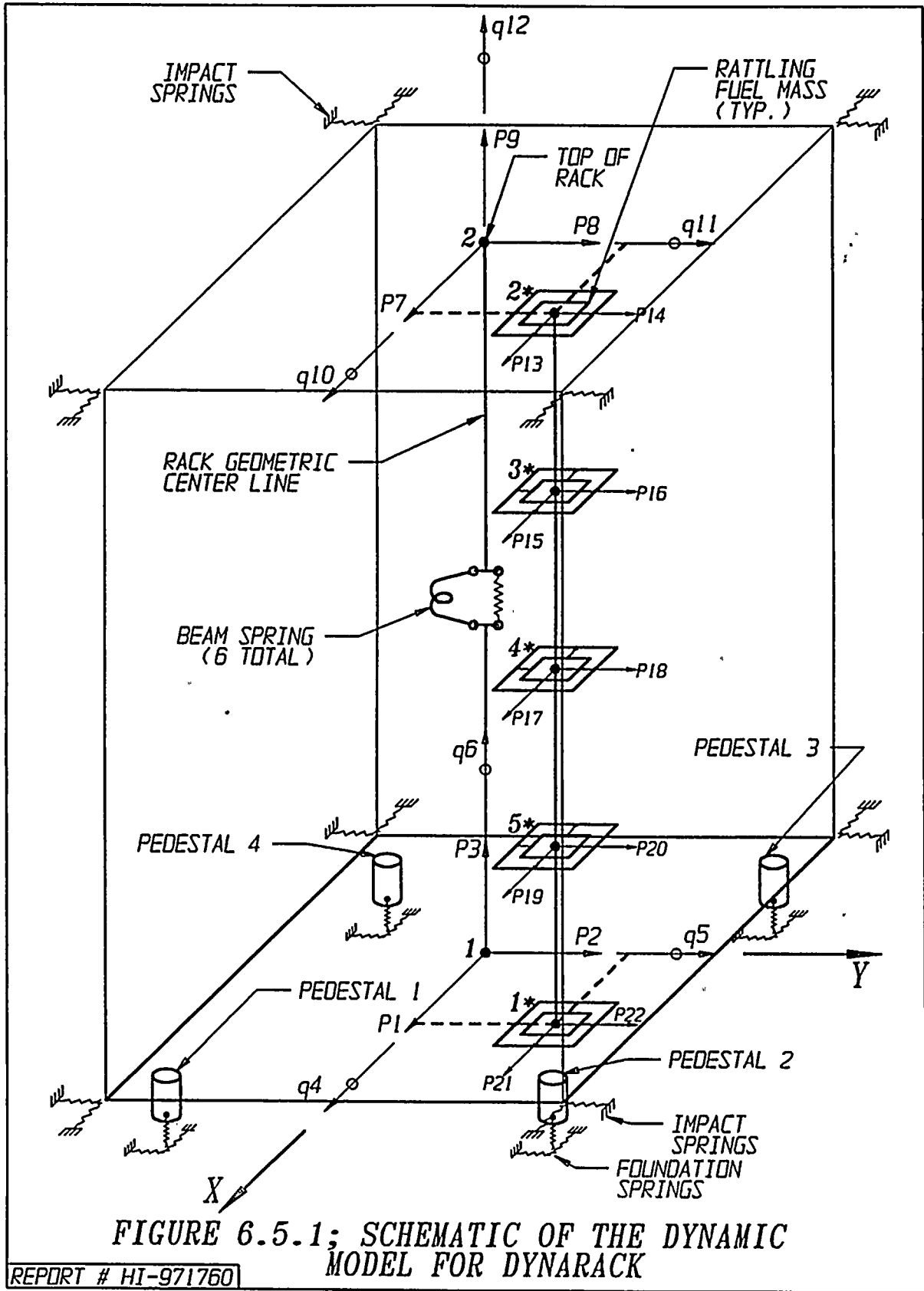


FIGURE 6.5.1; SCHEMATIC OF THE DYNAMIC MODEL FOR DYNARACK

REPORT # HI-971760

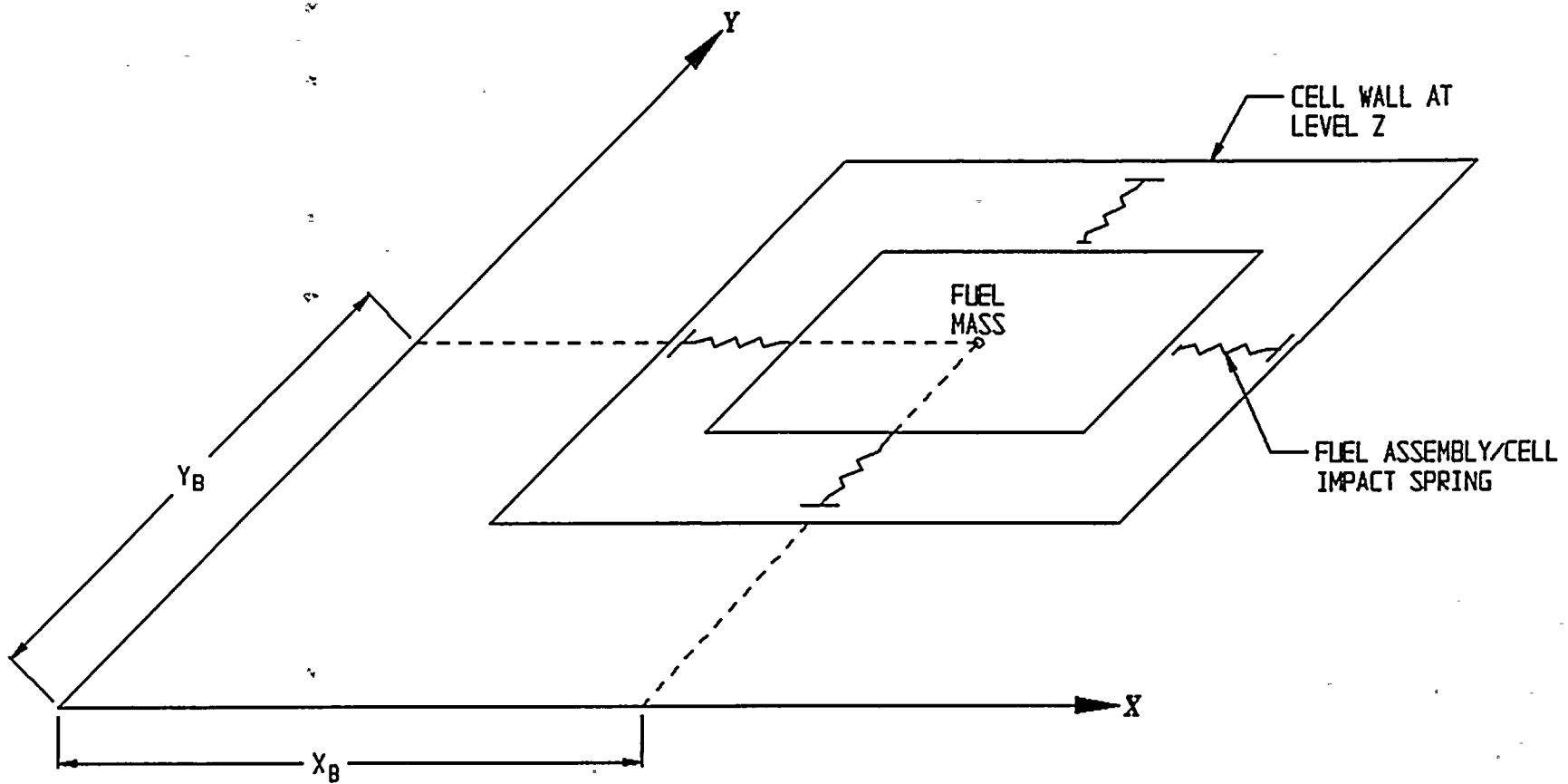


FIGURE 6.5.2; FUEL-TO-RACK IMPACT SPRINGS AT LEVEL OF RATTLING MASS

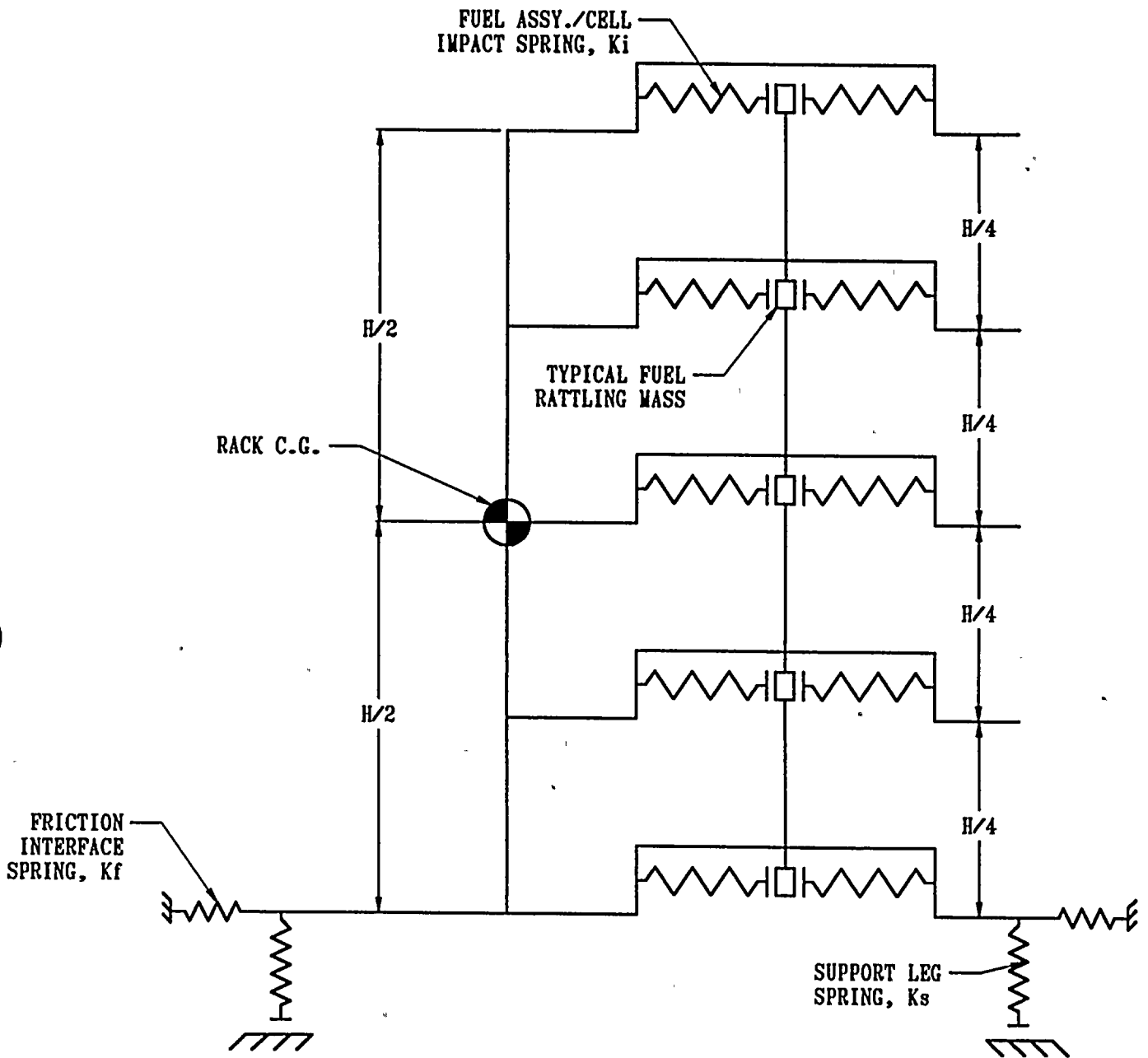
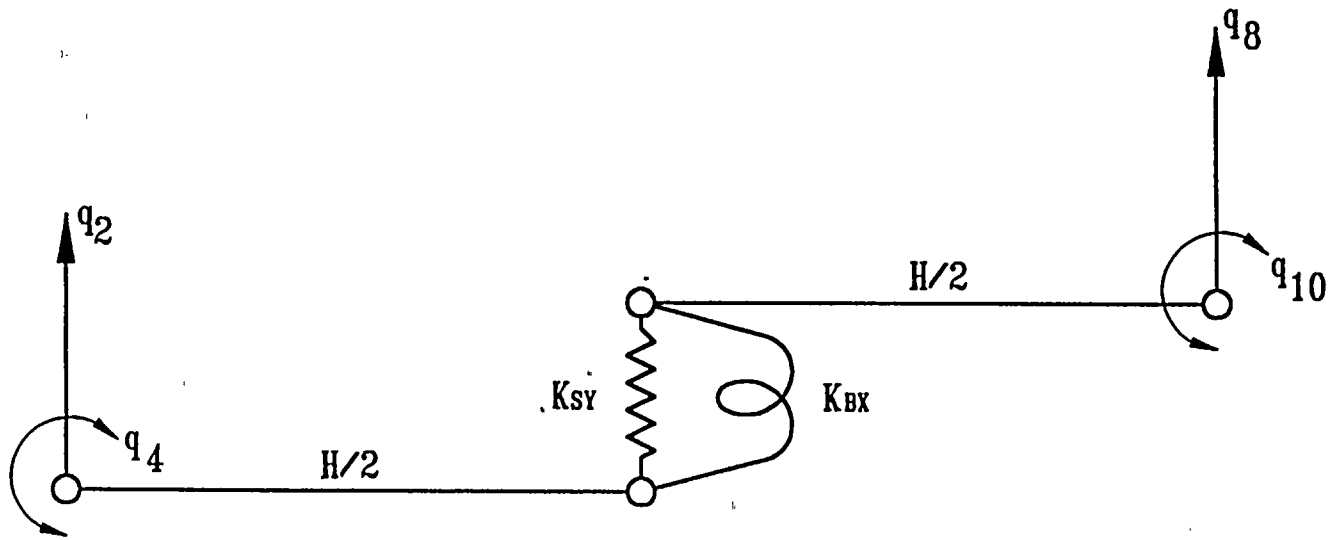


FIGURE 6.5.3; TWO DIMENSIONAL VIEW OF THE  
 SPRING-MASS SIMULATION

REPORT # HI-971760



RACK DEGREES-OF-FREEDOM FOR Y-Z PLANE BENDING WITH SHEAR AND BENDING SPRING

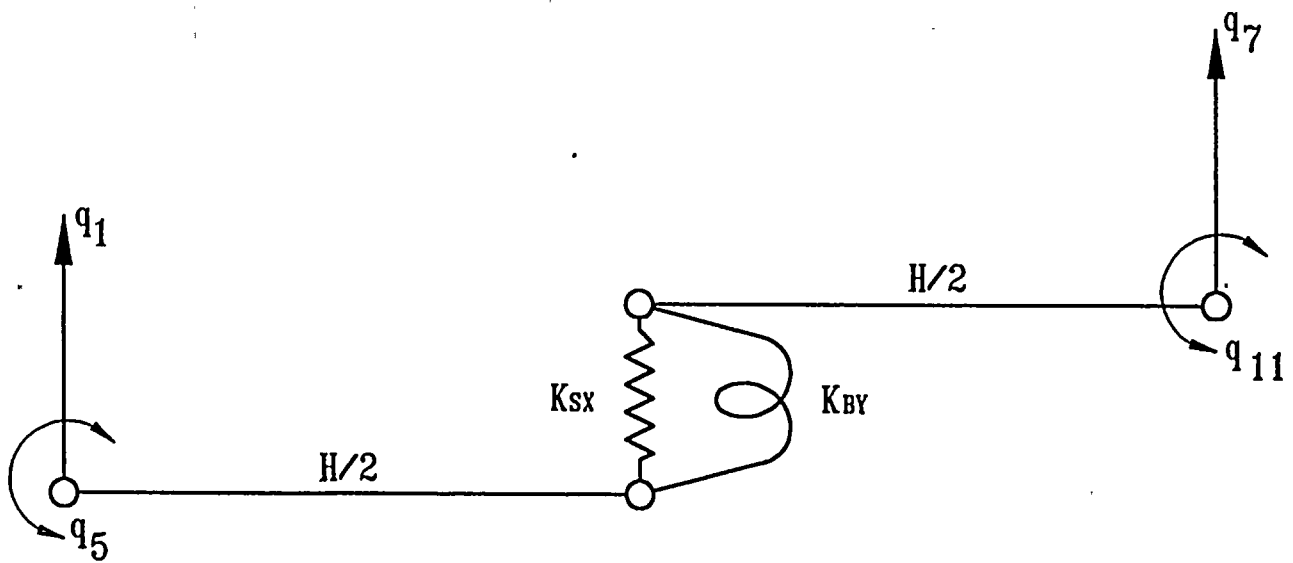


FIGURE 6.5.4; RACK DEGREES-OF-FREEDOM FOR X-Z PLANE BENDING WITH SHEAR AND BENDING SPRING

REPORT # HI-971760

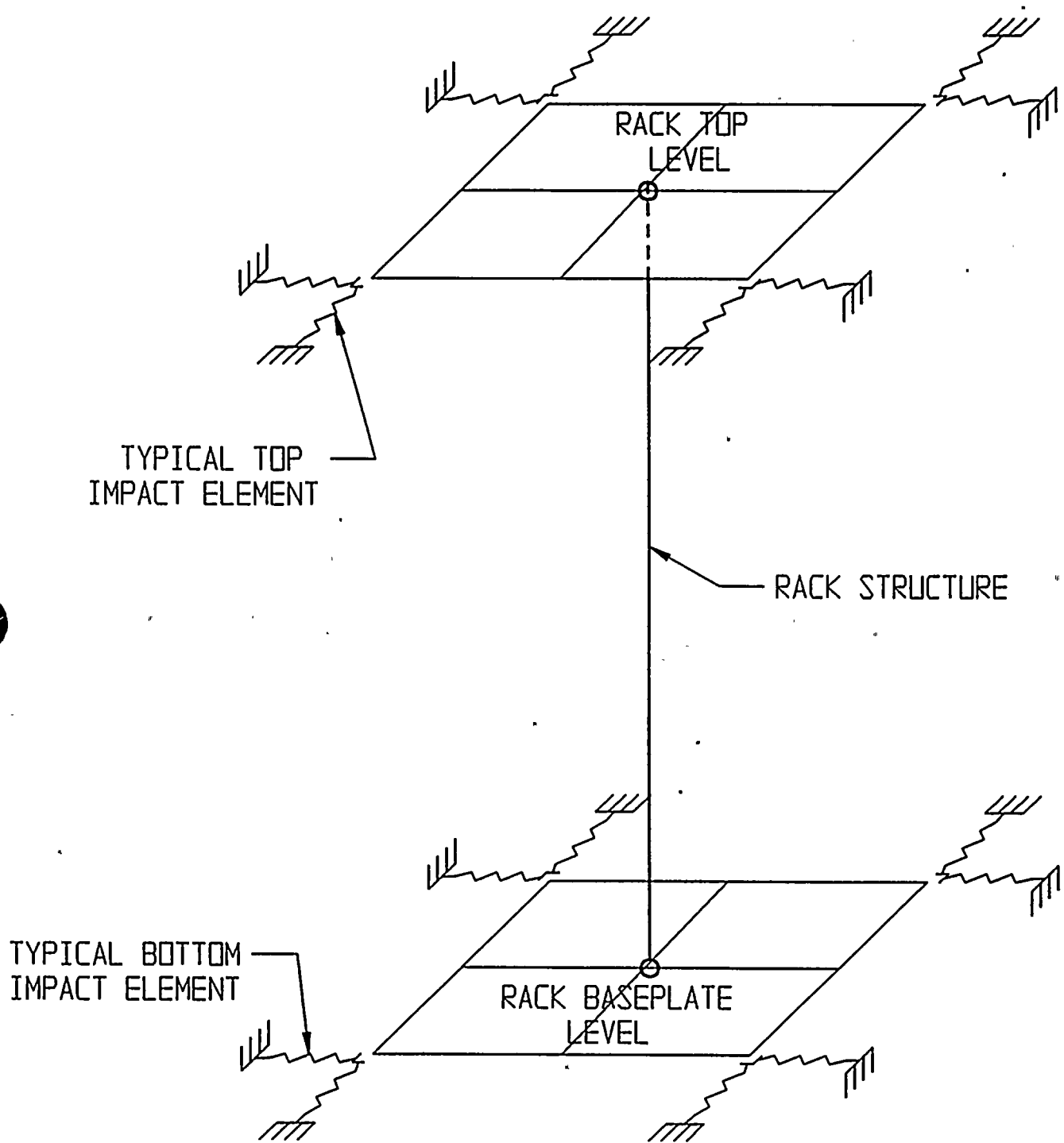
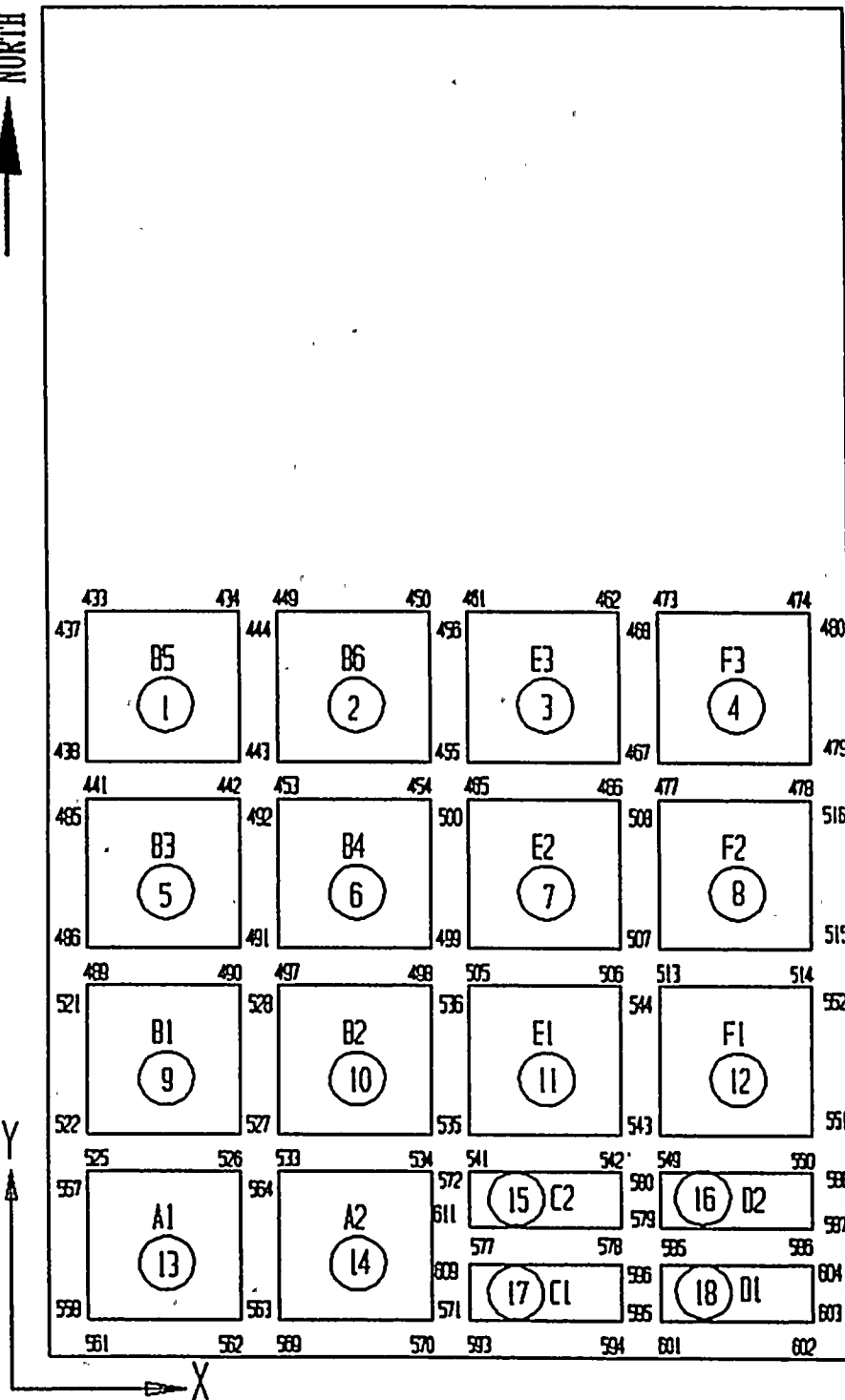


FIGURE 6.5.5; RACK-TO-RACK IMPACT SPRINGS

REPORT # HI-971760



MODEL  
COORDINATE  
AXES

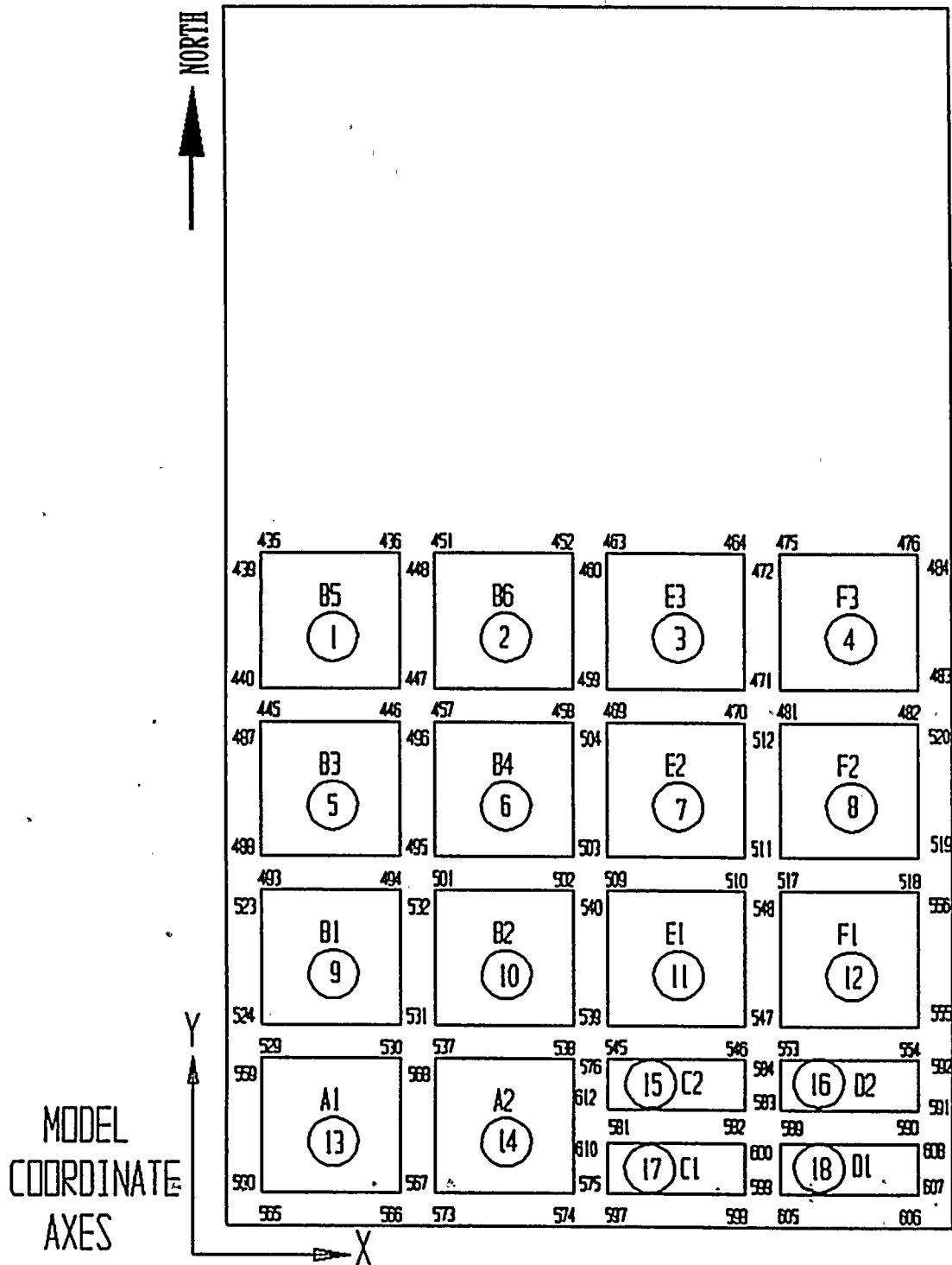


### HARRIS SPENT FUEL POOL C

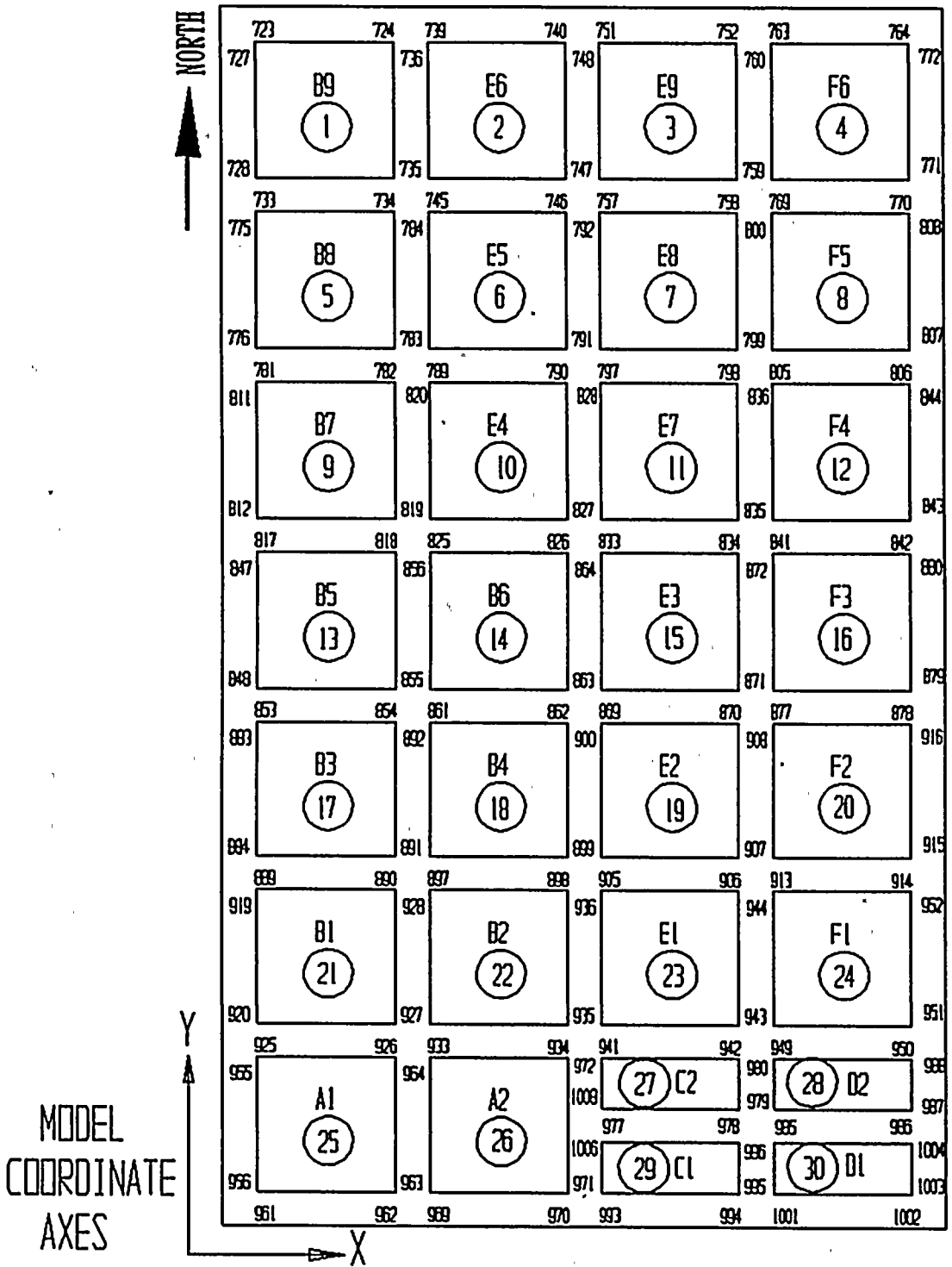
FIGURE 6.5.6; RACK IMPACT SPRING NUMBERING SCHEME (BOTTOM)  
CAMPAIGN I

HI -971760







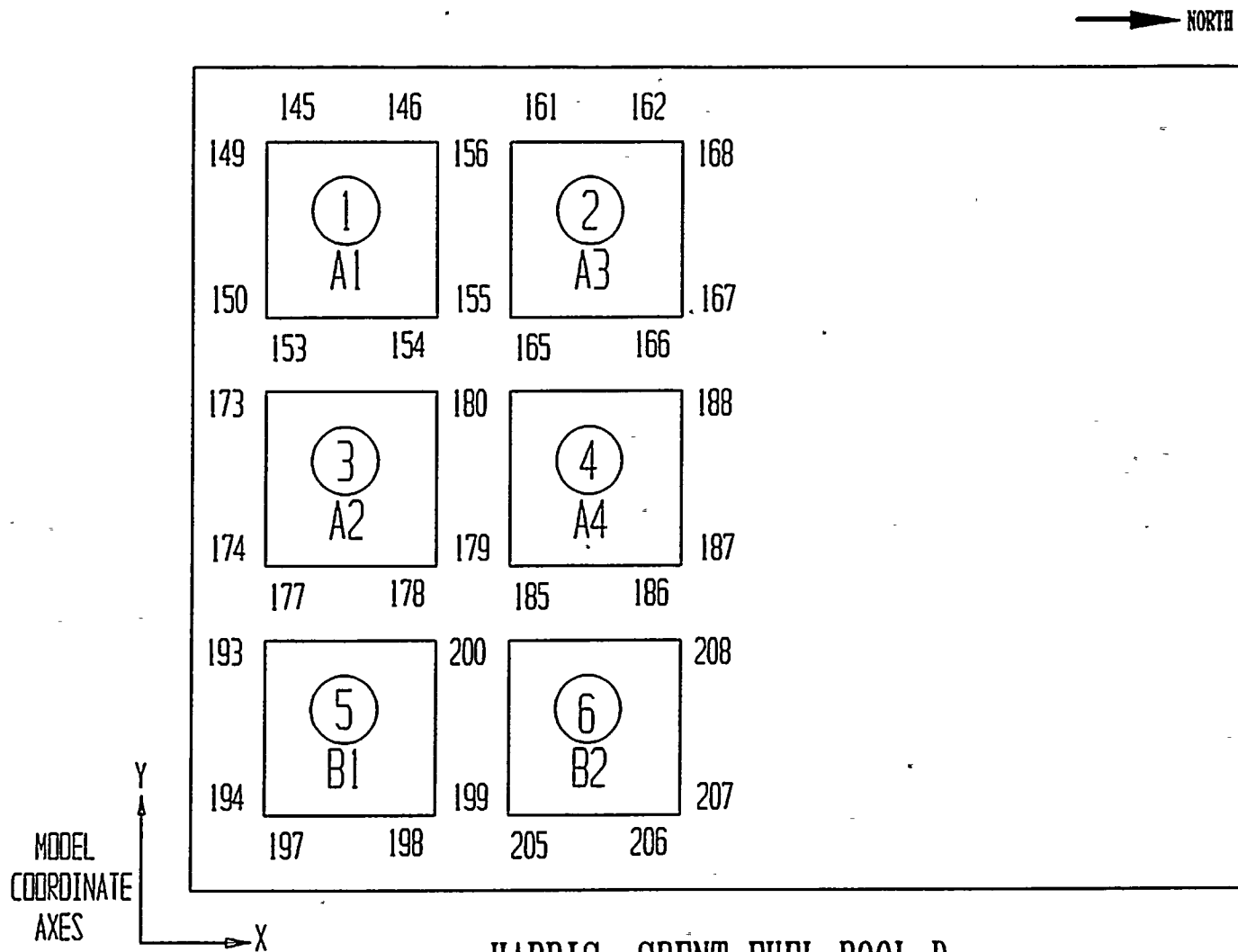


HARRIS SPENT FUEL POOL C

FIGURE 6.5.9; RACK IMPACT SPRING NUMBERING SCHEME (TOP)  
CAMPAIGNS II AND III

HI -971760

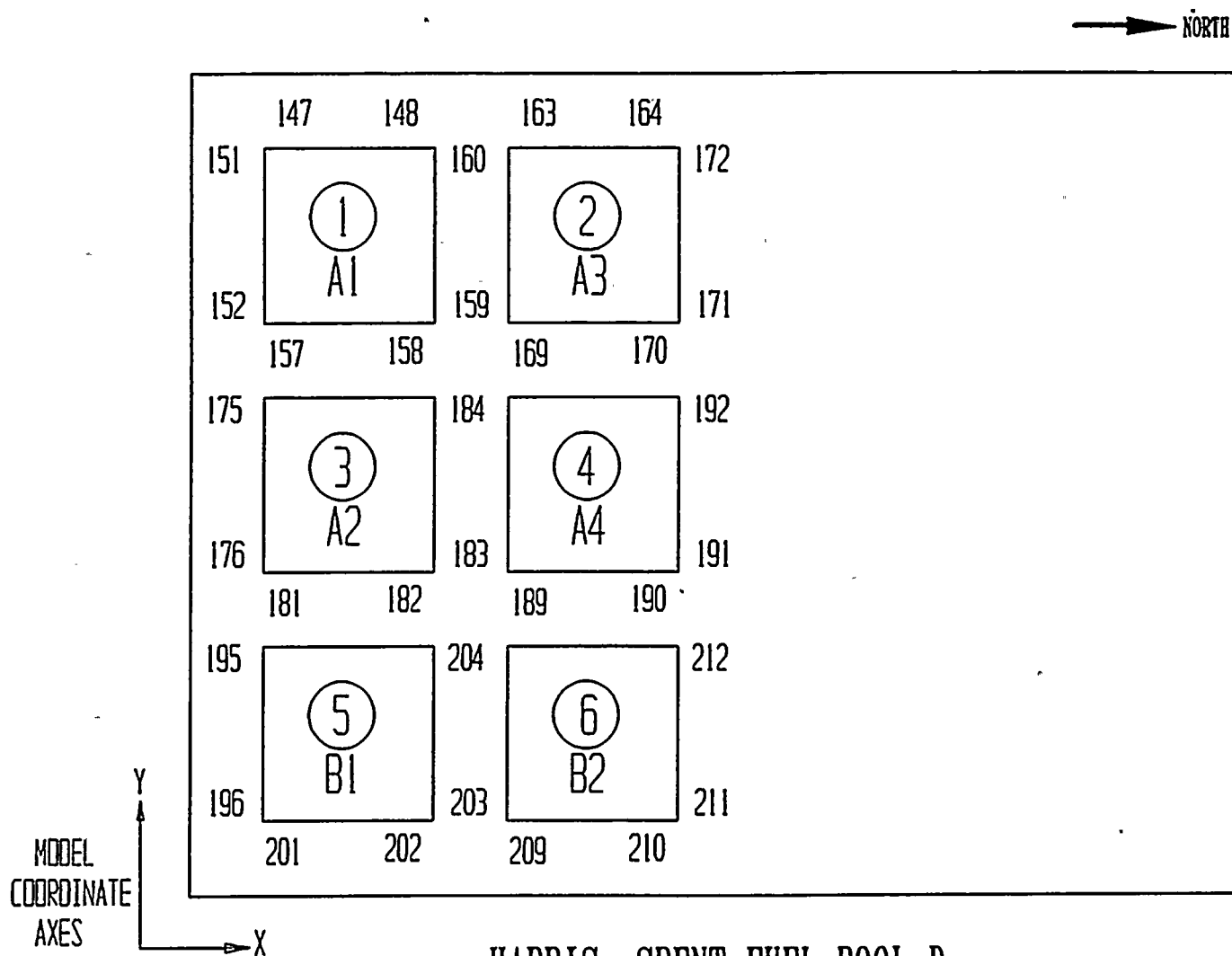




HARRIS SPENT FUEL POOL D

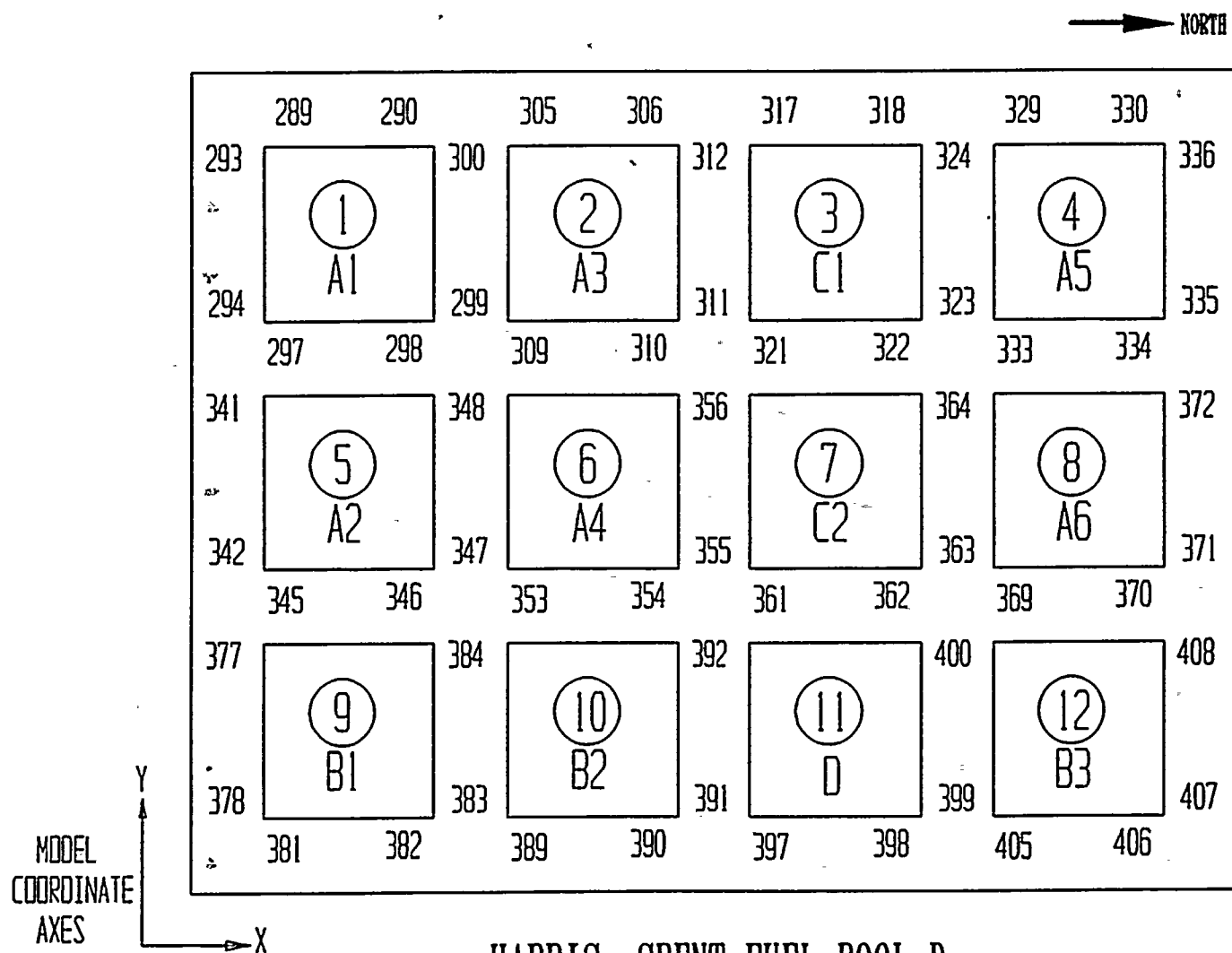
FIGURE 6.5.10; RACK IMPACT SPRING NUMBERING SCHEME (BOTTOM) CAMPAIGN I





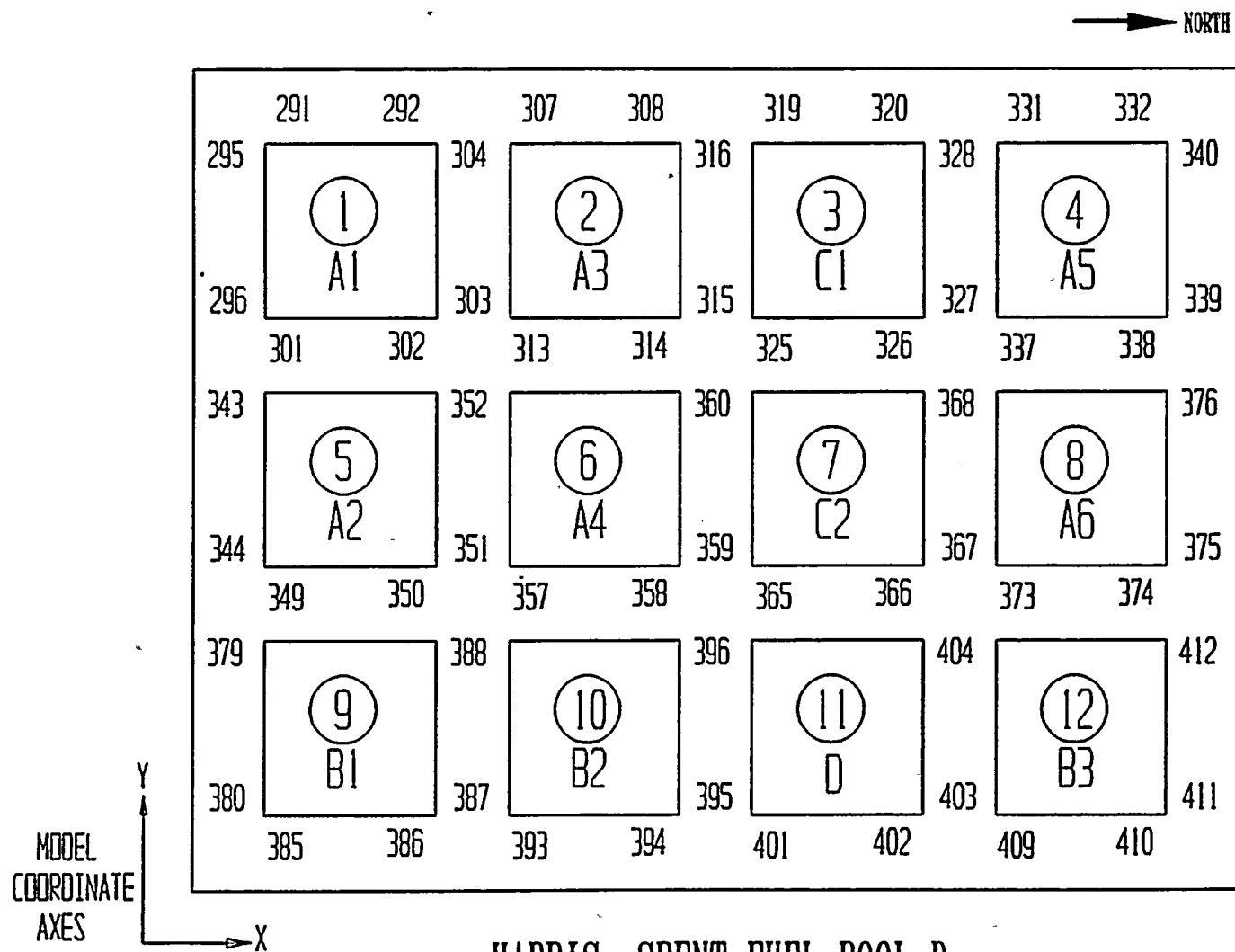
HARRIS SPENT FUEL POOL D

FIGURE 6.5.11; RACK IMPACT SPRING NUMBERING SCHEME (TOP)  
CAMPAIGN I



HARRIS SPENT FUEL POOL D

FIGURE 6.5.12; RACK IMPACT SPRING NUMBERING SCHEME (BOTTOM)  
 CAMPAIGN II



HARRIS SPENT FUEL POOL D

FIGURE 6.5.13; RACK IMPACT SPRING NUMBERING SCHEME (TOP)  
CAMPAIGN II

Harris Pool C Run 4  
Vertical Pedestal SSE Time History Loading  
Rack 5, Pedestal 2

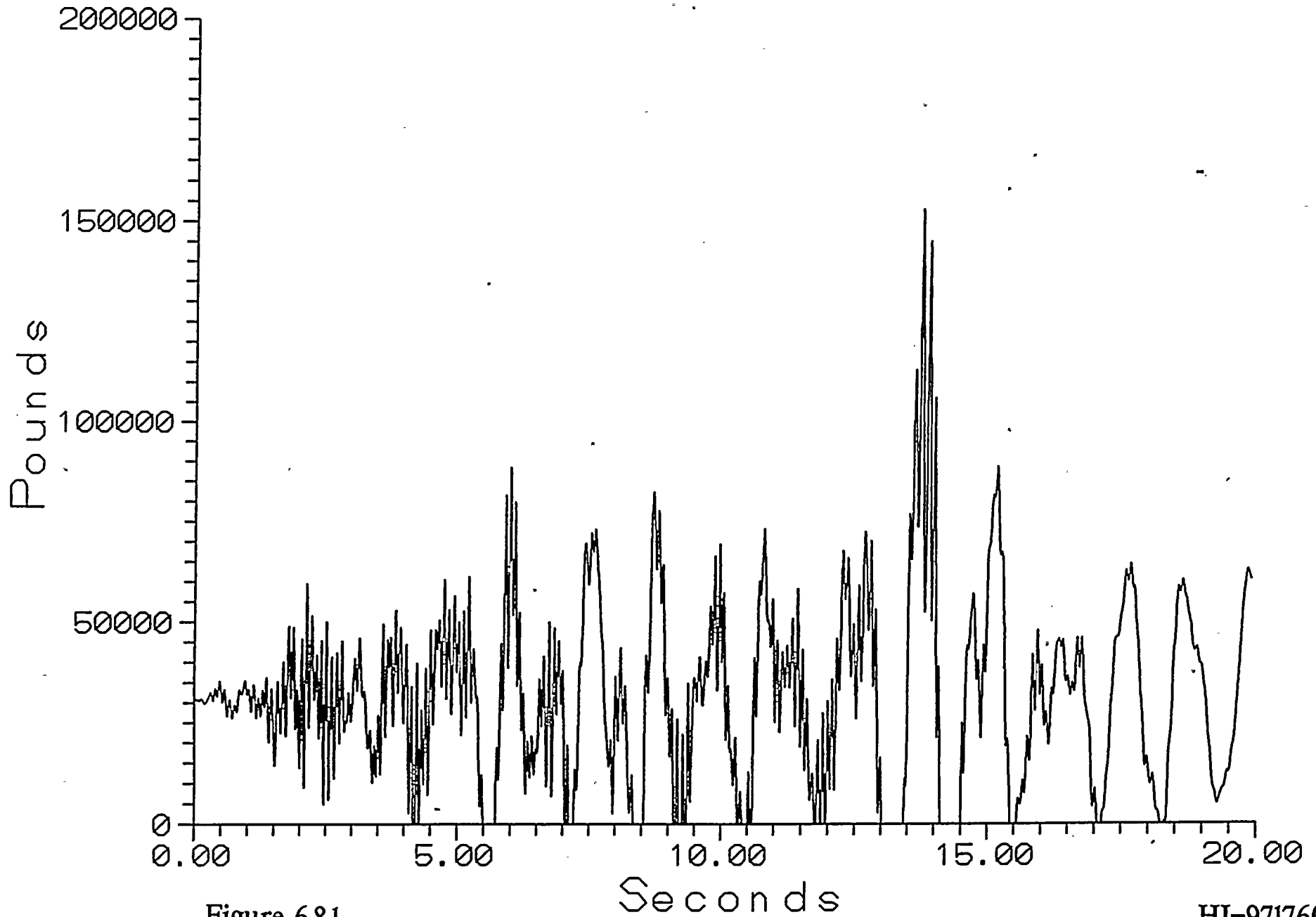
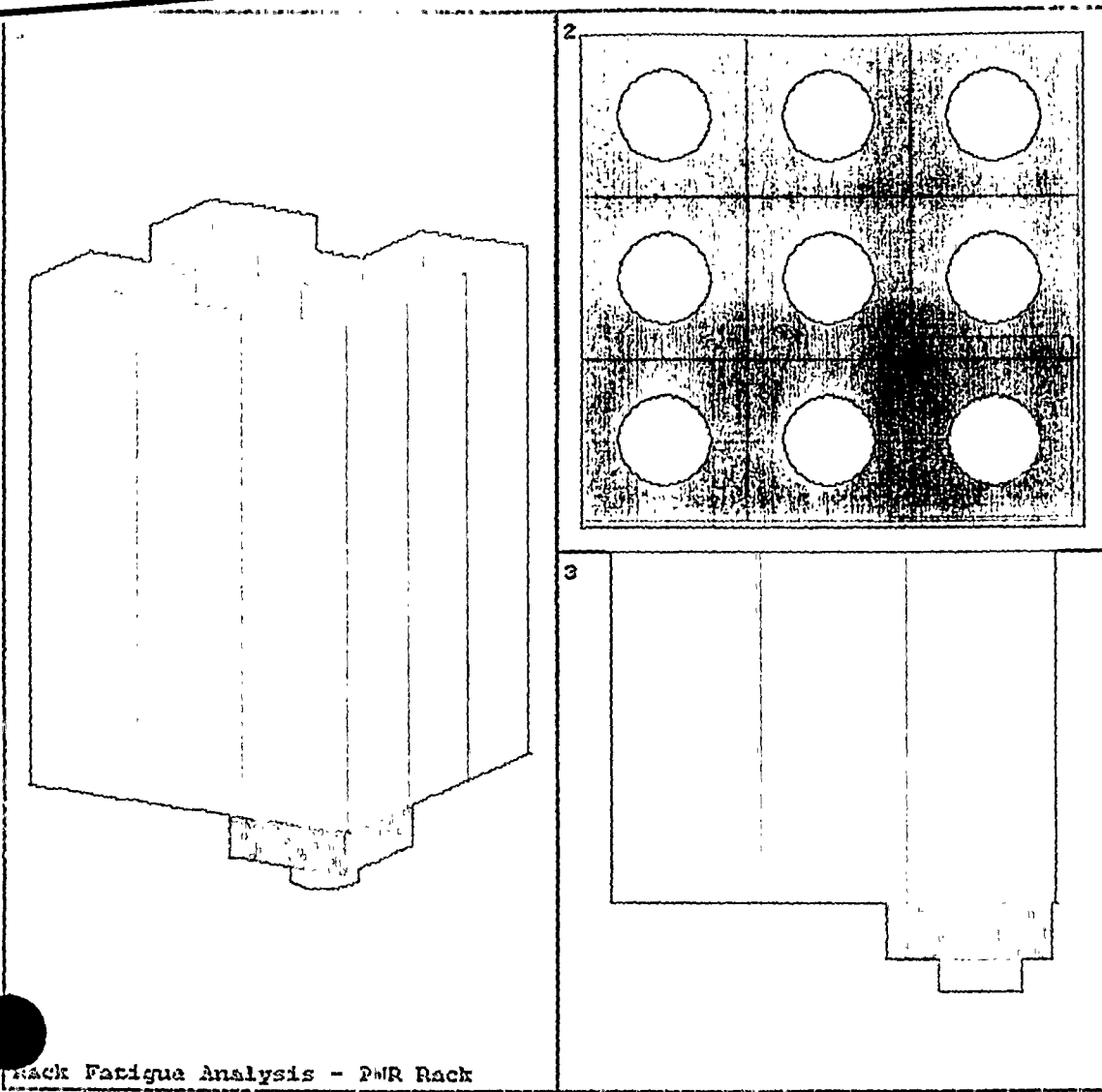


Figure 6.8.1

HI-971760





ANSYS 5.3  
 JAN 16 1998  
 15:58:12  
 ELEMENTS  
 TYPE NUM  
 XV =.482963  
 YV =-.836516  
 ZV =.258819  
 DIST=.41.117  
 XF =-8.861  
 YF =0.861  
 ZF =17.25  
 A-ZS=-65.854  
 PRECISE HIDDEN  
 EDGE

WIND=2  
 ZV =1  
 DIST=15.05  
 XF =-8.861  
 YF =8.861  
 ZF =17.25  
 2-BUFFER  
 EDGE

WIND=3  
 YV =-1  
 DIST=16.78  
 XF =-9.027  
 YF =8.861  
 ZF =5.108  
 2-BUFFER  
 EDGE

Figure 6.9.1; Rack Fatigue Analysis Model

## 7.0 FUEL HANDLING AND CONSTRUCTION ACCIDENTS

### 7.1 Introduction

The USNRC OT position paper [7.1] specifies that the design of the rack must ensure the functional integrity of the spent fuel racks under all credible drop events in the spent fuel pool. This section contains synopses of the analyses carried out to demonstrate the regulatory compliance of the proposed racks under postulated fuel assembly drop scenarios germane to HNP pools C and D.

In addition to the postulated fuel assembly free-fall scenarios, a gate drop accident event was also considered. In this case, the ability of the pool structure to avert primary structural damage (leading to rapid loss of water) needs to be demonstrated.

### 7.2 Description of Fuel Handling Accidents

Two categories of fuel assembly accidental drop events are considered. In the so-called "shallow drop" event, a fuel assembly, along with the portion of handling tool which is severable in the case of a single element failure, is assumed to drop vertically and hit the top of the rack. The "depth" of damage to the affected cell walls must be demonstrated to remain limited to the portion of the cell above the top of the "active fuel region", which is essentially the elevation of the top of the Boral neutron absorber. To meet this criterion, the plastic deformation of the rack cell wall should not extend more than 21.3 inches (downwards) from the top of a PWR rack. The distance separating the top of the rack from the Boral in the BWR racks in pools C and D is 13.75 inches. Therefore, to be conservative the smaller BWR dimension of 13.75 inches is selected as the maximum depth of damage of an object falling onto the tops of storage racks.

By observation, the drop of a PWR assembly onto a PWR rack is more limiting than any other combination of the two fuel types (PWR vs. BWR) with the two rack (PWR vs. BWR) types. This is obvious because of two reasons. The PWR assembly drop is a more severe case than the BWR assembly case, since the effect of the weight differences (approximately 1600 vs. 680 lbs, respectively) far exceeds the effect of the differences in the impact cross-section zone (about 8.4 vs. 5.5 inches, respectively). The PWR storage rack cell controls as an impact zone over the BWR cell because it is larger (8.4 vs. 6.06 inches, respectively) resulting in less capacity to withstand top of cell or baseplate impacts. (The nominal cell wall thicknesses of the two rack types is identical).

In order to utilize an upper bound of kinetic energy at impact, the impactor is assumed to weigh 2,100 lbs and the free-fall height is assumed to be 36 inches. The impactor weight corresponds to the heaviest fuel (plus handling tool) which will be handled in pools C and D.

It is readily apparent from the design of the rack modules described in Section 3, that the impact resistance of a rack at its periphery is less than its interior. Accordingly, the potential shallow drop scenario is postulated to occur at the periphery in the manner shown in Figure 7.2.1.

Finally, the fuel assembly assemblage is assumed to hit the rack in a manner to inflict maximum damage. The impact zone is chosen to minimize the cross sectional area which experiences the deformation. Placement of the impact at the corner would reduce the impact zone area, but actually increases the cross-sectional area experiencing deformation. Impact at the corner would involve the crushing of two cell walls under the dynamic impact. Therefore, impact on only one cell wall is chosen to simulate the worst case accident. Figure 7.2.2 depicts the impacted rack in plan view.

The second class of "fuel drop event" postulates that the impactor falls through an empty storage cell impacting the rack baseplate. This so-called "deep drop" scenario threatens the structural integrity of the "baseplate". If the baseplate is pierced, then the fuel assembly might damage the pool liner (which at 3/16" is rather thin) and create an abnormal condition of the enriched zone of fuel assembly outside the "poisoned" space of the fuel rack. To preclude damage to the pool liner, and to avoid the potential of an abnormal fuel storage configuration in the aftermath of a deep drop event, it is required that the baseplate remain unpierced and that the maximum lowering of the fuel assembly support surface is less than the distance from the bottom of the baseplate to the liner.

The deep drop event can be classified into two scenarios, namely, drop through cell located above a support leg (Figure 7.2.3), and drop in an interior cell away from the support pedestal (Figure 7.2.4).

In the former deep drop scenario (Figure 7.2.3), the baseplate is buttressed by the support pedestal and presents a hardened impact surface, resulting in a high impact load. The principal design objective is to ensure that the support pedestal does not pierce the lined, reinforced concrete pool slab.

The baseplate is not quite as stiff at cell locations away from the support pedestal (Figure 7.2.4). Baseplate severing and large deflection of the baseplate (such that the liner would be impacted) would constitute an unacceptable result.

### 7.3 Description of the Rack Drop Accident

The drop of a rack above spent fuel stored within in-place rack modules is precluded, since racks will not be lifted above spent fuel. The drop of a rack module during installation is also extremely remote, due to the defense-in-depth approach discussed in Sections 3.5 and



11.1. Despite the unlikelihood of this possibility, a rack dropping to the pool floor has been considered. To evaluate the consequences of an accidental, uncontrolled lowering of the heaviest rack module, a 13x13 BWR module conservatively considered with a submerged weight of 16140 lb (actual maximum nominal dry weight is only 15700 lb), from a height of 480 inches above the pool liner is considered (Figure 7.3.1). The objective of the analysis is to ensure that a rapid loss of pool water will not occur, leading to loss of shielding to the stored nuclear fuel.

#### 7.4 Mathematical Model

In the first step of the solution process, the velocity of the dropped object (impactor) is computed for the condition of underwater free fall. Table 7.1 contains the results for the three drop events.

In the second step of the solution, an elasto-plastic finite element model of the impacted region on Holtec's computer Code PLASTIPACT (Los Alamos Laboratory's DYNA3D implemented on Holtec's QA system) is prepared. PLASTIPACT simulates the transient collision event with full consideration of plastic, large deformation, wave propagation, and elastic/plastic buckling modes. For conservatism, the impactor in all cases is assumed to be *rigid*. The physical properties of material types undergoing deformation in the postulated impact events are summarized in Table 7.2.



## 7.5 Fuel Drop Results

### 7.5.1 Shallow Drop Events

Figure 7.5.1 shows the finite element model utilized in the shallow drop impact analysis.

Dynamic analyses show that the top of the impacted region undergoes severe localized deformation. Figure 7.5.2 shows an isometric view of the post-impact geometry of the rack for the shallow drop scenario. The maximum depth of plastic deformation is limited to 11 inches, which is below the design limit of 13.75 inches. Figure 7.5.3 shows the plan view of the post-collision geometry. Approximately 10% of the cell opening in the impacted cell is blocked.

### 7.5.2 Deep Drop Events

The deep drop scenario depicted in Figure 7.5.4(b), wherein the impact region is located above the support pedestal, is found to produce a negligible deformation on the baseplate. The vertical force in the support pedestal remains below the loads generated during seismic events (see Section 6). Therefore, it is concluded that the pool liner will not be damaged.

The deep drop condition through an interior cell depicted in Figure 7.5.4(a) does produce some deformation of the baseplate and localized severing of the baseplate/cell wall welds (Figure 7.5.5). However, the fuel assembly support surface is lowered by a maximum of 2.89 inches, which is less than the minimum distance of 6 inches from the bottom of the baseplate to the liner. Therefore, the deformed baseplate will not strike the liner during this drop event and the pool liner will not be damaged. As stated in Subsection 4.7.2, criticality evaluations performed for this baseplate deformation have shown that the storage configuration remains acceptable.

## 7.6 Results of Other Drop Scenarios

Since the primary structural integrity of the slab is unimpaired subsequent to a rack drop to the pool floor liner, catastrophic loss of pool water would not occur. Therefore, catastrophic failure of the pool structure or rapid loss of pool water will not occur.

No other credible in-pool drops have been identified. An object potentially carried over the pools is one of the 4,000 pound gates which isolate the pools. These gates are long rectangular metallic structures with a base area of 8 inches by 41 inches. During handling the gate is lifted using a single failure proof crane and double rigging. The rigging complies with the safety margin requirements of NUREG-0612. An accidental drop of the gate is not a credible event, because of the above mentioned defense-in-depth approach to the lifting of this heavy load. Additionally the gates are not located within the pools, but are installed inside of slots within adjacent transfer canals. Nevertheless, analyses were carried out for this accident scenario. A gate drop during handling from 40 feet above the pool liner was evaluated and it has been determined that a primary failure of the water retaining concrete structure will not occur. A gate drop during handling from 15 inches above the top of a PWR rack loaded with fuel was also evaluated. A schematic of the 3D finite element model is depicted in Figures 7.6.1 and 7.6.2. The gate is conservatively considered to strike only three rack storage cell walls, as shown in Figure 7.6.3. This impact zone is conservative, since the dimensions of the gate would span at least four cell walls. The gate is shown to penetrate the rack to a depth of less than 5 inches, as shown in Figures 7.6.4 and 7.6.5. Since this penetration remains above the tops of the stored fuel assemblies, no fuel damage occurs.

## 7.7 Closure

The fuel assembly and gate drop accident events evaluated for the HNP fuel pools were analyzed and found to produce localized damage well within the design limits for the racks. A construction accident event wherein the heaviest rack falls from a 40 foot height onto the pool floor was also considered. Analyses show that the pool structure will not suffer any primary structural damage. A similar conclusion is reached with regard to a gate drop event.

7.8 References

- [7.1] "OT Position for Review and Acceptance of Spent Fuel Storage and Handling Applications," dated April 14, 1978.

**TABLE 7.1****IMPACT EVENT DATA**

Case	Impactor Weight (lbs)	Impactor	Drop Height (inches)	Impact Velocity (inch/sec)
1. Shallow drop event	2,100	Fuel Assembly	36	152
2. Deep drop event	2,100	Fuel Assembly	205	353
3. Construction event	16,140	Rack Module	480	304

**TABLE 7.2**

**MATERIAL DEFINITION**

Material Name	Type	Density	Elastic Modulus	Stress		Strain	
		(pcf)	(psi)	First Yield	Failure	Elastic	Failure
				(psi)	(psi)		
Stainless steel	SA240-304L	490	2.760e+07	2.130e+04	6.620e+04	7.717e-04	3.800e-01
Stainless steel	SA240-304	490	2.760e+07	2.500e+04	7.100e+04	7.717e-04	3.800e-01
Stainless steel	SA564-630	490	2.760e+07	1.063e+05	1.400e+05	3.851e-02	3.800e-01
Concrete	4000 psi	150	3.605e+06	4.000e+03	2.022e+04	1.110e-03	5.500e-02



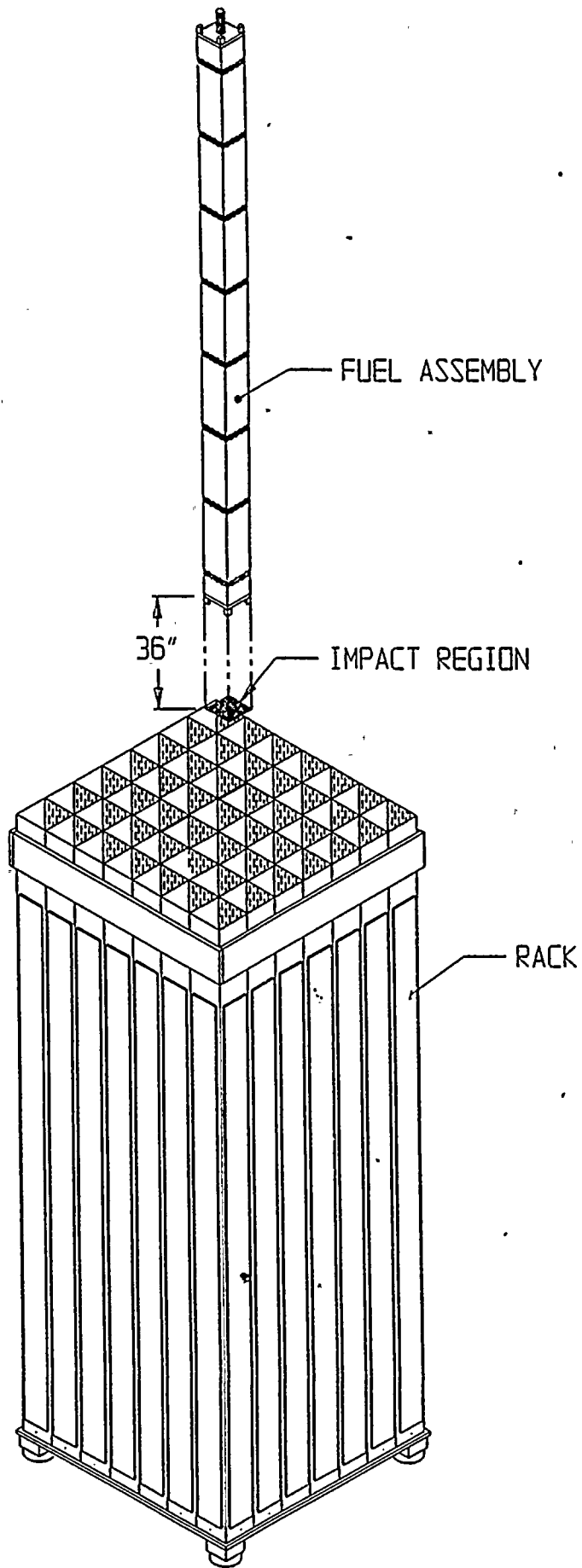


Figure 7.2.1; Shallow Drop on a Peripheral Cell



IMPACTOR

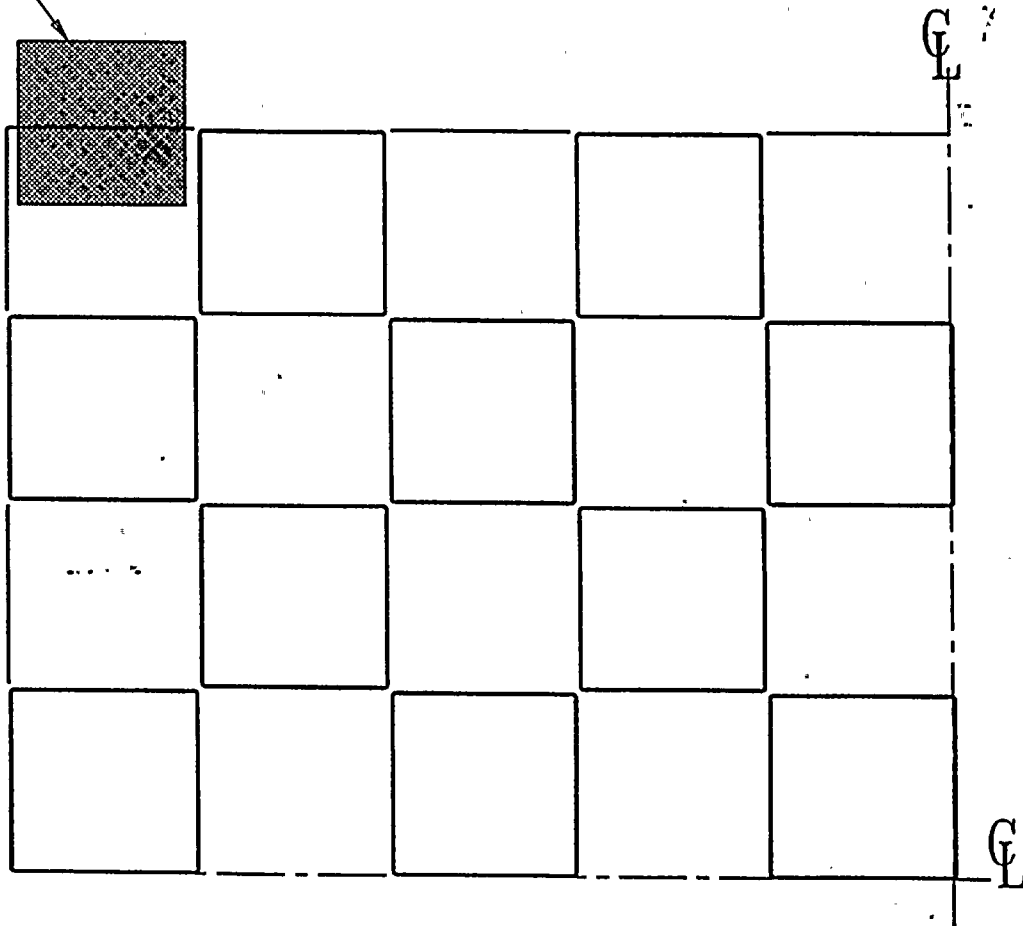


Figure 7.2.2; Plan View of Impactor and Impact Zone  
(Shallow Drop Event)



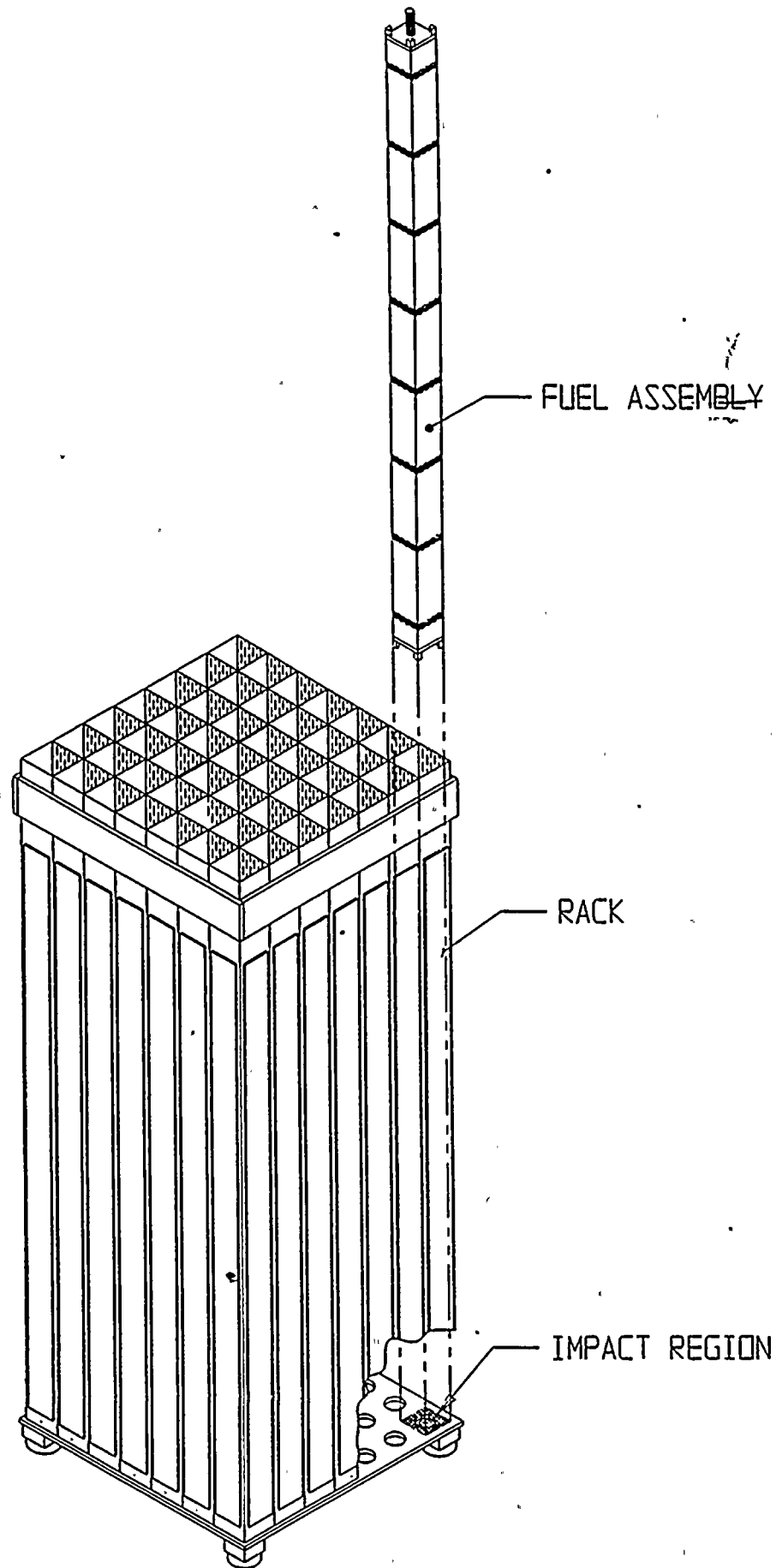


Figure 7.2.3; Deep Drop on a Support Leg Location



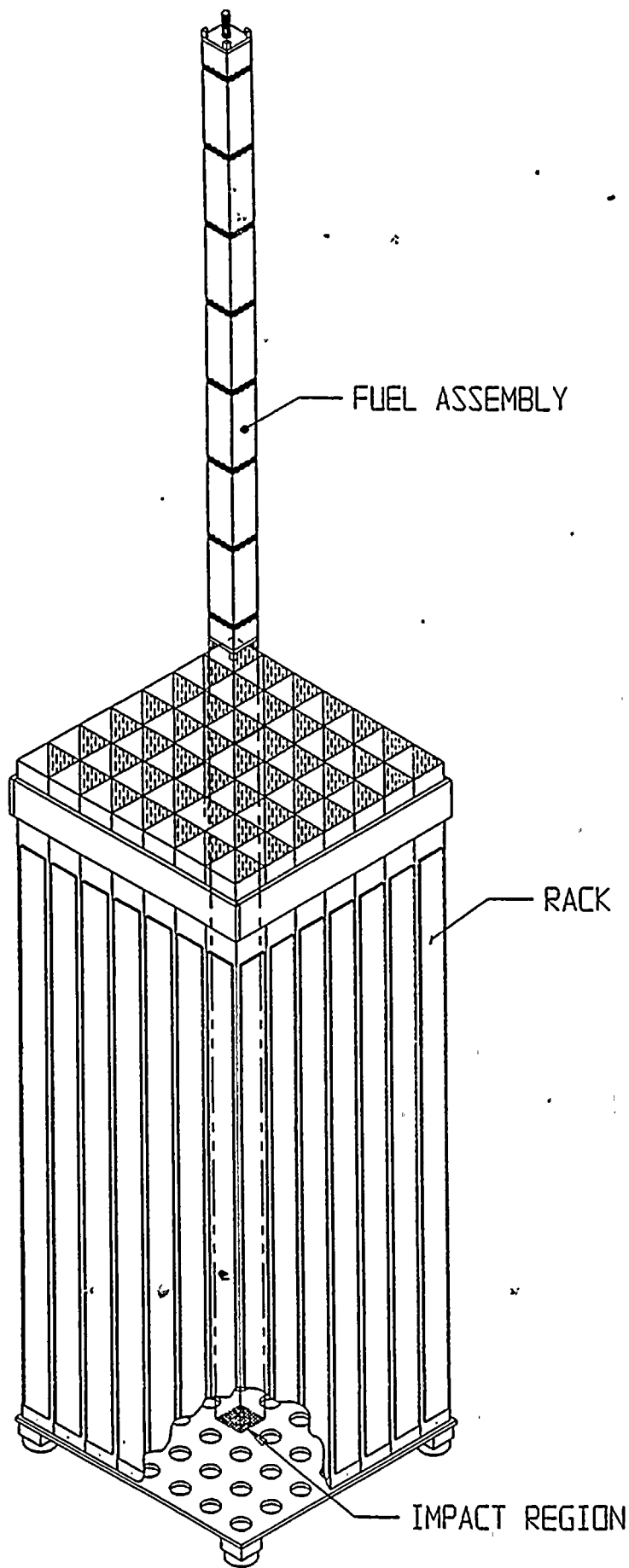


Figure 7.2.4; Deep Drop on a Center Cell Leg Location

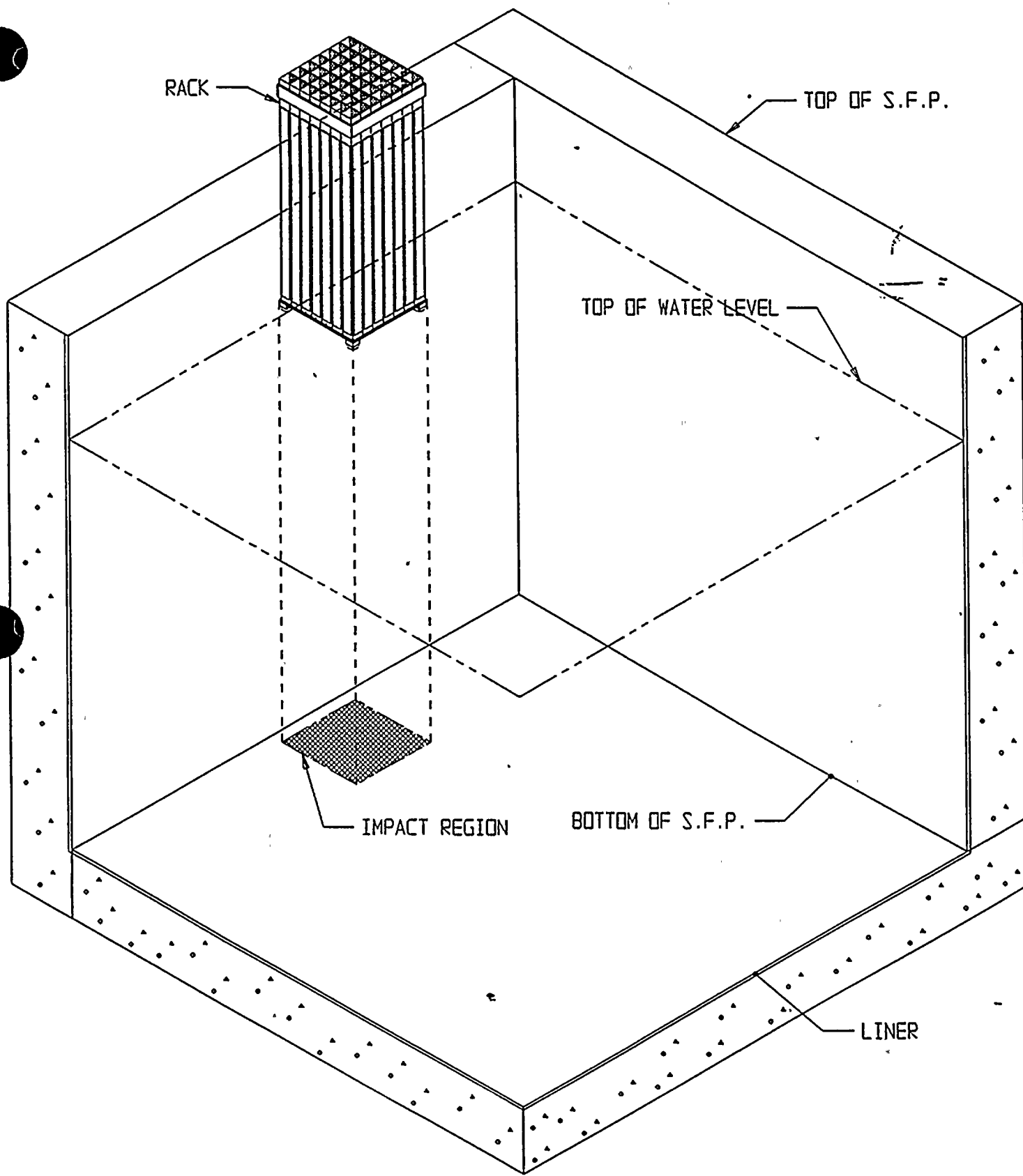


Figure 7.3.1; Heaviest Rack Drop



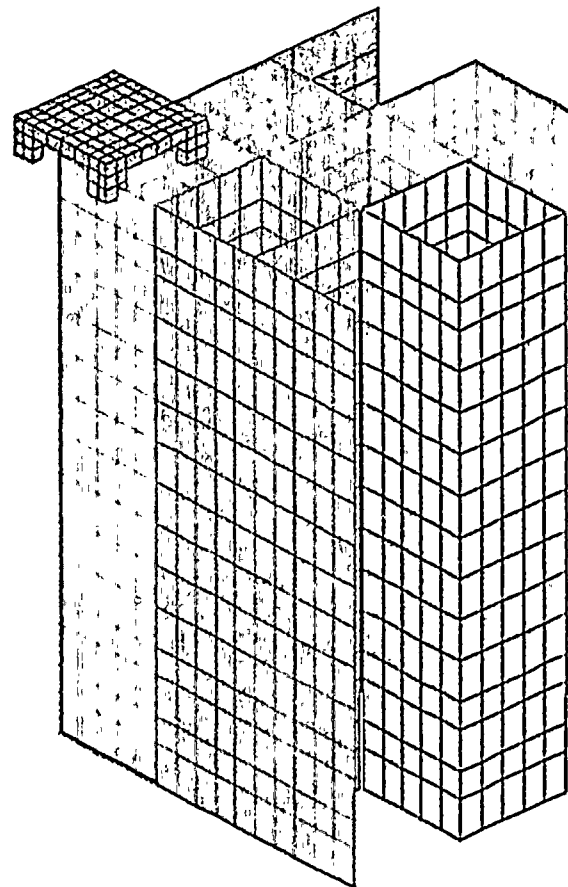
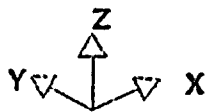


Figure 7.5.1; Shallow Drop: Finite Element Model Detail Impacted Region

HARRIS - SPENT FUEL RACK UPPER EX  
STEP 19 TIME = 6.6499516E-002

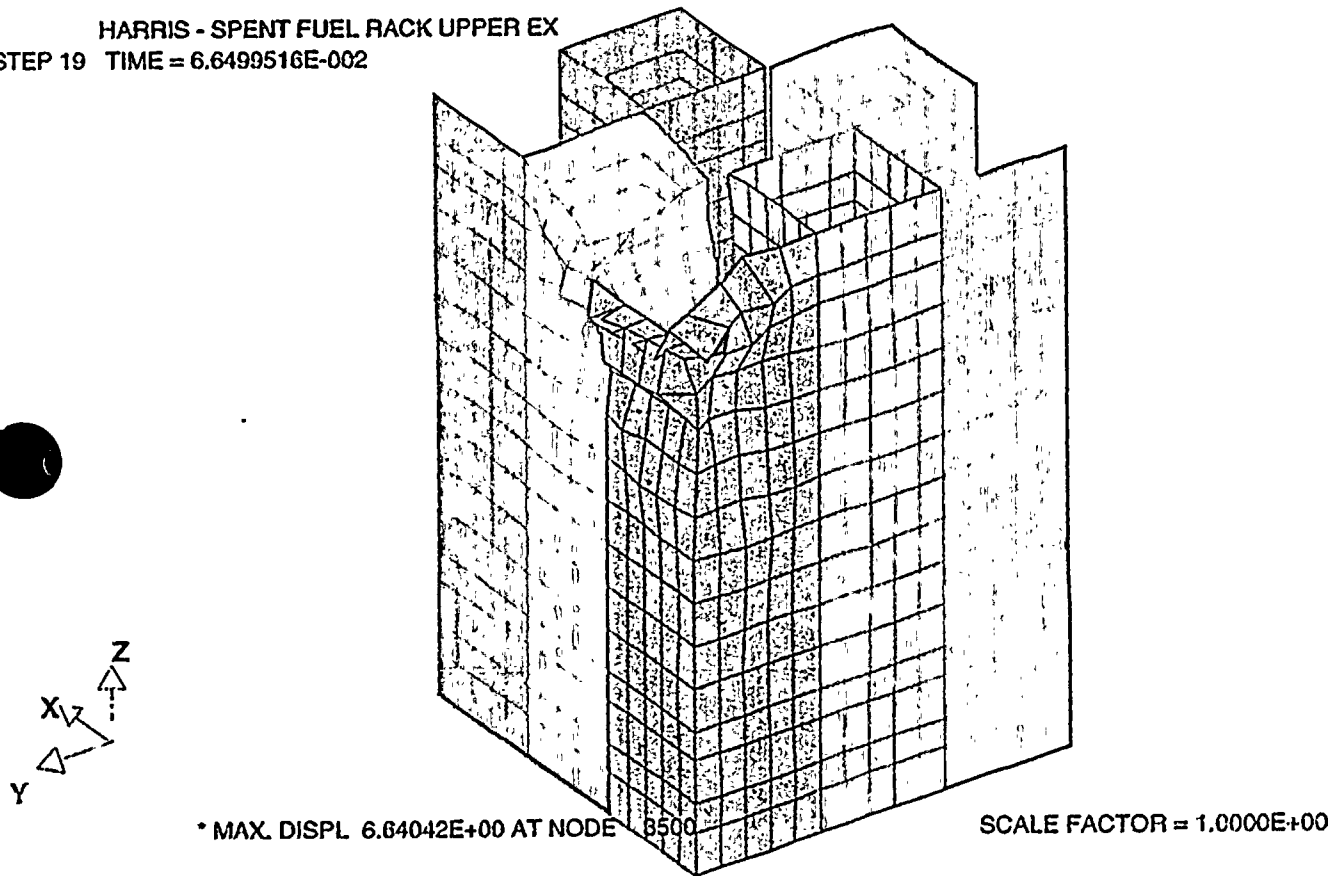


Figure 7.5.2; Maximum Cell Deformation for Shallow Drop on Exterior Cell

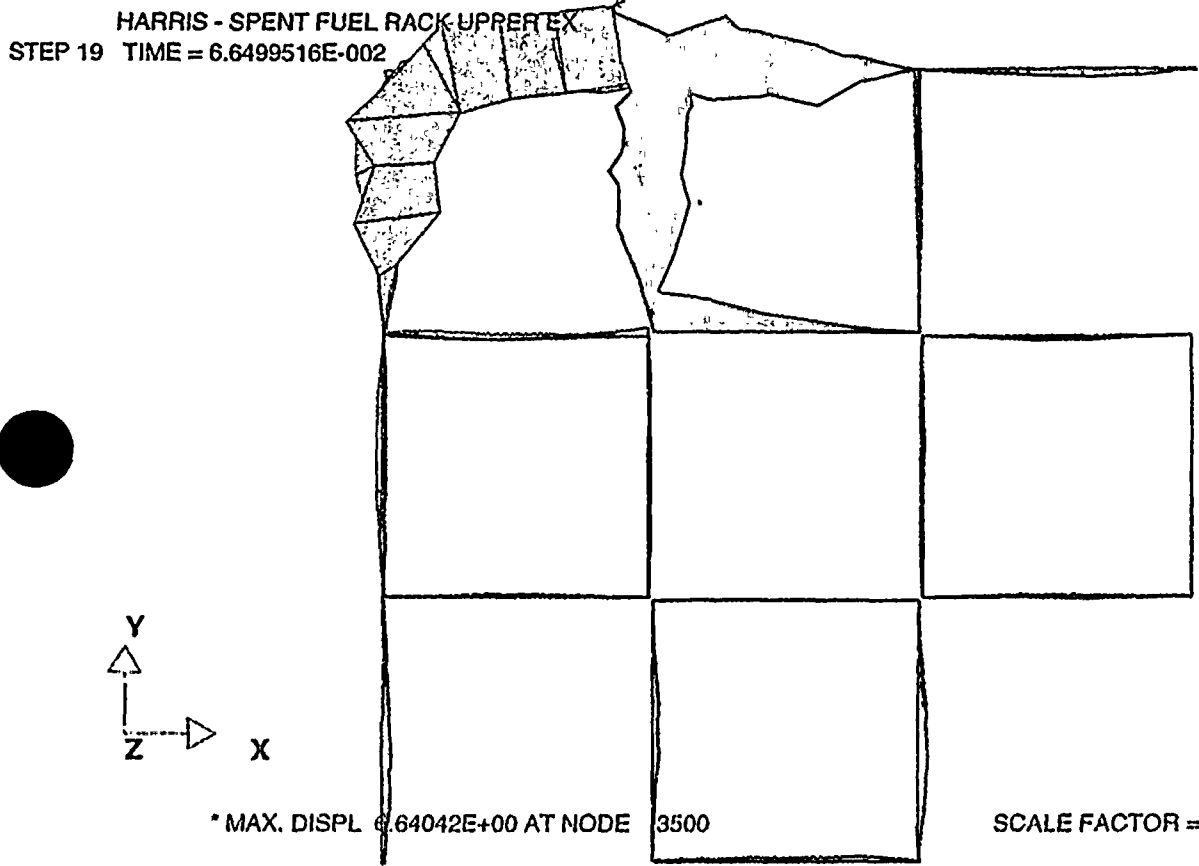
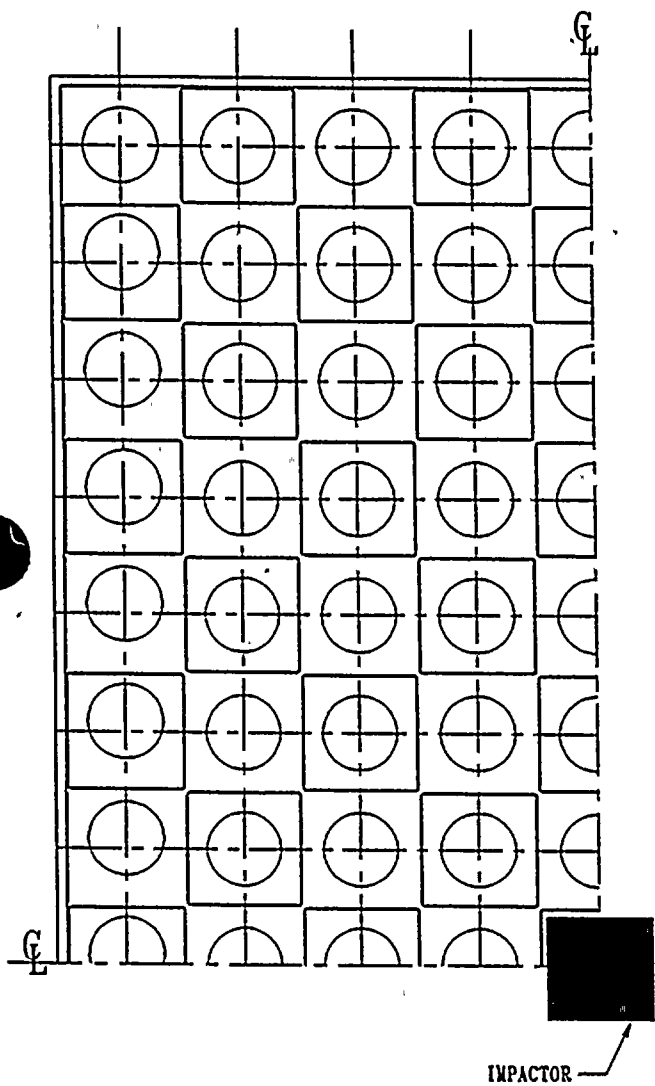
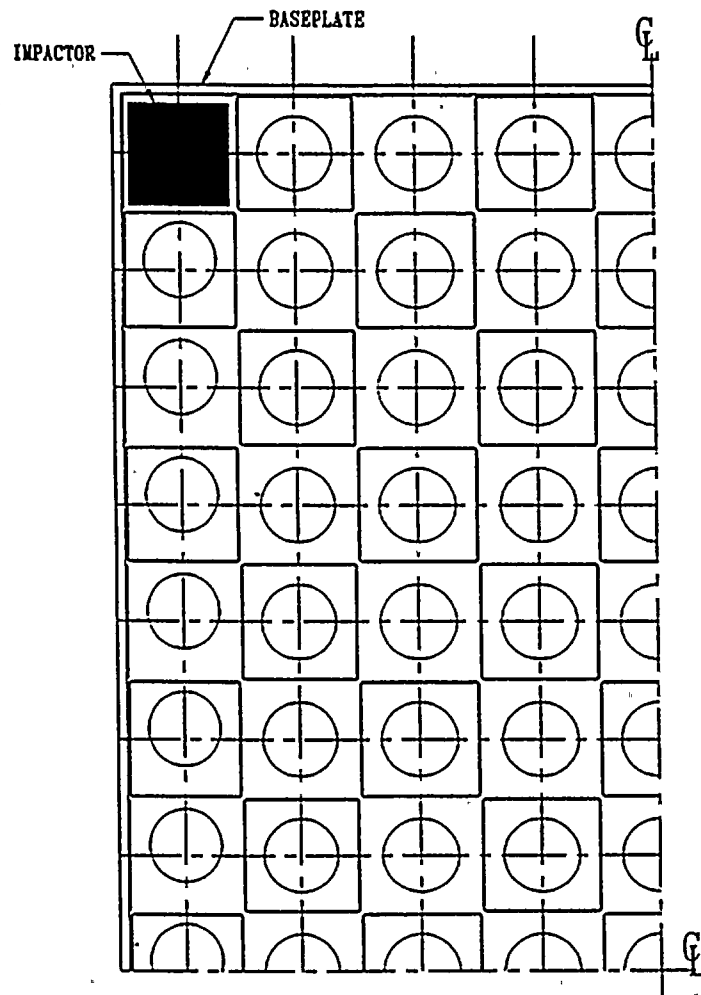


Figure 7.5.3; Shallow Drop: Maximum Cell Deformation  
 Impacted Region Plan



(a) SCENARIO SC1



(b) SCENARIO SC2

Figure 7.5.4; Plan View of Deep Drop Scenarios

STEP 27 TIME = 1.3499989E-002  
TOTAL DISPLACEMENT

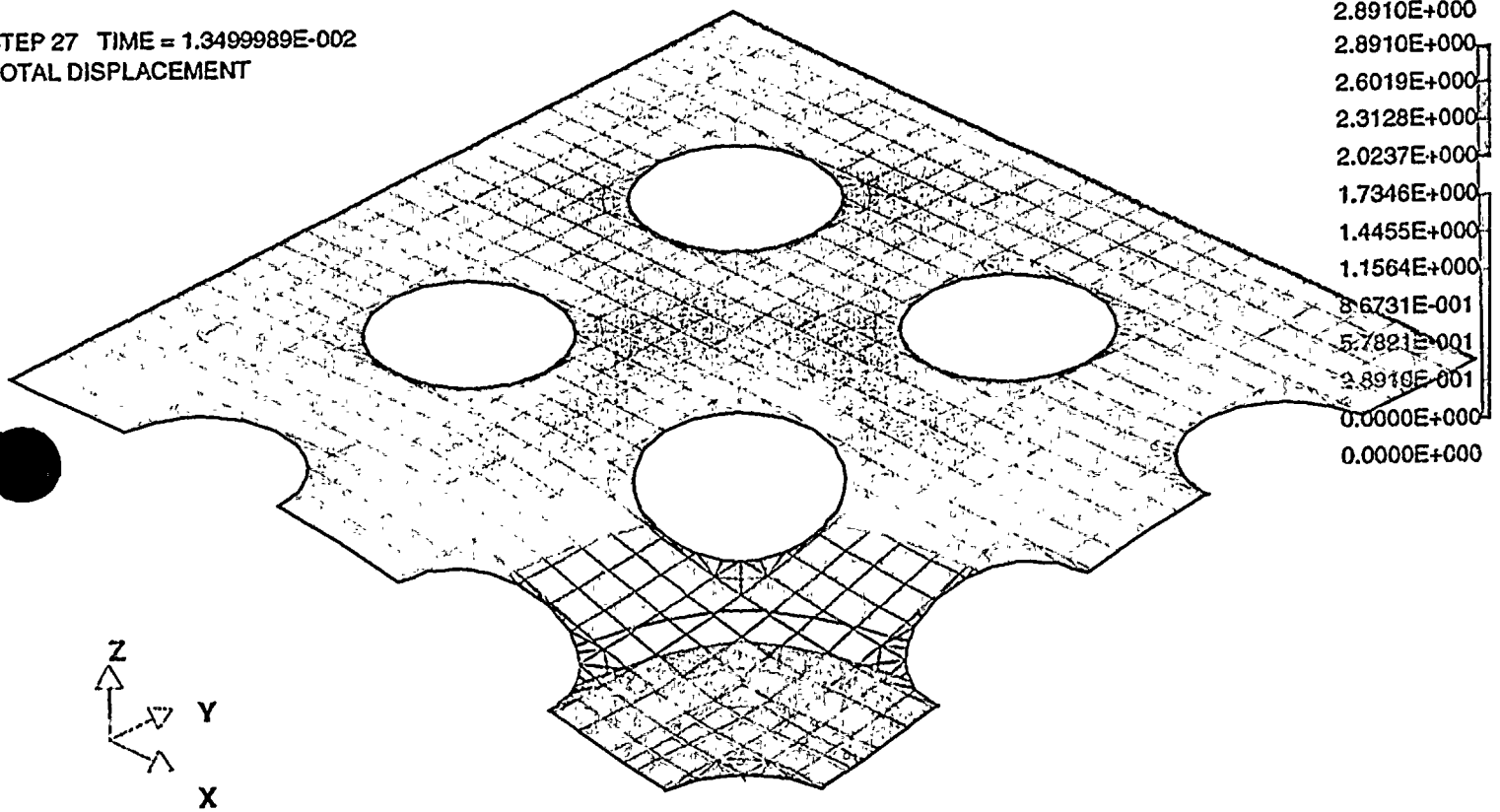


Figure 75.5; Maximum Baseplate Deformation from Deep Drop Scenario



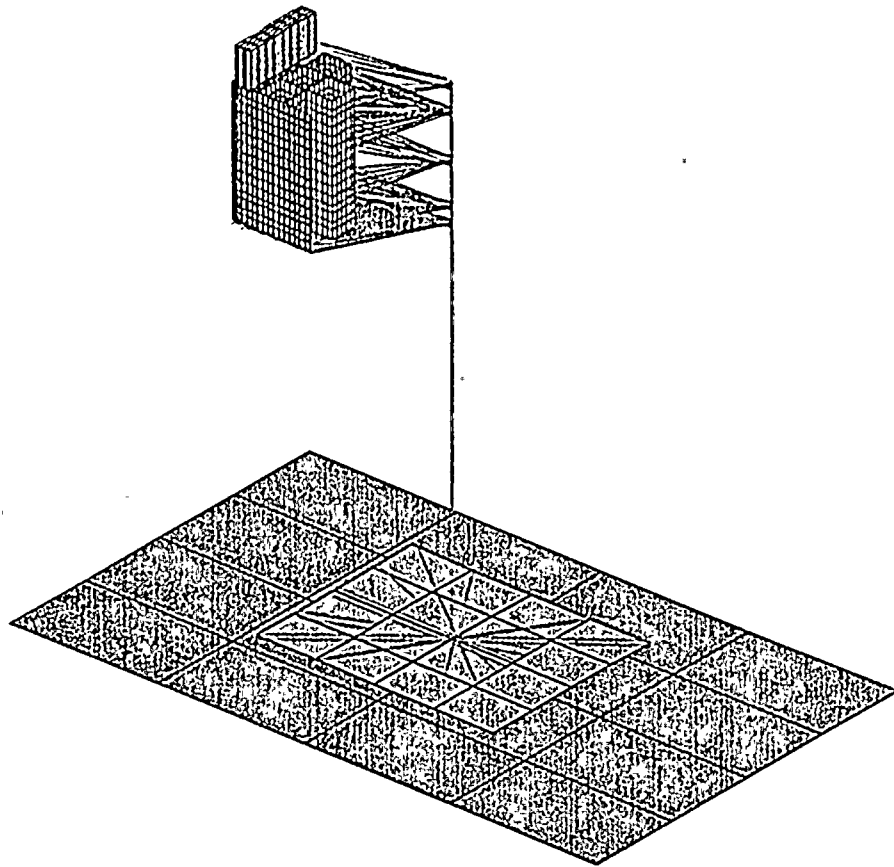
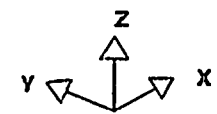


Figure 7.6.l; Gate Drop Finite-Element Model

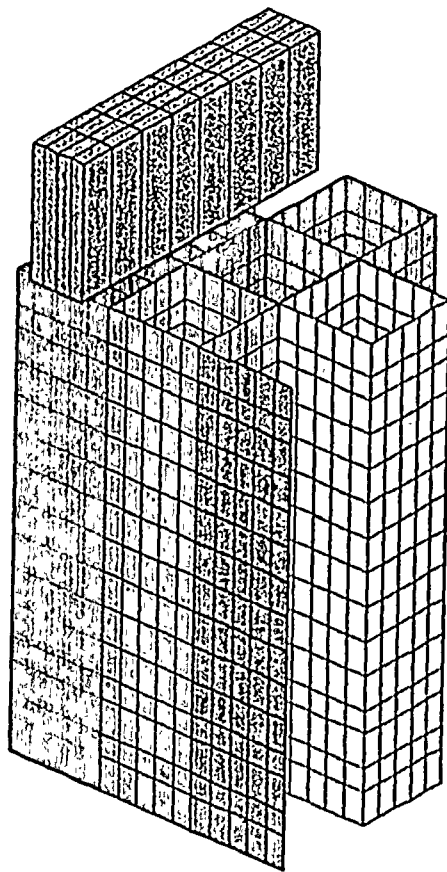
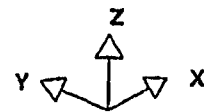


Figure 7.6.2; Gate Drop Finite-Element Model, Detail of Impacted Region

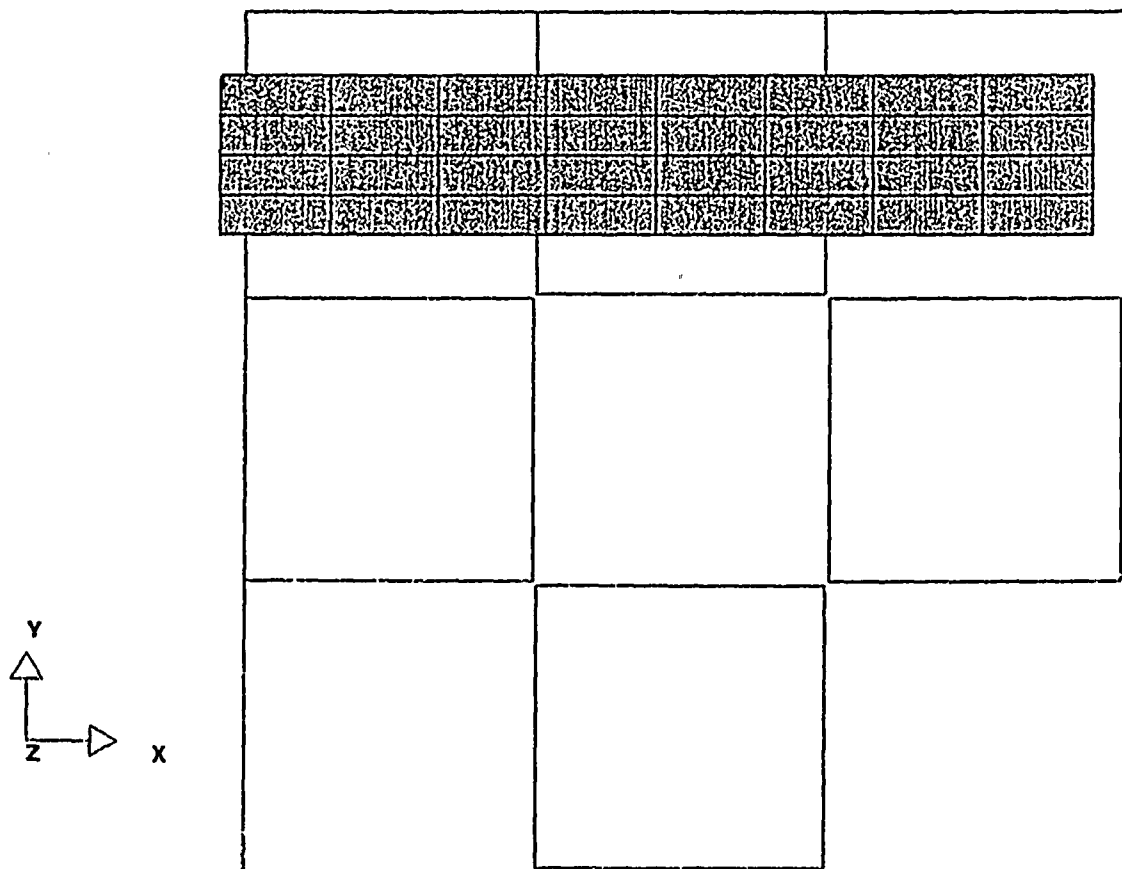
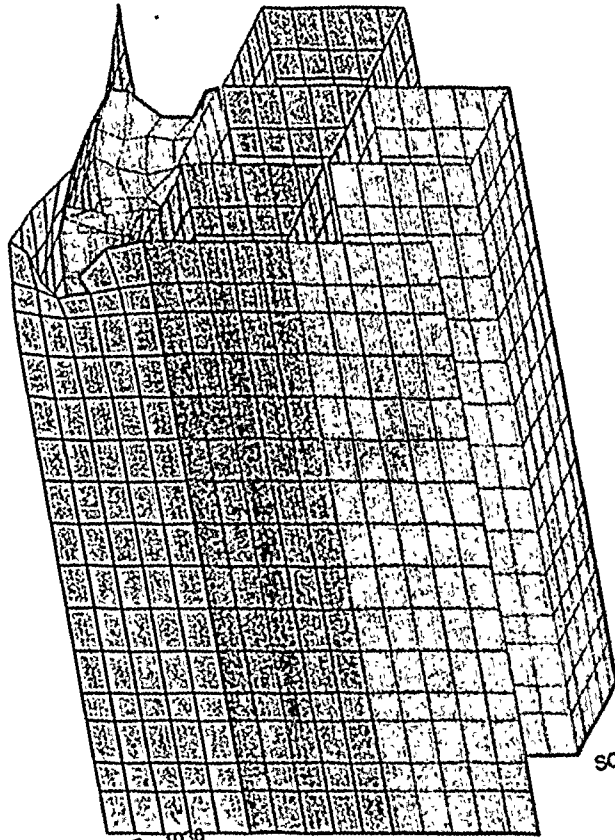


Figure 7.6.3; Gate Drop Finite-Element Model  
Detail of Impacted Region (Plan)

EP 17 TIME = 5.9499886E-002



SCALE FACTOR = 1.0000E+00

\* MAX. DISPL 4.50589E+00 AT NODE 1038

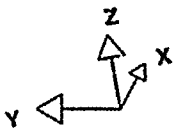


Figure 7.6.4; Gate Drop Maximum Deformation

HI-971760

STEP 17 TIME = 5.9499886E-002

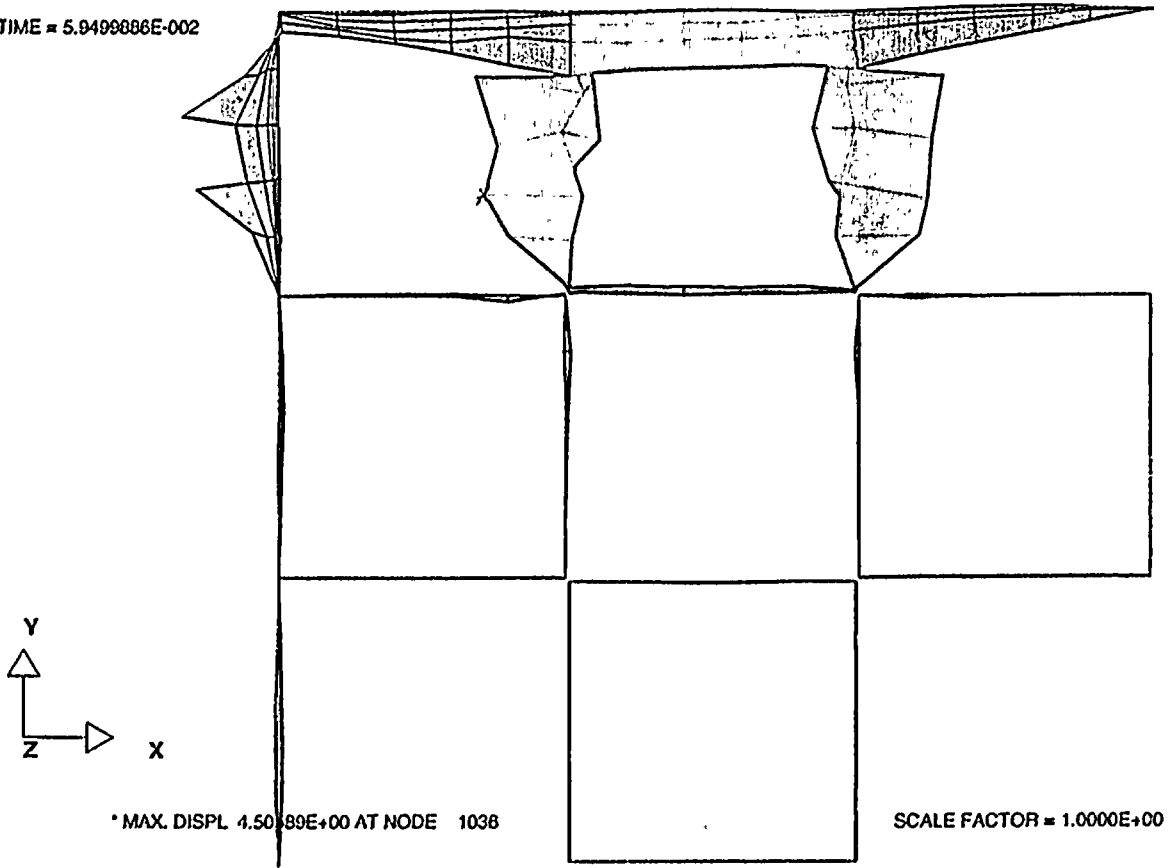


Figure 7.6.5; Gate Drop Maximum Deformation  
Impacted Region Plan

## 8.0 FUEL POOL STRUCTURE INTEGRITY CONSIDERATIONS

### 8.1 Introduction

The Harris Spent Fuel Pools (SFPs) C and D are safety related, seismic category I, reinforced concrete structures. Spent fuel is to be placed within storage racks located in both of these areas and they will be collectively referred to herein as the fuel pool structure. This section describes the analysis to demonstrate structural adequacy of the pool structure, as required by Section IV of the USNRC OT Position Paper [8.1.1].

The pool regions are analyzed using the finite element method. Results for individual load components are combined using factored load combinations mandated by SRP 3.8.4 [8.1.2] based on the "ultimate strength" design method of the American Concrete Institute (ACI 318) [8.1.3]. It is demonstrated that for the critical bounding factored load combinations, structural integrity is maintained when the pools are assumed to be fully loaded with spent fuel racks, as shown in Figures 1.2 and 1.3 with all storage locations occupied by fuel assemblies.

The regions examined in the SFPs are the floor slabs, and the highly loaded wall sections adjoining the slabs. Both moment and shear capabilities are checked for concrete structural integrity. Local punching and bearing integrity of the slab in the vicinity of a rack module support pedestal pad is evaluated. All structural capacity calculations are made using design formulas meeting the requirements of ACI 318.

### 8.2 Description of Pool Structures

The SFPs are located inside the Fuel Handling Building and are supported by a two way, reinforced concrete slab. The minimum thickness of the slab is 12.0 feet, including grout. The SFPs are separated by reinforced concrete walls and transfer canals.

Figure 1.1 shows the layout of the majority of the Fuel Handling Building. A plan of the building area of concern is shown in Figure 8.2.1, which shows the major structural dimensions of the

pools. The floor liner plate of the SFPs are located at elevation 246.0 The spent fuel area operating floor is at elevation 286.0.

### 8.3 Definition of Loads

Pool structural loading involves the following discrete components:

#### 8.3.1 Static Loading (Dead Loads and Live Loads)

- 1) Dead weight of pool structure includes the weight of the Fuel Handling Building concrete upper structure.
- 2) Maximum dead weight of rack modules and fuel assemblies in the fully implemented storage configuration, as shown in Figures 1.2 and 1.3.
- 3) Dead weight of a shipping cask including yoke of 250 kips.
- 4) The Cask Crane, Auxiliary Crane and Spent Fuel Handling Machine (Refueling Platform) are designed to move along the N-S direction. The dead weight and the rated lift weight of these cranes are considered as live load.
- 5) The hydrostatic water pressure.

#### 8.3.2 Seismic Induced Loads

- 1) Vertical loads transmitted by the rack support pedestals to the slab during a SSE or OBE seismic event.

- 2) Hydrodynamic inertia loads due to the contained water mass and sloshing loads (considered in accordance with TID-7024 [8.3.1]) which arise during a seismic event.
- 3) Hydrodynamic pressures between racks and pool walls caused by rack motion in the pool during a seismic event.
- 4) Seismic inertia force of the walls and slab.

### 8.3.3 Thermal Loading

Thermal loading is defined by the temperature existing at the faces of the pool concrete walls and slabs. Two thermal loading conditions are evaluated: The normal operating temperature and the accident temperature.

## 8.4 Analysis Procedures

### 8.4.1 Finite Element Analysis Model

The finite element model encompasses the two SFPs, the Fuel Transfer Canal, the Cask Loading Pool, and adjacent transfer canals and building structure. The interaction with the rest of the Fuel Handling Building reinforced concrete, which is not included in the finite-element model, is simulated by imposing appropriate boundary conditions. The structural area of interest for the reracking project includes only two pools which are involved in the fuel storage capacity increase. However, by augmenting the area of interest, by considering in the constructed finite-element model and numerical investigation the additional areas described above, the perturbation induced by the boundary conditions on the stress field distribution for the area of interest is minimized. A finite element 3D view of the structural elements considered in the numerical investigation is shown in Figure 8.4.1.



The preprocessing capabilities of the STARDYNE computer code [8.4.1] are used to develop the 3-D finite-element model. The STARDYNE finite-element model contains 13,353 nodes, 3,564 solid type finite-elements, 7,991 plate type finite-elements and 24 hydro-dynamic masses. Figure 8.4.1 depicts an isometric view of the three-dimensional finite element model without the water and concentrated masses (racks, cask, etc.).

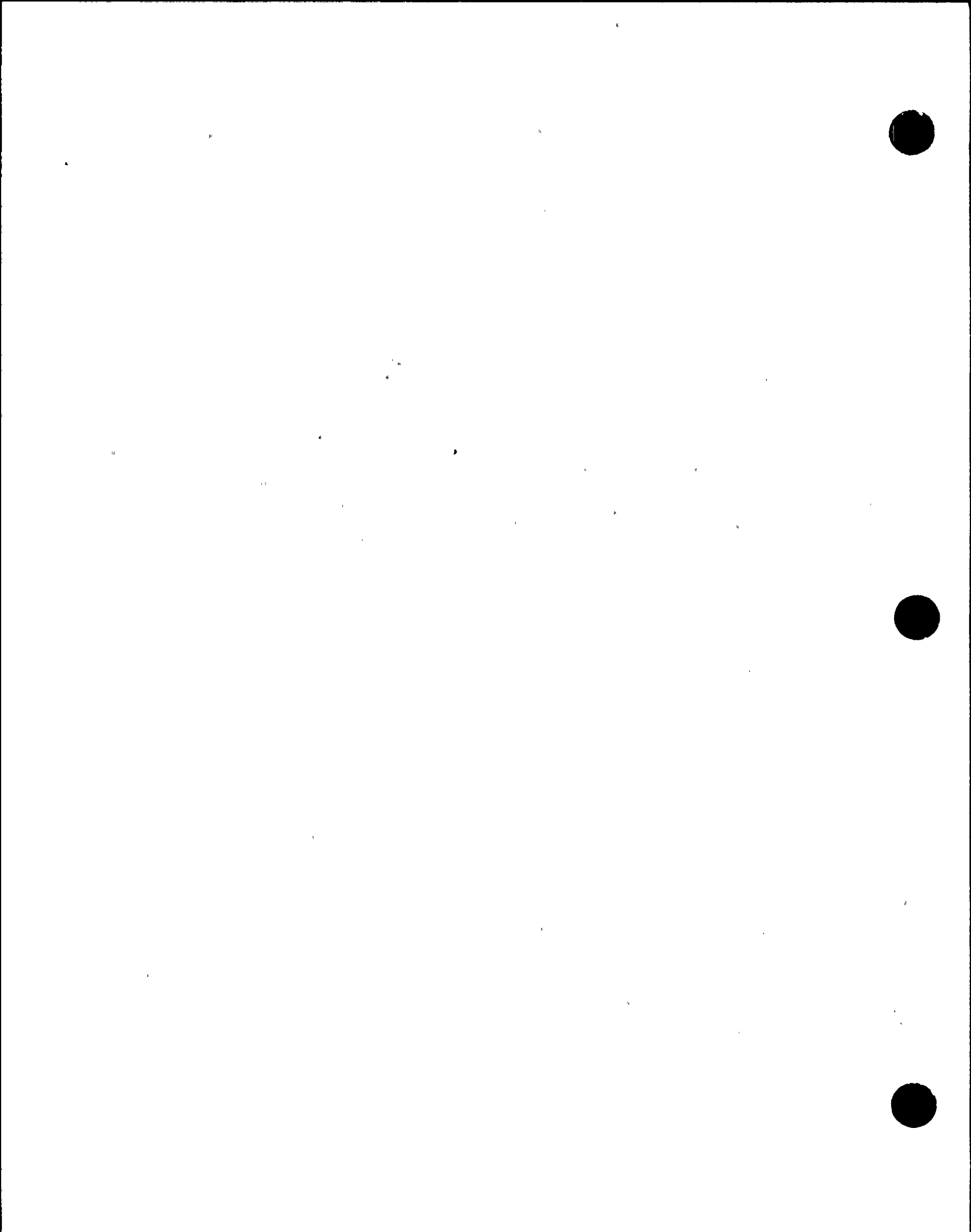
The dynamic behavior of the water mass contained in the SFPs and Transfer Canal during a seismic event is modeled according to the guidelines set in TID-7024.

To simulate the interaction between the modeled region and the rest of the Fuel Handling Building a number of boundary restraints were imposed upon the described finite-element model.

The behavior of the reinforced concrete existing in the structural elements (walls, slab and mat) is considered elastic and isotropic. The elastic characteristics of the concrete are independent of the reinforcement contained in each structural element for the case when the un-cracked cross-section is assumed. This assumption is valid for all load cases with the exception of the thermal loads, where for a more realistic description of the reinforced concrete cross-section the assumption of cracked concrete is used. To simulate the variation and the degree of cracking patterns, the original elastic modulus of the concrete is modified in accordance with Reference [8.4.2].

#### 8.4.2 Analysis Methodology

The structural region of concern, from column lines 43 to 73 and from line L to N, is isolated from the Fuel Handling Building. This region is numerically investigated using the finite element method. The pool walls and their supporting reinforced concrete slab are represented by a 3-D finite-element model.



The individual loads considered in the analysis are grouped in five categories: dead load (weight of the pool structure, dead weight of the rack modules and stored fuel, dead weight of the reinforced concrete Fuel Handling Building upper structure, the hydro-static pressure of the contained water), live loads (weights of the Cask Crane, Auxiliary Crane, and SFHM and their maximum suspended loads), thermal loads (the thermal gradient through the pool walls and slab for normal operating and accident conditions) and the seismic induced forces (structural seismic forces, interaction forces between the rack modules and the pool slab, seismic loads due to self-excitation of the pool structural elements and contained water, and seismic hydro-dynamic interaction forces between the rack modules and the pool walls for both OBE and SSE conditions). The dead and thermal loads are considered static acting loads, while the seismic induced loads are time-dependent.

The material behavior under all type of loading conditions is described as elastic and isotropic representing the uncracked characteristics of the structural elements cross-section, with the exception of the thermal load cases where the material elasticity modulus is reduced in order to simulate the variation and the degree of the crack patterns. This approach [8.1.3] acknowledges the self-relieving nature of the thermal loads. The degree of reduction of the elastic modulus is calculated based on the average ultimate capacity of the particular structural element.

The numerical solution (displacements and stresses) for the cases when the structure was subjected to dead and thermal loads is a classical static solution. For the time-dependent seismic induced loads the displacement and stress field are calculated employing the spectra (shock) method. This method requires a prior modal eigenvector and eigenvalues extraction. Natural frequencies of the 3-D finite-element model are calculated up to the rigid range, considered as greater than 34 Hz. Three independent orthogonal acceleration spectra are applied to the model. The acceleration spectra are considered to act simultaneously in three-directions. The SRSS method is used to sum the similar quantities calculated for each direction.

Results for individual load cases are combined using the factored load combinations discussed below. The combined stress resultants are compared with the ultimate moments and shear capacities of all structural elements pertinent to the SFPs, which are calculated in accordance with the ACI 318 to develop the safety factors.

#### 8.4.3 Load Combinations

The various individual load cases are combined in accordance with the NUREG-0800 Standard Review Plan [8.1.2] requirements with the intent to obtain the most critical stress fields for the investigated reinforced concrete structural elements.

For "Service Load Conditions" the following load combinations are:

- Load Combination No. 1 =  $1.4 * D + 1.7 * L$
- Load Combination No. 2 =  $1.4 * D + 1.7 * L + 1.9 * E$
- Load Combination No. 3 =  $1.4 * D + 1.7 * L - 1.9 * E$
- Load Combination No. 4 =  $0.75 * (1.4 * D + 1.7 * L + 1.9 * E + 1.7 * T_o)$
- Load Combination No. 5 =  $0.75 * (1.4 * D + 1.7 * L - 1.9 * E + 1.7 * T_o)$
- Load Combination No. 6 =  $1.2 * D + 1.9 * E$
- Load Combination No. 7 =  $1.2 * D - 1.9 * E$

For "Factored Load Conditions" the following load combinations are:

- Load Combination No. 8 =  $D + L + T_o + E'$
- Load Combination No. 9 =  $D + L + T_o - E'$
- Load Combination No. 10 =  $D + L + T_a + 1.25 * E$
- Load Combination No. 11 =  $D + L + T_a - 1.25 * E$
- Load Combination No. 12 =  $D + L + T_a + E'$
- Load Combination No. 13 =  $D + L + T_a - E'$

where:

- D = dead loads;
- L = live loads;
- $T_o$  = thermal load during normal operation;
- $T_a$  = thermal load under accident condition;
- E = OBE earthquake induced loads;
- $E'$  = SSE earthquake induced loads.

### 8.5 Results of Analyses

The STARDYNE computer code is used to obtain the stress and displacement fields for the 1 individual load cases.

The STARDYNE postprocessing capability is employed to form the appropriate load combinations and to establish the limiting bending moments and shear forces in various sections of the pool structure. A total of 13 load combinations are computed. Section limit strength

formulas for bending loading are computed using appropriate concrete and reinforcement strengths. For Harris, the concrete and reinforcement allowable strengths are:

$$\begin{aligned} \text{concrete } f_c' &= 4,000 \text{ psi} \\ \text{reinforcement } f_y &= 60,000 \text{ psi} \end{aligned}$$

Table 8.5.1 shows results from potentially limiting load combinations for the bending and shear strength of the slab and walls. For each section, we define the limiting safety margins as the limited strength bending moment or shear force defined by ACI for that structural section divided by the calculated bending moment or shear force (from the finite element analyses). The major regions of the pool structure consist of the four concrete walls and floors delimiting each of the SFPs. Each area is searched independently for the maximum bending moments in different bending directions and for the maximum shear forces. Safety margins are determined from the calculated maximum bending moments and shear forces based on the local strengths. The procedures are repeated for all the potential limiting load combinations. Therefore, limiting safety margins are determined. Table 8.5.1 demonstrates that the limiting safety margins for all sections are above 1.0, as required.

## 8.6 Pool Liner

The pool liners are subject to in-plate strains due to movement of the rack support feet during the seismic event. Analyses are performed to establish that the liner will not tear or rupture under limiting loading conditions in the pool. These analyses are based on loadings imparted from the most highly loaded pedestal in the pool assumed to be positioned in the most unfavorable position. Bearing strength requirements are shown to be satisfied by conservatively analyzing the most highly loaded pedestal located in the worst configuration with respect to underlying leak chases.

## 8.7 Conclusions

Regions affected by loading the fuel pool completely with high density racks are examined for structural integrity under bending and shearing action. It is determined that adequate safety margins exist assuming that all racks are fully loaded with a bounding fuel weight and that the factored load combinations are checked against the appropriate structural design strengths. It is also shown that local loading on the liner does not compromise liner integrity under a postulated fatigue condition and that concrete bearing strength limits are not exceeded.

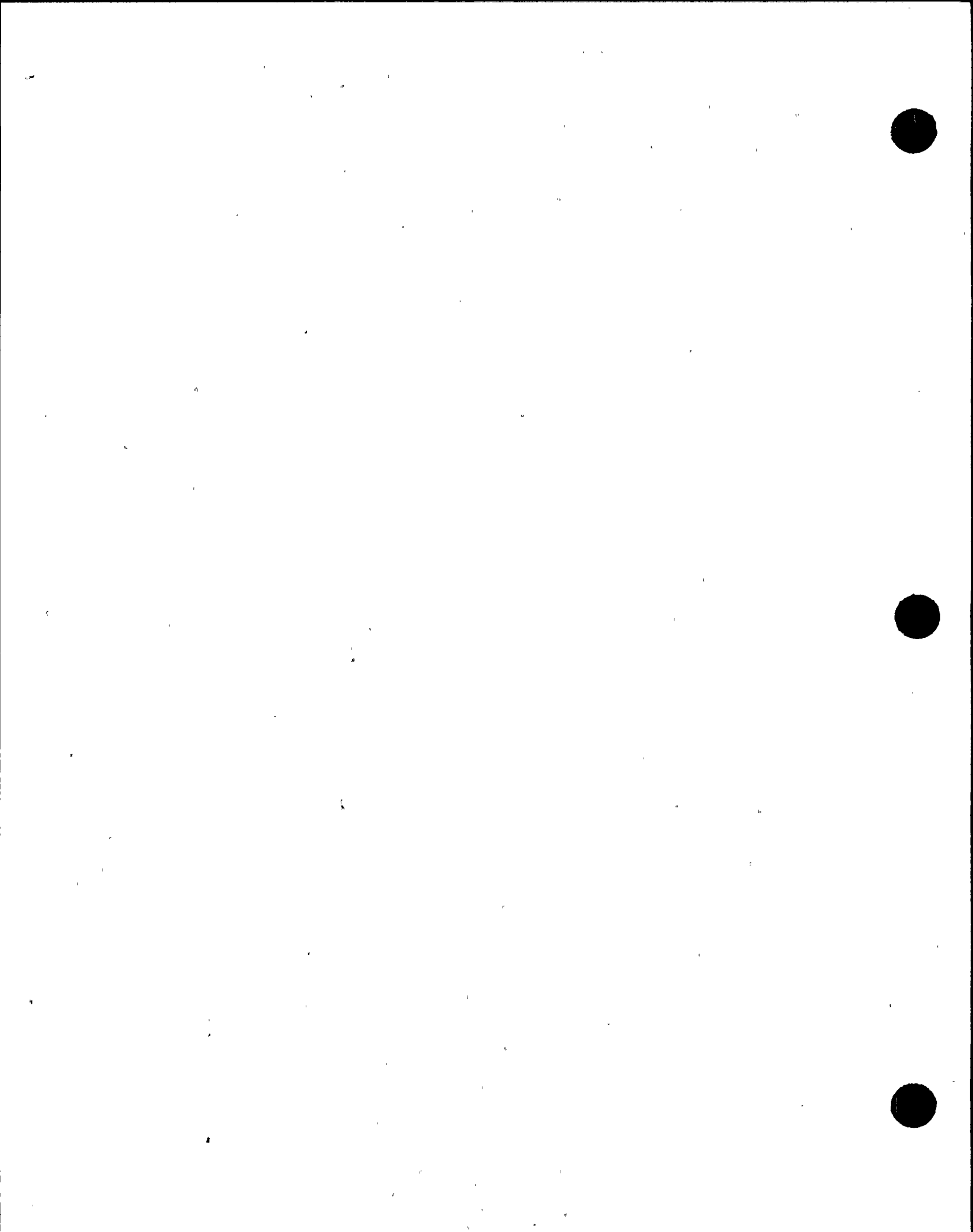
## 8.8 References

- [8.1.1] OT Position for Review and Acceptance of Spent Fuel Handling Applications, by B.K. Grimes, USNRC, Washington, D.C., April 14, 1978.
- [8.1.2] NUREG-0800, SRP-3.8.4, Rev. 1., July 1981.
- [8.1.3] ACI 318-95 and ACI 318R-95, "Building Code Requirements for Structural Concrete and Commentary," American Concrete Institute, 1995.
- [8.3.1] "Nuclear Reactors and Earthquakes, U.S. Department of Commerce, National Bureau of Standards, National Technical Information Service, Springfield, Virginia (TID 7024).
- [8.4.1] STARDYNE User's Manual, Research Engineers, Inc., Rev. 4.4, July 1996.
- [8.4.2] ACI 349-85, Code Requirements for Nuclear Safety Related Concrete Structures, American Concrete Institute, Detroit Michigan.

Table 8.5.1

## BENDING AND SHEAR STRENGTH EVALUATION

Pool	Location	Limiting Safety Margin	Critical Flexure Load Combinations (see Section 8.4.3)	Limiting Safety Margin	Critical Shear Load Combinations (see Section 8.4.3)
C	North Wall	1.97	2	1.31	2
	South Wall	3.51	2	2.20	3
	East Wall	1.72	2	1.10	5
	West Wall	1.05	10	1.06	4
	Pool Floor Slab	2.1	2	2.71	2
D	North Wall	2.32	2	3.43	3
	South Wall	1.30	10	1.08	3, 7
	East Wall	1.48	2, 6	1.07	3, 7
	West Wall	1.05	4	1.06	2
	Pool Floor Slab	2.01	2	1.64	3



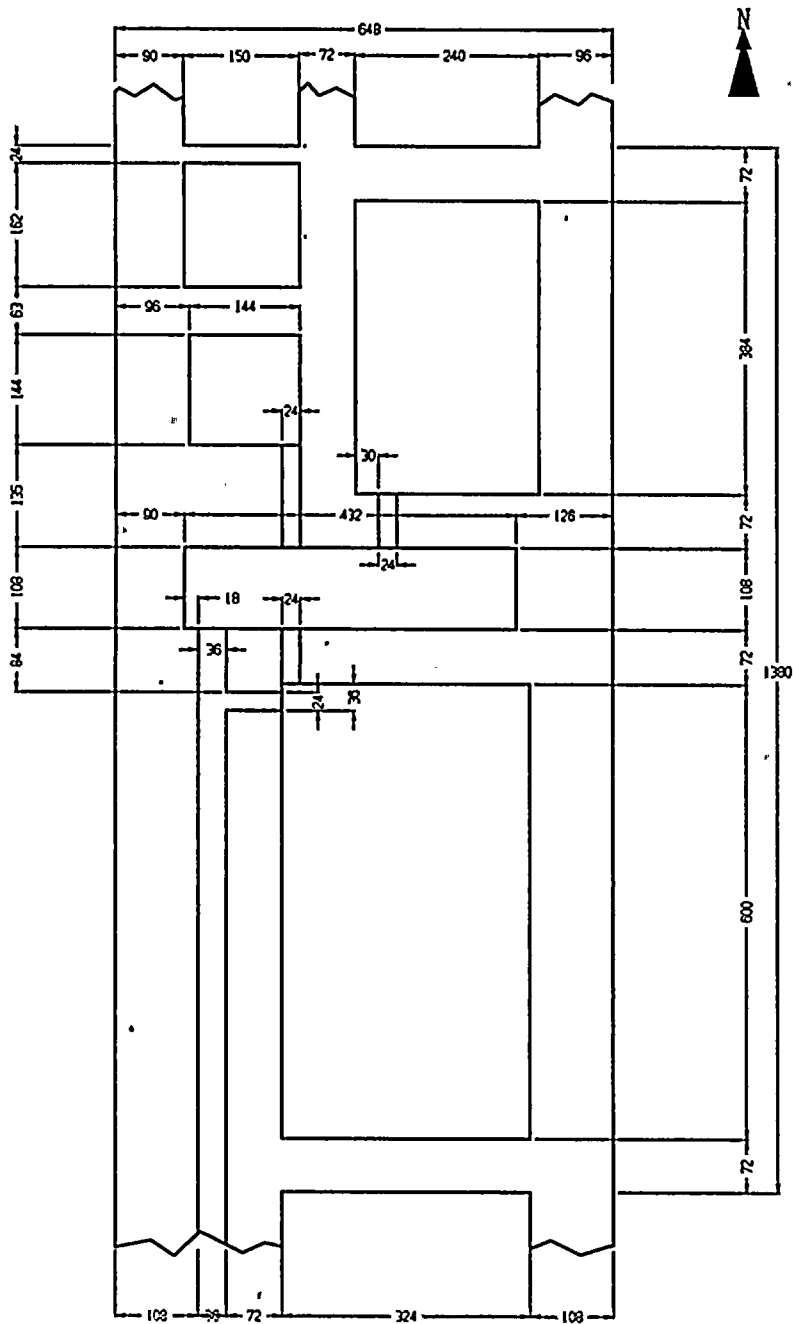


Figure 8.2.1; Pool Structure Dimensions

V1  
L9  
C1

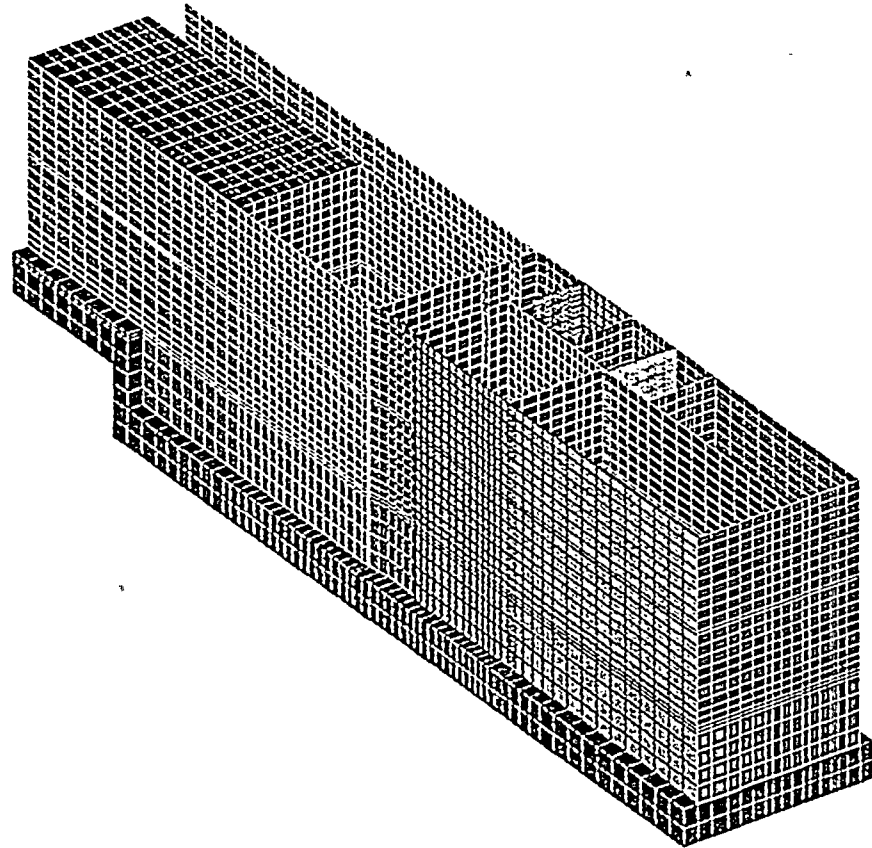


Figure 8.4.1; Fuel Handling Building  
Finite Element Model

## 9.0 RADIOLOGICAL EVALUATION

### 9.1 Solid Radwaste

No significant increase in the volume of solid radioactive wastes is expected from operating with the expanded storage capacity. The necessity for pool filtration resin replacement is determined primarily by the requirement for water clarity, and the resin is normally expected to be changed about once a year. During racking operations, a small amount of additional resins may be generated by the pool cleanup system on a one-time basis.

### 9.2 Gaseous Releases

Gaseous releases from the fuel storage area are combined with other plant exhausts. Normally, the contribution from the fuel storage area is negligible compared to the other releases and no significant increases are expected as a result of the expanded storage capacity.

### 9.3 Personnel Doses

During normal operations, personnel working in the fuel storage area are exposed to radiation from the spent fuel pool. Operating experience has shown that area radiation dose rates originate primarily from radionuclides in the pool water. As expected, subsequent to the removal of transhipped fuel from the shipping casks, Harris has experienced increases in the pool water radionuclide concentrations due to sloughing of crud and other contaminants associated with fuel handling. Additionally, radionuclide concentration increases are also experienced subsequent to the discharge of fuel from the Harris Unit 1 reactor. These two conditions represent the the previously analyzed conditions for pool water radionuclide concentrations and will not be significantly changed by the capacity expansion of storing spent fuel in pools C and D. Therefore, no additional evaluations for pool water radionuclides are required for the proposed change.

Radiation dose rates in accessible areas around the SFPs will be determined for comparison with existing zone designations. Any changes required to the zone designations will be identified and included in an update to the Harris FSAR, if necessary.

Operating experience has also shown that there have been negligible concentrations of airborne radioactivity in the Spent Fuel Pool area. No increase in airborne radioactivity is expected as a result of the expanded storage capacity.

#### 9.4 Anticipated Dose During Re-racking

All of the operations involved in racking will utilize detailed procedures prepared with full consideration of ALARA principles. Similar operations have been performed in a number of facilities in the past, and there is every reason to believe that racking can be safely and efficiently accomplished at Harris, with low radiation exposure to personnel. The Harris racking project represents lower radiological risks due to the fact that the pools currently contain no spent fuel.

- Total dose for the racking operation is estimated to be between 2 and 3 person-rem, as indicated in Table 9.4.1. While individual task efforts and doses may differ from those in Table 9.4.1, the total is believed to be a reasonable estimate for planning purposes. Divers will be used only if necessary, but the estimated person-rem burden includes a figure for their possible dose.

The existing radiation protection program at Harris is adequate for the re-racking operations. Where there is a potential for significant airborne activity, continuous air monitors will be in operation. Personnel will wear protective clothing as required and, if necessary, respiratory protective equipment. Activities will be governed by a Radiation Work Permit, and personnel monitoring equipment will be issued to each individual. As a minimum, this will include



thermoluminescent dosimeters (TLDs) and self-reading dosimeters. Additional personnel monitoring equipment (i.e., extremity TLDs or multiple TLDs) may be utilized as required.

Work, personnel traffic, and the movement of equipment will be monitored and controlled to minimize contamination and to assure that dose is maintained ALARA.

Table 9.4.1

PRELIMINARY ESTIMATE OF PERSON-REM DOSE DURING RACKING

Step	Number of Personnel	Hours	Estimated Person-Rem Dose
Clean and vacuum pool	3	25	1.5 to 2.0
Remove underwater appurtenances	4	5	0.4 to 0.8
Installation of new rack modules	5	20	0.1 to 0.2
Total Dose, person-rem			2 to 3

## 10.0 INSTALLATION

### 10.1 Introduction

The construction phase of the Harris Spent fuel pool rack installation will be executed by Carolina Power & Light. CP&L will also be responsible for specialized services, such as underwater diving and welding operations, if required. All construction work at Harris will be performed in compliance with NUREG-0612 (refer to Section 3.0), and site-specific procedures.

Crane and fuel bridge operators are to be adequately trained in the operation of load handling machines per the requirements of ANSI/ASME B30.2, latest revision, and the plant's specific training program.

The lifting devices designed for handling and installation of the new racks and removal of the old racks at Harris are remotely engageable. The lifting devices comply with the provisions of ANSI N14.6-1978 and NUREG-0612, including compliance with the primary stress criteria, load testing at a multiplier of maximum working load, and nondestructive examination of critical welds.

An intensive surveillance and inspection program shall be maintained throughout the rack installation phase of the project. A set of inspection and QC hold points will be implemented which have been proven to eliminate any incidence of rework or erroneous installation in numerous previous rack installation campaigns in Pools A and B.

Holtec International and CP&L have developed a complete set of operating procedures which cover the entire gamut of operations pertaining to the rack installation effort. Similar procedures have been utilized and successfully implemented by Holtec International on previous rack installation projects. These procedures assure that ALARA practices are followed and provide detailed requirements to assure equipment, personnel, and plant safety. The following is a list of procedures which will be available for use in implementing the rack installation phase of the project.

A. Installation/Handling Procedure:

This procedure provides direction for the handling/installation of the new high density modules. The procedure delineates the steps necessary to receive a new high density rack on site, and the proper method for unloading and uprighting the rack, staging the rack prior to installation, and installation of the rack. The procedure also provides for the installation of new rack bearing pads, adjustment of the new rack pedestals and performance of the as-built field survey.

B. Receipt Inspection Procedure:

This procedure delineates the steps necessary to perform a thorough receipt inspection of a new rack module after its arrival on site. The receipt inspection includes dimensional measurements, cleanliness inspection, visual weld examination, and verticality measurements.

C. Cleaning Procedure:

This procedure provides for the cleaning of a new rack module, if it is required, in order to meet the requirements of ANSI 45.2.1, Level C. Permissible cleaning agents, methods and limitations on materials to be employed are provided.

D. Pre-Installation Drag Test Procedure:

This procedure stipulates the requirements for performing a functional test on a new rack module prior to installation into Pools C or D. The procedure provides direction for inserting and withdrawing a "dummy" fuel assembly into designated cell locations, and establishes an acceptance criteria in terms of maximum kinetic drag force.



E. Post-Installation Drag Test Procedure:

This procedure stipulates the requirements for performing a functional test on a new rack module following installation into Pools C or D. The procedure will provide direction for inserting and withdrawing a "dummy" fuel assembly into designated cell locations, and establishes an acceptance criteria in terms of maximum kinetic drag force.

F. Underwater Diving Procedure:

Underwater diving operations may be required to assist in the positioning of new rack modules. This procedure describes the method for introducing a diver into Pools C or D, provides for radiological monitoring during the operation, and defines the egress of the diver from the fuel pool following work completion. Furthermore, this procedure requires strict compliance with OSHA Standard 29CFR-1910, Subpart T, and establishes contingencies in the event of an emergency.

G. ALARA Procedure:

Consistent with Holtec International's ALARA Program, this procedure provides details to minimize the total man-rem received during the rack installation project, by accounting for time, distance, and shielding. Additionally, a pre-job checklist is established in order to mitigate the potential for an overexposure.

H. Liner Inspection Procedure:

In the event that a visual inspection of any submerged portion of the Spent Fuel Pool liner is deemed necessary, this procedure describes the method to perform such an inspection using an underwater camera and describes the requirements for documenting any observations.

I. Leak Detection Procedure:

This procedure describes the method to test the Spent Fuel Pool liner for potential leakage using a vacuum box. This procedure may be applied to any suspect area of the pool liner.

J. Underwater Welding Procedure:

In the event of a positive leak test result, an underwater welding procedure will be implemented which will provide for the placement of a stainless steel repair patch over the area in question. The procedure contains appropriate qualification records documenting relevant variables, parameters, and limiting conditions. The weld procedure is qualified in accordance with AWS D3.6-93, Specification for Underwater Welding or may be qualified to an alternate code accepted by CP&L and Holtec International.

K. Job Site Storage Procedure:

This procedure establishes the requirements for safely storing a new rack module on-site, in the event that long term job-site storage is necessary. This procedure provides environmental restrictions, temperature limits, and packaging requirements.

10.2 Rack Arrangement

Pools C and D at Harris have been previously unused. The new rack arrangement has been prepared to maximize flexibility in the number and type (PWR vs. BWR) fuel assemblies stored. The new rack arrangement for Pool C consists of a mixture of free-standing PWR and BWR Holtec racks.



A breakdown of the number of racks and storage cells in the first campaign and completely filled configuration of Pool C is as follows:

	First Campaign		Filled Pool	
	Cells	Racks	Cells	Racks
PWR Cells	360	4	927	11
BWR Cells	1320	10	2763	19
Total	1680	14	3690	30

Pool D will store a maximum of 1025 PWR assemblies in 12 rack modules. Racks will be added to the pools on an as needed basis. A schematic plan view depicting the Spent Fuel Pools in the new maximum density configuration can be seen in Figure 1.1.

### 10.3 Pool Survey and Inspection

A pool inspection shall be performed to determine if any items attached to the liner wall or floor will interfere with the placement of the new racks or prevent usage of any cell locations subsequent to installation.

In the event that protrusions are found which would pose any interference to the installation process, it is anticipated that underwater diving operations and mechanical cutting methods would be employed to remove the protrusions.

## 10.4 Pool Cooling and Purification

### 10.4.1 Pool Cooling

The pool cooling system shall be operated in order to maintain the pool water temperature at an acceptable level. It is anticipated that specific activities, such as bearing pad elevation measurements, may require the temporary shutdown of the Spent Fuel Pool cooling system. At no time, however, will pool cooling be terminated in a manner or for a duration which would create a violation of the Harris Technical Specification or procedures.

Prior to any shutdown of the Spent Fuel Pool cooling system, the duration to raise the pool bulk temperature to 137°F will be determined. A margin temperature of 112°F is chosen such that the cooling system may be restarted prior to reaching this temperature. This will ensure that the pool bulk temperature will always remain below 137°F.

### 10.4.2 Purification

The existing Spent Fuel Pool filtration system shall be operational in order to maintain pool clarity. Additionally, an underwater vacuum system shall be used as necessary to supplement fuel pool purification. The vacuum system may be employed to remove extraneous debris, reduce general contamination levels prior to diving operations, and to assist in the restoration of pool clarity following any hydrolasing operations.

## 10.5 Installation of New Racks

The new high density racks shall be delivered in the horizontal position. A new rack module shall be removed from the shipping trailer using a suitably rated crane, while maintaining the horizontal configuration, and placed upon the upender and secured. Using two independent overhead hooks, or a single overhead hook and a spreader beam, the module shall be uprighted into vertical position.

The new rack lifting device shall be installed into the rack and each lift rod successively engaged. Thereafter, the rack shall be transported to a pre-levelled surface where the appropriate quality control receipt inspection shall be performed.

In preparing Pool C or D for the initial rack installation, the pool floor shall be inspected and any debris which may inhibit the installation of bearing pads will be removed. New rack bearing pads shall be positioned in preparation for the rack modules which are to be installed. Elevation measurements will then be performed in order to gage the amount of adjustment required, if any, for the new rack pedestals.

The new rack module shall be lifted with the Auxiliary Crane and transported along the safe load path. The rack pedestals shall be adjusted in accordance with the bearing pad elevation measurements in order to achieve module levelness after installation.

It is anticipated that the rack modules shall be lowered into the Pools C and D using the Cask Handling Crane. A hoist with sufficient capacity will be attached to the Auxiliary Crane for installation and removal activities in order to eliminate contamination of the main hook during lifting operations in the pools. The rack shall be carefully lowered onto its bearing pads.

Movements along the pool floor shall not exceed six inches above the liner, except to allow for clearance over floor projections.

Elevation readings shall be taken to confirm that the module is level and as-built rack-to-rack and rack-to-wall offsets shall be recorded. The lifting device shall be disengaged and removed from the fuel pool under Radiation Protection direction.

## 10.6 Safety, Radiation Protection, and ALARA Methods

### 10.6.1 Safety

During the rack installation phase of the project, personnel safety is of paramount importance, outweighing all other concerns. All work shall be carried out in strict compliance with applicable approved procedures.

### 10.6.2 Radiation Protection

Radiation Protection shall provide necessary coverage in order to provide radiological protection and monitor dose rates. The Radiation Protection department shall prepare Radiation Work permits (RWPs) that will instruct the project personnel in the areas of protective clothing, general dose rates, contamination levels, and dosimetry requirements.

In addition, no activity within the radiologically controlled area shall be carried out without the knowledge and approval of Radiation Protection. Radiation Protection shall also monitor items removed from the pool or provide for the use of alarming dosimetry and supply direction for the proper storage of radioactive material.

### 10.6.3 ALARA

The key factors in maintaining project dose As Low As Reasonably Achievable (ALARA) are time, distance, and shielding. These factors are addressed by utilizing many mechanisms with respect to project planning and execution.

#### Time

Each member of the project team will be properly trained and will be provided appropriate education and understanding of critical evolutions. Additionally, daily pre-job briefings will be employed to acquaint each team member with the scope of work to be performed and the proper



means of executing such tasks. Such pre-planning devices reduce worker time within the radiologically controlled area and, therefore, project dose.

### Distance

Remote tooling such as lift fixtures, pneumatic grippers, a support levelling device and a lift rod disengagement device have been developed to execute numerous activities from the pool surface, where dose rates are relatively low. For those evolutions requiring diving operations, diver movements shall be restricted by an umbilical, which will assist in maintaining a safe distance from irradiated sources. By maximizing the distance between a radioactive sources and project personnel, project dose is reduced.

### Shielding

During the course of the rack installation, primary shielding is provided by the water in the Spent Fuel Pool. The amount of water between an individual at the surface (or a diver in the pool) and an irradiated fuel assembly is an essential shield that reduces dose. Additionally, other shielding, may be employed to mitigate dose when work is performed around high dose rate sources.

## 10.7 Radwaste Material Control

Radioactive waste generated from the rack installation effort shall include vacuum filter bags, miscellaneous tooling, and protective clothing.

Vacuum filter bags shall be removed from the pool and stored as appropriate in a suitable container in order to maintain low dose rates.

Contaminated tooling shall be properly stored per Radiation Protection direction throughout the project. At project completion, an effort will be made to decontaminate tooling to the most practical extent possible.

11.0 ENVIRONMENTAL COST/BENEFIT ASSESSMENT

11.1 Introduction

Article V of the USNRC OT Position Paper [11.1] requires the submittal of a cost/benefit analysis for the chosen fuel storage capacity enhancement method. This section provides justification for selecting rack installation in Pools C and D as the most viable alternative.

11.2 Imperative for Increased Storage Capacity

The specific need to increase the limited existing storage capacity at the Harris facility is based on the continually increasing inventory in Pools A and B due to core offloads at Harris and transshipments from the Robinson and Brunswick plants, the prudent requirement to maintain full-core offload capability, and a lack of viable economic alternatives.

Based on the current number of stored assemblies and estimated discharge and transshipment rates, the Harris fuel pool is projected to lose the capacity to discharge one full core in 2001. This projected loss of storage capacity in the Harris pool would affect CP&L's ability to operate the reactors. CP&L does not have an existing or planned contractual arrangement for third party fuel storage or fuel reprocessing.

11.3 Appraisal of Alternative Options

CP&L has determined that rack installation at the Harris pools is by far the most viable option for increasing spent fuel storage capacity in comparison to other alternatives.

The key considerations in evaluating the alternative options are:

- Safety: minimize the number of fuel handling steps
- Economy: minimize total installed and O&M cost
- Security: protection from potential saboteurs, natural phenomena
- Non-intrusiveness: minimize required modification to existing systems
- Maturity: extent of industry experience with the technology
- ALARA: minimize cumulative dose due to handling of fuel

Rack installation was found by CP&L to be the most attractive option in respect to each of the foregoing criteria. An overview of the alternatives is provided in the following.

#### Rod Consolidation

Rod consolidation has been shown to be a potentially feasible technology. Rod consolidation involves disassembly of spent fuel, followed by the storage of the fuel rods from two assemblies into the volume of one and the disposal of the fuel assembly skeleton outside of the pool (this is considered a 2:1 compaction ratio). The rods are stored in a stainless steel can that has the outer dimensions of a fuel assembly. The can is stored in the spent fuel racks. The top of the can has an end fixture that matches up with the spent fuel handling tool. This permits moving the cans in an easy fashion.

Rod consolidation pilot project campaigns in the past have consisted of underwater tooling that is manipulated by an overhead crane and operated by a maintenance worker. This is a very slow and repetitive process.

The industry experience with rod consolidation has been mixed thus far. The principal advantages of this technology are: the ability to modularize, compatibility with DOE waste management system, moderate cost, no need of additional land and no additional required surveillance. The disadvantages are: potential gap activity release due to rod breakage, potential for increased fuel cladding corrosion due to some of the protective oxide layer being scraped off, potential interference of the (prolonged) consolidation activity which might interfere with ongoing plant operation, and lack of sufficient industry experience.

### On-Site Cask Storage

Dry cask storage is a method of storing spent nuclear fuel in a high capacity container. The cask provides radiation shielding and passive heat dissipation. Typical capacities for PWR fuel range from 21 to 37 assemblies that have been removed from the reactor for at least five years. The casks, once loaded, are then stored outdoors on a seismically qualified concrete pad. The pad will have to be located away from the secured boundary of the site because of site limitations. The storage location will be required to have a high level of security which includes frequent tours, reliable lighting, intruder detection, (E-field), and continuous visual monitoring.

The casks, as presently licensed, are limited to 20-year storage service life. Once the 20 years has expired the cask manufacturer or the utility must recertify the cask or the utility must remove the spent fuel from the container.

There are several plant modifications required to support cask use. Tap-ins must be made to the gaseous waste system and chilled water to support vacuum drying of the spent fuel and piping must be installed to return cask water back to the Spent Fuel Pools. A seismic concrete pad must be made to store the loaded casks. This pad must have a security fence, surveillance protection, a diesel generator for emergency power and video surveillance.



1942

...

...

...

...

...

...

...

...

...

...

...

...

...

...

...

...

Finally, the cask facility must have equipment required to vacuum dry the cask, backfill it with helium, make leak checks, remachine the gasket surfaces if leaks persist, and assemble the cask on-site. For casks which have closure gaskets, the space between the inner and outer lid must be continuously monitored to check for inner seal failure.

Presently, no MPC cask has been licensed. Because of the continued uncertainty in the government's policy, the capital investment to develop a dry storage system is considered to be an inferior alternative for Harris at this time.

### Modular Vault Dry Storage

Vault storage consists of storing spent fuel in shielded stainless steel cylinders in a horizontal configuration in a reinforced concrete vault. The concrete vault provides radiation shielding and missile protection. It must be designed to withstand the postulated seismic loadings for the site.

A transfer cask is needed to fetch the storage canisters from the fuel pool. The plant must provide for a decontamination bay to decontaminate the transfer cask, and connection to its gaseous waste system and chilled water systems. A collection and delivery system must be installed to return the pool water entrained in the canisters back to the fuel pool. Provisions for canister drying, helium injection, handling, and automatic welding are also necessary.

The storage area must be designed to have a high level of security similar to that of the nuclear plant itself. Due to the required space, the vault secured area must be located outside the secured perimeter. Consideration of safety and security requires it to have its own video surveillance system, intrusion detection, and an autonomous backup diesel generator power source.

Some other concerns relating to the vault storage system are: inherent eventual "repackaging" for shipment to the DOE repository, the responsibility to eventually decommission the new facility,



large "footprint" (land consumption), potential fuel handling accidents, potential fuel/clad rupture due to high temperature and high cost.

At the present time, no MPC technology based vault system has yet been offered for licensing to the USNRC. Therefore, this option is considered to be unavailable at this time.

### Horizontal Silo Storage

A variation of the horizontal vault storage technology is more aptly referred to as "horizontal silo" storage. This technology suffers from the same drawbacks which other dry cask technologies do, namely,

- i. No fuel with cladding defects can be placed in the silo.
- ii. Concern regarding long-term integrity of the fuel at elevated temperature.
- iii. Potential for eventual repackaging at the site.
- iv. Potential for fuel handling accidents.
- v. Relatively high cumulative dose to personnel in effecting fuel transfer (compared to rack installation).
- vi. Compatibility of reactor/fuel building handling crane with fuel transfer hardware.
- vii. Potential incompatibility with DOE shipment for eventual off-site shipment.
- viii. Potential for sabotage.



The following information was obtained from the records of the  
 Department of the Interior, Bureau of Land Management, on  
 the subject of the above-captioned tract of land.  
 The tract of land described in the above-captioned  
 instrument is situated in the County of [County Name],  
 State of [State Name], and is more particularly  
 described in the instrument above referred to.  
 The tract of land is situated in the [Section] of  
 the [Township] of the [Range] of the [Meridian].  
 The tract of land is situated in the [Quarter] of  
 the [Section] of the [Township] of the [Range] of the [Meridian].  
 The tract of land is situated in the [Quarter] of  
 the [Section] of the [Township] of the [Range] of the [Meridian].



This instrument was recorded in the County of [County Name],  
 State of [State Name], on the [Date] day of [Month], [Year].



### 11.3.1 Alternative Option Summary

An estimate of relative costs in 1997 dollars for the aforementioned options is provided in the following:

Rack Installation:	\$12 million
Horizontal Silo:	\$35-45 million
Rod consolidation:	\$25 million
Metal cask (MPC):	\$68-100 million
Modular vault:	\$56 million

The above estimates are consistent with estimates by EPRI and others [11.2, 11.3].

To summarize, there are no acceptable alternatives to increasing the on-site spent fuel storage capacity of Harris. First, there are no commercial independent spent fuel storage facilities operating in the U.S. Second, the adoption of the Nuclear Waste Policy Act (NWPA) created a de facto throw-away nuclear fuel cycle. Since the cost of spent fuel reprocessing is not offset by the salvage value of the residual uranium, reprocessing represents an added cost for the nuclear fuel cycle which already includes the NWPA Nuclear Waste Fund fees. In any event, there are no domestic reprocessing facilities. Third, at over \$½ million per day replacement power cost, shutting down the Harris reactor is many times more expensive than simply installing racks in the existing Spent Fuel Pools.

### 11.4 Cost Estimate

The proposed construction contemplates installation of storage modules in Harris Pools C and D using free-standing, high density, poisoned spent fuel racks. The engineering and design is completed for rack installation in the pools. This rack installation project will provide sufficient pool storage capacity to maintain full-core offload capability until the end of the current plant license.

The total capital cost is estimated to be approximately \$12 million as detailed below.

Engineering, design, project management:	\$2 million
Rack fabrication:	\$7 million
Rack installation:	\$3 million

As described in the preceding section, many alternatives were considered prior to proceeding with rack installation, which is not the only technical option available to increase on-site storage capacity. Rack installation does, however, enjoy a definite cost advantage over other technologies.

#### 11.5 Resource Commitment

The expansion of the Harris Spent Fuel Pool capacity is expected to require the following primary resources:

Stainless steel:	250 tons
Boral neutron absorber:	20 tons, of which 15 tons is Boron Carbide powder and 5 tons are aluminum.

The requirements for stainless steel and aluminum represent a small fraction of total world output of these metals (less than 0.001%). Although the fraction of world production of Boron Carbide required for the fabrication is somewhat higher than that of stainless steel or aluminum, it is unlikely that the commitment of Boron Carbide to this project will affect other alternatives. Experience has shown that the production of Boron Carbide is highly variable and depends upon need and can easily be expanded to accommodate worldwide needs.

Prior to the proposed modification, Pools C and D were maintained full of water with levels consistent with those of Pools A and B. Although water was allowed to be exchanged between all four pools at various times, there was no heat load associated with Pools C and D. Therefore, the bulk pool temperatures in Pools C and D have always been maintained at or below the temperatures in Pools A and B. Due to the heat load arising from the spent fuel inventory, the pool cooling system will be connected to Pools C and D to provide adequate heat removal capabilities. The maximum normal bulk pool temperature will be realized when the capacity is maximized for Pools C and D, but will still be  $\leq 137^{\circ}\text{F}^{\dagger}$ .

Maintaining four pools (instead of the previous two pools) in the Fuel Handling Building with bulk pool temperatures  $\leq 137^{\circ}\text{F}^{\dagger}$  will result in an increase in the pool water evaporation rate. This pool water evaporation increase has been determined to increase the relative humidity of the Fuel Building atmosphere by less than 10%. This increase is within the capacity of both the normal and the ESF Ventilation Systems. The net result of the increased heat loss and water vapor emission to the environment is negligible.

---

<sup>†</sup> The  $137^{\circ}\text{F}$  limit is consistent with that currently in the Harris FSAR and procedures for pools A and B. CP&L is in the process of re-evaluating systems and components to allow for an increase the allowable bulk pool temperature.

- [11.1] OT Position Paper for Review and Acceptance of Spent Fuel Storage and Handling Applications, USNRC (April 1978).
- [11.2] Electric Power Research Institute, Report No. NF-3580, May 1984.
- [11.3] "Spent Fuel Storage Options: A Critical Appraisal", Power Generation Technology, Sterling Publishers, pp. 137-140, U.K. (November 1990).